

THE SPATIAL DISTRIBUTION OF METALS IN
DISC GALAXIES, VIA SIMULATIONS AND
OBSERVATIONS

Maidier Sancho Miranda

A THESIS SUBMITTED IN PARTIAL FULFILMENT
OF THE REQUIREMENTS FOR THE DEGREE OF
DOCTOR OF PHILOSOPHY

Jeremiah Horrocks Institute for Maths, Physics and Astronomy
University of Central Lancashire

July 2017

Declaration

The work presented in this thesis was carried out at the Jeremiah Horrocks Institute for Maths, Physics and Astronomy, University of Central Lancashire.

I declare that while registered as a candidate for the research degree, I have not been a registered candidate or enrolled student for another award of the University or other academic or professional institution.

I declare that no material contained in the thesis has been used in any other submission for an academic award. Data and models used in this thesis that are not my own are clearly cited in the text.

I also declare that all the work presented in this thesis is solely my own work. In my PhD I was working in a team with more collaborators and that is the reason why I use the first person plural throughout the thesis, but everything included in it is my personal contribution.

Maiden S

Abstract

In this thesis we are interested in the evolution of disc galaxies. One of the most common ways to study it is by a deep analysis of the distribution of chemical abundances in the stellar populations of the disc component. Abundance gradients let us reconstruct the puzzle of the formation and evolution of this type of galaxies, once we learn about the different elements that are released to the interstellar medium at each stage of the life of stars.

In this work we pay special attention to the so-called thick disc component of spiral galaxies, believing that it is a relic of the early galaxy and its understanding opens the door for a complete galaxy formation scenario. We analyse thick discs both with observational data and simulations because we want to have a wider view of the situation and we think that such complementary approaches can help us maximise our knowledge and results.

Our simulations with an enhanced feedback are the ones that best reproduce the measured data from the Milky Way. The trend for the variation of the mean metallicity with galactic radius at different heights from the plane matches that in the Galaxy. It is negative in the mid-plane of galaxies and then becomes positive at greatest heights. According to simulations, this behaviour is due to a population of relatively young and metal-rich stars formed in situ in the outer galaxy, which is missing in the inner thick disc.

When looking at the same magnitudes but via observations from the CALIFA local universe galaxy sample, we see that the external galaxies exhibit a variety of

different behaviours both for the metallicity and age radial gradients with height, in addition to the trend found in simulations and the Milky Way. We deduce that thick discs probably do not form through a unique mechanism but from a combination of many of them.

Finally we want to know the influence of the galactic mass in the chemical evolution of a disc galaxy. By using a fiducial set of simulations and comparing the results to observational data we conclude that the smallest systems in our set might have an incorrect feedback efficiency, and suggest that a mass-dependent modulation of feedback might improve the result.

Contents

Declaration	ii
Abstract	iii
Acknowledgements	xvi
1 INTRODUCTION	1
1.1 Background	1
1.2 Disc galaxies	3
1.3 Chemical evolution	8
1.4 Thick disc	13
1.5 Future outlook	24
1.6 Thesis outline	25
2 ORIGIN OF THE METALLICITY DISTRIBUTION IN THE THICK DISC	27
2.1 Introduction	28
2.2 Simulations	31
2.3 Results	35
2.3.1 Radial Metallicity Gradients	35
2.3.1.1 [Fe/H] gradients	36
2.3.1.2 [O/Fe] gradients	44

2.3.2	Vertical Metallicity Gradients	46
2.3.3	Rotational Velocity Gradients	49
2.4	Discussion	51
2.4.1	Distribution Functions	51
2.4.2	Formation Radius	56
2.5	Summary	62
3	THE STELLAR POPULATIONS IN THE THICK DISC	67
3.1	Introduction	68
3.2	Sample	71
3.3	Analysis	73
3.3.1	Bulge-disc division	73
3.3.2	Extraction of the spectra	74
3.3.3	Cleaning from emission	77
3.3.4	Obtaining ages and metallicities	78
3.4	Results	81
3.4.1	Age gradient	81
3.4.2	Metallicity gradient	84
3.4.3	Velocity field	87
3.4.4	General trends	88
3.5	Conclusions	94
4	ON THE EVOLUTION OF SIMULATED GALAXIES: GETTING CLOSER TO ANY-MASS GALAXY REPRODUCTION	97
4.1	Introduction	98
4.2	Sample	101
4.2.1	Scaling relations	105
4.3	Results	105

4.3.1	Metallicity gradient	110
4.4	Conclusions	117
5	GENERAL CONCLUSIONS	119
A	EXTRA MATERIAL REGARDING CHAPTER 2	123
A.1	Figures of MaGICC-g15784	123
A.2	Tables	124
B	EXTRA MATERIAL REGARDING CHAPTER 3	132
C	LIST OF PUBLISHED ARTICLES FROM THIS WORK	175

List of Tables

2.1	Primary characteristics of the MaGICC, MUGS and RAMSES-CH simulations	32
3.1	Primary characteristics of the six galaxies from the CALIFA survey	72
4.1	Primary characteristics of the 16 fiducial simulations, when they are at redshift 0	103
4.2	Primary characteristics of the fiducial set, when they are at high redshifts	104
A.1	[Fe/H] radial gradients with increasing height for our five simulated galaxies	128
A.2	Same as Table 2.2, but considering sub-populations selected by [O/Fe], for galaxy MaGICC-g15784	129
A.3	[O/Fe] radial gradients with increasing height for our five simulated Milky Way-like galaxies	130
A.4	[Fe/H] vertical gradients with increasing radius for our galaxies	131

List of Figures

1.1	Image from NASA of the spiral galaxy Messier 74	4
1.2	Rotation curve of galaxy NGC3198, including the measured data, the result from the stars in the galaxy and the curve needed for the dark matter to recover the measurements	6
1.3	Density distribution with distance from the mid-plane, for the Milky Way galaxy	15
1.4	Age- $[\alpha/\text{Fe}]$ relation for stars in the solar neighbourhood, with the separation between the thin and thick discs proposed by Haywood et al. (2013)	19
1.5	Spatial separation of thick and thin discs, taken from Kasparova et al. (2016)	20
1.6	$[\alpha/\text{Fe}]$ vs $[\text{Fe}/\text{H}]$ plane for the Milky Way, when using G-type dwarfs from the SEGUE survey	21
2.1	Age-metallicity relation for the simulated galaxy MaGICC-g15784 . .	37
2.2	Radial abundance gradient as a function of height from the plane . .	38
2.3	$[\text{O}/\text{Fe}]$ vs. age distribution for the galaxy MaGICC-g15784	41
2.4	Radial $[\text{Fe}/\text{H}]$ gradient vs. height inferred from isolating a thick disc via chemical characteristics	43
2.5	$[\text{O}/\text{Fe}]$ radial gradient as a function of distance from the galactic plane	45

2.6	Vertical metallicity gradient as a function of radius, for the geometrical thick disc	48
2.7	Rotational velocity of solar neighbourhood stars as a function of height above the plane	50
2.8	Metallicity distribution functions for the thick disc and thin disc populations associated with simulation MaGICC-g15784	53
2.9	Distribution of the ages of thin and thick discs for MaGICC-g15784	54
2.10	Distribution of the radii of formation for thick and thin disc populations selected by $ z $, in the case of MaGICC-g15784	55
2.11	Density plots of the metallicity for the thick and thin discs in terms of the formation radius of the stars, alongside the evolution of the metallicity gradient with time, for galaxy MaGICC-g15784	57
2.12	Cumulative distribution function of the distance travelled by each star normalised to the average migration, for MaGICC-g15784	60
2.13	Same as Fig. 2.11, but separating stars by abundance instead of morphologically	61
3.1	Radial surface brightness profile for galaxy IC5376	75
3.2	Reproduction of the slits we study in galaxy NGC0955	76
3.3	Age in terms of radius for three galaxies in the set	82
3.4	Age against radius for the other three galaxies	83
3.5	Radial profile of the total metallicity for three galaxies considered in this work	85
3.6	Metallicity versus radius for the other three galaxies in our set	86
3.7	Rotation curve of galaxy UGC08267	89
3.8	Radial age gradients for increasing values of height	90
3.9	Radial metallicity gradients for increasing values of height	91

3.10	Scalelength vs. velocity lag and maximum line-of-sight velocity vs. scalelength	95
4.1	Scaling relations fulfilled by the fiducial set of 16 simulations	106
4.2	Mass density in terms of radius for a subset of our galaxy sample	108
4.3	Same as Fig. 4.2 but for the case of higher redshifts	109
4.4	Oxygen abundance in terms of radius for some galaxies in the sample	111
4.5	Same as Fig. 4.4 but showing all individual gas particles instead of the mean oxygen at each radial bin	112
4.6	Oxygen gradient versus stellar mass, including observations and MaG-ICC simulations at different redshifts	114
4.7	Same as Fig. 4.4 but using the R_{25} scale for the radius	115
4.8	Same as Fig. 4.6 but for gradients measured in the relative scale dex R_{25}^{-1}	116
A.1	Radial metallicity profile at different heights for MaGICC-g15784	125
A.2	Same as Fig. 2.14 but for $[O/Fe]$	126
A.3	Vertical metallicity for increasing radius for galaxy MaGICC-g15784	127
B.1	Galaxy IC0540, age vs. radius on the left and metallicity vs. radius on the right – weighted by light	133
B.2	Galaxy IC0540, age vs. radius on the left and metallicity vs. radius on the right – weighted by light	134
B.3	Galaxy IC0540, age vs. radius on the left and metallicity vs. radius on the right. Bottom row: radial age gradient with height on the left and the same for metallicity on the right – weighted by light	135
B.4	Galaxy IC0540, age vs. radius on the left and metallicity vs. radius on the right – weighted by mass	136

B.5	Galaxy IC0540, age vs. radius on the left and metallicity vs. radius on the right – weighted by mass	137
B.6	Galaxy IC0540, age vs. radius on the left and metallicity vs. radius on the right. Bottom row: radial age gradient with height on the left and the same for metallicity on the right – weighted by mass	138
B.7	Galaxy IC0540, rotation curve in the top and radial surface brightness profile in the bottom	139
B.8	Galaxy IC5376, age vs. radius on the left and metallicity vs. radius on the right – weighted by light	140
B.9	Galaxy IC5376, age vs. radius on the left and metallicity vs. radius on the right – weighted by light	141
B.10	Galaxy IC5376, radial age gradient with height on the left and the same for metallicity on the right – weighted by light	142
B.11	Galaxy IC5376, age vs. radius on the left and metallicity vs. radius on the right – weighted by mass	143
B.12	Galaxy IC5376, age vs. radius on the left and metallicity vs. radius on the right – weighted by mass	144
B.13	Galaxy IC5376, radial age gradient with height on the left and the same for metallicity on the right – weighted by mass	145
B.14	Galaxy IC5376, rotation curve in the top and radial surface brightness profile in the bottom	146
B.15	Galaxy NGC0781, age vs. radius on the left and metallicity vs. radius on the right – weighted by light	147
B.16	Galaxy NGC0781, age vs. radius on the left and metallicity vs. radius on the right – weighted by light	148

B.17 Galaxy NGC0781, age vs. radius on the left and metallicity vs. radius on the right. Bottom row: radial age gradient with height on the left and the same for metallicity on the right – weighted by light 149

B.18 Galaxy NGC0781, age vs. radius on the left and metallicity vs. radius on the right – weighted by mass 150

B.19 Galaxy NGC0781, age vs. radius on the left and metallicity vs. radius on the right – weighted by mass 151

B.20 Galaxy NGC0781, age vs. radius on the left and metallicity vs. radius on the right. Bottom row: radial age gradient with height on the left and the same for metallicity on the right – weighted by mass 152

B.21 Galaxy NGC0781, rotation curve in the top and radial surface brightness profile in the bottom 153

B.22 Galaxy NGC0955, age vs. radius on the left and metallicity vs. radius on the right – weighted by light 154

B.23 Galaxy NGC0955, age vs. radius on the left and metallicity vs. radius on the right – weighted by light 155

B.24 Galaxy NGC0955, age vs. radius on the left and metallicity vs. radius on the right. Bottom row: radial age gradient with height on the left and the same for metallicity on the right – weighted by light 156

B.25 Galaxy NGC0955, age vs. radius on the left and metallicity vs. radius on the right – weighted by mass 157

B.26 Galaxy NGC0955, age vs. radius on the left and metallicity vs. radius on the right – weighted by mass 158

B.27 Galaxy NGC0955, age vs. radius on the left and metallicity vs. radius on the right. Bottom row: radial age gradient with height on the left and the same for metallicity on the right – weighted by mass 159

B.28 Galaxy NGC0955, rotation curve in the top and radial surface brightness profile in the bottom	160
B.29 Galaxy UGC04197, age vs. radius on the left and metallicity vs. radius on the right – weighted by light	161
B.30 Galaxy UGC04197, age vs. radius on the left and metallicity vs. radius on the right – weighted by light	162
B.31 Galaxy UGC04197, radial age gradient with height on the left and the same for metallicity on the right – weighted by light	163
B.32 Galaxy UGC04197, age vs. radius on the left and metallicity vs. radius on the right – weighted by mass	164
B.33 Galaxy UGC04197, age vs. radius on the left and metallicity vs. radius on the right – weighted by mass	165
B.34 Galaxy UGC04197, radial age gradient with height on the left and the same for metallicity on the right – weighted by mass	166
B.35 Galaxy UGC04197, rotation curve in the top and radial surface brightness profile in the bottom	167
B.36 Galaxy UGC08267, age vs. radius on the left and metallicity vs. radius on the right – weighted by light	168
B.37 Galaxy UGC08267, age vs. radius on the left and metallicity vs. radius on the right – weighted by light	169
B.38 Galaxy UGC08267, radial age gradient with height on the left and the same for metallicity on the right – weighted by light	170
B.39 Galaxy UGC08267, age vs. radius on the left and metallicity vs. radius on the right – weighted by mass	171
B.40 Galaxy UGC08267, age vs. radius on the left and metallicity vs. radius on the right – weighted by mass	172

B.41 Galaxy UGC08267. Top row: metallicity vs. radius. Bottom row: radial age gradient with height on the left and the same for metallicity on the right – weighted by mass	173
B.42 Galaxy UGC08267, rotation curve in the top and radial surface bright- ness profile in the bottom	174

Acknowledgements

I warmly thank my supervisors Patricia Sanchez-Blazquez, Chris Brook and Brad Gibson for introducing me into such an amazing topic of research. I am indebted to Patricia and Chris because they were the ones who made my passion for research start, and who made it continue as well. Chris gave me my first opportunity to learn about this area of study and my first chance to publish a paper. And Patricia has been my greatest support during my PhD, who motivated me, taught me and who I worked with daily. Basically, she helped me finish this thesis. I acknowledge that in addition to working together they showed me their friendship by sharing good times together.

This experience would have been impossible without the funding of the University of Central Lancashire. A special thank you to Derek Ward-Thompson for giving me the freedom to make my own decisions, understanding every situation and allowing me to travel to all the conferences I thought were convenient for my academic growth. He has been my mentor and my guide. I want to thank Dimitris Stamatellos for his effort in helping me improve this thesis, and Nuala Jones for always being very friendly and efficient. Also a big thank you to Joss Bland-Hawthorn for his kindness and support since the time I met him.

Thank you to my lifelong friends Iratxe and Cris for being always close to me in spite of being hundreds of kilometres apart and for their visits both in Preston and Madrid. I am very pleased with all the new friends and colleagues that I met during this journey, and the old friends that are still there. I really liked to find

them all around the world, when we went to conferences and had a great time. We shared moments of joy and also very tense moments when we had to prepare and give talks.

This thesis is an achievement not only for me but also for Eloy, who has been by my side in the hardest times. A huge thank you for sharing his incredibly valuable scientific mind with me.

Finally, I feel a huge gratitude to my family for their infinite support. I would have never made it without them and their continuous encouragements. Special thanks to my Ama for being with me everyday, and everyday giving me the best advice. To all the members of my family thanks a lot for loving me so much and for being the best family in the world, in particular to my sisters Lorea and June, Amama and Tia. And to my Aitite because he always bet on me.

Chapter 1

INTRODUCTION

1.1 Background

‘A galaxy is a gravitationally bound collection of stars whose properties cannot be explained by a combination of baryons and Newton laws of gravity’ – Willman & Strader (2012). The word ‘galaxy’ comes from the Greek word ‘galaxias’ which means ‘milky’, due to the appearance of the Milky Way as a milky band in the sky. In addition to stars, galaxies also contain dark matter, interstellar gas, dust and stellar remnants, and they behave as a body with a form. Galaxies have typical sizes of hundreds of parsecs to tens of kiloparsecs and usually contain between 10^9 and 10^{14} stars. The Universe is thought to contain $\sim 2 \times 10^{12}$ galaxies (Conselice et al. 2016). Galaxies are thought to be mostly collisionless systems, although they can interact with each other and with the intergalactic gas, suffering environmental influences. Star formation takes place in dense regions of the interstellar gas, sometimes triggered by these interactions.

Galaxies are observed to have a variety of different shapes. These morphologies are summarised in the Hubble Sequence of Galaxies (Hubble & Rosseland 1936), also known as the ‘tuning fork’ diagram. It arranges galaxies in a continuous sequence with elliptical galaxies at the left end and spirals at the right, leaving lenticular

galaxies in the middle. The spirals are split into two branches: barred spirals and non-barred spirals. Apart from these galaxy types, there are also dwarf galaxies which have low luminosity, irregular galaxies which do not have a rotational symmetry nor clear components, etc. In 1959 de Vaucouleurs (1959) made the revised Hubble sequence, which contained a larger range of morphological types.

The nature of dark matter is still unknown but it predetermines the existence of galaxies. White & Rees (1978) pointed out that formation of galaxies was accomplished during two stages: the dark matter clustered under the influence of gravity and the gas cooled into the dark matter haloes. In a more complete formation scenario for galaxies, van der Kruit & Freeman (2011) claimed that dark matter haloes, after forming gravitationally, relax to virial equilibrium. Then infalling gas is shock-heated to the halo virial temperature, to finish cooling radiatively. In this step the disc is gradually built and stars form quiescently. From then on, the star formation history of the disc is very different for each galaxy. The most popular and complete scenario for galaxy formation is the so-called ‘inside-out’ growth model (e.g. Bouwens et al. 1997; Kepner 1999). In this scenario the bulge was formed first at high redshift and then the disc grew starting from the inner part to the outskirts, via gas infall. This model describes the general features of galaxies but it does not predict the detailed formation of an individual one.

According to the phenomenon of downsizing, star formation in the early universe took place primarily in the larger galaxies and later shifted to the smaller ones (Heavens et al. 2004). This relation between the mass and star formation history of galaxies is reflected in their colour distributions. At low redshifts, there is a bimodal colour distribution. Low mass galaxies are forming stars and therefore they appear blue, whereas more luminous systems with very low or null star formation rate form the red sequence (e.g. Kauffmann et al. 2003). The red sequence persists to beyond $z = 2$, which means that some galaxies had completed their star-forming lives by

this time.

1.2 Disc galaxies

In this thesis we focus on spiral galaxies, because we want to explore the galaxy we live in, the Milky Way (the Galaxy). Figure 1.1 is an example of a spiral galaxy. Spiral galaxies have a disc-like appearance, with spiral arms emerging from their central regions. The spiral pattern can be double (maintaining a symmetry) or a more complicated configuration. The light distribution of spiral galaxies consists of a rotating disc of stars and interstellar medium (within which the spiral arms lie), in addition to a central bulge, similar in character to an elliptical galaxy or a disc. In the case of barred spirals, which constitute roughly two-thirds of all spirals, the central bulge has an elongated (or spherical + a bar) appearance, and the spiral arms originate from the end of the bar. Our own Milky Way is a barred spiral galaxy.

Spiral galaxies are classified as Sa, Sb, Sc and Sd, according to the degree of openness of the spiral arms and the relative luminosity of the central bulge, both decreasing from Sa to Sd. We indicate that a spiral galaxy has a bar by the letter B, e.g. SBa. Intermediate stages along the sequence are also defined, e.g. Sab. Sa galaxies finished forming the disc with sufficient gas left to support star formation at a low level up to the present, while later types (Sc and Sd) had more gas left and could form stars more vigorously thus far (Sandage et al. 1970).

The majority of the mass in spiral galaxies is in the form of a semi-spherical halo of dark matter, which extends far beyond the visible galaxy, as demonstrated by the galaxy rotation curves (Rubin et al. 1980; Williams et al. 2009). The rotation curve measures the rotational speed of visible stars or gas around the centre of the galaxy with radial distance. The rotation curve predicted from the distribution of visible matter has a maximum in the galactic bulge and decreases with radial distance



Figure 1.1: Messier 74 is an almost face-on spiral galaxy. It has symmetrical spiral arms emanating from the central bulge. M74 is located ~ 32 million light-years away from us. The image has been taken from the webpage of NASA: www.nasa.gov.

from the galactic centre. On the other hand, observations find that the curve does not decrease but it is flat, indicating a constant rotation outside the bulge. This discrepancy suggests the existence of dark matter as the material responsible for the extra mass needed to maintain the rotation. An example of this discrepancy is shown in Fig. 1.2. According to Ostriker & Peebles (1973), dark haloes help stabilise spiral galaxies, which could suffer bar instabilities if the halos were missing.

The observed surface brightness distribution in most spirals can be expressed with two components, a spheroidal component associated to the bulge and a disc component. The luminosity profile of the spheroidal component can be represented by a de Vaucouleurs $r^{1/4}$ law (de Vaucouleurs 1948). de Vaucouleurs (1958) established the universal exponential description of the radial light distribution in galactic discs as:

$$I(r) = I_0 \exp[-(r/r_l)], \quad (1.1)$$

where r_l is the scalelength of the disc and I_0 is the central surface brightness. Observations of edge-on spiral galaxies demonstrate that their vertical light distribution can be approximated by an isothermal sheet (Camm 1950):

$$I(z) = I_0 \operatorname{sech}^2[z/z_h], \quad (1.2)$$

where z_h is the scaleheight of the disc. The scaleheight is independent of radial distance (van der Kruit & Searle 1981).

Disc galaxies follow various scaling laws, i.e. relations between observable parameters and luminosity or stellar mass of the galaxy. Some of these scaling relations describe the stellar component of the galaxies (e.g. stellar mass-metallicity relation, luminosity-radius relation), while others link the properties of stars to the ones of dark matter (e.g. Tully-Fisher relation).

The Tully-Fisher law (Tully & Fisher 1977), in its original form, relates the

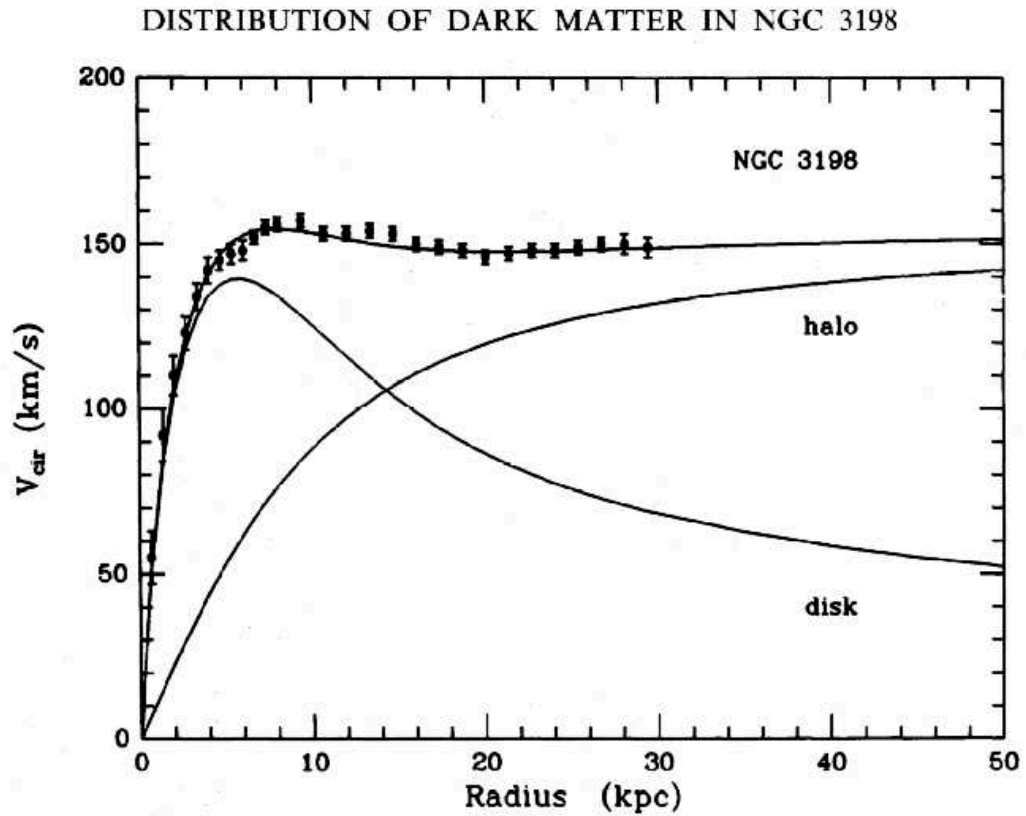


Figure 1.2: Rotation curve of galaxy NGC3198, taken from the webpage of David P. Bennett: <http://bustard.phys.nd.edu/Phys171/lectures/dm.html>. The points with error bars come from Doppler shift measurements of the 21.1 cm line. The solid line labeled 'disk' is the rotation curve due to the stars in the galaxy and the solid line labeled 'halo' indicates the rotation curve due to the dark matter halo of the galaxy, which is needed to match the observed data.

absolute blue magnitude M_B and the velocity width of the integrated HI profile of a galaxy. It is useful for measuring the absolute magnitudes and distances of galaxies from their HI profile width. Depending on the processes involved in the formation and evolution of disc galaxies, the slope, zero-point and scatter of the Tully-Fisher relation will change.

The tight correlation between stellar mass (or luminosity) and metallicity (e.g. Lequeux et al. 1979; Tremonti et al. 2004) refers to the baryonic component of the galaxies. The mass-metallicity relation reflects that bright, massive galaxies tend to be more metal-rich. A possible explanation is that more massive galaxies retain the metal enriched feedback of supernovae in a more effective way due to their deeper potential wells (Larson 1974). On the other hand, Tassis et al. (2008) argued that the cause of the mass-metallicity relation may not be the supernova ejections, but the inefficient conversion of gas into stars in low mass systems. This law also illustrates that galaxies with a given stellar mass were less enriched in the past, thus we can say that this relation evolves with time (Erb et al. 2006).

Another scaling law relates the luminosity and rotation velocity of galaxies, e.g. see Courteau et al. (2007). In that work they analysed the distribution of luminosity (L) and rotation velocity (V_c) for 1300 galaxies and found a relation of $V_c \propto L^{0.29}$ (more luminous galaxies rotate faster) in the I -band. The relation does not show any morphological dependence.

In this thesis we are only interested in the discs of spiral galaxies. These contain a substantial fraction of the baryonic matter and angular momentum in the galaxy, and much of the activity related to their evolution, such as the formation of stars, takes place in the disc. This is why exploring the discs is particularly important for understanding the formation and evolution of spiral galaxies, which is the main aim of our work.

1.3 Chemical evolution

The chemical composition of galaxies and the distribution of abundances within them provide interesting insight into the formation and evolution of disc galaxies, because it is the result of a combination of physical mechanisms like star formation processes, supernovae winds, gas infall, etc. This is why there has been important progress in this field in the last years.

In astronomy, the metallicity or Z is the fraction of mass of an astronomical object that is in chemical elements different from hydrogen or helium, and it constitutes a fundamental property of galaxies. We define it that way because most of the physical matter in the Universe is in the form of hydrogen or helium. Metallicity includes elements referred to as ‘ α -process elements’ because they are the outcome of fusion processes involving helium; they are made of helium nuclei (α particles) stuck together. Such elements are C, N, O, Ne, Mg, Si, S, Ar, Ca and Ti. Other important metals for chemical evolution are the so-called ‘iron-peak elements’, which are among the heaviest stable elements produced in stars. These are V, Cr, Mn, Fe, Co and Ni. As stated in observational works like Tomkin et al. (1985), Reddy et al. (2006) and (Kobayashi et al. 2006), α -process elements (or just ‘ α -elements’) are produced in the galaxies on shorter timescales ($\sim 10^7$ yr) than iron-peak elements ($\sim 10^8$ – 10^9 yr). This is related to the conditions in which a star is found in the final stages of its life when it may erupt as a supernova (SN). The two main types of SN observed are SN II and SN Ia. The latter have a strong ionised silicon line (Si II) apart from lacking hydrogen lines, which are very strong in the former SN type. Type II supernovae result from the explosion at the end of the life of a massive star ($8 < M_{\star} < 50 M_{\odot}$) – see for example recent explanation by Gilmore (2004) – and produce mostly α -elements. SN Ia occur in binary systems where one of the stars must be a white dwarf and the other can range from a giant to a smaller star than a white dwarf, and produce primarily iron-peak elements. As the process for a SN II

explosion happens in a shorter timescale than for a SN Ia, the metallicity $[\text{Fe}/\text{H}]$ ¹ at which $[\alpha/\text{Fe}]$ begins to drop is indicative of the time when Type Ia supernovae begin to contribute to the chemical enrichment of a galaxy.

Studies of the chemical evolution in the Galactic disc found the so-called G-dwarf problem in the Simple Model of chemical evolution (Schmidt 1963; Pagel 1997). In the Simple Model the Galactic disc starts as pure gas with zero metallicity and without subsequent inflow or outflow, and then the result is a much higher fraction of low-metallicity, long-lived stars (as G-dwarfs) than is observed in the solar neighbourhood. There are extensions of the model rectifying this result (e.g. Tinsley 1980).

The mean metallicity of stars and gas in galactic discs depends on the luminosity of the galaxy (e.g. Gallazzi et al. 2005; Lee et al. 2006, called the mass-metallicity relation and explained in Section 1.2) and usually reveals a radial gradient, according to Tremonti et al. (2004) and other studies. For example, the LMC has a lower luminosity than the Milky Way and its metallicity distribution function is shifted towards lower metallicities, even though the shapes of the two metallicity distribution functions are similar (McWilliam 1990).

There are works in the literature who study the chemical evolution in high redshift discs. For example, Ma et al. (2016b) argue that it follows four steps. First gas flows in quickly forming a rotating gas disc. After that there is a starburst in the disc triggered by fast gas infall. This creates a negative radial metallicity gradient, with lower metallicity stars in the outer galaxy than in the inner one. Then, feedback from the starburst drives intense gas outflow, mixing the gas and metals and flattening the disc metallicity gradient. Finally gas falls back and reconstructs the disc, going back to the first step of the process. In the work by Ma et al. (2016b)

¹The notation $[A/B]$ used for element abundance ratios indicates:

$[A/B] \equiv \log_{10}(N_{A,\star}/N_{B,\star}) - \log_{10}(N_{A,\odot}/N_{B,\odot})$, where N is the number of atoms of a particular element. We obtain the same value of $[A/B]$ if we use the mass instead of the number of atoms.

this happens at $z > 0.7$ and they give evidence that feedback is the main component which flattens the metallicity gradient, as the epochs when the gas outflow rate is higher overlap with the ones for the flat abundance gradients. At $z < 0.7$ the stellar feedback is no longer strong enough to disrupt the gas disc. Then, a negative metallicity gradient is formed and does not change with time too much any more.

Searle (1971) predicted that the mean metal abundance of the stars in a disc is that of the gas plus an effective yield (the net production of heavy elements, modified by effects of zero-metal inflow or enriched gas outflow). They made a model capable of reproducing the radial gradients of metal abundance in the gas of disc galaxies in the local Universe. These gradients are negative, which means that metallicity is higher in the inner disc than in the outer one (Zaritsky et al. 1994; Sánchez et al. 2012b). Ma et al. (2016b) probe via cosmological zoom-in simulations that the strong gas-phase negative metallicity gradients only occur in galaxies with a rotating disc (rotationally supported), whilst strongly perturbed systems always show flat gradients. This is because rotationally supported discs have higher gas surface density in the centre, and therefore the star formation efficiency is higher in that area as well. Thus, metal enrichment is faster in the inner disc than in the outer one, making a negative metallicity gradient. On the other hand, strong perturbations, which are generally induced by mergers, violent gas infall or outflows, stir the gas in the interstellar medium and force gas mixing. Hence it leads to metal mixing in the galactic disc, producing flat metallicity gradients in these perturbed galaxies. This is also supported by other works like Perez et al. (2011).

There are studies which claim that non-interacting galaxies show no signs of correlation between the slope of the gas-phase metallicity gradients (when normalised to some characteristic radius like the effective radius or disc scalelength) and galaxy properties such as morphology, magnitude or stellar mass (e.g. Sánchez et al. 2014; Ho et al. 2015). They also find that the correlation appears when no normalisation

is used, because there exists a relation between these galaxy properties and the size of the disc, e.g. a relation between the mass and disc size. This is explained by Ho et al. (2015), who propose that gas and stellar discs co-evolve under virtually closed-box assumptions. Magrini et al. (2007) modelled the chemical evolution of M33, being able to reproduce the observational constraints, and found that metallicity in the disc increases with time at all radii. Also in their model, the radial abundance gradient flattens continuously for the past 8 Gyr.

When looking at the abundance gradient for young stars in the disc of the Milky Way, Luck et al. (2006) find a value of ~ -0.06 dex kpc^{-1} using the Cepheids, which is in good agreement with the gas-phase gradient presented by Shaver et al. (1983) (~ -0.07 dex kpc^{-1}). Sánchez-Blázquez et al. (2014) found negative stellar metallicity gradients in local galaxies. El-Badry et al. (2016) point out that even though stellar metallicity gradients and gas-phase metallicity gradients develop in the same way while stars form in the disc, the former are less vulnerable to strong feedback, especially in massive galaxies.

The ‘inside-out’ growth model for galaxy formation (explained in Section 1.1) creates a negative radial age gradient in the disc of galaxies, with older stars in the inner disc than in the outer one. At short radii stars form from the gas enriched by the stars that preceded them. This means that at redshift zero the radial abundance gradient has a negative slope. But different studies find contradictory trends for increased redshifts. Stanghellini & Haywood (2010), using Galactic planetary nebulae, suggest that the metallicity gradients are relatively flat and temporally invariant. This is in agreement with the cosmological hydrodynamical simulations used in Gibson et al. (2013) that include a feedback recipe which distributes energy and recycled material from the interstellar medium over large scales and counts with strong radial gas flows (MaGICC simulations, Brook et al. 2012a). On the other hand, Yuan et al. (2011) observed that the radial metallicity gradient is steep at

high redshift and it weakens with time, for the case of a lensed spiral galaxy. This behaviour of flattening gradients with time is also found in simulations from Pilkington et al. (2012a) and Gibson et al. (2013) that incorporate weak feedback (they do not include feedback from massive stars prior to exploding as supernovae).

Several authors have shown that the flattening of metallicity gradients with time can be due to the presence of radial migration, star formation, feedback etc. Radial migration is the redistribution of stars in galactic discs, which makes it possible for us to find stars at a different galactocentric radius from their birth radius. It happens in galaxies with bars or spiral arms. Stars gain or lose angular momentum (e.g. Lynden-Bell & Kalnajs 1972) and this way they can move outward or inward, respectively. Sellwood & Binney (2002) studied through N-body simulations the impact of transient spiral arms in the radial migration of stars. They found that the largest changes in angular momentum happen when stars are nearly at corotation with a spiral pattern. Other works highlighted the influence of bars on radial migration (e.g. Di Matteo et al. 2013; Kubryk et al. 2013). There are two main types of radial migration. The first is called ‘churning’ and refers to the change of guiding radius as the reason why the stars appear to be at a different galactocentric distance than previously (terminology used in Schönrich & Binney 2009). The other type is ‘blurring’, which is the radial migration due to epicyclic excursions around a fixed guiding radius. Halle et al. (2015) use an SPH simulation to prove that in galaxies dominated by a bar the main source of migrators by churning is the corotation of the bar and that this effect happens specially in the first 1–3 Gyr of the simulation, within the outer Lindblad resonance. In turn, blurring dominates towards the outer disc and at later times.

Recently there has been a new terminology called ‘Galactic Archaeology’ by Freeman & Bland-Hawthorn (2002), which aims to reconstruct the lost stellar substructures of the Galaxy through its detailed chemical and dynamical studies. The

idea is to make it possible to reconstruct a plausible view of the protogalaxy, similar to what archaeologists who study the relics on the Earth do. The focus of galactic archaeologists is to build up the unified picture in which the bulge and disc were formed, by a compilation of kinematic, age and chemical composition information of a large number of stellar relics. In other words, they search for ‘fossil’ remnants of the early Galaxy and its formation.

1.4 Thick disc

The thick disc is a complement to the more well known thin disc and represents an excess of light or stars beyond the canonical exponential vertical profile of the thin disc. Thick discs were first identified in edge-on S0 galaxies by Burstein (1979) and Tsikoudi (1979), and thereafter they have been detected in the majority of disc galaxies.

The classical picture of the Milky Way disc has been one of a two-component structure with a thin disc enshrouded by a thicker stellar disc. The existence of the second stellar component close to the Galactic plane was first noted by Yoshii (1982). He suggested that it was part of the halo, even though its density was 10 times that of the local halo. The Milky Way thick disc per se was identified by Gilmore & Reid (1983), and since then it has been the subject of much controversy. Gilmore & Reid (1983) discovered that the stellar number density distribution as a function of $|z|$ (distance from the Galactic plane) was not well fitted by a single density profile, but it was best fit by two components, one with a scaleheight of ~ 300 pc and the other with ~ 1350 pc (this is shown in Fig. 1.3). These are called the geometrically defined thin and thick discs respectively.

The thick disc was originally thought to contain a distinct or discrete population of stars relative to those of the thin disc. Such a ‘discrete’ thick disc picture is consistent with evidence provided for some external disc galaxies, revealing that

thick discs may be quite generic features of late-type galaxies (e.g. Yoachim & Dalcanton 2006; Comerón et al. 2011a; Freeman 2012). In spite of it being found in many systems, the thick disc could be a non-ubiquitous component, as suggested by Fry et al. (1999) when they studied the late-type spiral galaxy NGC4244 (but cf. Comerón et al. 2011b). Even being ubiquitous or not, the fact that they are found in many disc galaxies, as well as the similarity of their properties, suggests that whatever process is responsible for their existence it is important in the formation and evolution of disc galaxies. Yoachim & Dalcanton (2006) suggest that the ratio of thick disc to thin disc stars is about 10% for large spirals like the Milky Way and about 50% for smaller galaxies. Thus, it depends on the luminosity or circular velocity of the system.

The thin and thick disc populations in the Milky Way are distinct whether divided by age (e.g. Haywood et al. 2013), kinematics (e.g. Soubiran et al. 2003; Pasetto et al. 2012), vertical distributions (e.g. Gilmore & Reid 1983) and chemical abundances (e.g. Bensby et al. 2003; Lee et al. 2011). Structurally, the Galactic thin disc scaleheight is shorter than the one of the thick disc (100 – 500 pc thin disc and 800 – 1350 pc thick disc, the exact values still being unknown). The velocity dispersions are also larger in the thick disc than in the thin disc, $\sigma_{U,V,W} = 50 \pm 6, 45 \pm 4, 36 \pm 4 \text{ km s}^{-1}$ and $\sigma_{U,V,W} = 41 \pm 2, 31 \pm 2, 25 \pm 1 \text{ km s}^{-1}$, respectively (Soubiran et al. 2003). This means that the thick disc is kinematically hotter. As a whole the thick disc is a more slowly rotating stellar system than the thin disc, seen by the lag in its rotation curve. Additionally, the thick disc stars are older (it mainly contains stars with $6.6 < \text{age} < 9.8 \text{ Gyr}$) than the thin disc stars ($< 6.6 \text{ Gyr}$). Analyses by Gilmore & Wyse (1985), Wyse & Gilmore (1995) and Chiba & Beers (2000) established that the two populations were distinct in $[\text{Fe}/\text{H}]$. The thick disc is metal poor, with a peak metallicity around $[\text{Fe}/\text{H}] = -0.6$, in contrast to the thin disc, which has a peak metallicity around $[\text{Fe}/\text{H}] = -0.2$. Finally, high-resolution

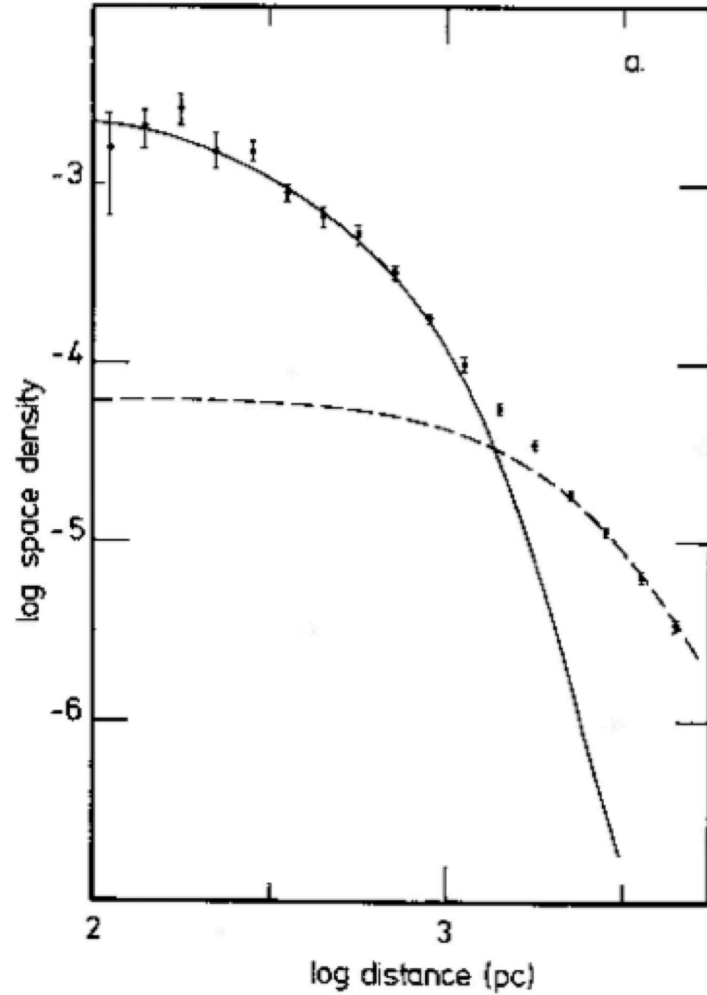


Figure 1.3: Density distribution with distance from the Galactic mid-plane, for stars with $4 \leq M_V \leq 5$, taken from Gilmore & Reid (1983). The observational data (individual points with error bars) have been fitted with two curves with different scaleheight, corresponding to the thick and thin discs.

spectra of kinematically selected nearby thick disc stars in the solar neighbourhood showed enhanced α -elements abundance with respect to the iron abundance, $[\alpha/\text{Fe}]$, compared to thin disc stars with similar $[\text{Fe}/\text{H}]$ (e.g. Prochaska et al. 2000; Feltzing et al. 2003), indicating a more rapid history of chemical evolution in the component highest from the plane. As the thick disc is the oldest disc part, the properties of its stars can be used as a ‘fossil record’ of the very earliest stages of the disc formation. This component is very interesting for galactic archaeologists.

The properties of the thin disc suggest that it was largely formed gradually from a disc made of rotating, high angular momentum gas in the mid-plane (e.g. Chiappini et al. 1997). However, the thick disc formation scenario is not proven yet and appears to be more complex. It remains a primary topic of debate for galactic structure. The most popular scenarios can be categorised as:

- Brook et al. (2004) suggest that discs are formed thick during the intense gas-rich merger phase at high-redshift; this scenario is supported by observations such as those of Gilmore et al. (2002), Wyse et al. (2006) and Comerón et al. (2011a).
- Abadi et al. (2003b) postulate that the thick disc formed from the direct accretion of debris from a now-disrupted SMC-mass satellite; such a satellite mass is required to give the correct stellar metallicities (Freeman 2012). The results by Yoachim & Dalcanton (2008) of a counter-rotating thick disc favour this mechanism.
- Quinn & Binney (1992), Kazantzidis et al. (2008), Villalobos & Helmi (2008) and Qu et al. (2011) favour a scenario in which the thick disc originated from kinematic heating of a pre-existing thin disc. Later the rest of the gas settled to form the present thin disc.
- Schönrich & Binney (2009) and Loebman et al. (2011) propose that the thick

disc populations were created in the inner region where the star formation efficiency was higher, and were taken to the outer disc by radial migration (but cf. Minchev et al. 2012; Vera-Ciro et al. 2014).

- Kroupa (2002) and Assmann et al. (2011) suggest that the thick disc originated via the ‘popping’ of star clusters.
- Bournaud et al. (2009) introduce a scenario in which massive clumps scatter stars to high velocity dispersions and form thick discs.
- According to Haywood et al. (2013) the thick disc formed through the birth of stars in a gas layer made thick by turbulence.

The first four scenarios are the principal ones and the last three are mentioned for completeness, but they are just flavours of the previous ones.

The study of stellar populations and kinematics of thin and thick discs can help us disentangle the correct scenarios. In principle, we will expect that internal evolution scenarios where thick discs are dynamically heated from thin disc stars will produce a range of properties changing smoothly with the distance from the plane. On the other hand, if it was formed via an external mechanism, it should be very different from the thin disc component. If a negative radial age gradient is observed in the thick disc, then it could have formed via thin disc flaring as a consequence of radial migration, because the stars from the thin disc that are flared to high heights are younger than thick disc stars. If thick discs are old and α -enhanced, without steep radial metallicity gradients, then they were probably formed rapidly at high redshift. According to van der Kruit & Freeman (2011), the Galactic thick disc probably did not suffer much secular heating since it was formed, as its stars spent the largest part of their lives away from the mid-plane. Probably the changing potential field of the Galaxy (linked to its continuing growth from the time of thick disc formation) was the source of the dynamical evolution of the thick disc.

This picture of a two-disc component has been called into question by multivariate mixture models (e.g. Nemeč & Nemeč 1993) and, more recently, by Bovy et al. (2012), who claim a single, continuous disc is in better agreement with observations. They use a large number of relatively low-resolution spectra of G-dwarfs from SDSS/SEGUE data, and define mono-abundance populations by dividing the stars depending on their location in the $[\alpha/\text{Fe}]$ vs $[\text{Fe}/\text{H}]$ plane. Then they analyse the stellar mass density distribution in that plane and find no clear separation. According to them, the scaleheights of the mono-abundance populations show a smooth transition from thin to thick as a function of $[\alpha/\text{Fe}]$.

This leads us to the question: ‘Are there distinct thick and thin discs?’ The answer to it depends on the definition one adopts for thin and thick discs. According to (most part of) the literature, there are at least two different types of discs in the Milky Way. However, there are still important open questions on how to best define these two types of discs (chemically, kinematically, geometrically or by age?). Figures 1.4, 1.5 and 1.6 reveal the diversity of possible ways to separate thick and thin discs in the literature.

Jurić et al. (2008) believe that the ideal definition is geometrical because this is the only way that thick and thin discs can be separated in external galaxies. In this interpretation, the two disc components are divided purely by spatial distribution of stars: the ones at higher heights correspond to the geometrical thick disc and the ones closer to the mid-plane are part of the geometrical thin disc. Jurić et al. (2008) suggested that the scalelength of the geometrical thick disc in the Milky Way is larger than that of the thin disc. After that, Minchev et al. (2015) specified that even if the chemically decomposed thick disc ($[\alpha/\text{Fe}]$ -high stars) is more radially compact than the thin disc ($[\alpha/\text{Fe}]$ -low population), the flaring of thin disc stars can contribute to the geometrical thick disc at outer radii and lead to a larger geometrical thick disc than the chemical one.

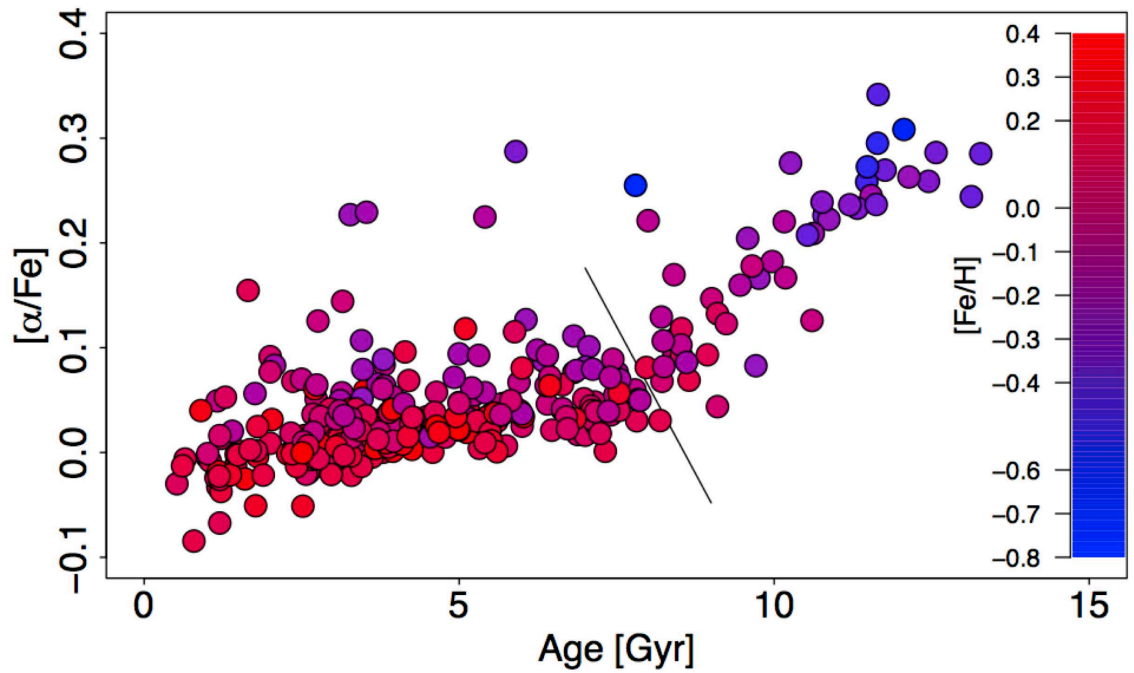


Figure 1.4: Age- $[\alpha/\text{Fe}]$ relation for stars in the solar neighbourhood, with the color scale coding metallicity. It is taken from Haywood et al. (2013). The values of $[\text{Fe}/\text{H}]$ can be seen in the inset. The diagonal solid black line represents the separation between thick (stars to the right of the line) and thin (stars to the left of the line) discs chosen in that work. They make a division purely based on age.

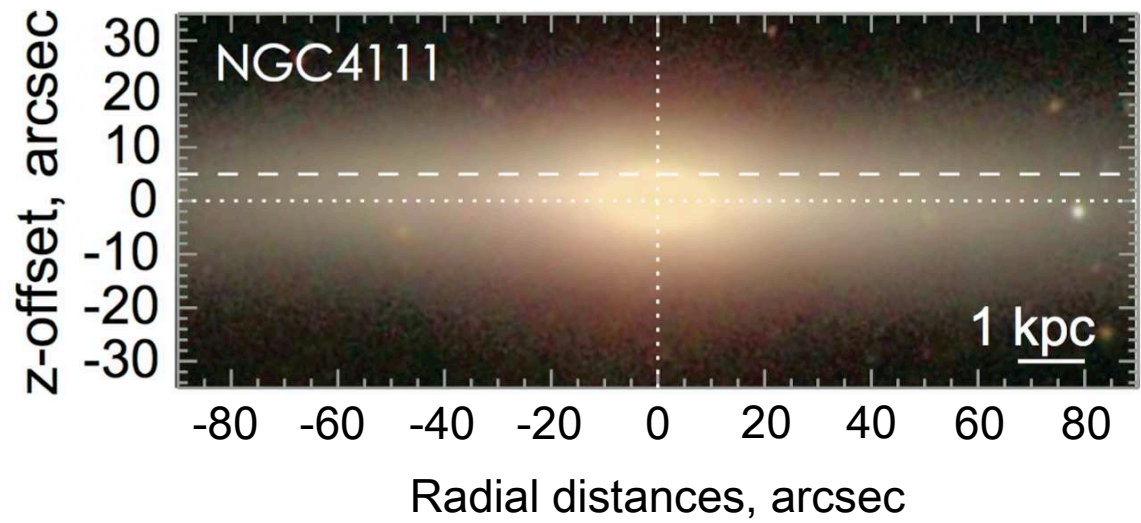


Figure 1.5: Spatial separation of thick and thin discs, taken from Kasparova et al. (2016). They show an image of the edge-on disc galaxy NGC4111 and analyse a slit located in the geometrical thick disc (horizontal dashed line) and another in the geometrical thin disc (horizontal dotted line).

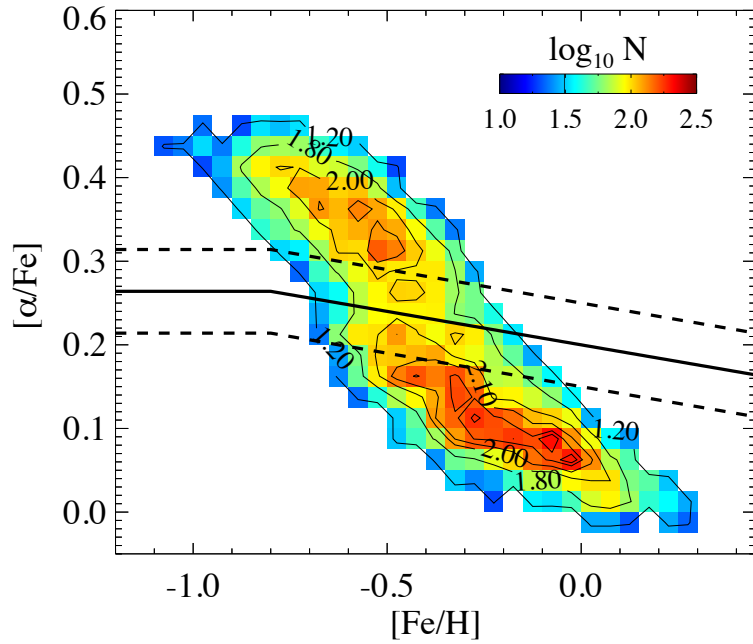


Figure 1.6: $[\alpha/\text{Fe}]$ vs $[\text{Fe}/\text{H}]$ plane, overplotted with density contours. This is taken from the work by Lee et al. (2011), where they use G-type dwarfs from the SEGUE survey. The solid line is the division between likely thin and thick disc populations. The dashed lines located at either side of the solid line indicate the starting points for the $[\alpha/\text{Fe}]$ -high and $[\alpha/\text{Fe}]$ -low partition they choose.

Navarro et al. (2011), Lee et al. (2011) and other studies suggest that thick and thin discs should be defined by their chemical properties only. The current high-resolution spectroscopic surveys clearly show a bimodal distribution in the $[\alpha/\text{Fe}]-[\text{Fe}/\text{H}]$ plane (e.g. Adibekyan et al. 2012; Bensby et al. 2014), not only in the solar neighbourhood but also in a large range of Galactic radii (e.g. Anders et al. 2014; Hayden et al. 2015). Thus, chemical abundance seems a reasonable way to divide the two populations of the Galactic disc. Mikolaitis et al. (2014) divided the disc stars from the Gaia-ESO survey into $[\alpha/\text{Fe}]$ -high and $[\alpha/\text{Fe}]$ -low and found that the $[\alpha/\text{Fe}]$ -low stars (the chemically defined thin disc) present negative radial and vertical metallicity gradients, while the $[\alpha/\text{Fe}]$ -high ones (chemical thick disc) follow a flat radial and a shallow negative vertical metallicity gradients. Similar results were exposed in Cheng et al. (2012a) using SEGUE data. Hayden et al. (2015), also using the chemical decomposition of disc stars, concluded that the chemical elements of the thick disc are radially well mixed, but the vertical negative metallicity gradient was not washed out. Results by RAVE are exposed in Boeche et al. (2013) and Boeche et al. (2014), showing that the radial abundance gradients flatten with increasing height from the mid-plane and in some cases invert. An interpretation of this behaviour is given in Minchev et al. (2014) and Miranda et al. (2016), and will be explained in Chapter 2. This evidence suggests that these two populations formed in a different way from each other.

On the other hand, Fuhrmann (2011) notes that the best way to classify thick and thin discs seems to be by age only. The problem with this criteria is the difficulty in determining accurate ages for a large volume of stars. Haywood et al. (2013) divide their stellar sample by age and by chemical abundances. They detect a connection between $[\alpha/\text{Fe}]$ -high disc stars and age-old ones, in agreement with Fuhrmann (2011). How they are related is still not clear because of the lack of large samples with accurate age estimates. The age is key information for galactic

archaeology and will provide details for the chronological order of the formation of galactic discs.

All these thick and thin disc definitions are different from each other and the populations in each case do not match entirely. Depending on the galactic formation history, the most meaningful magnitude would be a different one. For example, if during the galaxy formation there is an event that affects the whole galactic disc (e.g. gas expelled by strong feedback makes star formation stop in the whole disc), then the age would be the most relevant magnitude to differentiate the two populations. On the other hand, if, for example, there is a period when the $[\alpha/\text{Fe}]$ -low disc starts to form in the inner region while the $[\alpha/\text{Fe}]$ -high is still forming (this is found for example in the cosmological simulation by Brook et al. 2012b), then the age distribution of the chemical thin and thick discs may have a significant overlap, making chemical information more essential.

In order to clarify which is the formation mechanism for the thick disc (or if there is influence of a combination of them), there are three main approaches which could be applied. The three of them are complementary to each other and give useful information to improve the rest of them. The first is fitting the observational data with a galactic model which could distinguish each component, e.g. stellar populations model. The second approach is a semi-analytic model which studies chemical or chemodynamical evolution analytically and can relate the observed chemical signatures with the star formation history. The last approach is that of using cosmological simulations, which have a higher difficulty to match the observational data compared to the rest of the approaches, but are more useful to create a global idea of the situation in time and space.

An example of the first approach is Sanders & Binney (2015), who fitted the observational data with the distribution function of age and metallicity, including the effect of radial migration. They successfully fitted the Geneva-Copenhagen

Survey data applying different distribution functions to the two disc components.

Within the second approach, we have Chiappini et al. (2001), who try to explain the discontinuity in the $[\alpha/\text{Fe}]$ plane. They consider that there was an early intense star formation epoch which assembled the $[\alpha/\text{Fe}]$ -high disc, followed by a brief halt of the star formation, lowering the $[\text{Fe}/\text{H}]$ of the interstellar medium due to the fresh gas accretion. Then, the $[\alpha/\text{Fe}]$ -low disc is built from lower $[\text{Fe}/\text{H}]$.

Related to the third approach, Brook et al. (2004) found that cosmological simulations with Cold Dark Matter (CDM) hierarchical clustering galaxy formation, naturally create, at high redshift, geometrical thick discs which are kinematically hot, if there are multiple mergers of building blocks taking place. These building blocks are tiny, gas-rich galaxies and drive in-situ star formation in the central gas-rich disc after they merged. This situation is suitable for short timescale intense star formation to build up the $[\alpha/\text{Fe}]$ -high disc stars. Thus, this is the geometrical thick disc and its well-mixed metal abundances are produced in those high-redshift gas-rich mergers driven in-situ. Once the mergers stop, the star formation becomes less intense and there is a continuous low-level gas accretion, building the $[\alpha/\text{Fe}]$ -low disc component.

1.5 Future outlook

The present and future surveys will provide the missing information needed to solve this mystery. ESA's Gaia mission will supply 6D phase space distribution of about hundred millions of giant stars covering a large volume in the Galactic disc. This information will be complemented with the chemical abundances from the high resolution spectroscopic surveys, such as Gaia-ESO, APOGEE, GALAH, etc. For nearby population studies, SEGUE and RAVE focus on kinematic and chemical characteristics of a very large sample of stars in the Galactic disc and halo. Furthermore, the K2 mission with Kepler will add accurate ages of the giant stars. These data

will provide us clues on the formation scenario of the Galactic disc, and finally, disc galaxies in general.

1.6 Thesis outline

This thesis is a compilation of the work done following our concerns about disc galaxies and their universal properties, focusing on chemical evolution especially. We are interested both in simulations and the observational aspect of astronomy, and thus in my PhD we study the two points of view in our main three projects. The first two studies pursue the same purpose of trying to complete the picture of thick discs and their formation mechanism, but looking from the two different perspectives already mentioned (simulations and real data). The last work makes a comparison of the chemistry in galaxies with different masses, because it is also very important to know how our predictions are affected by mass.

For the first investigation we use five simulated spiral galaxies, with different star formation and feedback strengths, all with masses similar to the Milky Way. We look at various important behaviours for disc formation and compare them with measures of the Galaxy. We find that feedback plays a key role in the distribution of chemical elements in galaxies and that the ones with stronger feedback reproduce the observations better as a general rule. We select the simulation that best recreates the Milky Way and make a more extensive study of it. We then conclude that the inverted positive radial metallicity gradient we find in the thick disc of some simulations is due to (and might be the reason for the same result in the Galaxy as well) a population of younger and more metal-rich stars formed in situ in the outer galaxy, which is missing in the inner thick disc.

The second study is totally related to the first one, and the aim is exactly the same, but this time we examine observational data taken from the CALIFA integral field spectroscopic survey. We use a suite of six edge-on spiral galaxies from CALIFA

and look at their vertical properties. First we split the galaxies in various horizontal slits at diverse heights, trying to mimic the long-slit spectroscopy technique, and calculate the ages, metallicities and line-of-sight velocities of the stellar populations in the radial bins of each slit. We show the age and metallicity radial gradients of the stars with increasing height from the mid-plane, and find a variety of different behaviours: some gradients are negative, others positive and there are also some with an inversion point when moving up above the plane. It looks like the thick disc of galaxies did not form through a unique, simple mechanism, but in a more complicated way, potentially through a combination of various of the well known possible scenarios. Nowadays simulations and models are still not able to reproduce these results.

In the last project of this thesis we change topics slightly. This work, just like the former two, helps us have a more ample understanding of the evolution of disc galaxies, but in this case we look at the influence that galactic mass has on the distribution of chemical elements. We want to know if the chemical evolution is similar for all-mass galaxies irrespective of morphology. We take a fiducial set of sixteen simulated galaxies (one of them already used in the first study of this thesis) spanning a wide range in mass, and analyse the total oxygen radial gradients of the gas in terms of mass. Our gradients have similar amplitude to observational works (see Chapter 4 for details on the observational data) but the trends are not reproduced for lowest mass galaxies. They find steeper negative gradients for low mass galaxies (when the gradients are measured in an absolute distance scale), while in our case those galaxies show the flattest oxygen gradients. We suggest that a mass-dependent modulation of feedback and star formation efficiency in simulations might eradicate this inconsistency. Another explanation would be low number statistics in observations and simulations.

Chapter 2

ORIGIN OF THE METALLICITY DISTRIBUTION IN THE THICK DISC

Abstract

Using a suite of cosmological chemodynamical disc galaxy simulations, we assess how (a) radial metallicity gradients evolve with scale-height; (b) the vertical metallicity gradients change through the thick disc; and (c) the vertical gradient of the stellar rotation velocity varies through the disc. We compare with the Milky Way to search for analogous trends.

In this work we analyse five simulated spiral galaxies with masses comparable to the Milky Way. The simulations span a range of star formation and energy feedback strengths and prescriptions, particle- and grid-based hydrodynamical implementations, as well as initial conditions/assembly history. Disc stars are identified initially via kinematic decomposition, with *a posteriori* spatial cuts providing the final sample

from which radial and vertical gradients are inferred.

Consistently, we find that the steeper, negative, radial metallicity gradients seen in the mid-plane flatten with increasing height away from the plane. In simulations with stronger (and/or more spatially-extended) feedback, the negative radial gradients invert, becoming positive for heights in excess of ~ 1 kpc. Such behaviour is consistent with that inferred from recent observations. Our measurements of the vertical metallicity gradients show no clear correlation with galactocentric radius, and are in good agreement with those observed in the Milky Way's thick disc (locally). Each of the simulations presents a decline in rotational velocity with increasing height from the mid-plane, although the majority have shallower kinematic gradients than that of the Milky Way.

All in all, simulations employing stronger/more extended feedback prescriptions possess radial and vertical metallicity and kinematic gradients more in line with recent observations. The inverted, positive, radial metallicity gradients seen in the simulated thick stellar discs originate in a population of younger, more metal-rich, stars formed *in situ*, superimposed upon a background population of older migrators from the inner disc; the contrast provided by the former increases radially, due to the inside-out growth of the disc. A similar behaviour may be responsible for the same flattening as seen in the radial gradients with scaleheight in the Milky Way.

2.1 Introduction

As previously explained, the thick disc is a precious component when studying the formation and evolution of disc galaxies. Its different properties from the thin disc make the vertical structure of these galaxies very exciting.

The kinematics of the Milky Way thick disc has attracted much attention, no doubt due, in part, to the extraordinary wealth of information to be provided by the Gaia mission (e.g. Rix & Bovy 2013). Ahead of the Gaia Data Releases, the exploitation of extant datasets is both timely and essential for shaping the rapid analysis and dissemination of Gaia’s data. Recent, important, efforts in this area include that of Pasetto et al. (2012), who, using data from RAVE (Steinmetz et al. 2006), suggest the thick and thin discs are discrete and separable using stellar kinematics. Similar studies have been performed using data from SDSS (e.g. Carollo et al. 2010), obtaining analogous results. Alternative ways in which to probe and/or isolate thick and thin discs include those of chemistry (e.g. Navarro et al. 2011) and distances (e.g. Carrell et al. 2012, who select stars spatially using only dwarf stars).

In what follows, we examine how the velocity of the stars associated with the disc changes as a function of height above the plane. Observationally, vertical gradients in the rotational velocity of disc stars have been found (e.g. Bond et al. 2010; Casetti-Dinescu et al. 2011; Bovy & Tremaine 2012), with Moni Bidin et al. (2012) claiming a gradient of $dV_\phi/d|z| \approx -25 \text{ km s}^{-1} \text{ kpc}^{-1}$. By comparison with our simulations, these gradients allow us to probe the nature of kinematic transition from thin to thick disc (e.g. is it discrete or continuous?).

The metallicity of the thick disc has been well studied within the Milky Way (e.g. Bensby et al. 2003; Reddy et al. 2006; Ivezić et al. 2008). The spatial variations of the metallicity allow us to test galaxy formation and evolution scenarios. Metallicity gradients within the Milky Way have been studied since Shaver et al. (1983) recognised that the metals were not distributed homogeneously. Since then, radial (e.g. Simpson et al. 1995; Aflerbach et al. 1997), vertical (e.g. Marsakov & Borkova 2005; Soubiran et al. 2008) and azimuthal (e.g. Luck et al. 2011) gradients have been studied extensively in the Milky Way.

In the thin disc of late-type spirals, including the Milky Way, radial metallicity

gradients (whether measured in the gas-phase, or young stellar probes) are typically $-0.05 \text{ dex kpc}^{-1}$ (decreasing outwards through the thin disc). Moving away from the mid-plane, into the thick disc ($\sim 1\text{--}3 \text{ kpc}$ from the mid-plane), the gradient progressively flattens (Cheng et al. 2012b) and, indeed, eventually inverts (increasing outwards through the thick disc: Carrell et al. 2012; Anders et al. 2014). Such inversions of the radial metallicity gradient in the thick disc have also been seen in the chemodynamical simulations of Rahimi et al. (2013) and Minchev et al. (2014).

Boeche et al. (2014) have shown recently (using red giant branch stars) how the radial metallicity gradient of the Galaxy changes as a function of height $|z|$ above the plane. Only a small region in $|z|$ is covered by the RAVE sample employed, and therefore the results are mainly for stars with $|z| < 1 \text{ kpc}$, in the radial range 4.5 to 9.5 kpc. In Boeche et al. (2013), the team also determined radial gradients from the dwarf stars in the Geneva Copenhagen survey (GCS: Nordström et al. 2004).

Similarly, many studies have checked the vertical metallicity gradient in the Milky Way disc. Kordopatis et al. (2013) have inferred a vertical gradient of $-0.22 \pm 0.17 \text{ dex kpc}^{-1}$ along the line-of-sight to Sculptor, which corresponds roughly to the vertical plane. They interpret this decrease in metallicity as the transition from a thin disc to a thick disc dominated population, as opposed to any intrinsic thick disc gradient. Peng et al. (2013) also claim that there is no notable intrinsic vertical gradient in the thick disc. Conversely, there are studies which claim the existence of significant vertical gradients for this disc (Ruchti et al. 2011). Chen et al. (2011) measured the vertical gradient of the Milky Way using SDSS data. With fits over the range $1 < |z| < 3 \text{ kpc}$ they suggest a typical gradient of $-0.23 \pm 0.07 \text{ dex kpc}^{-1}$. Unlike Kordopatis et al. (2013), Chen et al. (2011) attributed this gradient to be intrinsic to the thick disc. As discussed below, when we separate thin and thick discs based upon observationally-motivated vertical slices in $|z|$, we are unable to draw conclusions as to whether the thick disc has an intrinsic

gradient or whether we are seeing the transition from thin to thick disc, because thin and thick disc stars are mixed in each vertical bin.

Recently, in Pilkington et al. (2012a) and Gibson et al. (2013) we have focused our work on how the radial gradients of Milky Way-scale simulations change as the galaxy evolves. Here, we extend that work to include how the radial metallicity gradient changes as a function of height above the plane (e.g. Bond et al. 2010; Carrell et al. 2012; Cheng et al. 2012b) and how the vertical metallicity gradient changes as a function of radius (e.g. Carrell et al. 2012). Our goal is to test the efficacy of our various energy feedback schemes in recovering the inverted metallicity gradients claimed for thick disc stars in the Milky Way and identify *why* these simulations are successful in doing so. This does not constitute *sufficient* proof of a direct analogy to the Milky Way, but is a *necessary* condition for any putative picture for the formation and evolution of the thick disc, as our galaxies are not one-to-one Milky Way models, but disc galaxies of a similar mass and environment.

2.2 Simulations

The codes and specific simulations employed here have been detailed in Stinson et al. (2010) (MUGS: McMaster Unbiased Galaxy Simulations), Brook et al. (2012a) (MaGICC: Making Galaxies In a Cosmological Context) and Few et al. (2014) (109-CH). Here, we only provide a summary of their primary characteristics.

Four of our simulations were performed with the smoothed particle hydrodynamics (SPH) code GASOLINE (Wadsley et al. 2004). Two variants of what have been referred to in earlier studies as galaxies `g1536` and `g15784` were generated, one (MUGS) using the more conservative feedback scheme described by Stinson et al. (2010), and one (MaGICC) using the more energetic approach outlined by Brook et al. (2012a). After Gibson et al. (2013), we refer to these four simulations as MUGS-`g1536`, MUGS-`g15784`, MaGICC-`g1536` and MaGICC-`g15784`. The main

Galaxy	IMF	c_\star	ϵ_{SNe}	SR	T_{max}	n_{th}	M
MUGS-g1536	Kroupa	0.05	40%	0%	15000	0.1	7.0
MUGS-g15784	Kroupa	0.05	40%	0%	15000	0.1	14.0
MaGICC-g1536	Chabrier	0.1	100%	10%	10000	9.3	6.8
MaGICC-g15784	Chabrier	0.1	100%	10%	10000	9.3	14.3
109-CH	Kroupa01	0.01	100%	–	–	0.3	7.1

Table 2.1: Primary characteristics of the simulations analysed in this work. Information for each column: 1. Simulation label; 2. Initial mass function (Kroupa \equiv Kroupa et al. 1993; Kroupa01 \equiv Kroupa 2001; Chabrier \equiv Chabrier 2003); 3. Star formation efficiency; 4. Thermalised SNe energy fraction coupled to the interstellar medium (ISM); 5. Thermalised massive star radiation energy fraction coupled to the ISM; 6. Maximum allowable gas temperature for star formation (K); 7. Minimum gas density needed for star formation (cm^{-3}); 8. Total mass of the galaxy ($10^{11} M_\odot$).

characteristics of each of the simulations used in our work are listed in Table 2.1.

Within GASOLINE, stars can form when gas has become sufficiently cool (MUGS: $T_{\text{max}} < 15000$ K; MaGICC: $T_{\text{max}} < 10000$ K) as well as sufficiently dense (MUGS: $n_{\text{th}} > 0.1 \text{ cm}^{-3}$; MaGICC: $n_{\text{th}} > 9.3 \text{ cm}^{-3}$). When a gas particle is eligible for star formation, stars form according to: $dM_\star/dt = c_\star M_{\text{gas}}/t_{\text{dyn}}$, where M_\star is the mass of stars formed in time dt , M_{gas} is the mass of a gas particle, t_{dyn} is the dynamical time of gas particles, and c_\star is the star formation efficiency – i.e., the fraction of gas that will be converted into stars.

Supernova feedback follows the blastwave model of Stinson et al. (2006) with

thermal energy (MUGS: 0.4×10^{51} erg; MaGICC: 10^{51} erg) deposited to the surrounding ISM from each supernova. Cooling is disabled in the blast region (~ 100 pc) for ~ 10 Myr. All the simulations include heating from a uniform UV ionising background radiation field (Haardt & Madau 1996). Cooling within the simulations takes into account both primordial gas and metals. The metal cooling grid is derived using CLOUDY (v.07.02: Ferland et al. 1998) and is described in detail in Shen et al. (2010).

The MaGICC simulations also include radiation feedback from massive stars (Hopkins et al. 2011). While a typical massive star might emit $\sim 10^{53}$ erg of radiation energy during its pre-SN lifetime, these photons do not couple efficiently to the surrounding ISM; as such, we only inject 10% of this energy in the form of thermal energy into the surrounding gas, and cooling is not disabled for this form of energy input. Of this injected energy, typically 90–100% is radiated away within a single dynamical time.

Raiteri et al. (1996) give a full description of the chemical evolution prescription in GASOLINE; here we summarise the main points. In the MUGS runs only oxygen and iron were tracked, and the overall metallicity (Z) was assumed to be $Z \equiv O + Fe$, which led to an under-prediction in Z of ~ 0.2 dex. However, as described in Pilkington et al. (2012a), this does not affect the metallicity gradients. The MaGICC runs track seven elements from SNe and AGB stars, and assume $Z \equiv O + Fe + C + N + Ne + Mg + Si$. Metal diffusion is included (in both MUGS and MaGICC), such that unresolved turbulent mixing is treated as a shear-dependent diffusion term (Shen et al. 2010). This allows proximate gas particles to mix their metals. Metal cooling is calculated based on the diffused metals.

Simulation 109-CH was run with the Adaptive Mesh Refinement (AMR) code RAMSES (Teyssier 2002), extended with the chemical evolution patch RAMSES-CH (Few et al. 2012a, 2014). RAMSES-CH tracks eight elements (H, C, N, O, Mg, Ne,

Si, Fe) and the global metallicity Z . The gas density threshold for star formation is 0.3 cm^{-3} ; once gas cells are eligible to form stars, they do it according to $c_{\star} \rho_{\text{gas}}/t_{\text{ff}}$, where c_{\star} is the star formation efficiency, ρ_{gas} is the gas density, and t_{ff} is the local free-fall time of the gas.¹

Feedback from SNe II events is presumed to be kinetic, while that from SNe Ia and AGB stars is thermal. Kinetic feedback deposits density, momentum, energy, and metals into all gas cells within a radial sphere of radius equivalent to two grid cells. The energy from each of these SNe II events is set to be $E_{\text{SN}} = 10^{51}$ erg. Kinetic feedback energy is determined by integrating the IMF for each stellar particle, and the momentum imparted to the gas depends then on the mass of the ejected material with an additional amount of swept-up material equal to the ejected gas mass times a factor f_w ($f_w = 10$ for 109-CH – see Few et al. 2014). The thermal feedback is much simpler and only spread over the gas cell in which the star particle is located. The thermal energy feedback from SNe Ia assumes $E_{\text{SN}} = 10^{51}$ ergs; the physical scale over which this energy is deposited has an impact on the slope of the resulting metallicity gradient (Pilkington et al. 2012a; Gibson et al. 2013).

In RAMSES, cooling is computed assuming photoionisation equilibrium (with a uniform UV background; Haardt & Madau 1996) as a function of temperature for different metallicities and densities. The metal cooling grid is derived from calculations from the CLOUDY code (Ferland et al. 1998). Gas that is colder than 10^4 K is cooled with metal fine-structure rates from Rosen & Bregman (1995).

¹RAMSES-CH uses the free-fall time to infer the star formation rate, while GASOLINE uses the dynamical time; RAMSES-CH also does not employ an explicit variable called c_{\star} , but we have calculated its equivalent to frame the discussion here.

2.3 Results

We focus our analysis on the disc stars associated with each of the five simulations described in Section 2.2. To isolate disc stars from spheroid stars, we employ the Abadi et al. (2003a) kinematic decomposition methodology, as used in earlier works. We decompose the full sample in two sub-populations according to the probability distribution function of J_z/J_{circ} : we take the distribution to the negative side and its mirror distribution as the spheroid stars and the rest constitute the disc stars, which all have positive values of J_z/J_{circ} . That way we reduce the bias because we remove the hottest population, most of them spheroid stars. When taking all the stars without doing any kinematical decomposition the results change $\sim 1\%$ and the trends remain the same. Further, while our simulations are ‘Milky Way-like’, they should not be construed as being *identical* to the Milky Way or thought of as direct Milky Way models; any such analysis will be necessarily qualitative. We believe that it is the trends that are important here, rather than the absolute values. For example, while the vertical scaleheights of our ‘thick discs’ are not dissimilar to that of the Milky Way ($\sim 1\text{--}1.5$ kpc – Gilmore & Reid 1983), the radial scalelengths are $\sim 1.5\text{--}2\times$ longer (cf. Bovy & Rix 2013). Even though the analysis which follows isolates radial regions in the disc by ‘kpc’, rather than ‘disc scalelength’, it is important to emphasise that our results are robust and not contingent upon the selected radial range.

2.3.1 Radial Metallicity Gradients

Radial abundance gradients within the MUGS and MaGICC simulations were the focus of Pilkington et al. (2012a) and Gibson et al. (2013), with their emphasis being the redshift evolution of the gas-phase abundance gradients. Both works demonstrated the powerful diagnostic that gradients can play in constraining the nature and physical extent of feedback. Here, we move beyond the in situ radial

abundance gradients and examine the impact on gradients when transitioning from the thin to the thick disc, contrasting with the behaviour seen in recent observational work and other simulations (e.g. Cheng et al. 2012b; Carrell et al. 2012).

2.3.1.1 [Fe/H] gradients

We begin looking at the distribution of the metallicity of stars with different ages. Figure 2.1 includes all disc stars in the radial range 5–10 kpc for one of our simulated galaxies, MaGICC–g15784 (the trend is very similar for the rest of them). The inner 5 kpc was avoided in order to filter out any remaining spheroid stars that were not removed by the kinematic decomposition. We also limit our sample to stars with $|z| < 3$ kpc. As expected, the mean metallicity increases very rapidly during the first ~ 4 Gyr of time and after that it remains almost constant.

Now we are ready to have a look at the gradients. In Fig. 2.2 we show the radial metallicity gradients (weighted by mass) for our five Milky Way-scale simulations, as a function of absolute height above the plane, including all disc stars in the radial range $5 < r < 10$ kpc (we choose a similar radial range as that used in most studies in the literature). In the figure, data from observations is represented by lines and results from simulations with symbols, as noted in the inset. Although the radial ranges employed by the rest of the studies are not always exactly the same as ours, it does not impact upon the results. We have checked the influence on changing the radial and vertical bins by ± 2 kpc and the trends remain the same, even if the exact numbers vary somewhat. All the values shown in the plot are representative of the mid-point of each vertical height bin in every simulation and observation; they have not been weighted by the density distribution. This does not introduce any dramatic bias because all the data have been analysed in the same way.

From Fig. 2.2, one can see that the gradients are negative at low scaleheights, but gradually flatten when moving to greater heights above the plane. The gradient

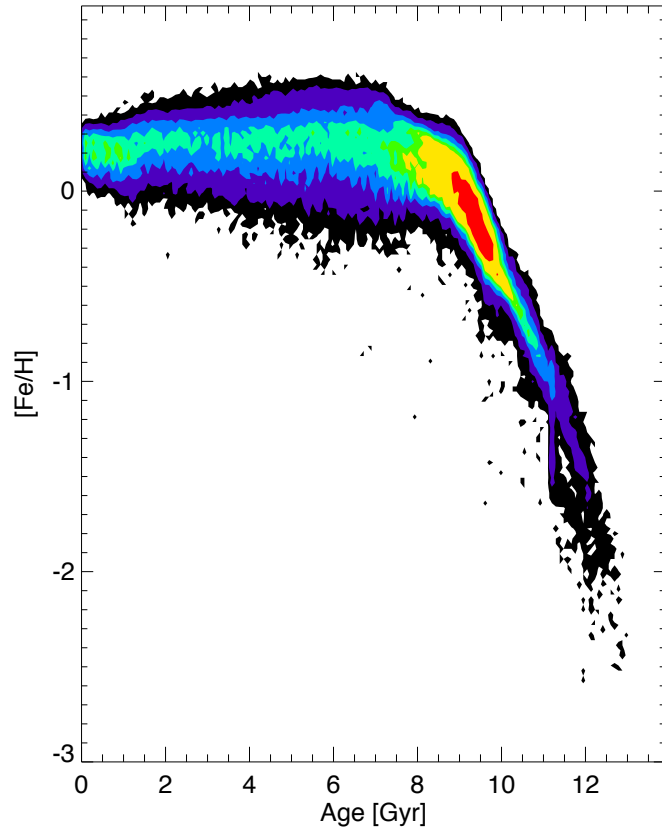


Figure 2.1: Age-metallicity relation for the disc stars which fulfil the conditions $5 < r < 10$ kpc and $|z| < 3$ kpc. Old stars have a low value of $[\text{Fe}/\text{H}]$, but it rapidly increases due to the SN Ia enrichment of the ISM. This figure corresponds to the galaxy MaGICC-g15784, but the relation is analogous for the rest of the simulations in our sample.

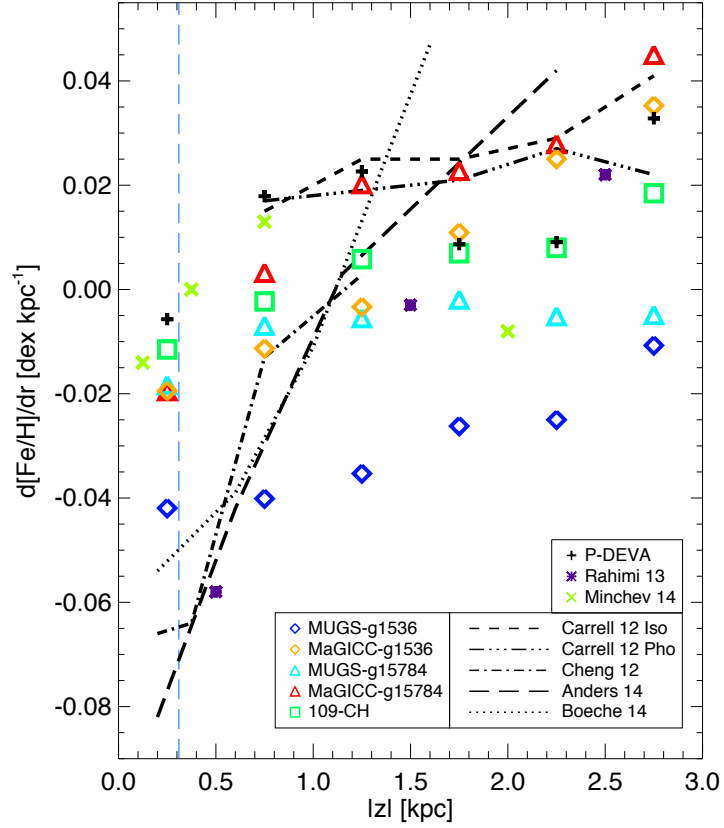


Figure 2.2: Radial abundance gradient as a function of height from the plane. The figure includes our five simulations, MUGS-g1536 (blue diamonds), MaGICC-g1536 (orange diamonds), MUGS-g15784 (cyan triangles), MaGICC-g15784 (red triangles) and 109-CH (green squares), for all disc stars in the radial range $5 < r < 10$ kpc. We also present recent observational data and results from other simulations overplotted in the panel (with the caveat that their radial and vertical selection criteria do not exactly match ours). Simulations from Rahimi et al. (2013) are represented with purple asterisks and the ones from Minchev et al. (2014) with light green crosses. The values for P-DEVA are indicated with black plus signs. Observational data from Carrell et al. (2012) (short dashed and triple dot dashed lines), Cheng et al. (2012b) (dot dashed line), Anders et al. (2014) (long dashed line) and Boeche et al. (2014) (dotted line), are shown. The blue vertical dashed line corresponds to the effective force resolution of the simulations, i.e. 314 pc.

within the MaGICC runs, with their substantially greater energy feedback, actually inverts (becoming positive) at heights $\gtrsim 1$ kpc. This transition occurs at heights which are also thought of as the transition between the thin and thick stellar discs of the Milky Way, in terms of the number counts of the latter beginning to dominate over the former (Jurić et al. 2008). Simulations which distribute the energy from supernovae over larger spatial scales, such as 109-CH, regardless of whether that feedback is ‘conventional’ or ‘strong’ energy-wise, also show gradient inversions when reaching heights associated with the classical thick disc. Conversely, the more conservative approaches to feedback, such as those applied to our MUGS realisations, while flattening with scaleheight, do not invert. The values of the radial gradients for the simulations employed here are listed in Table A.1. Figure A.1 contains the breakdown of the gradient at each height, for galaxy MaGICC-g15784.

The inversion of the radial metallicity gradient with height is also suggested by observations of the Milky Way disc. In Fig. 2.2 we have included some of these studies, each of which typically possesses a slope uncertainty of ~ 0.005 dex kpc $^{-1}$: Cheng et al. (2012b) checked the radial metallicity gradient of old main-sequence turnoff stars from the SEGUE survey, in a radial range from 6 to 16 kpc; Carrell et al. (2012) studied a sample of F, G and K dwarf stars from SDSS DR8, through two different distance measurements – isochrone and photometric distances (their radial range extends from 7 to 10.5 kpc); Anders et al. (2014) explored the APOGEE data, investigating the red giant sample with $6 < r < 11$ kpc. Each of these studies finds trends that are reflected in our simulations.

Several complementary works to ours have also examined this behaviour, and in Fig. 2.2 we therefore incorporate the prediction for three of these models drawn from the literature. Each of them was performed using different methodologies and simulations from those in our extended suite: Minchev et al. (2014) employed a chemodynamical model to study the radial gradients between $5 < r < 10$ kpc and

Rahimi et al. (2013) searched between 7 and 10 kpc in radii through their cosmological simulation. We also include one realisation of a Milky Way-like system run using the P-DEVA SPH code (Martínez-Serrano et al. 2008, 2009). It is interesting to note that in the Minchev et al. (2014) simulation, at a distance from the mid-plane greater than ~ 2 kpc, the gradient reverts from ‘inverted’ to ‘negative’ again. This is related to the flaring of the younger disc in this run; this flaring is not sufficient at that scaleheight to allow a population of younger, more metal-rich, stars to populate that region, which is ultimately the reason for the gradient reverting back to negative.

There are other studies analysing the radial metallicity gradients. For example, values from Boeche et al. (2013) agree well with our simulation results apart from stars with $|z| > 0.8$ kpc where they find a more positive gradient ($0.056 \text{ dex kpc}^{-1}$). The small number of stars in their sample though (middle panel of their figure 3) makes this inferred steep positive gradient somewhat uncertain.

Other trends for MUGS and MaGICC galaxies have previously been contrasted (e.g. Gibson et al. 2013; Obreja et al. 2013; Domínguez-Tenreiro et al. 2014). In all these cases, the consistency of our sets of galaxies with observational data is very satisfactory. The underlying physical processes responsible for the properties of these galaxies look the same for both the P-DEVA and the GASOLINE sets, including the origin of the spheroidal stellar components versus the disc ones (Domínguez-Tenreiro et al. 2015).

Because defining a thick disc can be done either spatially, as we have carried out by default (to allow for comparison with external edge-on discs), or chemically, we now check that our conclusions are robust to that thick disc definition. In order to do so, we show the relation between $[\text{O}/\text{Fe}]$ and stellar age for one of our simulated galaxies (MaGICC-g15784), in Fig. 2.3, and state that the trends are equivalent for the other simulations. The normalisation to solar abundances has been taken from

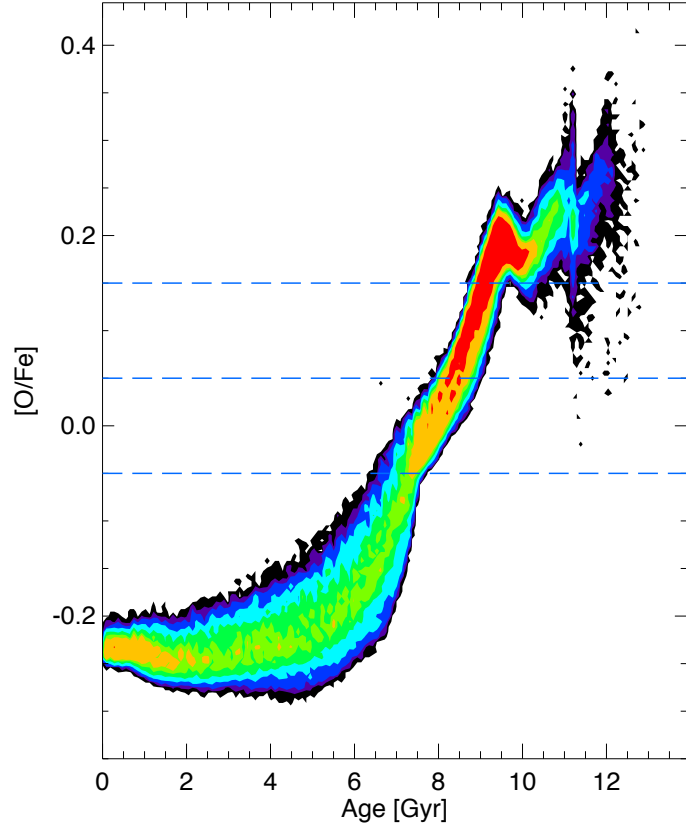


Figure 2.3: $[O/Fe]$ vs. age distribution for all disc stars included in Fig. 2.2 ($5 < r < 10$ kpc and $|z| < 3$ kpc), for the galaxy MaGICC-g15784. The densest (i.e., most populated) regions are shown in red and the least dense in black. Blue horizontal dashed lines indicate the high- α cuts that are used in Fig. 2.4 to investigate the radial gradients of chemically selected populations, as opposed to spatially selected populations exposed in Fig. 2.2. We have two main peaks, with different age and $[O/Fe]$, i.e. young α -poor and old α -rich stars. We call ‘thick disc’ to those disc stars with $[O/Fe] > -0.05$ dex and ‘thin disc’ to those with $[O/Fe] < -0.05$ dex.

Anders & Grevesse (1989). Except for a shift to lower $[\text{O}/\text{Fe}]$ values in the model, we can appreciate the similarity of this Figure with observational works, such as figure 6 of Haywood et al. (2013), who present the same relation for a sample of solar neighbourhood stars (see also Snaith et al. 2015). We define our chemically selected thick disc as the stars which fulfil the condition $[\text{O}/\text{Fe}] > -0.05$ dex and thin disc the stars with $[\text{O}/\text{Fe}] < -0.05$ dex, following the two main peaks or populations identified in Fig. 2.3.

We next return to the radial $[\text{Fe}/\text{H}]$ gradients and their variation with height, but this time examining the effect produced by separating the thick disc via the selection of α -enhanced stars (rather than simply a spatial cut). Figure 2.4 includes observational data and results from MaGICC-g15784, both with the same symbols and linestyles as in Fig. 2.2. Now we add the gradients for the sub-populations chemically separated according to the α -cuts denoted by the blue horizontal lines in Fig. 2.3. We represent with orange squares and black circles the chemically defined thick and thin discs, respectively. The figure reveals the similarity of results when changing the thick disc selection criteria. The conclusion does not change: the thick disc has a positive radial metallicity gradient and it is negative for the thin disc. In Fig. 2.4 we have also included more extreme thick disc conditions: blue asterisks show the result for sub-population with $[\text{O}/\text{Fe}] > 0.05$ dex and green diamonds for stars with $[\text{O}/\text{Fe}] > 0.15$ dex. When increasing these high- α criteria, the contamination of the thin disc gets smaller and the gradients are even more positive (at low $|z|$ they are less and less negative) and flatter, which agrees with our conclusions. Table A.2 contains the values of the gradients in the figure.

Increasing $|z|$ implies increasing age but not uniformly as a function of radius. While the outer disc is composed of stars with a range of ages at any height above the plane (due to flaring, etc.), the inner disc is exclusively old at high $|z|$. This causes the inversion from negative to positive $d[\text{Fe}/\text{H}]/dr$, or positive to more positive as

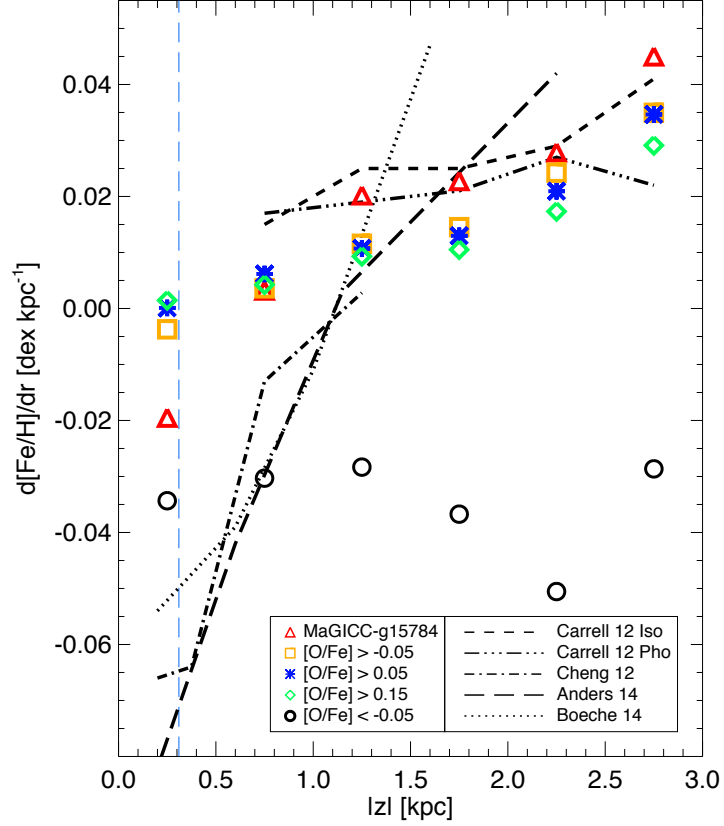


Figure 2.4: Radial $[\text{Fe}/\text{H}]$ gradient vs. height inferred from isolating a thick disc via chemical characteristics, i.e. the high- α population. We repeat some data previously presented in Fig. 2.2: observational data and results from galaxy MaGICC-g15784, both indicated with the same linestyles and symbols as before. We overplot the gradients for the three high- α cuts displayed in Fig. 2.3 through the horizontal blue dashed lines ($[\text{O}/\text{Fe}] > -0.05$ dex in orange squares, $[\text{O}/\text{Fe}] > 0.05$ dex in blue asterisks and $[\text{O}/\text{Fe}] > 0.15$ dex in green diamonds) and the low- α cut ($[\text{O}/\text{Fe}] < -0.05$ dex in black circles).

seen in Table A.2 for an individual $[\text{O}/\text{Fe}]$ cut. For any $|z|$ slice, increasing $[\text{O}/\text{Fe}]$ results in flatter gradients because the higher the $[\text{O}/\text{Fe}]$ cut, the smaller the age range available for the interplay of inside-out formation and disc flaring.

We have proved the consistency between our thick disc morphological selection and the chemical cut; indeed, our conclusions are unchanged by this choice. Whether α -selected or spatially-selected, the radial metallicity gradients are positive for the thick disc and negative for the thin disc.

The phenomenon of the inversion of the radial metallicity gradient is discussed in more detail in Section 2.4. Except for the next subsection concerning radial $[\text{O}/\text{Fe}]$ gradients, in the rest of the chapter we study the populations below and above 1 kpc separately, referring to them as thin and thick discs, respectively. We define the thick disc morphologically in contrast to a chemical/age cut because these $|z|$ slices allow better comparison with the Milky Way and external galaxies, as the latter are difficult to separate using detailed chemical abundances; such a spatial cut is a common means by which to separate thin and thick discs (e.g. Robin et al. 1996; Ojha 2001; Jurić et al. 2008; Hayden et al. 2015), but as stated earlier it is important to stress that our conclusions are robust to the choice of spatial vs. chemical definitions for the thick disc. Our approach is analogous to these aforementioned empirical thick disc works, and neatly avoids the ongoing debate regarding the use of the gap in the $[\alpha/\text{Fe}]-[\text{Fe}/\text{H}]$ plane to isolate disc components.

2.3.1.2 $[\text{O}/\text{Fe}]$ gradients

The variation of the radial gradients in $[\text{O}/\text{Fe}]$ as a function of $|z|$ is shown in Fig. 2.5 (the values are listed in Table A.3 and the detailed gradients at each height for MaGICC-g15784 are presented in Fig. A.2). Here, we use $[\text{O}/\text{Fe}]$ as a proxy for $[\alpha/\text{Fe}]$. Lines are used to represent observational results and symbols for simulations. We do not see any clear differences between our five simulations, and,

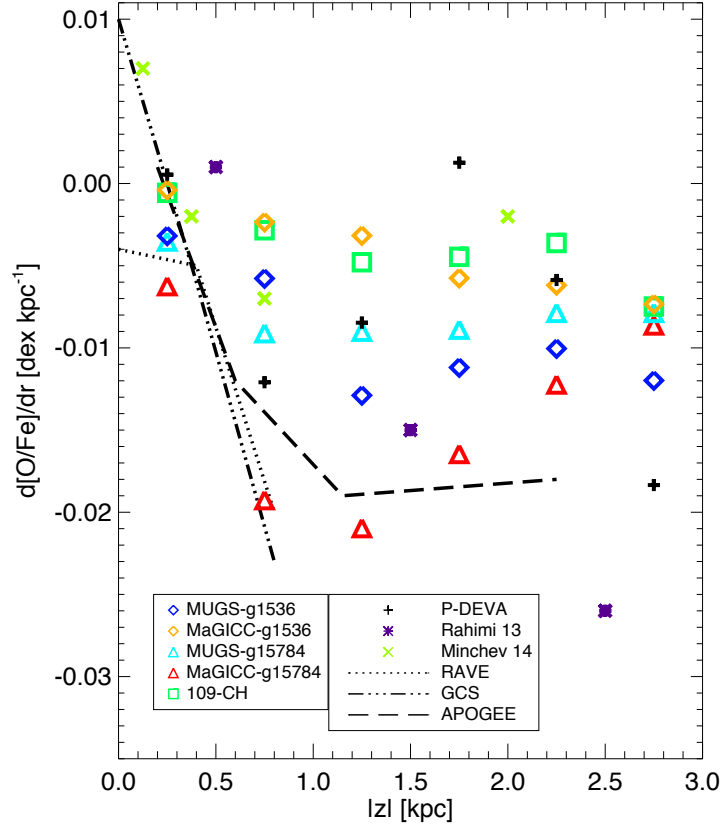


Figure 2.5: $[O/Fe]$ radial gradient as a function of distance from the galactic plane $|z|$. The disc stars with $5 < r < 10$ kpc of our five simulations are plotted: MUGS-g1536 in blue diamonds, MaGICC-g1536 in orange diamonds, MUGS-g15784 in cyan triangles, MaGICC-g15784 in red triangles and 109-CH in green squares. Results from some external simulations are also shown (P-DEVA in black plus signs, Rahimi et al. (2013) in purple asterisks and Minchev et al. (2014) in light green crosses), alongside the observational data from Boeche et al. (2013) (RAVE: dotted line; GCS survey: triple dot dashed line) and Anders et al. (2014) (APOGEE: dashed line).

furthermore, most seem to agree with the observational work from Boeche et al. (2013). In that work, they measured the $[\alpha/\text{Fe}]$ radial gradient as a function of height from the galactic plane for their sample of dwarf stars. They defined the α -enhancement as $[\alpha/\text{Fe}] = ([\text{Mg}/\text{Fe}] + [\text{Si}/\text{Fe}])/2$. They carried out a similar analysis on the RAVE and GCS survey stars to check the consistency of their results. These two observations are shown by the dotted and triple dot dashed lines of Fig. 2.5, respectively. Both the RAVE and GCS results are somewhat limited by the scaleheights which their data probe. Our simulations are also consistent with a number of other studies, including observations from APOGEE (Anders et al. 2014) and simulations from Minchev et al. (2014), which are also included in Fig. 2.5. The P-DEVA galaxy (Martínez-Serrano et al. 2008, 2009) also follows the same trends. Rahimi et al. (2013) found a steeper negative gradient at high $|z|$, although in the mid-plane their results are comparable to ours.

Gibson et al. (2013) presented the radial $[\text{O}/\text{Fe}]$ gradients for the discs of galaxies MUGS-g1536 and MaGICC-g1536 and concluded that both are relatively flat ($< -0.005 \text{ dex kpc}^{-1}$). Pilkington & Gibson (2012) analysed how the $[\text{O}/\text{Fe}]$ gradient of MUGS-g15784 evolves over time. Since redshift $z \sim 1$, stars have been born with relatively flat $[\text{O}/\text{Fe}]$ gradients. At earlier times, the gradient was steeper, due to the presence of α -enhanced stars in the inner disc (a natural byproduct of the inside-out growth of the disc). At the present epoch these have been distributed throughout the disc (due to various migration/heating/churning processes). This is similar to what was shown for $[\text{Fe}/\text{H}]$, for all of the MUGS galaxies, in Pilkington et al. (2012b).

2.3.2 Vertical Metallicity Gradients

Vertical metallicity gradients have been found to be different for the thin and thick discs of the Milky Way (e.g. Marsakov & Borkova 2005, 2006; Soubiran et al. 2008).

In Pilkington et al. (2012a), we studied the vertical metallicity gradients near the solar neighbourhood of the MUGS galaxies and found there to be no clear evidence for a two-component vertical structure in the density distribution. Given the force resolution (~ 300 pc), this should not be surprising given that the thin disc’s scale-height is more or less only one softening length in the MUGS and MaGICC runs. Here, we expand upon our initial work, but only concentrate on the vertical gradients 1–3 kpc from the mid-plane (our so-called thick disc stars), and how they vary as a function of galactocentric radius.

The primary observational constraint is provided by Carrell et al. (2012), in which a strong negative gradient was inferred, through the thick disc, near the solar neighbourhood (with a vertical metallicity gradient of ~ -0.10 to -0.15 dex kpc^{-1}); such a steep gradient is entirely consistent with that inferred earlier by Marsakov & Borkova (2005). Figure 2.6 shows this information (which is also listed in Table A.4 and detailed in Fig. A.3 for galaxy MaGICC–g15784) including our five simulations, the observational data from Carrell et al. (2012), and simulations from Rahimi et al. (2013) and P-DEVA galaxy. Both observations and simulations have used the same vertical range to identify thick disc stars: $1 < |z| < 3$ kpc.

The major conclusion to take from Fig. 2.6 is that the simulations undertaken with enhanced and/or more spatially-distributed feedback (MaGICC and 109-CH) each possess negative vertical metallicity gradients consistent with those observed in the solar neighbourhood of the Milky Way. A weak trend is also seen with galactocentric radius, the vertical gradients becoming shallower as one transitions from the inner to the outer disc. Conversely, the simulations with modest amounts of feedback (MUGS) show significantly flatter vertical gradients (at all galactocentric radii) than those observed in the Milky Way. We return to the underlying physics driving these trends in Section 2.4.

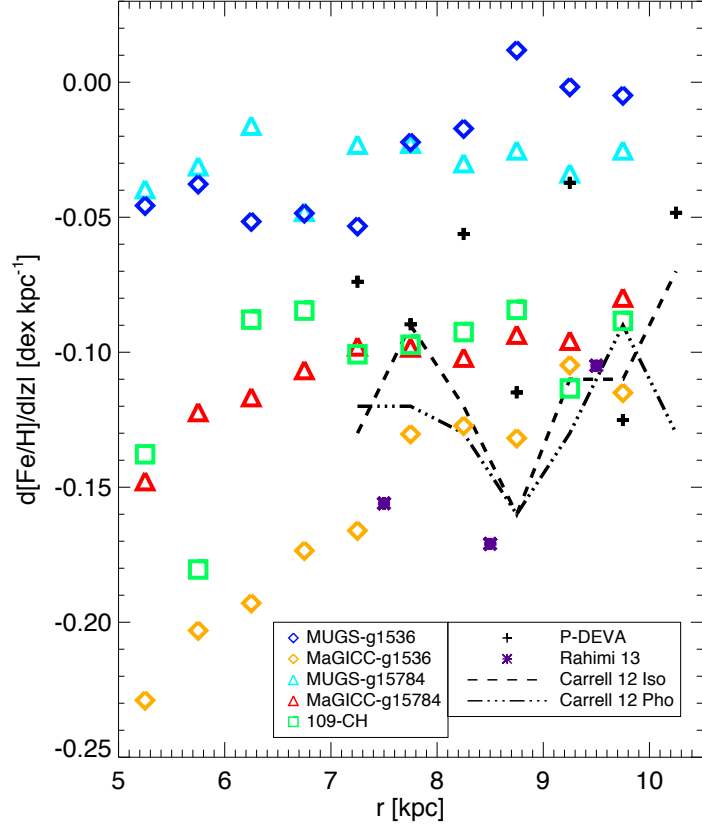


Figure 2.6: Vertical metallicity gradient as a function of radius. The figure includes data from our five simulations: two MUGS galaxies, the same two galaxies but with MaGICC feedback conditions and 109-CH. Observational data from Carrell et al. (2012) is shown with lines and results from the simulation in Rahimi et al. (2013) with purple asterisks. P-DEVA galaxy is indicated with black plus signs. All results are based upon stars selected from the vertical range $1 < |z| < 3$ kpc.

2.3.3 Rotational Velocity Gradients

Recent observations (e.g. Bovy & Tremaine 2012) have examined the kinematic properties of stars in the solar neighbourhood as a function of height above the mid-plane. For example, Moni Bidin et al. (2012) found vertical gradients in the rotational velocity component of $\sim -30 \text{ km s}^{-1} \text{ kpc}^{-1}$, in agreement with the work of Bond et al. (2010).

Figure 2.7 shows the rotational velocity V_ϕ as a function of height above the galactic plane for the analogous solar neighbourhoods of our suite of simulations. For each, this region was defined as an annulus spanning 7–10 kpc in galactocentric radius, and all stars assigned to the disc due to their kinematics were included in the derivation of the gradients. The change in radial range compared to the previous sections is done to make the comparison with observational results easier, as we have selected a range similar to theirs, but it should be noted that the results described here are not sensitive to the choice of the radial range. Four of the simulations (MUGS-g1536, MUGS-g15784, MaGICC-g1536 and 109-CH) all show vertical gradients of $dV_\phi/d|z| \simeq -10 \text{ km s}^{-1} \text{ kpc}^{-1}$. MaGICC-g15784 shows a much steeper vertical V_ϕ gradient of $\simeq -25 \text{ km s}^{-1} \text{ kpc}^{-1}$, more in line with the observational findings for the Milky Way from Girard et al. (2006), Bond et al. (2010) and Moni Bidin et al. (2012).

The galaxies MUGS-g1536, MaGICC-g1536 and 109-CH have a lower mass than the g15784 galaxies (Table 2.1). Even so, it is difficult to draw strong conclusions about the relation between the velocity gradient and mass, given the limited number of simulations in our sample. In addition, the effect of galaxy mass has not been well constrained observationally, due to limitations in resolving single stellar kinematics.

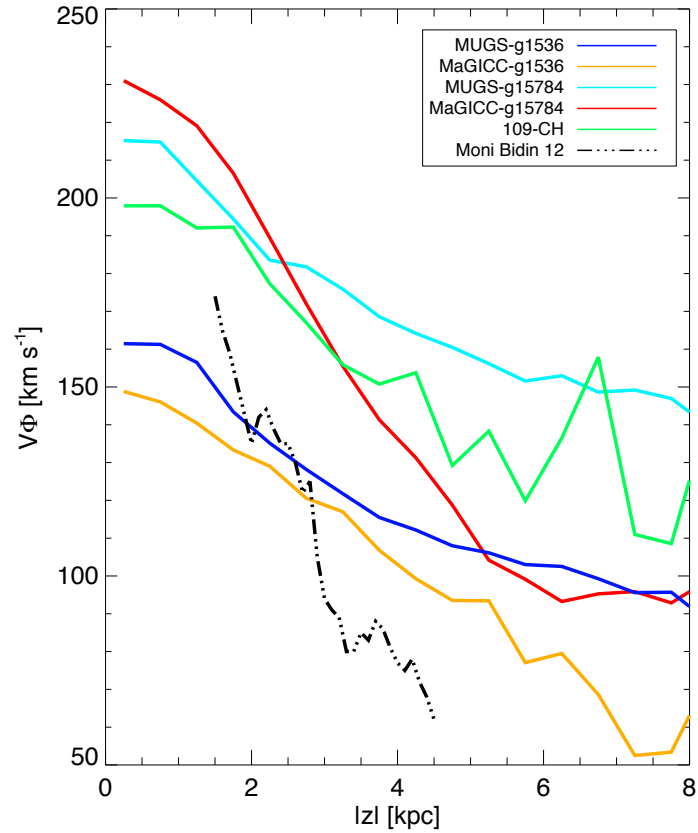


Figure 2.7: Rotational velocity of solar neighbourhood stars as a function of height above the plane. The four SPH simulations shown are MUGS-g1536 (blue line), MaGICC-g1536 (orange line), MUGS-g15784 (cyan line) and MaGICC-g15784 (red line), along with the AMR simulation 109-CH (green line). Observational results from Moni Bidin et al. (2012) are also included (black triple dot dashed line).

2.4 Discussion

Having shown the flattening of the radial metallicity gradient through the thick discs of our simulations, we now examine the mechanisms responsible for this behaviour. To do so, we concentrate on MaGICC-g15784, as its abundance and kinematic profiles are the best match to the Milky Way.

We examine the thick and thin disc stars separately following the $|z|$ division in Section 2.3, reminding the reader that, as we showed in Figs. 2.2 and 2.4, these two populations, when separated thusly, show opposite trends for the radial $[\text{Fe}/\text{H}]$ gradients. Furthermore, we sub-divide the disc into three radial bins – $7 < r < 8$ kpc, $10 < r < 11$ kpc, and $14 < r < 15$ kpc – in order to have a sample of stars which populate the extrema of our radial bin in Section 2.3 and to extend the conclusions to larger radii.

2.4.1 Distribution Functions

In Figs. 2.8, 2.9 and 2.10, we show the distribution functions of metallicity, age and formation radius for the stars associated with the aforementioned three radial bins, for two different vertical slices (corresponding to thick and thin discs).

The $[\text{Fe}/\text{H}]$ histograms in Fig. 2.8 are consistent with the radial metallicity gradients found in Fig. 2.2 (which were averaged at a given galactocentric radius). In Fig. 2.8, the top panel corresponds to the thick disc population while the bottom corresponds to the thin disc. The colour-coding in both panels represents the transition from inner disc (red), to middle (blue), to outer (green). The gradient in Fig. 2.2 has been determined from disc stars with galactocentric radii between 5–10 kpc. Beyond 10 kpc, the gradient actually starts to flatten. This is interesting because the chemically-defined thick disc more or less terminates at this radius, leaving a region defined by a single chemical component showing no significant radial metallicity gradient above the mid-plane. The thin disc, on the contrary, has a metallicity

gradient which extends out to the furthest measured radii.

On the other hand, negative age gradients for both the thick and thin discs exist, with no inversion encountered at higher scaleheights. This is illustrated in Fig. 2.9, with the thick disc in the top panel and the thin disc in the lower one.

The migration of stars from their birth location, whether via bar-/arm-driven resonances, churning, or kinematic heating/diffusion will act to flatten metallicity gradients (e.g. Loebman et al. 2011; Pilkington & Gibson 2012; Pilkington et al. 2012a; Kubryk et al. 2013). In our study, we do not separate between these different mechanisms, in part because we do not capture the physics of resonances correctly due to lack of resolution. Here, we use the term ‘radial migration’ to refer to the change between birth and present day radius, without specifying which mechanism is responsible for causing the change; the mechanism, while interesting, is not critical for the specific analysis here.

To quantify the influence on migrators versus non-migrators, we refer to Fig. 2.10, which shows the distribution of formation radii for stars in the thick (upper panel) and thin (lower panel) discs. Transition from the red line, to the blue, and finally to the green corresponds to moving outwards radially (note: the current radial position is also indicated by the vertical dashed lines in the same colours). We can see that the inner thick disc is dominated by migrated/diffused stars, but when moving outwards the in situ/locally-born population increases in relative importance. In the outermost bin (green line) one can define two different populations corresponding to each of the peaks in the distribution, where the inner peak would correspond to the migrators coming from the inner disc and the outer peak to the non-migrators/in situ population.

Referring to the bottom panel of Fig. 2.10, one can see that for the thin disc there are two different populations at all current radii (again, spanning current radii of 7–15 kpc). The in situ component is even more dominant, relatively speaking,

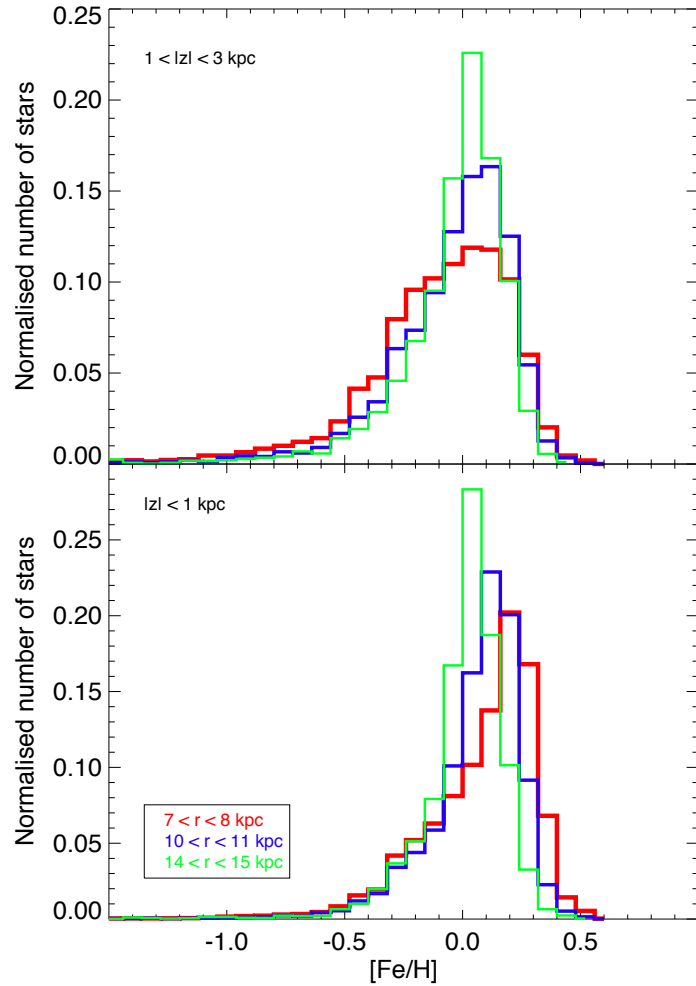


Figure 2.8: Metallicity distribution functions for the so-called thick disc population ($1 < |z| < 3$ kpc, upper panel) and thin disc population ($|z| < 1$ kpc, lower panel) associated with simulation MaGICC-g15784. Different colours correspond to different radial bins as indicated in the legend; when moving outwards we pass from red, to blue, to green.

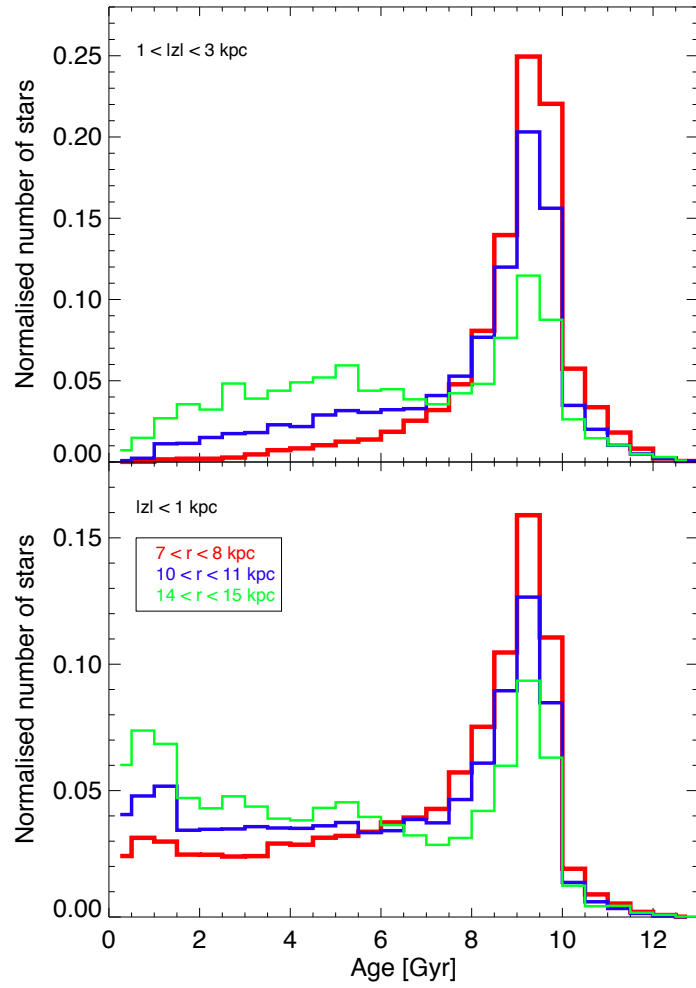


Figure 2.9: Distribution of the ages of the thin and thick discs, in the bottom and top panels, respectively. Colour-coding is the same as in Fig. 2.8 and is indicated in the inset as well.

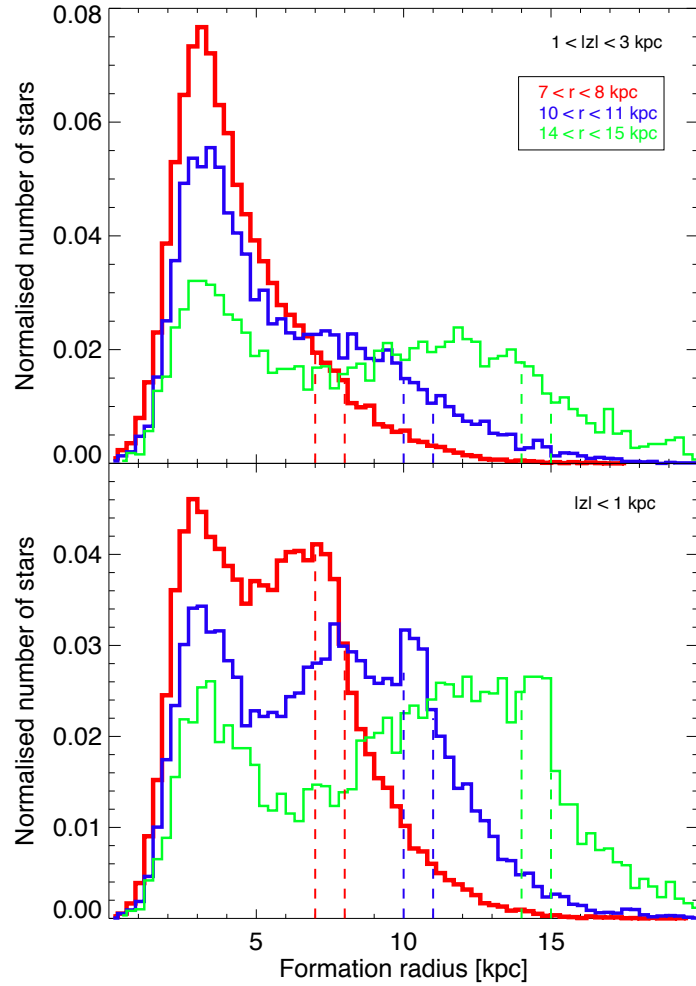


Figure 2.10: Distribution of the radii of formation for thick and thin disc populations selected by $|z|$, in the top and bottom panels, respectively. Colour-coding corresponds to different present-day radial bins, as per the legend and Fig. 2.8. The vertical dashed lines show that current position of the stars in the associated radial bin (as indicated by their colour).

than that seen for the thick disc (for each of the three radial bins), not surprisingly, given the inside-out growth of the thin disc.

2.4.2 Formation Radius

To explore the origin of the inverted metallicity gradients at high $|z|$, we build upon Fig. 2.10 and quantify the evolution of the stellar migration with time, metallicity and as a function of galactocentric radius. To relate this radial migration with the underlying metallicity gradients, in Fig. 2.11, we show the metallicity of the stars as a function of their formation radius for both thick (upper panels) and thin (lower panels) disc stars presently situated in the inner (left panels), middle (centre panels) and outer (right panels) disc of MaGICC-g15784; these present-day locations for said stars are denoted by the vertical dashed lines in each panel.

The solid lines in Fig. 2.11 reflect the mass-weighted radial $[\text{Fe}/\text{H}]$ gradients of the young stars (a proxy for the instantaneous gas-phase abundances), with each colour representing a different epoch (red = past; purple = present-day). These act to illustrate the time evolution of the abundance gradients (using all disc stars within $|z| < 3$ kpc and $5 < r < 15$ kpc). An earlier analogous version of this can be seen in figure 4 of Pilkington et al. (2012a), although in that case, they only examined MUGS-g15784 and Apollo (from the RaDES sample: Few et al. 2012b). The stronger feedback (with its enhanced redistribution of metals onto the largest scales) associated with the MaGICC galaxies (relative to MUGS or RaDES) acts to mitigate any significant evolution of the metallicity gradients, as identified by Gibson et al. (2013); we see that the slope of these lines in Fig. 2.11 does not change for different epochs in spite of the radial migration, as opposed to other studies.

What is readily apparent from Fig. 2.11 is that the ratio of so-called ‘in situ’ stars (those currently situated near to or within the vertical lines in each panel – i.e., those which have not moved significantly in a radial sense since birth) to those which have

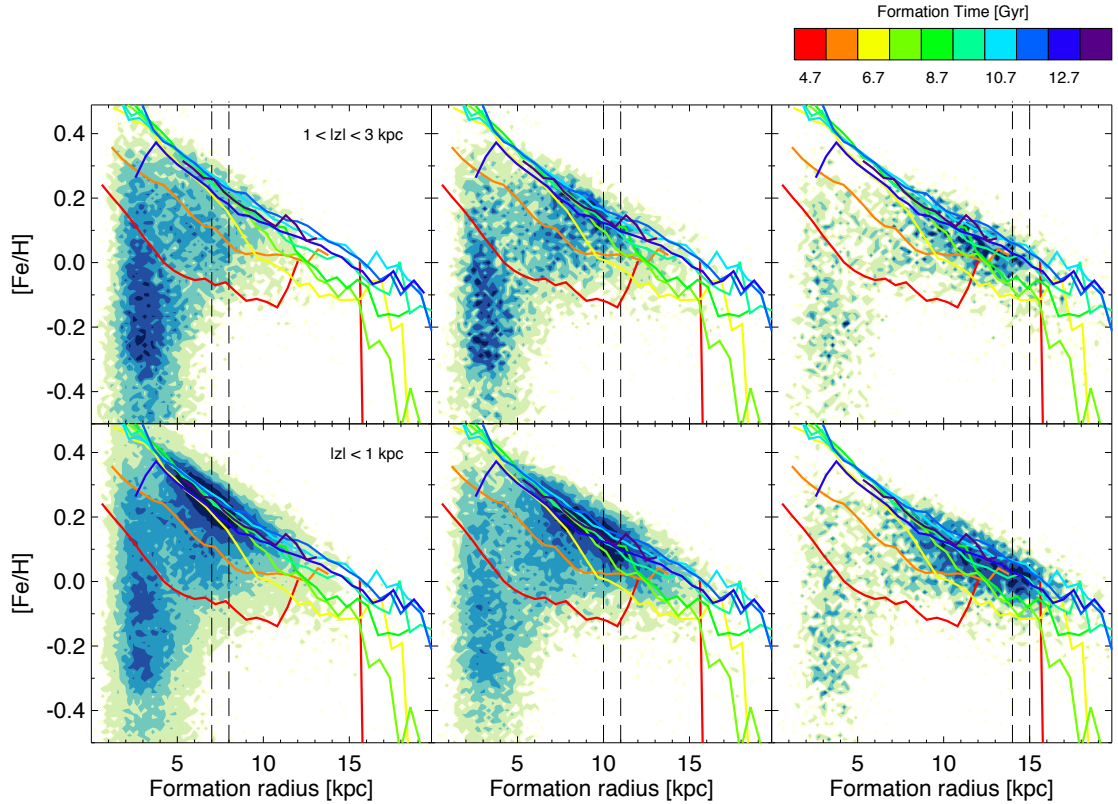


Figure 2.11: Density plots of the metallicity for the thick (upper row) and thin (lower row) discs in terms of the formation radius of the stars are shown alongside the evolution of the metallicity gradient with time (solid lines), for galaxy MaGICC-g15784. Stars have been selected according to our $|z|$ cut, as outlined in Section 2.3.1.1. The legend bar above the figure describes the difference in colour for the lines, which are the same in the six panels; each line indicates the behaviour of $[\text{Fe}/\text{H}]$ with the formation radius for new born stars, at different time steps. The density plots from left to right show the results for increasing current radii ranges, between $7 < r < 8$ kpc, $10 < r < 11$ kpc and $14 < r < 15$ kpc. The vertical dashed lines in each panel correspond to these radial bins.

migrated a significant distance (corresponding primarily, but not exclusively, to the density enhancement seen in each panel near ~ 3 kpc in formation radius) is higher in the outer regions for both the thick and thin discs. It is also readily apparent that the ‘in situ’ population within the thin disc dominates at each radial bin, today, as to be expected according to the inside-out disc growth.

Specifically, referring to the inner thick disc (upper left panel of Fig. 2.11), its membership is formed primarily near a galactocentric radius of ~ 3 kpc, $\gtrsim 10$ Gyr ago (inferred from the age distribution for the density peak near ~ 3 kpc), with metallicities $-0.3 \lesssim [\text{Fe}/\text{H}] \lesssim 0.0$. In contrast, the outer thick disc (upper right panel of Fig. 2.11) is also comprised of a tail of stars which formed nearby (in situ), $\sim 1\text{--}5$ Gyr ago, with metallicities $0.0 \lesssim [\text{Fe}/\text{H}] \lesssim +0.1$. Old stars are more centrally concentrated, which in turn is related to the disc inside-out formation.

In the thin disc, the situation is quite different. At all radii, the relatively metal-rich ‘in situ’ component formed over the previous $\sim 7\text{--}8$ Gyr dominates over any putative ‘migration’ component. That latter component exists at some level throughout the thin disc (which, for this simulation, is represented again by the density enhancement at relatively lower metallicities, originating near a galactocentric radius of ~ 3 kpc), but its contrast with respect to the ‘in situ’ component diminishes significantly with increasing radius. Unlike in the inner parts, the outermost region is quite similar for both thin and thick discs, which is telling us that thin disc stars can be found at high vertical distances; i.e. the disc of our simulated galaxy flares, consistent with Minchev et al. (2014).

We quantify the migration in Fig. 2.12, in which we compare the migration of stars drawn from each panel of Fig. 2.11. It is normalised to the average migration of each bin in the previously cited figure. Small values in the x -axis mean little travelling or migration. We can see that generally, in the three radial bins, thin disc stars have a greater ratio of in situ stars than those in the thick disc. Although this

quantity is very different when comparing the inner bin for the thick and thin discs (red and orange lines respectively), the difference reduces when moving to larger radial values, and finally, in our outermost radial bin the migration is quite similar for both discs (thick disc in green and thin disc in light green). Again, it is this ‘contrast’ that is the source of the inversion of the radial metallicity gradient in this simulation.

We make a consistency check and illustrate in Fig. 2.13 the same as in Fig. 2.11 but separating the stars by their chemistry. Here, the top row shows the thick disc according to the abundance cut made in Section 2.3.1.1 and the bottom row the thin disc. The trends and conclusions are the same as in Fig. 2.11: the outer thick disc is composed of (by mean) younger, more metal-rich stars than its inner counterpart, which pull the radial metallicity gradient up, and invert it. Once again, we state that our conclusions are robust to the thick disc selection criteria.

Minchev et al. (2015) suggested that thick discs result from the imbedded flares of mono-age stellar populations, which should always result in discs growing inside-out. Such flaring would naturally give rise to the inversion of chemical gradients with increasing distance from the disc mid-plane, as we find here. Therefore, our results may be generic, given the similarity of results with Minchev et al. (2015), in spite of the completely different simulation technique and chemical enrichment models employed.

Bringing together the different arguments from this section, we can summarise by saying that the negative radial metallicity gradient seen in the thin disc can be inferred directly from tracing the metallicity of the density peak of the in situ population (bottom row of Fig. 2.11); that population dominates at all radii and reflects the inside-out nature of disc growth. Conversely, the positive radial metallicity gradient seen in the thick disc is driven by a ‘contrast effect’ between the in situ and migrator populations; in moving from the inner thick disc, to the outer

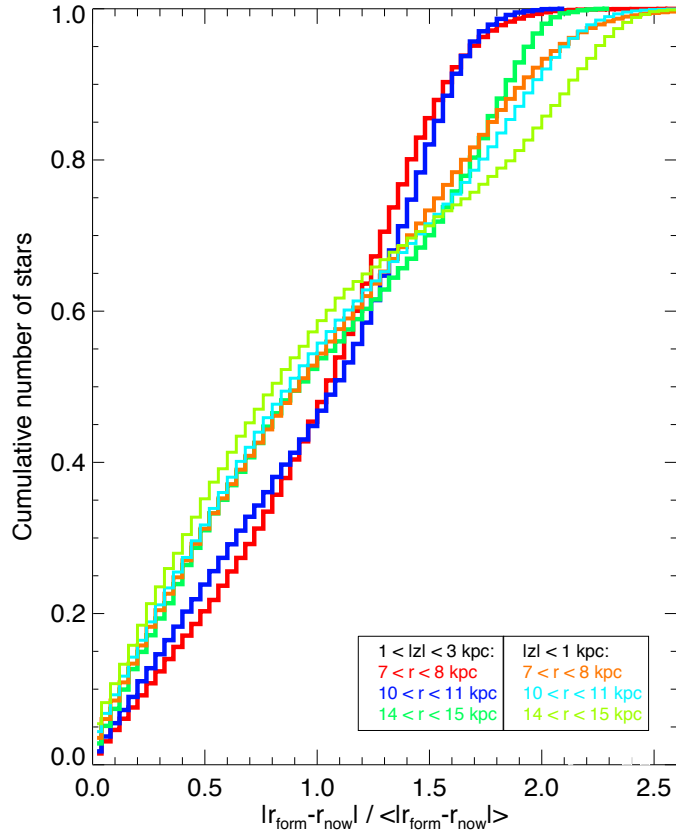


Figure 2.12: Cumulative distribution function of the distance travelled by each star normalised to the average migration. Each line indicates the migration corresponding to one of the panels in Fig. 2.11. Large values along the x -axis represent greater degrees of migration. Darker colours correspond to the thick disc: stars which are currently located in the range $7 < r < 8$ kpc are shown in red, the ones at $10 < r < 11$ kpc in blue, and the ones at $14 < r < 15$ kpc in green. Lighter colours match the same radial bin but in the thin disc, with orange corresponding to our innermost bin ($7 < r < 8$ kpc), cyan the medium bin ($10 < r < 11$ kpc), and light green the outermost one ($14 < r < 15$ kpc).

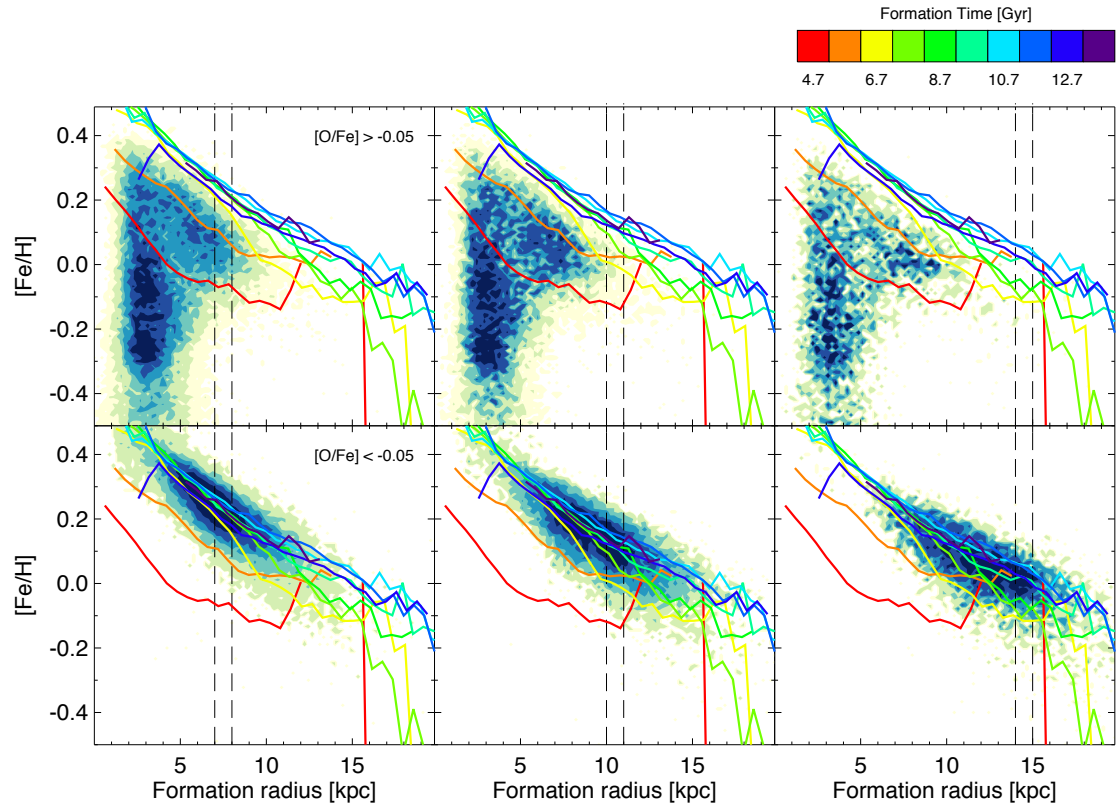


Figure 2.13: Same as Fig. 2.11, but separating stars by abundance instead of morphologically. In this case the top and bottom rows indicate the chemically defined thick and thin discs, respectively. The thin disc does not contain very old stars, as we saw in Fig. 2.3. On the contrary, the thick disc is missing new-born stars.

regions, the contribution from migrators drops dramatically, and the (relatively) more metal-rich in situ population gradually flattens and, in some cases, inverts the gradient. Consequently, it is the tail of younger, in situ stars (which is superimposed on a population of stars that have relocated from the centre) which shape the flattened/inverted gradients.

2.5 Summary

This work has analysed five simulations, two with lower feedback from the MUGS suite, the same two galaxies but with higher feedback from the MaGICC suite, and one with the new AMR code RAMSES-CH (109-CH). It complements the study of Stinson et al. (2013a), where they also looked at the formation of thin and thick discs, finding excellent agreement with observations from the Milky Way, when restricting the analysis to the examination of mono-abundance stellar populations.

We examine our suite of simulations in order to make an internal comparison between them and then judge the potential link to the Milky Way. Our simulations are slightly hotter, in a kinematic sense, than the Galaxy, thus we restrict the analysis simply to an identification of the similarity in trends. To expand upon the work presented in Pilkington et al. (2012a) and Gibson et al. (2013) (who considered only radial gradients, and only in the mid-plane of the disc) this analysis has focused on:

1. The change in the radial metallicity gradient with height above the galactic plane. We find that MaGICC and 109-CH simulations, which include increased feedback energy (mixing metals more efficiently) and distribution of the energy from supernovae on larger spatial scales, respectively, show better agreement with observations from the Milky Way and other simulations. When moving away from the plane of the disc, the gradient increases and becomes flatter in

all simulations, but only the MaGICC and 109-CH show it becoming inverted (it becomes positive, i.e. more metal-rich in the outskirts, relative to the inner parts of their respective discs, at $|z| \sim 1$ kpc). We define the thick disc population as the one with positive radial gradient ($1 < |z| < 3$ kpc) and thin disc the one with $|z| < 1$ kpc. We have chosen a spatial cut to separate thin and thick discs, as done observationally for extragalactic studies of thick discs (e.g. Yoachim & Dalcanton 2008; Comerón et al. 2016; Kasparova et al. 2016), and for many Milky Way studies (e.g. Hayden et al. 2015). That said, we have confirmed that the conclusions are not affected in a qualitative sense when applying a thick-thin disc discriminant based upon chemical arguments.

2. The change in the vertical metallicity gradient as a function of radius, for the morphologically selected thick disc stars. The vertical gradients in all five simulations analysed in this work show no dependence on radial distance from the galactic centre. The MaGICC and 109-CH simulations both present vertical gradients of $\simeq -0.12$ dex kpc^{-1} , which agrees very well with the observational results from Carrell et al. (2012). The MUGS galaxies exhibit shallower values. Observations of vertical gradients from Chen et al. (2011) and Kordopatis et al. (2013) both get vertical gradients in the thick disc with values $\simeq -0.2$ dex kpc^{-1} .
3. The change in the stellar rotational velocity at increasing $|z|$. One of our simulations (MaGICC-g15784) shows a vertical rotational velocity gradient in line with observations from Bond et al. (2010) and Moni Bidin et al. (2012) ($dV_\phi/d|z| \simeq -25$ km s^{-1} kpc^{-1}). The other four simulations illustrate much shallower velocity gradients.

We next focused on the simulated galaxy which best reproduces the observations of the Milky Way thick disc – MaGICC-g15784 – and made a detailed study of its

thin and thick disc stars (selected according to $|z|$) separately, at three different radial bins.

We analysed the distribution functions of $[\text{Fe}/\text{H}]$ and formation radius. The metallicity histograms clearly reflect the trends noted before: when moving outwards from the centre of the galaxy, the metallicity of the thin disc decreases but in the thick disc it increases. From the histograms of the formation radius of the stars, we conclude that there is a significant influence from stars which migrate from their original location during their lifetimes, both in the thin and thick discs. We do not separate the different mechanisms here, simply referring to this process as ‘migration’, without any pre-disposition as to whether it is systematic ‘churning’ or a more random ‘diffusion’.

To get a better understanding of the situation, in Fig. 2.11 we examined the relation between star formation history (by the time evolution of the metallicity gradients) and migration. This figure illustrates the situation for the thick and thin discs separately, for three radial bins. In the thick disc (top row), we see that from the left, to the middle and to the right panels, the centroid of the distribution moves from a very old low metallicity population to intermediate age metal-rich stars, making the metallicity gradient positive. In the thin disc (bottom row) the young population of in situ, metal-rich stars dominates at small radii (left panel), increasing the mean metallicity and making the gradient negative.

The greatest difference between the two discs when referring to migration is that in the thin disc the ratio of in situ stars to migrators is higher than in the thick disc. The contribution of the in situ stars is what makes the radial metallicity gradient invert in MaGICC–g15784. The migrators erase all the trends because they form a larger population than the non-migrators (flattening the gradients in the outer galaxy), but still the in situ population is what inverts the gradients in the thick disc. In other words, as shown in Fig. 2.12, the thin disc has a big influence on in situ

stars. The (spatially defined) outer thick disc has, as well, although these are also thin disc stars flaring upwards, which makes the thin and thick discs similar in terms of migration at our outermost radial bin. The innermost radial bin, however, is very different for each of the two disc components: the in situ peak which dominates in the thin disc is missing for the thick one.

Figure 2.13 proves that our conclusions do not depend on the thick disc selection criteria. Both chemically and morphologically selected thick discs appear to have a positive radial metallicity gradient. Stars move radially and there is a frosting of in situ star formation, with the latter dominating the further out in radius we go. Following the centroid of the points in the bottom row of any of these two figures one can confirm that the gradient is negative in the thin disc; similarly, following the centroid in the upper row it flattens and inverts. The difference between Fig. 2.11 and Fig. 2.13 lies in the presence, or lack thereof, of a tail of younger stars when doing the spatial cut.

Our simulations are somewhat kinematically hot, relative to the Milky Way (concluded from the proportion of stars which have migrated). From Fig. 2.11 we can make predictions concerning what might have happened had there been little or no migration (i.e., had the simulations been kinematically colder). In that case, the metallicity gradient would only be set by the temporal evolution of metallicity. In Fig. 2.11, stars would only ‘travel’ vertically as they would not change their radius. With a metallicity evolution such as that seen for MaGICC-g15784, the results would change quantitatively but not qualitatively; we would still see an inverted gradient in the thick disc and our conclusions would still be entirely valid. Put another way, the reason for the inversion of the metallicity gradient in our simulations is not stellar migration, but is driven by the stars that remain close to the radius at which they were born (the in situ population).

According to our simulations, to reproduce the effects observed in the Galaxy

we need to combine the high feedback employed in MaGICC and the contribution of the stars in the outer thick disc which have not migrated far from their birth location.

Our goal here has not been to undertake an internal comparison between different simulations, run with different codes and methodologies. Instead, we have aimed to provide a qualitative comparison of a broad suite of such simulations with the trends seen in the Milky Way, identify where the similarities lie, and then isolate the reasons for those similarities. The robustness of our conclusions are encouraging; larger and more precise datasets from Gaia, APOGEE, GALAH, WEAVE, 4MOST, etc, will prove invaluable in better constraining the underlying physical mechanisms we now believe responsible for the inverted gradients apparently intrinsic to the thick disc.

Chapter 3

THE STELLAR POPULATIONS IN THE THICK DISC

Abstract

Making use of six edge-on disc galaxies from the CALIFA sample, we aim to study their vertical structure and get new conclusions about the thick disc formation in galaxies. Our suite spreads from Sa to Sbc in type and includes a diversity of masses. We decompose the CALIFA cubes into slits parallel to the mid-plane of the systems, mimicking the results of long-slit spectroscopy, and make radial bins in each slit. Then we collect relevant information about ages, metallicities and line-of-sight velocities at the radial bins. This makes us able to have a complete study of the characteristics of our galaxy set. All our galaxies suffer velocity lag with increasing height, suggesting the existence of a thick disc in all of them. In addition, we find that the age and metallicity gradients exhibit a variety of trends, both increasing and decreasing when moving to larger radii. Thus, we discard the option of a single formation scenario for the thick disc, opposed to what simulations predict. We believe that

the evolution is complex and various scenarios take part in it.

3.1 Introduction

Even though there has been a great advance in cosmological simulations and astronomical instrumentation, the formation and evolution of galaxies is still one of the outstanding problems in astrophysics. The distribution of the stars in galaxies can help us answer some of the common questions in contemporary galactic astronomy. Special attention has been paid to the thick disc of spiral galaxies, as it contains fossil information about the early stages of disc formation. For more details about the thick disc see Section 1.4.

Kinematic analysis plays a significant role in disentangling the disc formation and thick disc existence. Over the past few years rotation curves for several external massive galaxies have been measured (Yoachim & Dalcanton 2008; Comerón et al. 2015; Guérou et al. 2016; Comerón et al. 2016; Kasparova et al. 2016), all of them showing a prograde thick disc rotation curve with a lag of a few kilometres per second with respect to the thin disc. Our own Milky Way has a prograde thick disc as well (Chiba & Beers 2000). In low-mass galaxies (defined by Yoachim & Dalcanton 2008 as the ones with $V_c < 120 \text{ km s}^{-1}$), rotation curves are more diverse: there are cases with an important lag, others show little net rotation lag and there is even a case of a counter-rotating thick disc (the thick disc rotates in the opposite direction to the thin disc, see Yoachim & Dalcanton 2005, 2008). If retrograde rotation is confirmed for a larger sample of galaxies, this will support an external origin for the stars in it, and will discard scenarios where the thick disc formed through kinematical heating of the thin disc.

Early type spirals usually have a more prominent dustlane along their mid-plane when comparing to later types, complicating the exploration of the thin disc near

the plane. Dalcanton et al. (2004) found that galaxies with maximum rotation velocities larger than 120 km s^{-1} have well-defined dustlanes, while in those with slower rotation the dust distribution is much more diffuse. They suggested that dustlanes are related to fragmentation of the gas component during a collapse, which happens due to gravitational instabilities in the disc that suffer galaxies with rotation speed above 120 km s^{-1} . Then it is easier to compare thin and thick disc characteristics in later type galaxies.

Metallicity gradients within the Milky Way have been studied since Shaver et al. (1983) realised that metals were not homogeneously distributed. In the thin disc of the Milky Way, radial metallicity gradients are negative, but when moving away from the mid-plane into the thick disc they flatten (e.g. Cheng et al. 2012b) and eventually invert (e.g. Carrell et al. 2012; Anders et al. 2014; Xiang et al. 2015). Such inversions in the radial metallicity gradient have also been found in the simulations of Rahimi et al. (2013), Minchev et al. (2015) and Miranda et al. (2016). For further details see Chapter 2. This has not been extensively examined in external galaxies yet and it is the aim of our work.

In addition, age gradients in the Milky Way have also been studied. Martig et al. (2016), when looking at giant stars from the APOGEE survey, find that the geometrically defined thick disc (stars higher than 1 kpc from the mid-plane, Jurić et al. 2008) in the Milky Way has a strong negative radial age gradient. This happens both in the thin and thick disc, in the latter being possibly due to the flaring of younger stars upward in the plane (Minchev et al. 2014). Such a result has also been found in simulations by Minchev et al. (2015) and Miranda et al. (2016). It implies that the inner parts of the geometrical thick disc (selection of the thin and thick discs just by position with respect to the plane) might have formed at high redshift, in a violent phase, whereas the outer parts are younger and were built later, possibly through flaring of thin disc populations.

In the Milky Way, the thick disc can be defined through a criterion in kinematics, geometrics, ages or abundances. Unfortunately, that detailed portrait cannot be obtained in external galaxies. As a result of observational difficulties, so far it is not possible to resolve the majority of external galaxies into individual stars. Instead, we study the mean values of ages and metallicities from integrated spectra (e.g. Sánchez-Blázquez et al. 2011; González Delgado et al. 2015). Although this type of studies is very common in elliptical galaxies, only recently has it become more popular in disc galaxies. Thick discs in these galaxies can only be examined geometrically, making the sample limited to edge-on galaxies and looking at the greatest heights enabled by the quality of the data. Even so we cannot completely separate thin and thick discs geometrically. We will always have the influence of both stellar components, though at greater heights the thick disc flux will dominate, and the mid-plane will be composed mostly by thin disc stars.

Nowadays only a few studies have been able to analyse the thick discs of external galaxies. An example of it is the work by Kasparova et al. (2016), who study three S0 galaxies and find very moderate (or flat) radial metallicity gradients in both the thin and thick disc, without significant difference with each other. Comerón et al. (2016) focus their analysis in the kinematics of an edge-on S0 galaxy. They visualise the ages and metallicities at two heights, one in the thick and the other in the thin disc. Another study in this field is completed by Yoachim & Dalcanton (2008), who take conclusions about the thick disc formation through a sample of nine edge-on disc galaxies with a slit in the mid-plane and another off-plane.

In this work we go one step further. We are interested in the vertical structure of external disc galaxies, and study the stellar populations and kinematics. We limit ourselves to a set of edge-on galaxies from the CALIFA survey (Sánchez et al. 2012a,b), expanding a range in morphological types and masses. Comparing to the studies previously mentioned, we have more slits (~ 7 slits per galaxy, depending on

the resolution of each system), which allows us to look at trends and gradients with height. This represents a challenge due to the typical low surface brightness of thick discs.

For this work we assume a flat Λ CDM cosmology with a Hubble constant of $H_0 = 70.2 \text{ km s}^{-1} \text{ Mpc}^{-1}$, $\Omega_\Lambda = 0.728$ and $\Omega_m = 1 - \Omega_\Lambda = 0.272$, consistent with observations from Planck Collaboration (2014).

3.2 Sample

The data used in the present study is taken from the CALIFA survey (Calar Alto Legacy Integral Field Area, Sánchez et al. 2012a,b). The survey observed a statistically well defined sample of ~ 600 galaxies in the local Universe, using 250 observing nights with PMAS/PPAK integral field spectrophotometer mounted at the Calar Alto 3.5 m telescope. The targets are randomly selected from the mother sample, which includes 939 galaxies from the SDSS DR7 (Abazajian et al. 2009). Some of the criteria for target selection are a redshift range of $0.005 < z < 0.03$, a latitude restriction to exclude the Galactic plane ($|b| > 20^\circ$), a flux limit of $PetroMag_r < 20$ and a declination limit of $\delta > 7^\circ$. Satisfying these selection criteria, the ~ 600 objects constitute a representative sample covering a wide range in galactic properties such as morphological types, luminosities, stellar masses and colours, with the advantage that a volume correction can be done to it. We refer to Sánchez et al. (2012a,b) for further specifications.

The spectra cover the range $3700 - 7000 \text{ \AA}$ in two overlapping setups, one in the red ($4300 - 7000 \text{ \AA}$) at a spectral resolution of $R = 850$ (V500 setup) and one in the blue ($3700 - 5000 \text{ \AA}$) at $R \sim 1650$ (V1200 setup), where the resolutions quoted are those at the overlapping wavelength range ($\lambda \sim 4500 \text{ \AA}$). In this work we use a combined version of the data (the COMBO) obtained by degrading the spectral resolution of the blue part of the spectra to match the resolution of the red using a

Galaxy	Type	Inclination	PA	z	r_l	r_{disc}	V_{LOS}	V_{lag}	B -mag
IC0540	Sab	90.0	170.8	0.007	1.44	0.24	118	35	14.70
IC5376	Sab	90.0	4.0	0.018	1.91	0.74	192	42	14.75
NGC0781	Sa	90.0	12.2	0.012	1.43	0.59	174	26	13.93
NGC0955	Sab	81.5	19.6	0.005	1.15	0.32	145	45	12.92
UGC04197	Sb	90.0	131.1	0.015	3.98	0.07	182	22	14.53
UGC08267	Sbc	84.7	40.5	0.025	5.96	0.00	166	15	15.39

Table 3.1: Primary characteristics of the galaxies analysed in this work. Information for each column: 1. Galaxy name within CALIFA; 2. Morphological type; 3. Inclination (degree); 4. Position angle (degree); 5. Redshift; 6. Scalelength (kpc); 7. Radius at which the bulge corresponds to 30% of the light and the disc to 70% (kpc); 8. Maximum of the line-of-sight velocity (km s^{-1}); 9. Line-of-sight velocity lag when moving 1 kpc in height ($\text{km s}^{-1} \text{kpc}^{-1}$); 10. Total B -magnitude (magnitude). Some of the values have been calculated by ourselves and others taken from HyperLeda (Makarov et al. 2014) or CALIFA databases.

wavelength-dependent Gaussian smoothing kernel.

The data reduction is explained in detail in Sánchez et al. (2012a) and Husemann et al. (2013). The basic tasks include cosmic ray rejection, optimal extraction, flexure correction, wavelength and flux calibration and sky subtraction. Then the final data cube is reconstructed, with a one arcsec spatial sampling. The two-dimensional spectral maps obtained for the sample are aimed to address fundamental issues in galaxy evolution.

For this work we have selected six disc galaxies from the CALIFA sample. We worked with DR2 and selected all edge-on (inclination $> 80^\circ$), spiral galaxies. After discarding the ones with very low quality, we had 11 galaxies left. Some of them had to be excluded afterwards due to low S/N (< 13) of the individual spaxels or because there were not enough radial bins with high S/N to measure the gradient, reducing the sample to six: IC0540, IC5376, NGC0781, NGC0955, UGC04197 and UGC08267. They form a suite of spiral galaxies with morphological types ranging from Sa to Sbc, all without signs of recent interactions and with an inclination $\sim 90^\circ$. We are only interested in edge-on galaxies because we want to analyse the vertical structure of the discs. The principal properties of the galaxies in our sample are summarised in Table 3.1.

3.3 Analysis

3.3.1 Bulge-disc division

We have a variety of galaxy types, ranging from Sa to Sbc, and some of them possess a considerable bulge. In this study we are only interested in the disc region of the galaxies; thus we need to get rid of the bulge. In order to do so, we take the SDSS r -band images of the six galaxies in our sample and, making use of the `iraf` task `ellipse`, we get the one-dimensional surface brightness profiles. In the region

dominated by the disc, the curve can be fitted by a pure exponential profile, using the classical formulae:

$$I = I_0 \exp[-(r/r_l)], \quad (3.1)$$

where r_l is the scalelength of the disc and I_0 the intensity at the centre. We fit that exponential to the external part of our profiles and take the exceeding flux above it in the central region as the contribution from the bulge. We define our bulge-disc separation at the radius where 30% of the light comes from the bulge and 70% from the disc, and we call that radius r_{disc} . We consider that it is the extent of the bulge in the mid-plane. We assume that the bulge has a spheroidal form and, therefore, its contribution decreases with the distance from the plane, having some slits which do not contain any part of it. An example of the decomposition is presented in Fig. 3.1, which shows the surface brightness profile for galaxy IC5376. For this galaxy, $r_{\text{disc}} = 0.74$ kpc. In the following analysis, we will only consider the stellar populations beyond that point, discarding the ones closer to the centre of the galaxy. We use the same exponential fit to calculate the scalelength of the disc, r_l . For galaxy IC5376, the value obtained is $r_l = 1.91$ kpc. The scalelengths and r_{disc} for the rest of the galaxies are summarised in Table 3.1, and the rest of surface brightness profiles are shown in Appendix B.

3.3.2 Extraction of the spectra

In order to analyse the stellar population gradients of the different disc components in our CALIFA sample, we extract spectra radially in apertures simulating long-slits and placed parallel to the plane at different heights (see Fig. 3.2).

For this purpose we make use of `PINGSOFT` (Rosales-Ortega 2011). The `PINGSOFT` software is a suite of IDL routines made to improve the visualisation, manipulation and analysis of integral field spectroscopy data. We adapted the original routine

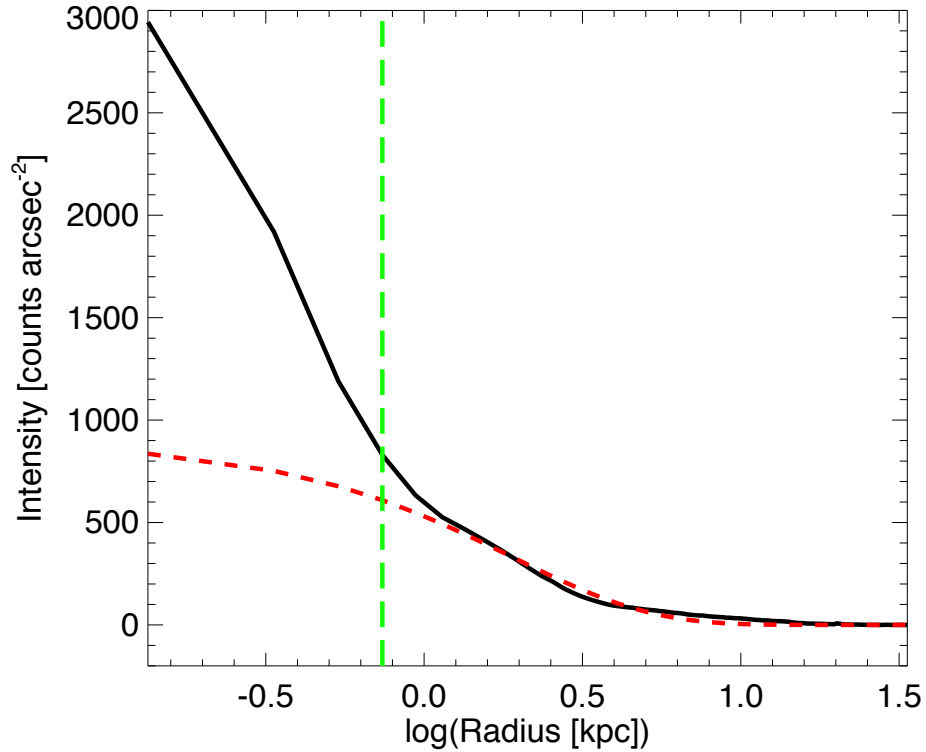


Figure 3.1: Radial surface brightness profile for one of the galaxies in our sample, IC5376, represented by the black line. The red short-dashed line is the exponential fit to the disc considering the radial range 1 – 30 kpc (0.0 – 1.5 dex in the logarithmic scale). The excess of light at low radii comes from the bulge. Following our criteria, the disc starts at the radius where the bulge constitutes 30% of the light ($r_{\text{disc}} = 0.74$ kpc for this galaxy, expressed in a logarithmic scale in the figure). This point is marked with the vertical green long-dashed line. We exhibit the x -axis in a logarithmic scale to have a better viewing of the area of interest, which is the cut between the dominance of the bulge and the disc.

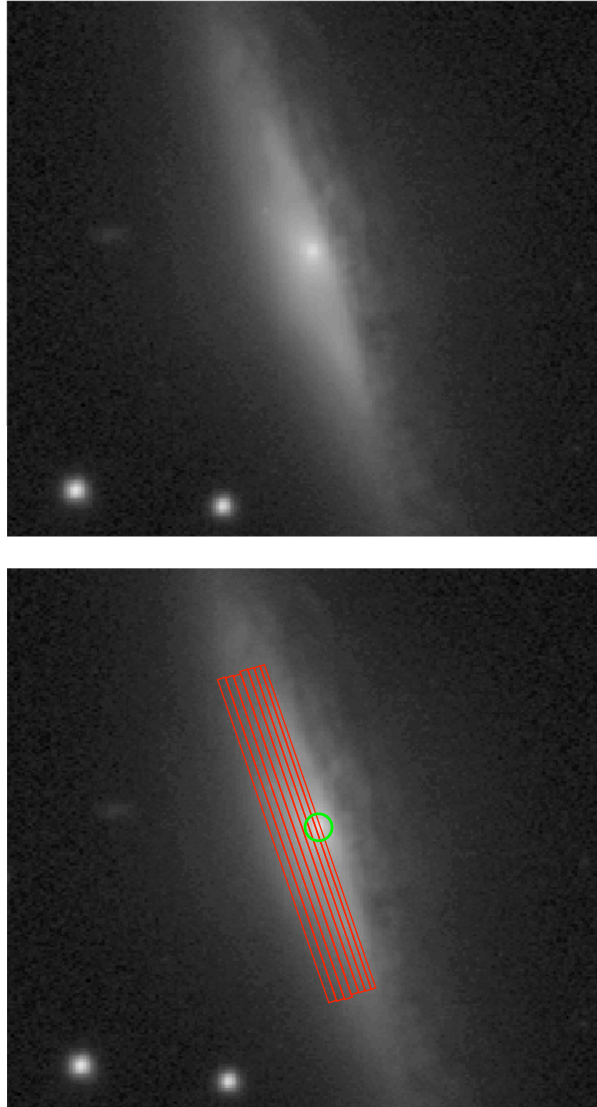


Figure 3.2: Reproduction of the slits we study in galaxy NGC0955. In the top panel we show the image of the galaxy from SDSS r -band and in the bottom one we overplot the slits as red rectangles. The green circle is the bulge, removed for the analysis.

which creates slits of a desired centre, height, length and position angle, to include as additional inputs the minimum S/N of the radial bins and the central wavelength and width of the band at which the S/N will be calculated. In the preprocessing steps we also mask the foreground and background sources and bad pixels.

Each slit covers the whole length of the galaxy and a thin layer in height (these range between 1 and 2 arcsec in height, depending on the S/N of the area). The galaxies contain ~ 7 slits in total distributed along the central heights, starting from the mid-plane and extending above and below it. The slits are then divided in radial bins with a required minimum $S/N \sim 22$ (this varies between $S/N > 25$ and $S/N > 20$ depending on the mean S/N of each galaxy).

An example of the slits overlapped in one of our galaxies (NGC0955) is shown in Fig. 3.2. The top panel is the r -band image of the galaxy from SDSS and the bottom panel includes the slits as calculated with PINGSoft (red rectangles) and the bulge to be removed (green circle). This galaxy has a dust lane, which makes us discard that side of the galaxy due to data being blurred. The side of the galaxy under study is the one including the slits.

3.3.3 Cleaning from emission

Studying the stellar populations of disc galaxies has always been a challenge. The difficulty stems from the fact that emission lines coming from star forming regions can fill the absorption lines used for stellar population analysis and, therefore, they need to be cleaned before. The development of software that allows the fitting of absorption and emission lines at the same time has helped solving the problem.

Here we use GANDALF (Sarzi et al. 2006) to perform this task in our radially binned spectra. GANDALF fits absorption and emission lines simultaneously, treating the latter as additional Gaussians. In the initial step, emission lines are masked and the absorption line spectrum is fitted with the Penalized Pixel-Fitting method, pPXF

(Cappellari & Emsellem 2004), using as templates the stellar population models of Vazdekis et al. (2010) based on the MILES stellar library (Sánchez-Blázquez et al. 2006; Cenarro et al. 2007; Falcón-Barroso et al. 2011)¹. In this stage, radial velocities and velocity dispersions are estimated for the stellar component. GANDALF then employs the best values of the velocity and velocity dispersion and the best template mix as initial values for the obtention of emission lines. In the second step, emission line equivalent widths, radial velocities and velocity dispersions are extracted for the gaseous component. For our analysis we subtract the emission line spectra from the observed spectra at each radius. For further specifications about GANDALF we refer the reader to Sarzi et al. (2006).

3.3.4 Obtaining ages and metallicities

The integrated light spectrum of disc galaxies contains the contribution of several generations of stars. Lately, numerical techniques have been developed to derive the star formation history with time basing the analysis on the information taken from spectra (Heavens et al. 2000; Cid Fernandes et al. 2005; Tojeiro et al. 2007; Koleva et al. 2009).

An example of these codes, and the one we have applied to the emission line-cleaned spectra in this work, is STECKMAP (STellar Content and Kinematics via Maximum A Posteriori likelihood, Ocvirk et al. 2006b,a)². It is a bayesian method for interpreting galaxy spectra in terms of their stellar populations. It projects the spectrum onto a temporal sequence of models of single stellar populations and determines the linear combination of these models that fits the observed spectrum best (via a penalised χ^2). The stellar content of the population will be fixed by the weights of the various components of this linear combination. As templates, we use the stellar population models by Vazdekis et al. (2010) based on the MILES library

¹The stellar population models and library are publicly available at <http://miles.iac.es>

²STECKMAP software package is public and can be obtained at <http://astro.u-strasbg.fr/~ocvirk/>

(Sánchez-Blázquez et al. 2006).

STECKMAP has been extensively tested and used in a variety of applications (e.g. Sharina & Davoust 2009; Pappalardo et al. 2010; Sánchez-Blázquez et al. 2011; Sánchez-Blázquez et al. 2014). The method is not parametric and does not make any a priori assumption regarding the shape of the star formation history. The only condition that STECKMAP imposes is that the different unknowns, namely the stellar age distribution, the age-metallicity relation and the line-of-sight velocity distributions or the broadening function have to be smooth in order to avoid extreme oscillating solutions that are not robust and most likely unphysical. The function to minimise is defined as

$$Q_\mu = \chi^2(s(x, Z, g)) + P_\mu(x, Z, g), \quad (3.2)$$

where s is the modelled spectrum resulting from the age distribution x , the age-metallicity relation Z and the broadening function g . The penalisation P_μ can be written as $P_\mu(x, Z, g) = \mu_x P(x) + \mu_Z P(Z) + \mu_v P(g)$, where the function P gives high values for solutions with strong oscillations (i.e. a rapid variation of the metallicity with age or a noisy broadening function) and small values for smoothly varying solutions. Adding the penalisation P to the function Q is equivalent to injecting an a priori probability density to the solution as $f_{prior}(x) = \exp(-\mu_x P(x))$. See Ocvirk et al. (2006a) for more details.

In this work we have not fitted simultaneously the star formation histories and the kinematics, but took the solution for kinematics obtained with pPXF when doing the correction from emission lines (see Section 3.3.3). The reason is that the existing degeneracy between metallicity and velocity dispersion (Koleva et al. 2008) biases the mean-weighted metallicities if both parameters are fitted at the same time. In Sánchez-Blázquez et al. (2011), they compare the age-metallicity degeneracy obtained by STECKMAP and other two widely used techniques, and prove that

the former is the one that reduces it more.

STECKMAP gives as output the stellar age distribution (the contribution in flux of each age component to the observed spectrum), the age-metallicity relation (the metallicity of each age component, with the metallicity of the Sun being 0.02 in these models), the stellar mass as a function of age (the mass that the given component had at the time of its birth) and the star formation rate as a function of lookback time. From these, various integrated quantities can be obtained. In this work, the ones that we are interested in are the mass- and luminosity-weighted age and metallicity:

$$\langle \log q \rangle_{\text{MW}} = \frac{\sum_i \text{mass}(i) \log(q_i)}{\sum_i \text{mass}(i)}, \quad (3.3)$$

$$\langle \log q \rangle_{\text{LW}} = \frac{\sum_i \text{flux}(i) \log(q_i)}{\sum_i \text{flux}(i)}, \quad (3.4)$$

where q is the physical parameter we want to obtain (age or metallicity), and $\text{mass}(i)$ and $\text{flux}(i)$ are, respectively, the reconstructed mass and flux contributions of the stars in the i th age bin, as returned by STECKMAP. We have chosen to weight our ages and metallicities in a base-10 logarithmic scale because these values are more similar to the SSP-equivalent parameters, as showed by Sánchez-Blázquez et al. (2011)³. Young stars are very luminous in the optical range, and thus they contribute more to the light-weighted values making them lower than the SSP-equivalent ones (the same trend is observed for metallicities). This means that the light-weighted values of age will be strongly biased towards the ages of the youngest stellar components. The mass-weighted values will be less biased towards the age and metallicity of the youngest components but they are also more uncertain. This is because galaxies are dominated in mass by an old stellar population, independently of the radius. These old stars are not very luminous and, therefore, their contribution to the

³The average values of ages and metallicities can change considerably if we added them linearly

observed spectrum is low. For this reason, mass-weighted ages are always higher than the SSP-equivalent ones. The mass-weighted metallicity, however, follows a similar trend to that of the luminosity-weighted one and, in the same way, agrees with the SSP-equivalent one for high-metallicity values.

3.4 Results

We use the values calculated in the previous sections to obtain valuable trends for our galaxy set. Combining all the results we will give some hints about the formation and evolution of spiral galaxies.

3.4.1 Age gradient

We start analysing how the age of the populations changes when moving from the central part of the disc to larger radii. Figures 3.3 and 3.4 illustrate the trends for our six galaxies, each of them in one row, when the logarithm of age has been weighted by light. We present the behaviours at two heights (the results for the rest of the slits are presented in Appendix B): the panels on the left column exhibit the results for slits close to the mid-plane and on the right the ones for greater heights, representative of the thin and thick discs, respectively. In those figures, the radius is expressed in units of kpc and scalelength. The black diamonds are the ages calculated with `STECKMAP`. The central black vertical dotted line indicates the centre of the galaxy. The blue vertical dashed lines at each side represent the bulge (which, as explained in Section 3.3.1, has been discarded in our work).

Three of our galaxies show a significant change of (both metallicity and age) trend at certain radius. We are interested in fitting gradients and therefore we need linear trends. The most important area for our study is the inner disc, thus, we discard the outer disc (all radial bins with larger radii than the outermost dotted vertical

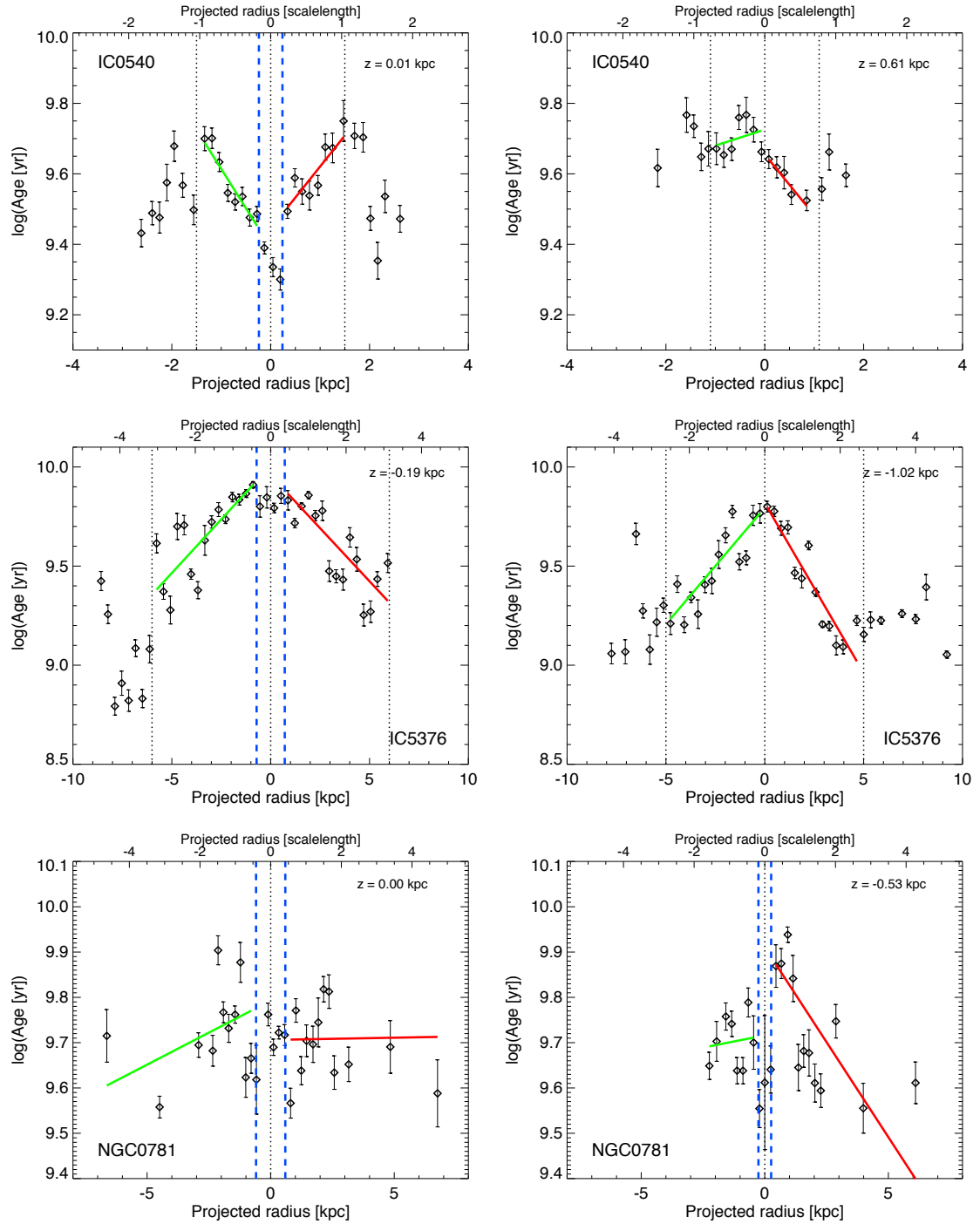


Figure 3.3: Age in terms of radius for populations in our galaxy set, showing galaxies IC0540, IC5376 and NGC0781 from top to bottom. On the left we show the trends for the slits in the mid-plane and on the right for higher slits. The black diamonds are the data. We colour the linear fits at each side of the centre with green and red solid lines.

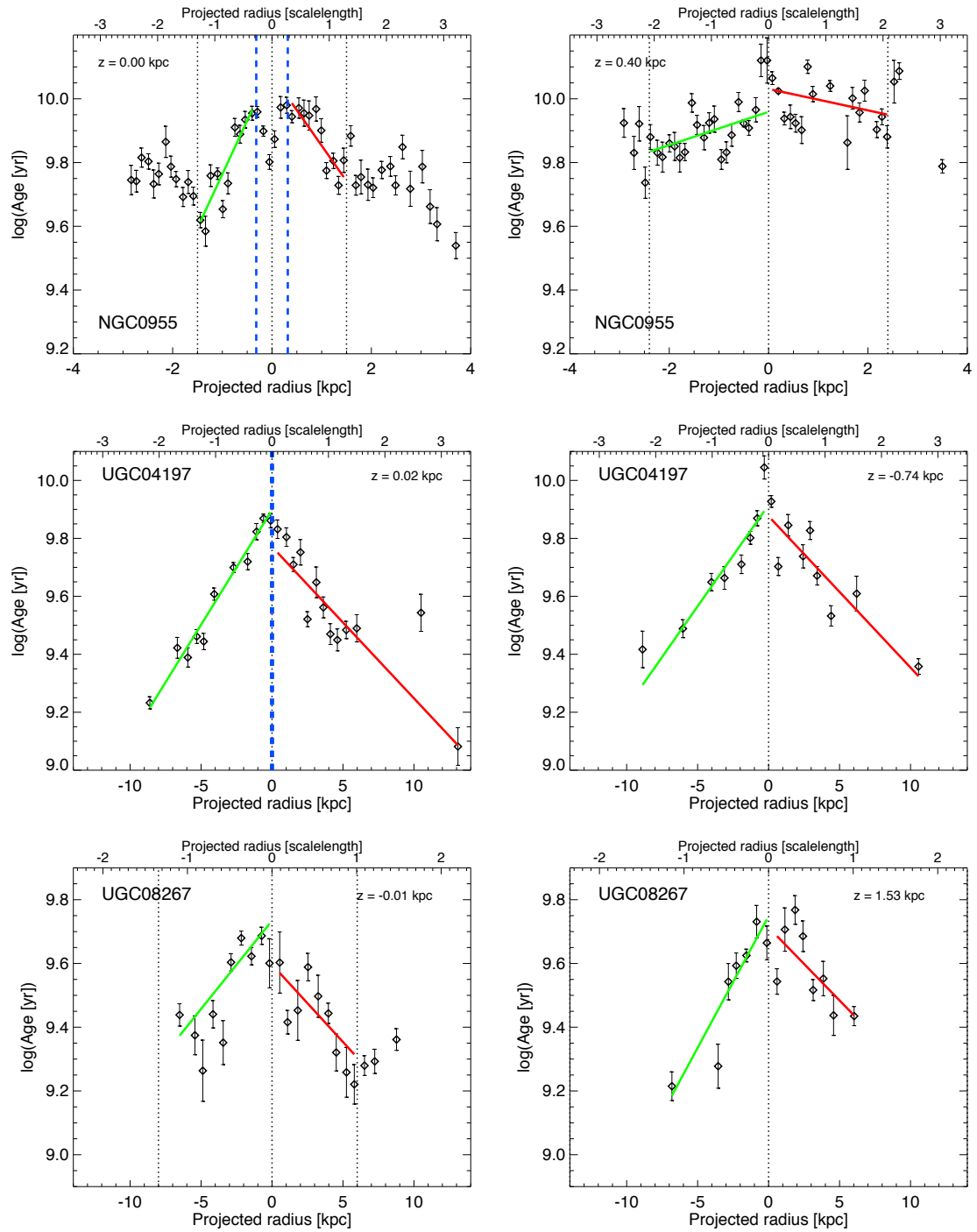


Figure 3.4: Same as Fig 3.3 (age against radius) but for the rest of galaxies in our sample, NGC0955, UGC04197 and UGC08267, from top to bottom.

lines in Figs. 3.3 and 3.4). The change in trend could be related to systematic errors in the outer disc region and must be analysed in more detail before being used. In the literature we can also find many cases of galaxies with a change in trend in, for example, the age profile (e.g. Ruiz-Lara et al. 2016).

To estimate the gradients and errors we use the bootstrap with replacement technique. The process is repeated 5000 times and the mean values and standard deviations of the slopes and intercepts are taken as our gradients. We adjust a linear fit at each side of the bulge (red and green solid lines in Figs. 3.3 and 3.4). The slope of these lines is the radial age gradient we are interested in and it will be explained in more detail in Section 3.4.4.

In Figs. 3.3 and 3.4 we can see that each galaxy has a different behaviour in age when moving up the plane. For example, in the mid-plane of galaxy IC0540 the age gradient is steep and positive, with age increasing when moving to larger radii. When shifting to greater heights, the age gradient inverts, becoming negative, with older populations in the inner galaxy. This change of trend could be related to the point where the thick disc of IC0540 starts to dominate over the thin disc. For the other five galaxies, we see that the age gradient is negative both in the plane and above (or below) it, but the values of the slopes change from the slits on the left column to the ones on the right. In addition to that, the mean age of the populations in a slit increases with height. This is one of the basic characteristics of the thick discs according to theory.

3.4.2 Metallicity gradient

We now study the light-weighted total metallicity in terms of radius. Figures 3.5 and 3.6 present these gradients for our CALIFA galaxies. The left column shows the trends for the slits closer to the mid-plane and the right one at greater heights, so that we can make a comparison of the behaviour when moving up. Each row refers

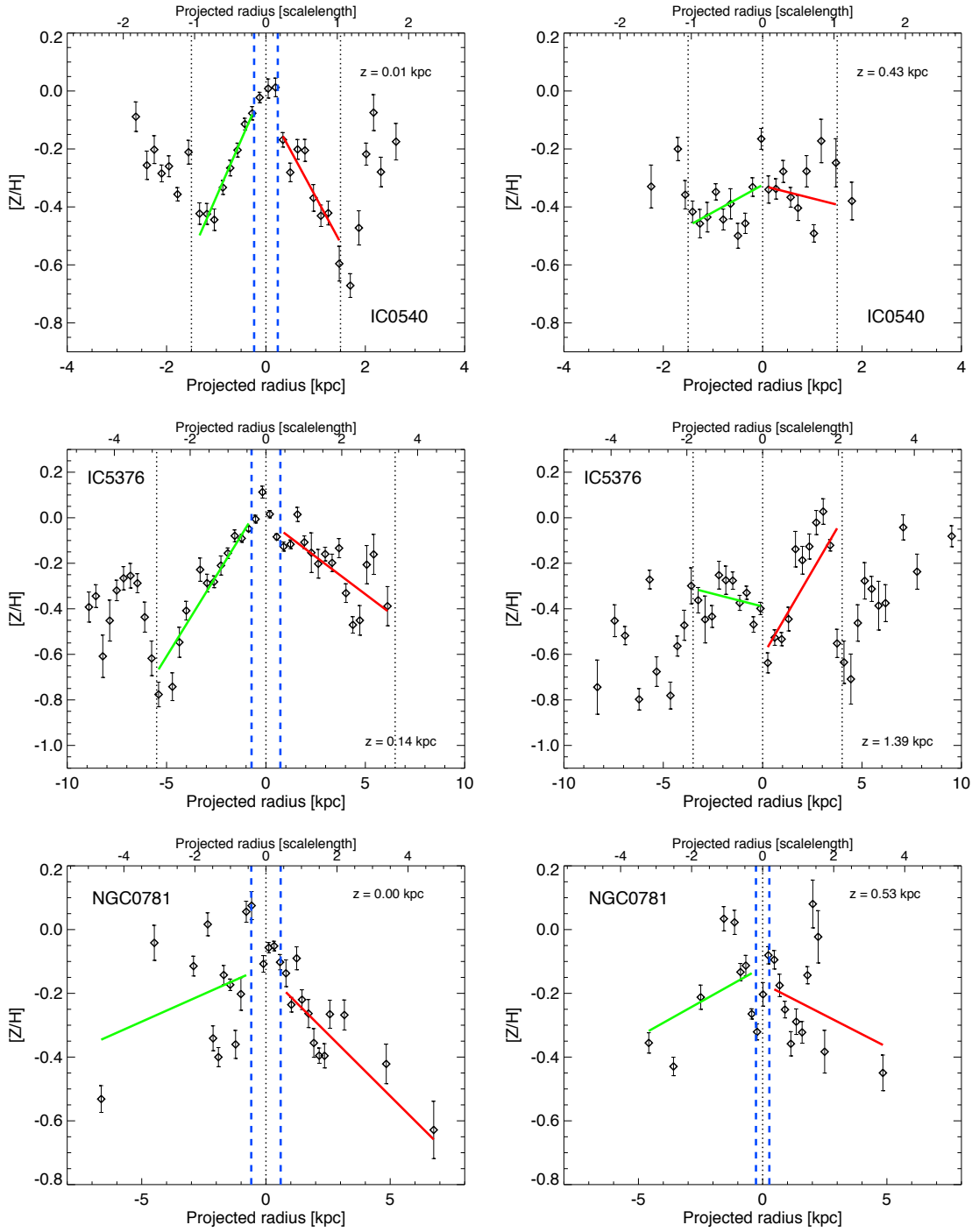


Figure 3.5: Radial profile of the total metallicity for three galaxies considered in this work, IC0540, IC5376 and NGC0781, from top to bottom. On the left there are the slits closer to the galactic plane and on the right the ones at greater heights. The linestyles and colours match those from Fig. 3.3.

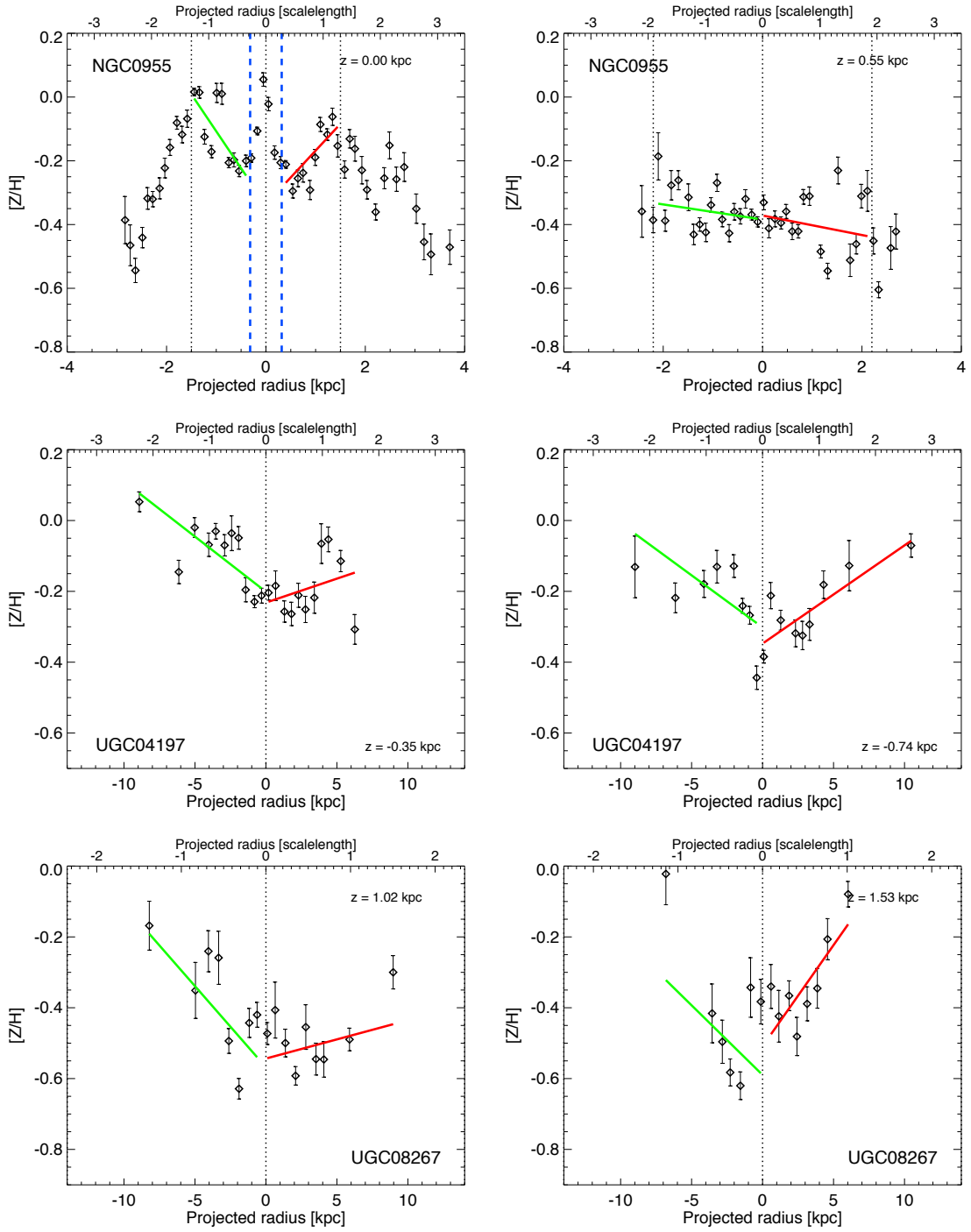


Figure 3.6: Same as Fig 3.5 (metallicity versus radius) but for the other three galaxies in our set, NGC0955, UGC04197 and UGC08267, from top to bottom.

to an individual galaxy. The behaviours for all the slits are exhibited in Appendix B.

There is a different trend for each galaxy, but generally the gradients are more positive (or less negative) in the geometrical thick disc than in the geometrical thin disc. Some of the galaxies go in accordance with the inside-out formation scenario of spiral galaxies and have a negative radial metallicity gradient close to the galactic plane. Above it there is an inversion and in the highest slits the radial metallicity gradient is positive, which means that the populations in the outer part have a higher metal content than the inner ones. This goes in line with results of the Milky Way (e.g. Anders et al. 2014; Xiang et al. 2015) and simulations (e.g. Miranda et al. 2016). In Figs. 3.5 and 3.6 we can also appreciate the decrease of the mean metallicity of each slit when moving to greater heights, which indicates that the thick disc is formed in a more primordial medium than the thin disc. Here we have only shown the results for certain slits and in Section 3.4.4 we will thoroughly explore the general radial metallicity gradients of our galaxy set.

We do not show the mass-weighted radial metallicity gradient due to the lower reliability of the results. The theoretical effect of having a higher light-weighted metallicity (reflects the values of the youngest stars) than a mass-weighted one (represents the metallicity of the old stars) is satisfied in our galaxies and exhibits the metallicity evolution of the galaxies, where new stars form from the gas enriched by the previous stellar generations.

3.4.3 Velocity field

We next study the line-of-sight velocity in each radial bin provided by pPXF. An example of this is presented in Fig. 3.7, which shows the rotation curve for UGC08267, with the slits above the mid-plane on the left panel and the ones below it on the right. In all slits, the absolute value of the line-of-sight velocity increases very rapidly with radius close to the bulge and becomes flatter at larger radii. The situation is quite

similar for the positive and negative z -s. The mean maximum line-of-sight velocity for this galaxy is $V_{LOS} = 166 \text{ km s}^{-1}$ and the values for the rest of our galaxies are summarised in Table 3.1. The rotation curves for the rest of the galaxies in the set can be found in Appendix B.

Theoretically, there is a lag between the rotation of the thin and the thick disc. We measure the difference in velocity when moving 1 kpc above and below the mid-plane, and define the lag as its mean value. Figure 3.7 reveals that, in the case of UGC08267, there is such a delay when moving up from the mid-plane, and it is also a common characteristic in our whole galaxy set. In the case of UGC08267 this effect is $V_{\text{lag}} \sim 15 \text{ km s}^{-1} \text{ kpc}^{-1}$, which is our smallest measured lag, and the others range from 22 to $45 \text{ km s}^{-1} \text{ kpc}^{-1}$. The exact values can be found in Table 3.1. We will discuss the implications of the velocity lag in Section 3.4.4.

3.4.4 General trends

Now we merge all the results found during the previous sections in order to have a detailed study of the galaxies involved in this work. Each panel in Figs. 3.8 and 3.9 is a compilation of the gradients in all slits for all the galaxies in our sample. Figure 3.8 shows the slope of the radial age gradient as a function of height above the plane while Fig. 3.9 represents the same for the total metallicity. We made this division of studying the trends at each side of the centre separately in order to see if they are totally equivalent or not. Now we can assess that their trends are generally similar with small discrepancies. This same happens when comparing the results above and below the mid-plane, shown in these figures with different symbols. The gradients are presented in two scales: dex kpc^{-1} and $\text{dex scalelength}^{-1}$. The latter is more appropriate if we want to contrast various galaxies from our sample.

In Figs. 3.8 and 3.9 we have not included all the slits taken from the CALIFA datacubes, but discarded many considering them too noisy or lacking radial bins. All

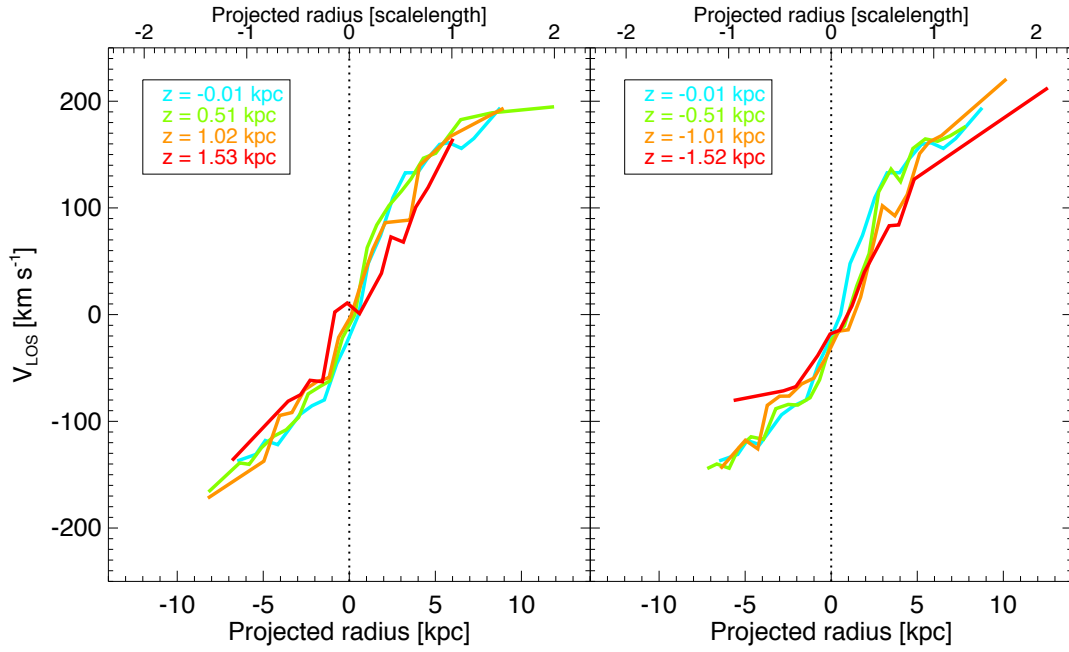


Figure 3.7: Rotation curve of UGC08267 for heights above the galactic plane on the left and below it on the right. The slit closest to the mid-plane is shown in both panels. Colour-coding goes according to the insets, changing from blue, green, orange and red when moving to greater heights. The legend in each panel relates the mean height with each rotation curve. There is a lag of velocity at the highest slits.

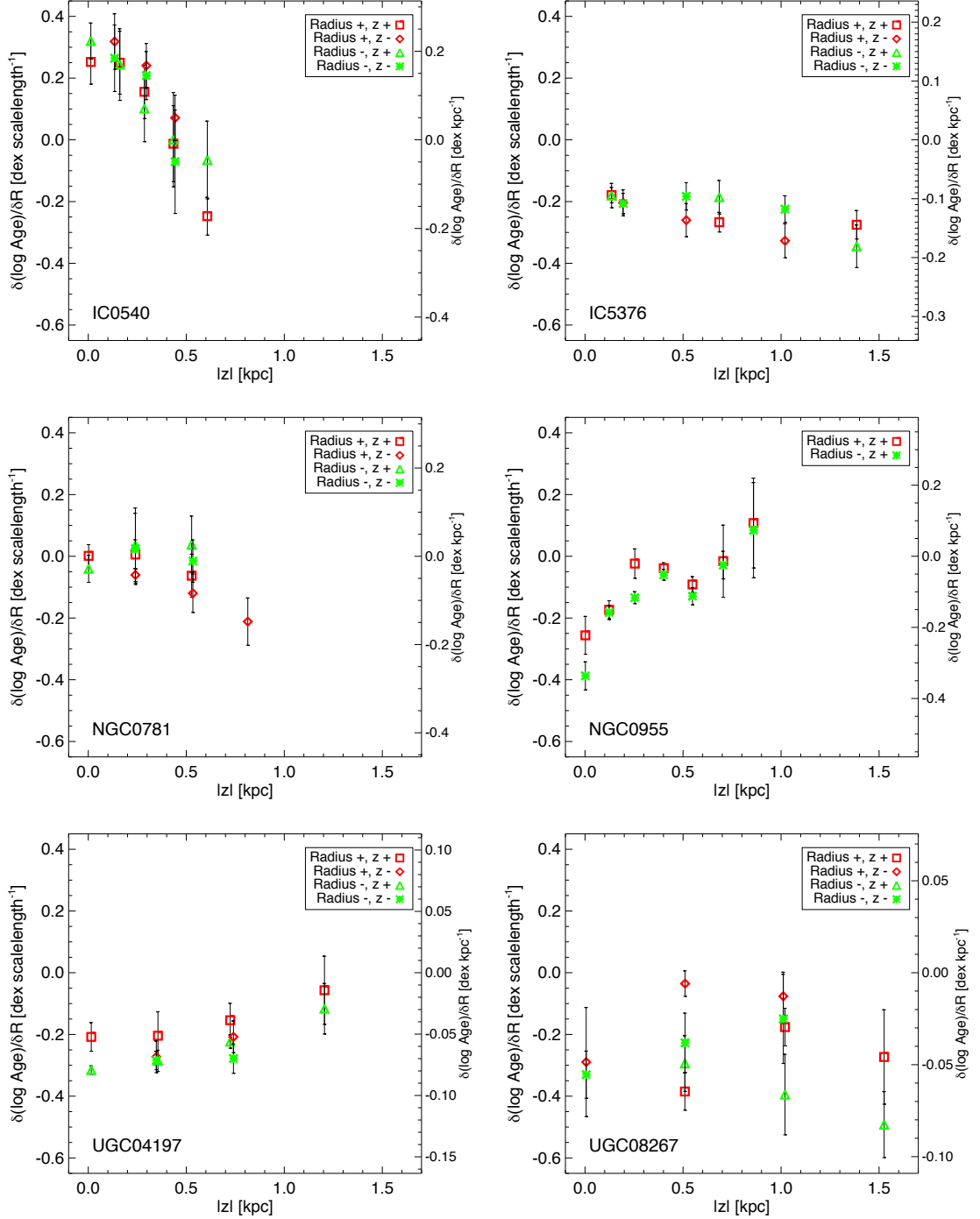


Figure 3.8: Radial age gradients for increasing values of height, including the six galaxies in our sample. Colour-coding is equivalent to the fittings in Figs. 3.3–3.6: red and green symbols here match the fits at both sides of the galactic centre in those figures. This is also mentioned in the legend, along with the symbols for positive and negative heights.

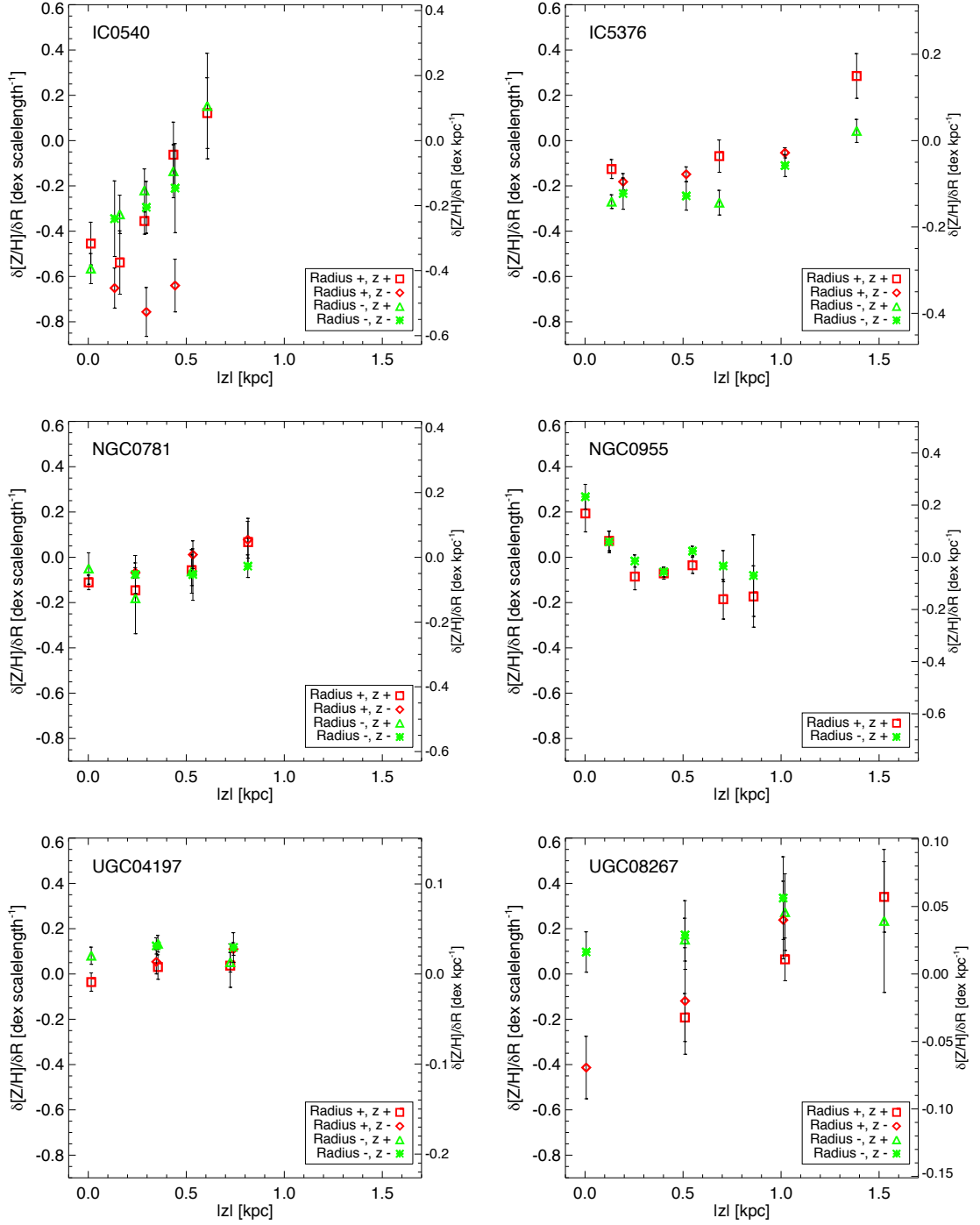


Figure 3.9: Same as Fig. 3.8 but for the radial metallicity gradients instead. We include our six galaxies.

the galaxies possess valuable slits at both sides of z , with the exception of NGC0955, which, as presented in Fig. 3.2, is covered by a dust lane in one side of the galaxy, making us discard it and limit our analysis to the other half (we only study the half with positive z).

A quick look at Fig. 3.8 shows that there is not a unique trend for the radial age gradients of all the galaxies, but a great variety of them. Three of our galaxies (IC0540, IC5376 and NGC0781) present a gradient which gets smoothly more negative with height, and in the case of the other three (NGC0955, UGC04197 and UGC08267) it appears that the gradient is more positive with height. Furthermore, IC0540, NGC0781 and NGC0955 exhibit a radial age gradient which is positive in some slits (older stars in the outer galaxy) and negative in others (younger stars in the outer galaxy), while for the other three galaxies the radial age gradient is negative at all heights. The latter case is consistent with Martig et al. (2016), who state that galaxies suffer flaring (the centre of the galaxies is dominated by old stars and the outer parts by younger ones that flare up in height) and this makes the radial age gradient to be negative at all heights. Some simulations also make this prediction (e.g. Miranda et al. 2016).

The situation is not so diverse for radial metallicity gradients, presented in Fig. 3.9. The main scenario is one in which it is negative in the mid-plane, which means that the metallicity is higher in the inner galaxy. When moving higher above and below the plane, there is a nice transitioning to a shallower gradient and it goes less and less negative. This same behaviour is found for the Milky Way (e.g. Carrell et al. 2012; Anders et al. 2014) and simulations (e.g. Miranda et al. 2016). We have one exception: NGC0955 shows a steep, positive radial metallicity gradient in the galactic plane and shallows when moving to the rest of the slits. All six galaxies seem to have an inversion point where the radial metallicity gradient changes sign. These inversion points could have an important significance in the formation of galaxies,

and give us clues about the formation scenarios taking place.

The inclination of a galaxy could change the results of the gradients with height. In our sample, we have two galaxies which are not completely edge-on (NGC0955 and UGC08267, according to HyperLeda). Inclination is a difficult magnitude to measure, and therefore we should not trust the values completely. We have tested the influence of inclination on the radial gradients, how they change when using these type of systems not completely edge-on. For that purpose we make use of two cosmological simulations from the MaGICC project (Making Galaxies In a Cosmological Context, Brook et al. 2012a). They were realised with the smoothed particle hydrodynamics code GASOLINE (Wadsley et al. 2004) and both are spiral galaxies with masses comparable to the Milky Way. We compare the radial age and metallicity gradients when these objects have an inclination of 90° and 80° . We find that in the latter case the trends are less pronounced, and the behaviours are flatter, but the same patterns remain. Inclination is an important factor which goes flattening the gradients when moving the galaxies from edge-on to face-on, but 80° is still an adequate inclination for looking at the vertical structure of the galaxies. In our sample, the lowest inclination is 81.5° . Even though quantitatively it is not the same as having it completely edge-on, qualitatively the result will be the same as if it was. Thus we can use our six galaxies for the purpose of measuring gradients at various heights.

Regarding the velocities, we see in Table 3.1 that our suite is composed of high-mass galaxies (these have rotational velocity $\geq 120 \text{ km s}^{-1}$). We only have one galaxy which is in the limit of high-mass system, with $V_{LOS} = 118 \text{ km s}^{-1}$. The six galaxies in our sample display a lag in velocity when moving to greater heights, ranging from 15 to $45 \text{ km s}^{-1} \text{ kpc}^{-1}$, in line to what is found for the Milky Way ($\sim 30 \text{ km s}^{-1} \text{ kpc}^{-1}$, see e.g. Chiba & Beers 2000). This is contrary to Yoachim & Dalcanton (2008), who claim that in high-mass galaxies there is not much difference

between thin and thick disc kinematics and therefore there is no lag.

Next we show in the top panel of Fig. 3.10 the relation between the velocity lag and the scalelength of our galaxies. There is a trend indicating that the galaxies with smallest lag are the ones with larger scalelength, which means that the systems with a steeper light profile will suffer a more prominent lag in the thick disc. In addition, the bottom panel of Fig. 3.10 exhibits the maximum line-of-sight velocity vs. scalelength for the six galaxies. We see that the line-of-sight velocity increases very rapidly with scalelength until it reaches a maximum and then decreases smoothly. This relation goes in accordance with the theory that larger scalelengths are usually characteristic of a bigger and more massive galaxy with a stronger rotational activity.

3.5 Conclusions

We take a sample of six edge-on disc galaxies from the CALIFA sample ranging from Sa to Sbc. We are interested in the vertical structure of these objects and thus analyse the radial age gradient with increasing height, radial metallicity gradient with height, rotation curve and velocity lag.

Velocity lag seems to be a very common characteristic of disc galaxies, and appears in all the elements of our set, ranging between 15 to 45 km s⁻¹ kpc⁻¹, in line with other studies as Comerón et al. (2016), who get a lag of 30–40 km s⁻¹ (in 2.4 kpc height) for the thick disc of their galaxy. This could indicate that thick discs are ubiquitous features of disc galaxies.

We find that neither the age nor the metallicity gradients follow one unique behaviour. In our set, some age gradients decrease with height, but others increase. Some are negative at all heights (this result is also found by Miranda et al. 2016 using simulations and Martig et al. 2016 using APOGEE data, who propose flaring as the cause of it) and others have an inversion point. Thick disc stars are older

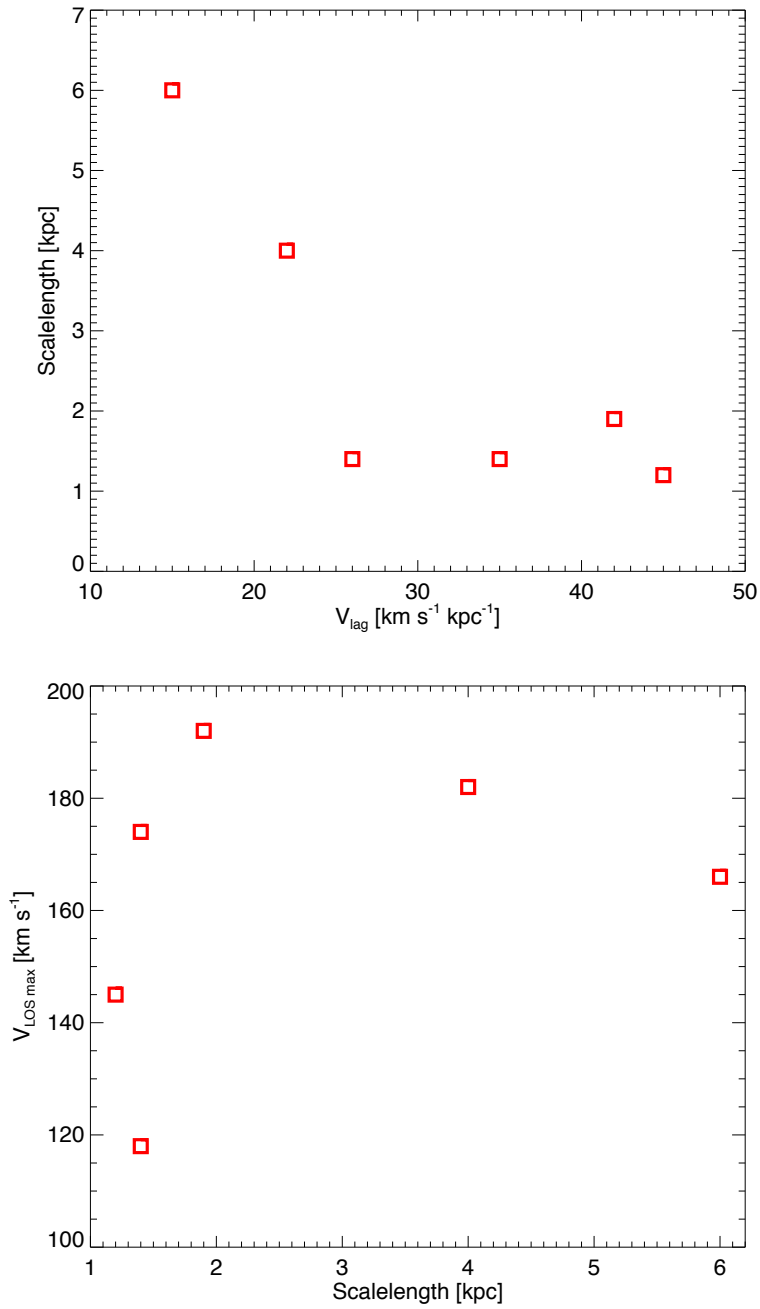


Figure 3.10: Top: scalelength vs. velocity lag. Bottom: maximum line-of-sight velocity vs. scalelength.

than thin disc ones, but the difference in age is small for some galaxies. This is because the spectra of old stars evolve little with time.

With respect to the metallicity gradient, there is a wider consensus, as all galaxies except one have an increasing trend when moving higher from the mid-plane. They even invert sign and go from negative close to the plane to positive in the thick disc, in accordance with the results from the Milky Way (e.g. Carrell et al. 2012; Anders et al. 2014; Xiang et al. 2015) and cosmological simulations (e.g. Rahimi et al. 2013; Miranda et al. 2016). Furthermore, all the galaxies experience a reduction of the mean metallicity in the highest slits, which implies that the thin disc has a longer evolution than the thick disc.

This variety of trends suggests that the thick disc formation scenarios might be diverse, as also stated by Kasparova et al. (2016). Galaxies have a complex evolutionary history. We believe that the wide range of behaviours might be explained if there are external processes taking part in the evolution of disc galaxies. For example, minor mergers could have played a role (see Abadi et al. 2003b), because they are external secular processes that affect in many distinct ways depending on the environment, galaxy mass, merging satellite mass etc, making the stellar populations distribute quite differently in each case. Another possible mechanism for obtaining results similar to ours would refer to thick discs being formed in-situ off the mid-plane during gas rich mergers, as advanced by Brook et al. (2004). Radial migration could contribute to redistribute the populations but it is not strong enough to flatten the radial gradients.

Nowadays models are still not able to reproduce these results. We propose that simulations should also consider different scenarios for the formation and evolution of disc galaxies. Further conclusions will be taken by studying a larger galaxy sample. For example, it will be possible to know if the trends found in this work are related to the galactic mass or any other intrinsic parameter.

Chapter 4

ON THE EVOLUTION OF SIMULATED GALAXIES: GETTING CLOSER TO ANY-MASS GALAXY REPRODUCTION

Abstract

Making use of a fiducial set of simulations of disc galaxies spanning a wide range in mass, we examine the variation of the radial metallicity gradient with stellar mass and compare it to observational trends.

The cosmological chemodynamical simulations employed here are drawn from the MaGICC project. The sample, consisting of 16 galaxies, forms a homogeneous and complete statistical suite of field galaxies and covers a range in masses of $10^6 \lesssim M_{\star} \lesssim 10^{11} M_{\odot}$. All of them are late type galaxies, and spirals or irregulars in morphology.

We study gas-phase radial oxygen gradients overplotting observations and simulations. We see that, contrary to what is found in real systems, the mean gradient in MaGICC galaxies does not get steeper at lower galactic masses. Our gradients are too flat for galaxies with stellar masses $M_\star < 10^9 M_\odot$, and this trend of the oxygen gradient with mass remains when we study the relation at different redshifts. The total metal content is consistent with empirical scaling relations like the oxygen abundance against stellar mass relation, but distributed incorrectly. We propose a mass-dependent modulation of feedback and/or star formation efficiency for simulated galaxies. Implementing such a mass dependency must be handled with care, in order not to violate said empirical scaling relations.

4.1 Introduction

Metallicity is a key characteristic of galaxies, and looking at its distribution, one can collect clues about their formation puzzle. One of the most used heavy elements in the interstellar medium of a galaxy is the oxygen abundance, which is defined as the number ratio of oxygen to hydrogen atom and expressed as $12 + \log(\text{O}/\text{H})$. The gas-phase oxygen abundance in the surrounding medium depends on various processes during the evolution of a galaxy, say the number of high-mass stars exploded as a supernova or releasing stellar winds around, the oxygen expelled to the circumgalactic medium or getting gravitationally unbound via feedback processes (see Section 1.3 for a more precise explanation). Gas inflows from the intergalactic medium could also vary the metallicity of a galaxy (Kewley et al. 2006; Rupke et al. 2008).

It is known that there is a tight correlation between global metallicity and stellar mass in star-forming galaxies, known as the mass-metallicity relation (Tremonti et al. 2004). It evolves with redshift, galaxies being more metal-rich at lower redshift

(e.g. Zahid et al. 2013), and thus it is a fundamental relation for measuring the chemical evolution of galaxies. This enrichment happens due to the subsequent stellar generations that live in galaxies. There are many physical processes that could be responsible for shaping the mass-metallicity relation, such as accretion of metal-free gas (Dalcanton et al. 2004), metal enriched outflows (Larson 1974) and variation in the star formation efficiency (Calura et al. 2009). The mass-metallicity relation is used to constrain feedback models in simulations (e.g. Davé et al. 2011; Torrey et al. 2014; Ma et al. 2016a).

The relations between metallicity and other fundamental properties of galaxies can also place tight constraints on the processes governing their evolution. Searle (1971) found that galaxies in the local Universe generally have negative gas-phase radial metallicity gradients. This indicates that galaxies are more metal-rich in the central part than in the outskirts (e.g. Zaritsky et al. 1994; van Zee et al. 1998). Werk et al. (2011) and other works noticed that in the majority of the galaxies where measurements out to large radii are possible, the metallicity gradients flatten in the outer discs, suggesting that there is a transportation of metals from the inner to outer disc. Isolated galaxies show steeper gas-phase metallicity gradients than interacting galaxies of similar mass (Vila-Costas & Edmunds 1992; Rupke et al. 2010b), which can be explained if interactions trigger radial inflows of low metallicity gas from the outskirts toward the galactic centre (Rupke et al. 2010a; Torrey et al. 2012).

Galaxies at higher redshifts show diverse metallicity gradients (Cresci et al. 2010; Swinbank et al. 2012; Wuyts et al. 2016), with a slope that can be negative, flat or positive. For example, in the sample studied by Leethochawalit et al. (2016) most galaxies have flat gas-phase metallicity gradients, in contrast to Jones et al. (2013) who get stronger metallicity gradients in their high-redshift galaxies. Ma et al. (2016b) suggest that starburst episodes make the metallicity gradient of high-redshift galaxies vary on \sim Gyr time-scales. According to them, when a starburst is triggered

in a gas disc, a negative metallicity gradient can be built up quickly. Then the strong feedback from the starburst drives intense outflows, which mix the metals on galactic scales and result in flat metallicity gradients. After that, negative gradients may form again. In any case, measurements at high redshift are complicated and plagued with systematic errors that are still not very well understood (e.g. Mast et al. 2014; Ho et al. 2015).

Statistical studies of metallicity gradients in the local Universe are introduced with the late advances in instrumentation (Sánchez et al. 2014). Some examples are multi-slit spectroscopy and wide-field integral field spectroscopy (IFS). The IFS surveys are especially useful due to the large number of spectra they collect simultaneously. In some cases this fact combines with a large wavelength coverage that allows to capture multiple key emission lines for deriving metallicity. For example, surveys as CALIFA (see Chapter 3 for more details), MANGA (Mapping Nearby Galaxies at APO, Bundy et al. 2015), SAMI (Sydney-AAO Multi-object Integral field spectrograph, Croom et al. 2012) and Hector Survey (Bland-Hawthorn 2015) are starting to do these statistical studies.

In the literature, Ho et al. (2015) studied the metallicity gradient with mass for a sample of local field galaxies, and concluded that galaxies of lower masses have on average a steeper negative metallicity gradient and possess a larger dispersion (comparing to their massive counterparts), when expressing the gradient in units of dex kpc⁻¹. On the other hand, when the sizes of galaxies are taken into account in the gradient, these results are not true any more. Roy et al. (1996) studied the oxygen abundance of dwarf galaxies and saw no global abundance gradient in their discs. Pilyugin et al. (2015) studied data of H II regions in a set of irregular galaxies and found out that they are inhomogeneous like spiral galaxies and therefore they exhibit radial abundance gradients.

Simulations have also been used to assess this behaviour. In the ones by Tissera

et al. (2016), the metallicity gradient for increasing mass follows the same trend as in Ho et al. (2015): galaxies with lower stellar masses have steeper negative metallicity gradients at $z = 0$. They also look at higher redshifts and find similar results. Conversely, Ma et al. (2016b) make use of cosmological simulations of galaxies in an ample range of mass and deduce that low mass galaxies are the ones with flatter metallicity gradients.

In this work we study the dependence of the oxygen metallicity gradient with mass for a set of cosmological simulations, and compare the results with observational data from the IFS survey CALIFA among others. We are interested in the effect that feedback produces on different mass galaxies. The confrontation of the chemical properties of simulated galaxies with observations is a powerful tool to set constraints on galaxy formation models.

4.2 Sample

We use a set of 16 cosmological zoom simulations from the Making Galaxies In a Cosmological Context project (MaGICC, Brook et al. 2012a; Stinson et al. 2013b)¹. They are run with the parallel SPH (Smoothed Particle Hydrodynamics) code GASOLINE (Wadsley et al. 2004). This statistical sample has initial conditions derived from the McMaster Unbiased Galaxy Simulations (MUGS, Stinson et al. 2010). Here we describe the most critical points and refer the reader to Wadsley et al. (2004), Stinson et al. (2010), Brook et al. (2012a) and Section 2.2 of this thesis for further details.

Each simulation contains 5–15 million particles within its virial radius at $z = 0$, with mean stellar particle mass of $\sim 4800 M_{\odot}$. Stars are formed when a gas particle reaches cool temperatures ($T \leq 10000$ K) in a dense environment ($n_{th} \geq 9.3 \text{ cm}^{-3}$).

¹In Brook et al. (2012a) they analyse a smaller sample, which was then extended to include all the galaxies in this work

Gas is converted into stars according to the Schmidt Law (Schmidt 1959). In these simulations, stars feed energy back into the surrounding gas via two types of thermal energy: supernovae and radiation feedback from massive stars.

Prior to the explosion as supernovae, massive stars inject energy into the surrounding gas (Hopkins et al. 2011). This has been included as pure thermal feedback, which is highly inefficient in these type of simulations (Katz 1992; Kay et al. 2002), with only 10% of the emitted energy being injected in the surrounding medium.

Supernova feedback deposits 10^{51} erg of energy into the interstellar medium at the end of the stellar lifetime of every star more massive than $8 M_{\odot}$. Metals are ejected from type II and type Ia supernovae and stellar winds driven from asymptotic giant branch stars. Metal abundances are based on the SN II yields of Woosley & Weaver (1995) and SN Ia yields of Nomoto et al. (1997).

All simulations have very similar baryon cycles, which means that the same key processes occur on the scales resolved. They span a wide range of mass, going from $\sim 10^6 M_{\odot}$ to $\sim 10^{11} M_{\odot}$, and they constitute a statistical sample of field galaxies. All of them are late type and have ongoing star formation. We split the set in three subgroups, labeled as Milky Way-like (5 galaxies), irregulars (7 galaxies) and dwarfs (4 galaxies). The Milky Way-like ones are characterised by their spiral structure. The irregulars and dwarfs are irregular galaxies, with less well defined structures. The characteristics of each galaxy in the set at redshift 0 are reflected in Table 4.1, and at higher redshifts in Table 4.2. We could not calculate the scalelength of some of the galaxies at certain redshifts due to the non-exponential profile they showed in those moments of their lives. The systems with the same name but belonging to a different subgroup have an equal merging history but are rescaled to a different mass.

Galaxy	Subgroup	$r_{l,0}$	R_{25}	$grad_{kpc}$	$grad_{R_{25}}$
g1536	MW	3.07	10.63	-0.033	-0.353
g15784	MW	3.11	20.96	-0.035	-0.736
g21647	MW	1.56	8.27	-0.043	-0.354
g5664	MW	2.10	8.87	-0.038	-0.340
g7124	MW	2.67	9.36	-0.009	-0.085
g1536	Irreg.	2.04	2.92	-0.003	-0.010
g15784	Irreg.	2.40	7.84	-0.020	-0.158
g15807	Irreg.	1.88	9.74	-0.017	-0.166
g21647	Irreg.	1.88	1.86	-0.003	-0.005
g22437	Irreg.	1.80	4.43	-0.013	-0.060
g5664	Irreg.	1.91	2.75	-0.004	-0.012
g7124	Irreg.	1.53	1.17	-0.006	-0.007
g1536	Dwarf	0.23	0.11	-0.058	-0.006
g15784	Dwarf	0.78	—	-0.001	—
g15807	Dwarf	1.23	—	-0.008	—
g22437	Dwarf	0.17	0.12	0.011	0.001

Table 4.1: Primary characteristics of the simulations analysed in this work, when they are at redshift 0. Information for each column: 1. Simulation label; 2. Galaxy subgroup (Milky Way-like – MW –, irregular or dwarf); 3. Scalelength at redshift 0 (kpc); 4. B -band isophotal radius at magnitude 25 (kpc); 5. Gas-phase oxygen radial gradient when $z = 0$ (dex kpc^{-1}); 6. Oxygen gradient when $z = 0$ (dex R_{25}^{-1}).

Galaxy	Subgroup	$r_{l,0.53}$	$r_{l,0.96}$	$r_{l,1.25}$	$grad_{0.53}$	$grad_{0.96}$	$grad_{1.25}$
g1536	MW	2.31	2.17	1.93	-0.041	-0.023	-0.016
g15784	MW	2.63	2.25	1.39	-0.038	-0.046	-0.051
g21647	MW	1.52	1.47	1.80	-0.011	-0.004	-0.018
g5664	MW	1.26	1.06	1.07	-0.025	-0.011	-0.036
g7124	MW	2.53	2.29	2.26	-0.005	-0.009	-0.006
g1536	Irreg.	2.43	1.50	—	-0.009	-0.014	—
g15784	Irreg.	1.87	—	—	-0.020	—	—
g15807	Irreg.	—	—	—	—	—	—
g21647	Irreg.	—	0.89	—	—	0.045	—
g22437	Irreg.	1.40	1.03	—	-0.009	0.002	—
g5664	Irreg.	—	—	—	—	—	—
g7124	Irreg.	—	—	—	—	—	—
g1536	Dwarf	—	—	—	—	—	—
g15784	Dwarf	—	—	—	—	—	—
g15807	Dwarf	—	—	—	—	—	—
g22437	Dwarf	—	—	—	—	—	—

Table 4.2: Primary characteristics of the simulations analysed in this work, when they are at high redshifts. Information for each column: 1. Simulation label; 2. Galaxy subgroup (Milky Way-like – MW –, irregular or dwarf); 3. Scalelength at redshift 0.53 (kpc); 4. Scalelength at redshift 0.96 (kpc); 5. Scalelength at redshift 1.25 (kpc); 6. Gas-phase oxygen radial gradient when $z = 0.53$ (dex kpc^{-1}); 7. Oxygen gradient when $z = 0.96$ (dex kpc^{-1}); 8. Oxygen gradient when $z = 1.25$ (dex kpc^{-1}).

4.2.1 Scaling relations

To test the accuracy of our simulations we have to judge their ability to simultaneously match a range of observational constraints. The MaGICC set reproduces many observed scaling relations and we present them in Fig. 4.1. Panel (a) shows the relationship between stellar mass and total mass. Panel (b) relates the rotational velocity (at 3.5 scalelengths) and luminosity in the I -band, also known as the Tully-Fisher relation. Panel (c) is the size (the scalelength) against luminosity in the I -band, (d) reveals size versus rotational velocity. Panel (e) indicates the total baryonic mass (all stars and cold gas) versus rotational velocity and (f) presents $12 + \log(\text{O}/\text{H})$ against stellar mass.

These figures show that most of the galaxies match the observational predictions (taken from Brook et al. 2012a), delimited by the green dashed lines in Fig. 4.1, except for panel (f) which shows the observations with black dots and also includes the results for other simulations from Brook et al. (2012a). The simulations have the correct amount and distribution of angular momentum, as they match the Tully-Fisher relation over a wide range in luminosities and they have adequate sizes without too large bulges ($B/T \lesssim 0.004$ for all galaxies). The fact that the fiducial set matches the baryonic mass-metallicity relation indicates that the baryon cycle should be correct and thereby the feedback used appropriate. Therefore the fiducials form a valid sample and can be used for other comparisons with observational data.

4.3 Results

We want to study the radial oxygen abundance gradient of the gas-phase in relation to the stellar mass, in order to see if the chemical evolution of a galaxy depends on its galactic mass, or if, on the contrary, all-mass galaxies evolve in the same way. We want to bring the analysis somewhat closer to the observers' plane and try to

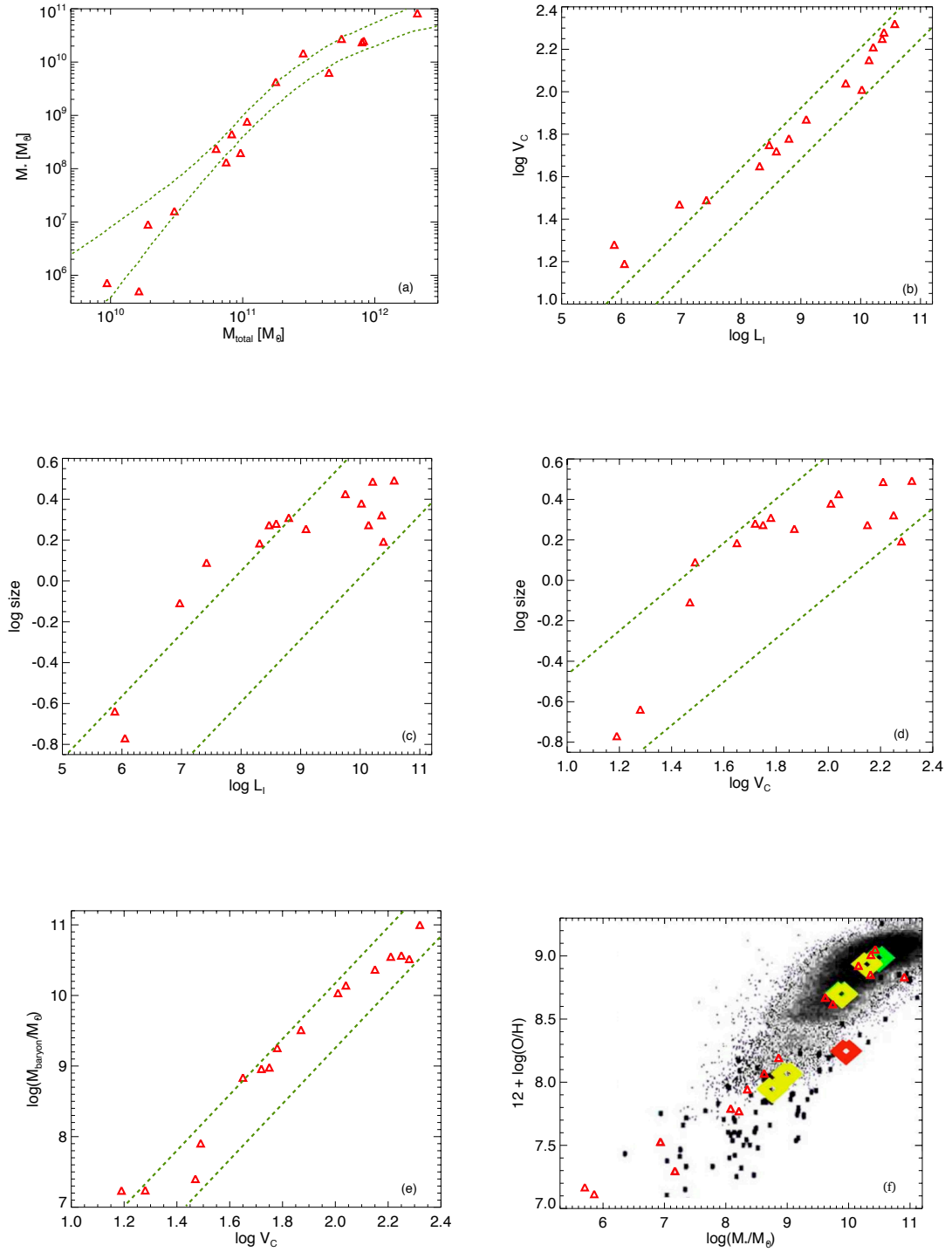


Figure 4.1: Some scaling relations fulfilled by the fiducial set. Our simulations are represented with red triangles and observational trends delimited by the green dashed lines and black dots.

reproduce the observational results as tight as possible, analysing the data in the same way as they do. Therefore, we derive the gradients employing a similar spatial resolution to the datasets in Ho et al. (2015), and use a radial bin size of 0.6 kpc (that is twice the softening length in the MW-scale runs in MaGICC and about 10x the softening length of the lowest mass dwarfs in the fiducial set)². We only select the low temperature gas particles ($T \leq 10000$ K), to resemble the conditions of the H II regions in the observations.

For normalising the metallicity gradients to a radial scale, we need to calculate the scalelength of each galaxy. Hence, we start the analysis by examining the mass density versus radius at redshift $z = 0$ for the MaGICC suite. In Fig. 4.2 we show the relation for a representative subsample of galaxies in our set: three MW-like galaxies, two irregulars and a dwarf. The black line in each panel is the result from a fiducial simulation and the red line is the exponential fit adjusted to the disc in order to calculate the scalelength, following this equation for the density:

$$\Sigma(r) = \Sigma_0 \times \exp[-(r/r_l)], \quad (4.1)$$

where r_l is the scalelength of the disc and Σ_0 is the central mass density. The values of the scalelengths for all galaxies at $z = 0$ are exposed in Table 4.1.

We are also interested in the temporal evolution of the gradients. Thus, we look at the density with radius of the galaxies in the set when they are at higher redshifts (some of these are shown in Fig. 4.3). The redshifts we focus on are 0.53, 0.96 and 1.25, which correspond to $t = 8.4$ Gyr, 6 Gyr and 5 Gyr, respectively. The scalelengths for all the simulations at these redshifts are indicated in Table 4.2.

²The radial bin used in the dwarfs is 0.1 kpc due to the small size of these galaxies

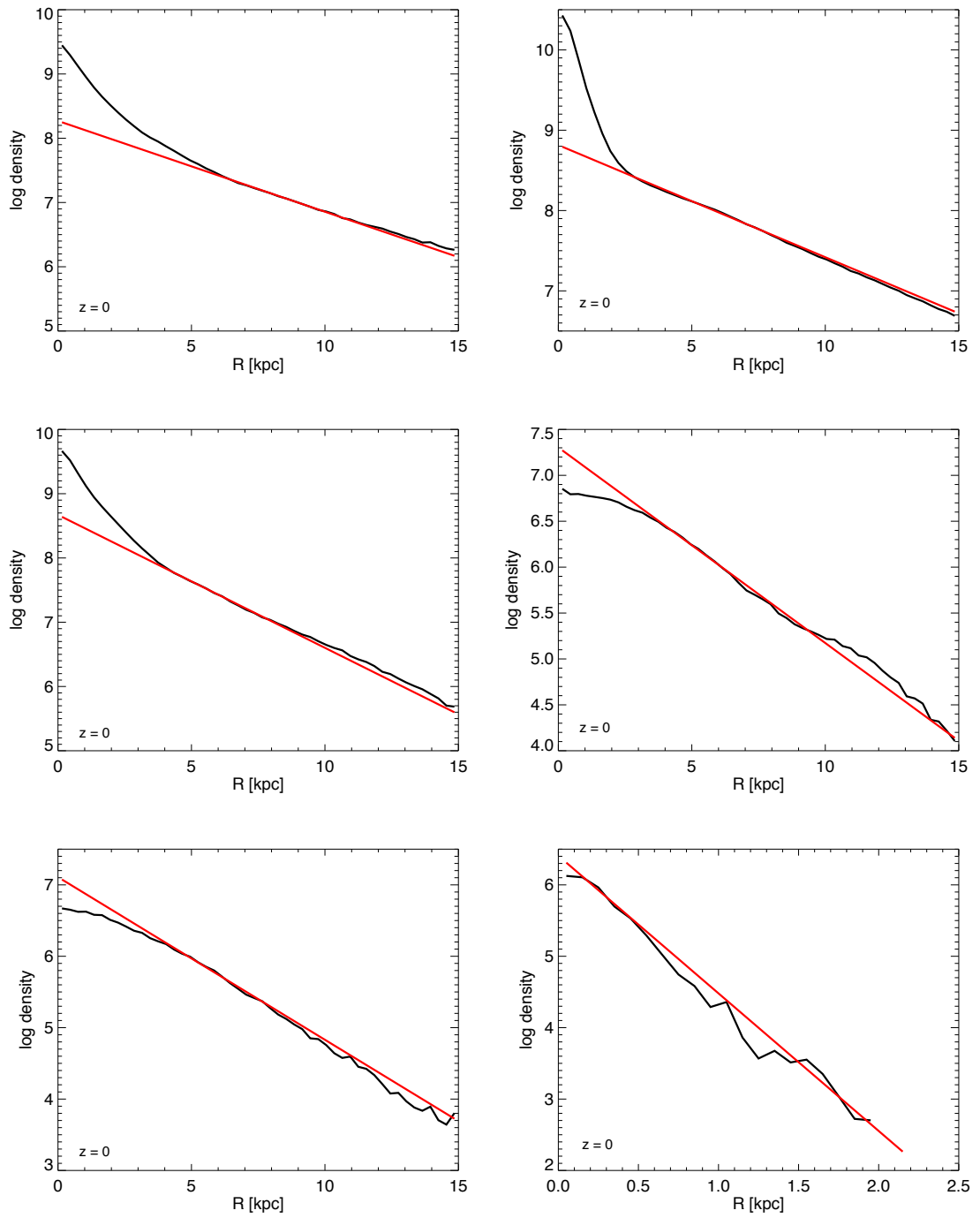


Figure 4.2: Mass density in terms of radius for a subset of our galaxy sample. The red lines are the exponential fits employed to calculate the scalelength of each galaxy.

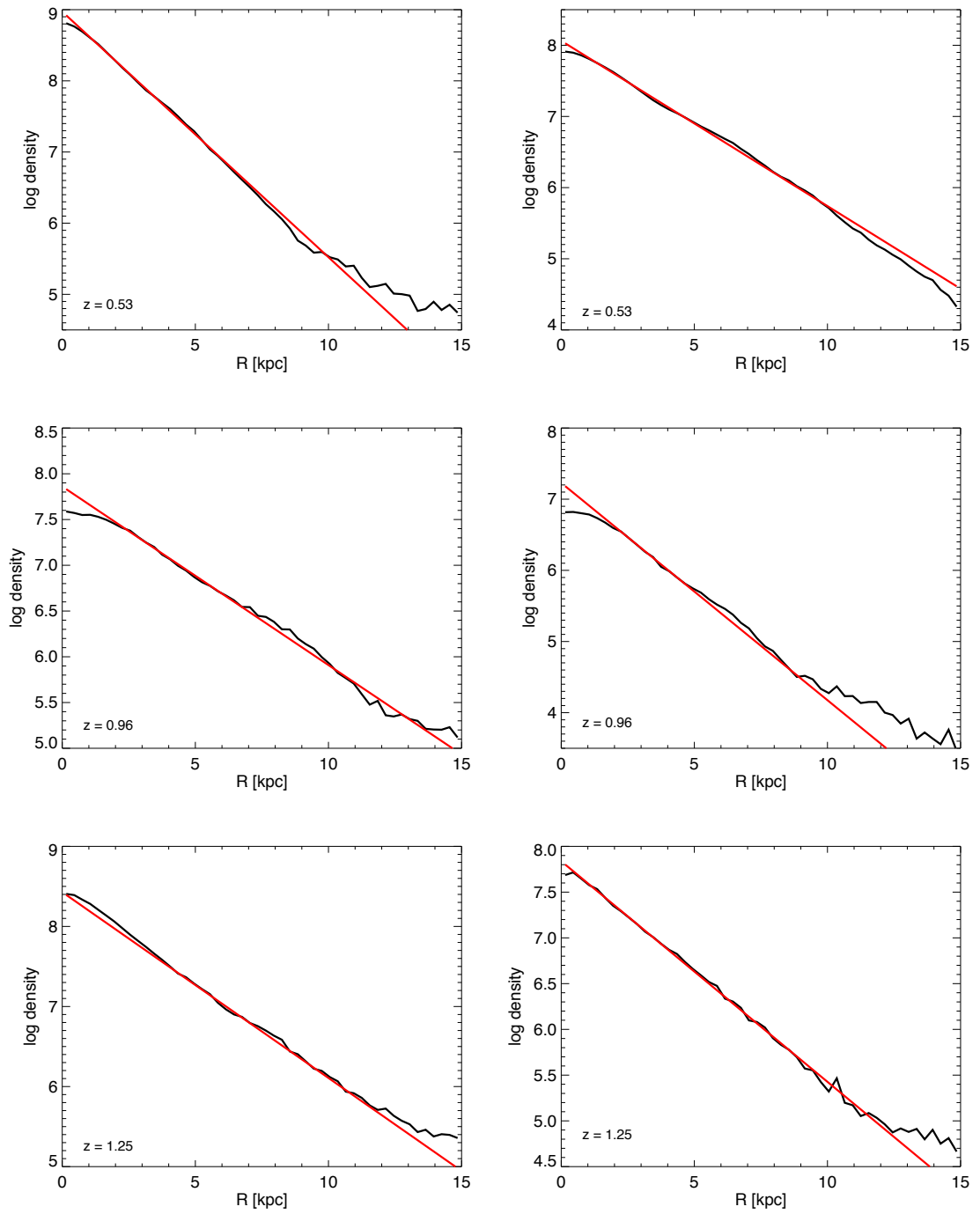


Figure 4.3: Same as Fig. 4.2 but for the case of higher redshifts. The z of each galaxy is expressed in its corresponding panel.

4.3.1 Metallicity gradient

We explore how the oxygen $12 + \log(\text{O}/\text{H})$ changes when moving from the inner to outer galaxy, and compare our findings with the observational data used in Ho et al. (2015). We make radial bins of 0.6 kpc (except for the dwarfs, for which we use 0.1 kpc) and take the mean oxygen abundance at each bin. We show the result for the mass weighted metallicity of the cold gas versus radius in Fig. 4.4 (black lines in the panels), including a subsample of our galaxy set at various redshifts. For this figure, we have discarded the inner part of the galaxies (the inner 1–2 kpc in the MW-like ones and 0.05–0.5 kpc in the dwarfs) to avoid any possible inhomogeneities or irregularities in their centre.

We want to obtain the values of the radial metallicity gradients, and therefore we need to adjust a linear fit to the metallicity. As explained in Section 4.1, the outer disc of some galaxies has an abrupt change in trend. We choose to study just the inner disc to resemble the observational studies, who usually cannot get accurate spectra of the outer discs. We use the least squares method to fit a line to the metallicity, selecting only the data between 1 and 3 disc scalelengths to avoid contamination from the bulge. This is illustrated via the red lines in Fig. 4.4. The slope of this linear fit will be our measurement of the gradient. We add Fig. 4.5 just to exhibit the oxygen abundance versus radius for all the individual gas particles composing each galaxy. Notice that the trends shown in this figure are well reproduced by the black lines in Fig. 4.4.

Next we look at the radial oxygen gradients with galactic mass in Fig. 4.6, when the gradients are expressed in dex kpc^{-1} . We include the values for all the redshifts under study. These are also exposed in Tables 4.1 and 4.2. Observational data from Ho et al. (2015) is overplotted with green asterisks. We see that MaGICC galaxies expand to lower masses, but the high-mass end is similar in simulations and observations. The latter suggest that the mean gradient steepens (and increases dispersion)

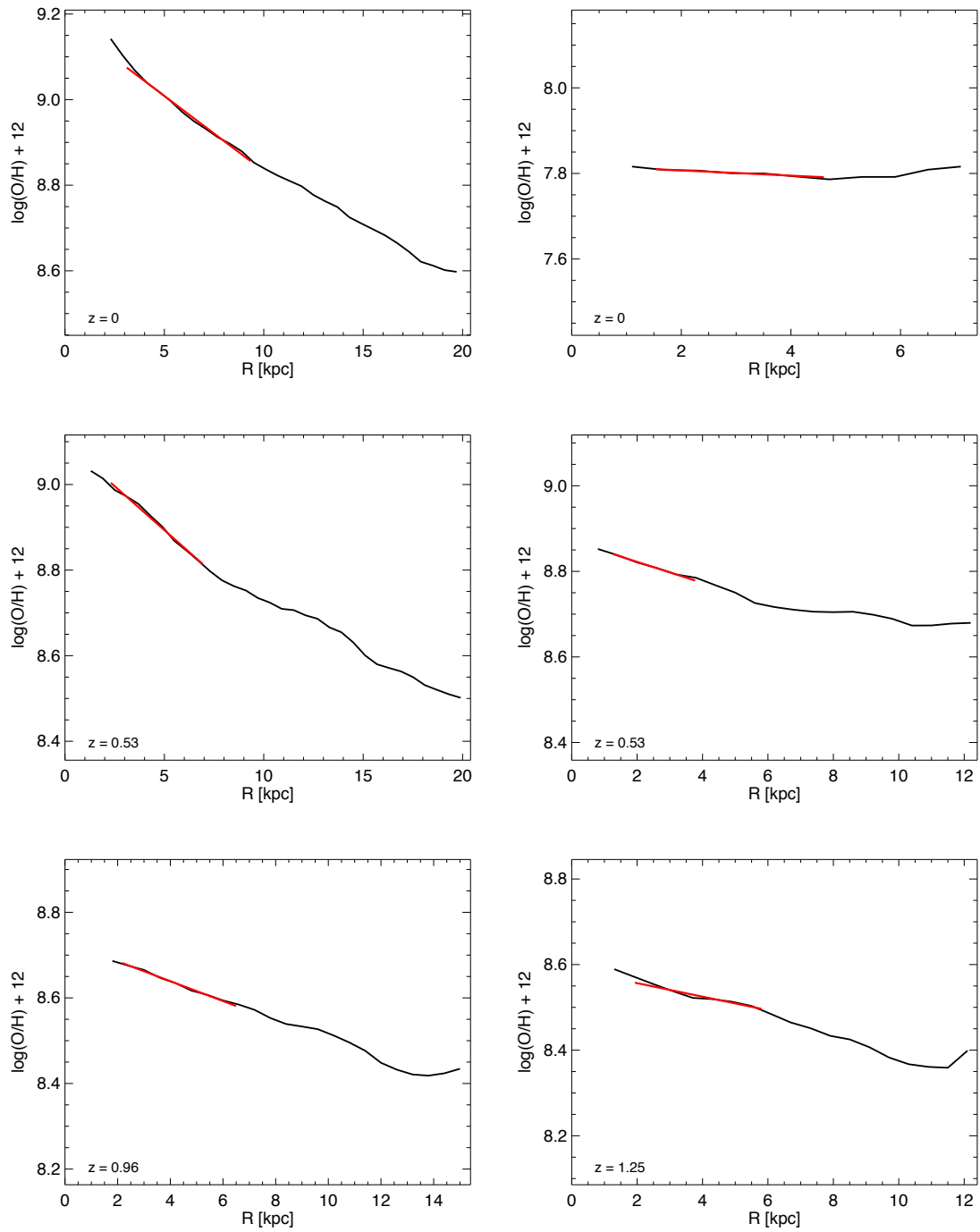


Figure 4.4: Oxygen abundance in terms of radius for some galaxies in the sample. The red line is the fit between 1 and 3 scalelengths. The radius is in units of kpc and the redshift of the galaxy is indicated in each panel.

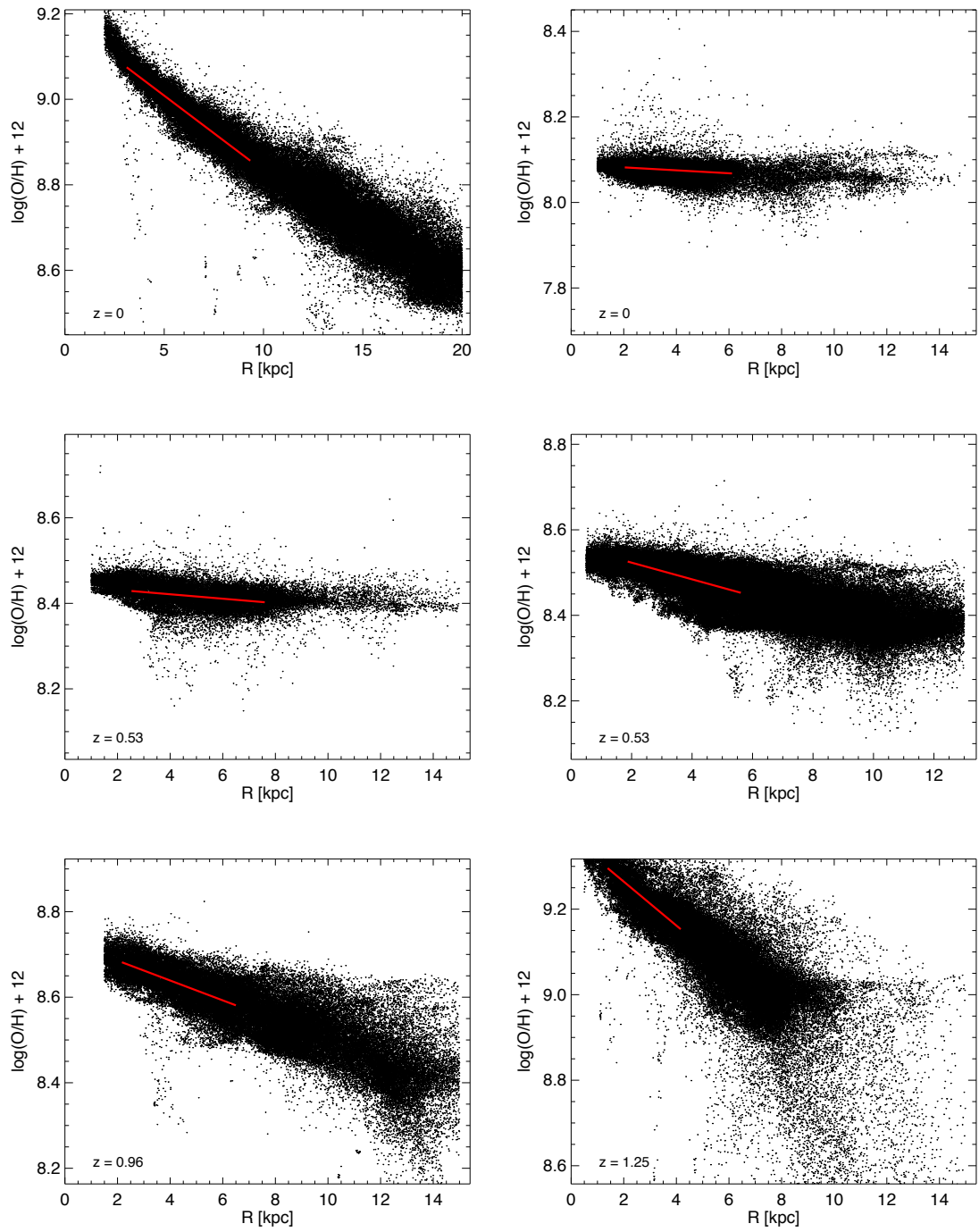


Figure 4.5: Same as Fig. 4.4 but showing all individual gas particles instead of the mean oxygen at each radial bin.

when moving to lower masses, becoming more negative, but our results do not reproduce that measured metallicity distribution, and generally become flatter with decreasing mass (except for one dwarf). Another conclusion from Fig. 4.6 is that the metallicity gradients of our set do not vary with redshift (since $z = 1.25$). Our results are in agreement with cosmological simulations from Ma et al. (2016b), not only qualitatively, but also quantitatively. On the other hand, Tissera et al. (2016) find the opposite trend, in accordance with Ho et al. (2015).

We repeat the analysis of the gradients but changing the scale in which they have been measured. Now we use a scale representative of the size of the galaxies, instead of an absolute scale as it is kpc. We study the variation of oxygen with increasing radius of the galaxy, with radius expressed in $R25$ (B -band isophotal radius at magnitude 25), in Fig. 4.7. We only look at $z = 0$ because we already know that the gradients do not vary with time. Again, the red lines show the fit between 1 and 3 scalelengths, and their slopes are then used in Fig. 4.8, which presents the oxygen gradient versus mass when distances are in units of $R25$. The steepening of the trend saw in Fig. 4.6 for the measured data from Ho et al. (2015) seems to dissipate when presenting the gradients in relative scales, with low-mass galaxies having slightly flatter metallicity gradients than high-mass galaxies. On the other hand we have MaGICC galaxies, which show the same behaviour of flattening gradients for lowest masses, when expressing the results in both $\text{dex } R25^{-1}$ and dex kpc^{-1} . Two of our dwarfs do not have magnitude 25 at any radii as they are very faint, and have been excluded from this part of the analysis. The values of the $R25$ and gradients for the rest of the systems are written in Table 4.1.

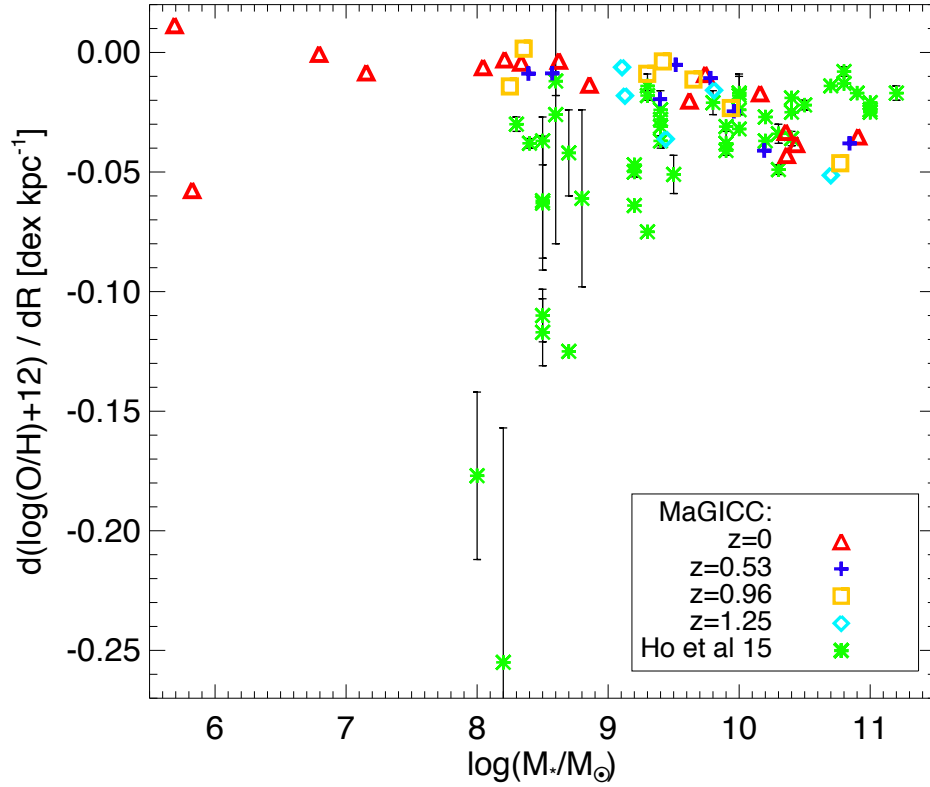


Figure 4.6: Oxygen gradient (in units of dex kpc^{-1}) versus stellar mass, including observations from Ho et al. (2015) (green asterisks) and MaGICC simulations at different redshifts ($z = 0$ in red triangles, $z = 0.53$ in blue crosses, $z = 0.96$ in orange squares and $z = 1.25$ in cyan diamonds). Each symbol indicates an individual galaxy. Our simulations go to lower masses than the measured data.

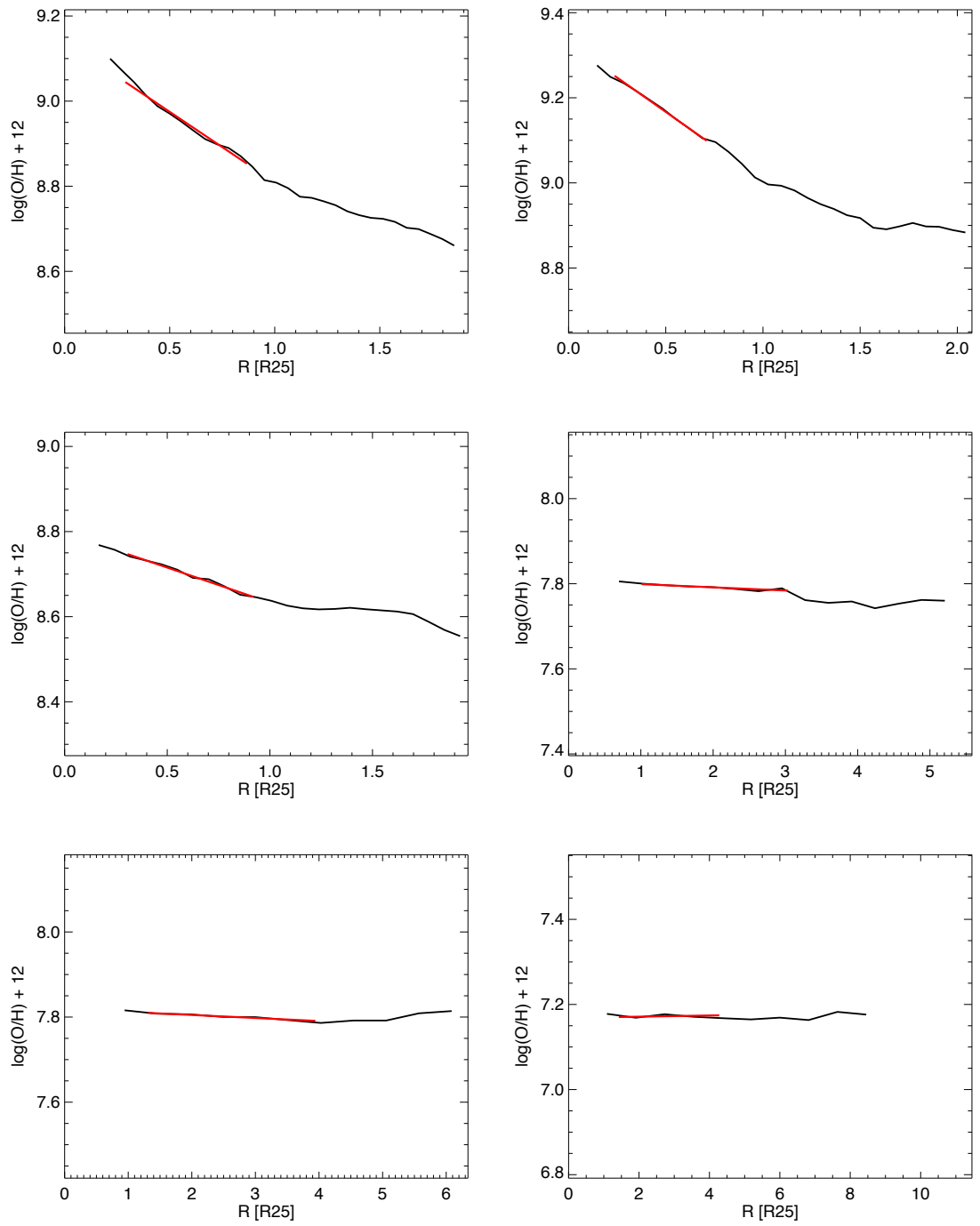


Figure 4.7: Same as Fig. 4.4 but using the R_{25} scale for the radius. The red lines are again the fit between 1 and 3 scalelengths.

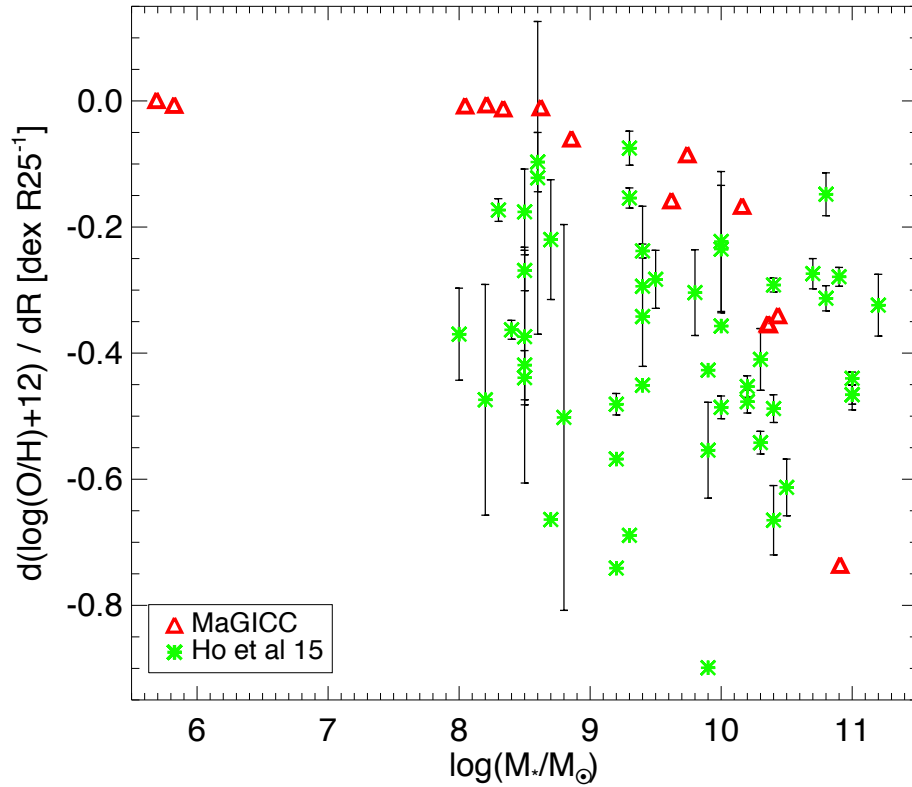


Figure 4.8: Same as Fig. 4.6 but for gradients measured in the relative scale dex $R25^{-1}$. This scale takes into account the galaxy size. Again, observations from Ho et al. (2015) are displayed with green asterisks and our fiducial simulations with red triangles. This time we only show values for simulations at redshift 0.

4.4 Conclusions

This work aims at studying the cold gas radial metallicity gradient in galaxies and its relation with galaxy mass. For that purpose we use a set of 16 cosmological simulations. We exhibit the oxygen gradient versus mass, when distances are measured both in an absolute scale (kpc) and relative scale ($R25$). We compare our results with other works from literature.

Ho et al. (2015), using various datasets, find that the mean gradient in kpc steepens when moving to lower galactic masses, while there is no trend for gradients in relative scales. This means that if we rescaled their observed galaxies to the same size, all-mass galaxies would have similar gradients. Said in another way, smaller galaxies have steeper negative gradients in dex kpc⁻¹ but then would be compensated when the galaxy sizes are taken into account. On the other hand, we find a similar trend for both distance scales, though it gets even more pronounced when using dex $R25^{-1}$. This is because the most massive galaxies are also the biggest and then their gradient gets even more steep when expressed in a scale that takes into account the size.

Our gradients in dex kpc⁻¹ show amplitudes similar to the observations used in Ho et al. (2015) and also simulations from Tissera et al. (2016) and Ma et al. (2016b), but the trend with stellar mass is reversed with respect to the two former studies (and in agreement with the latter), suggesting that the MaGICC dwarfs have been mixed too efficiently, giving them gradients which are flatter than the ones of their massive counterparts, in contrast to data from Ho et al. (2015). The discrepancy may just be due to the increased scatter and big errors at the low mass range in Ho et al. (2015), or due to the low number statistics in both observations and simulations.

MaGICC galaxies fulfil scaling relations like Tully-Fisher and mass-metallicity

but do not reproduce the measured metallicity distribution. The total metal content is consistent with empirical scaling relations (Pilkington et al. 2012b), but distributed incorrectly.

The disparity between observational data and our simulations could imply that we need a mass-dependent modulation of the feedback efficiency, in order to recover the mass-dependent gradient trend. One could thereafter calibrate that using the observations as a guide. This would be a powerful constraint on feedback and how it varies with mass. The feedback used in the fiducials is too strong for the dwarfs, and we should not use the same feedback recipe for the whole mass spectrum.

The fiducial suite has an increased feedback when compared to older simulations as for example MUGS (Stinson et al. 2010). Basically, when using weak feedback baryons born and die in the same point (or very close). In the centre of galaxies there are more star generations, and therefore metallicity is higher. This type of feedback does not distribute nor pull metals away and therefore it makes steeper negative metallicity gradients. High feedback, however, pushes the metals around and flattens the gradients. Thus, the baryonic cycle is different in each case. In figure 5 of Stinson et al. (2012), they show that MaGICC feedback reproduces some observational results, while the trend is not fitted any more when lowering feedback. This is not in disagreement with our idea of lowering feedback for low mass galaxies, as the observations in that figure are from high mass systems.

There is an interplay between the high star formation efficiency and strong feedback in galaxies. Lowering the star formation efficiency for the lowest mass simulations could also help fit the observational trends, as this makes gradients steeper as well. In summary, the most suitable solution would be to make mass dependent star formation efficiency and/or feedback simulations in the future, being careful to not violate the galactic scaling relations.

Chapter 5

GENERAL CONCLUSIONS

In this thesis we have focused on the distribution of the chemical abundances in disc galaxies, in order to improve the understanding about the evolution of such systems. We have studied (a) the metallicity gradients in the stars of thick discs through a detailed analysis of both real data and simulations, and (b) the metallicity in the cold gas-phase disc using a fiducial set of simulations. We have worked with observations from the CALIFA survey, and cosmological simulations from MaGICC, MUGS and RAMSES-CH.

First we study the thick disc of simulations and external galaxies. We look at the radial metallicity gradient with height in both samples. Chemodynamical simulations seem to reproduce the behaviour of the Milky Way, specially our simulations with higher feedback. The radial metallicity gradient is negative in the mid-plane of these galaxies (the inner area is more metal-rich than the outer counterpart), which is explained by the inside-out disc evolution. When increasing height the trend gets flat and then eventually inverts, finding lower metallicity stars at smallest radii. According to the simulations, this happens due to a population of young and metal-rich stars born in situ in the outer thick disc, which is missing in the inner part. These are superimposed upon older migrators coming from the inner thick disc, and that population can be found in its inner counterpart as well. On the other hand, in the

thin disc the metal-rich in situ population dominates at all radii. The fact that the outermost thick and thin discs are very similar makes us conclude that the stars of our simulations flare. In this study we also find out that our galaxies show no clear correlation between the vertical metallicity gradients in the thick disc and radius, in line with the results from the Milky Way. Kinematically, only one of our simulations predicts the same behaviour as the Galaxy for the rotational velocity with increasing height from the plane. This work was carried out by selecting the thick disc both spatially and by chemistry, and we can state that our conclusions are robust to the selection criteria.

The situation is quite different when looking at the gradients for the real data of the external galaxies we study from the CALIFA survey. In this case both the metallicity and age radial gradients show diverse behaviours when moving up from the mid-plane. Some galaxies follow the same trend as the Milky Way and simulations, but others do not. In our set, we find radial age gradients which decrease with height and others that increase. When analysing the radial metallicity gradients there is a wider consensus, all the galaxies except one having an increasing trend when moving higher from the mid-plane. All in all, the disc (and thick disc in particular) formation might be complex and various mechanisms might affect it. Then, the specific characteristics of each galaxy, like the environment, its mass, etc, might be essential in determining the resulting state. Simulations are still not able to reproduce these different results. We also find that all our galaxies suffer velocity lag at high heights, thus suggesting the thick disc existence. Our sample fulfils a relation between the scalelength and velocity lag, indicating that galaxies with a steeper light profile will have an increased lag in their thick discs. There is also a relation between the maximum line-of-sight velocity and scalelength, with maximum line-of-sight velocity increasing rapidly with scalelength until a maximum is reached and then decreasing smoothly.

We also study the difference in the radial abundance gradient of the cold gas-phase disc for a suite of simulations spanning a wide range in mass. Observational works find that low mass galaxies have a more steep negative metallicity gradient than their massive counterparts, when the gradients are expressed in an absolute distance scale, which goes in disagreement with what we find in our set. We see that simulated dwarf galaxies have the flattest gradients, and this trend does not change with redshift. We conclude that the feedback prescription in the simulations we have analysed is too strong for the lowest mass galaxies and thus it mixes the metals too efficiently, making the gradients flat. When expressing the gradient in a relative scale that takes into account the galaxy size, the observational trend between the metallicity gradient and mass disappears and all galaxies seem to have a universal metallicity gradient. In the case of our simulations, conversely, the same trend of flattening gradients for lower masses remains for both scales previously mentioned (absolute scale expressed in kpc and relative scale in $R25$). We propose a mass-dependent modulation of feedback and/or star formation efficiency in simulations might eradicate the inconsistency.

Simulations are a very powerful and valuable tool in order to give us new details, but nowadays they are not perfect and they do not reproduce the measured trends in some cases. An effort should be made to improve and implement them, for example trying to run a set of galaxies with a mass-modulated feedback. Furthermore, for the purpose of drawing solid conclusions we must have bigger samples both in simulations and observations, because low number statistics may be influencing our results. Even so, we can assert that the samples used in this thesis are big and robust enough to make an advance in science and make an approximate idea of the topic under study. Developing solutions to the problems encountered in simulations and observations at the same time, and using both approaches as a complement to each other, we will climb up and solve the mysteries in a faster pace.

This field still has a lot of work to do in order to answer some basic questions, as ‘How did the thick disc form?’, ‘Is the thick disc an ubiquitous component of disc galaxies?’, ‘How can we improve our simulations so that they completely match the observations?’. These questions are really challenging and answering them will make a big step in astronomy.

Appendix A

EXTRA MATERIAL

REGARDING CHAPTER 2

A.1 Figures of MaGICC–g15784

In this section we present some additional information for the galaxy which best matches the Milky Way, MaGICC–g15784.

First we show in Fig. A.1 the change in metallicity when increasing radius. We illustrate all disc stars from the centre of the galaxy up to $r = 20$ kpc. Starting from the top-left panel, end moving down, and then right, the value of $|z|$ increases, as indicated in each panel. The black line is the profile and the red one the fitting in the radial range $5 < r < 10$ kpc. These latter ones correspond to the red triangles in Fig. 2.2. We can see that moving through the panels, the slope of this line increases and then inverts, as we present more clearly in Fig. 2.2.

Figure A.2 is the same as Fig. A.1, but showing the $[O/Fe]$ radial profile instead of the $[Fe/H]$. It is related to Fig. 2.5. The red lines here correspond to the red triangles in that figure.

Finally we present the metallicity in terms of height above the mid-plane in

Fig. A.3. It is the detailed analysis of Fig. 2.6, and each red triangle in that image corresponds to one of the red lines here. We remind the reader that these images exhibit the vertical metallicity gradients only for the spatially selected thick disc. Starting from the top-left and moving down, and then right, we are going to larger values of the radius. The black lines show the profile for all disc stars up to $|z| = 5$ kpc.

A.2 Tables

This section contains Tables A.1, A.2, A.3 and A.4, which present the values for Figs. 2.2, 2.4, 2.5 and 2.6, in the same order as they appear throughout the text.

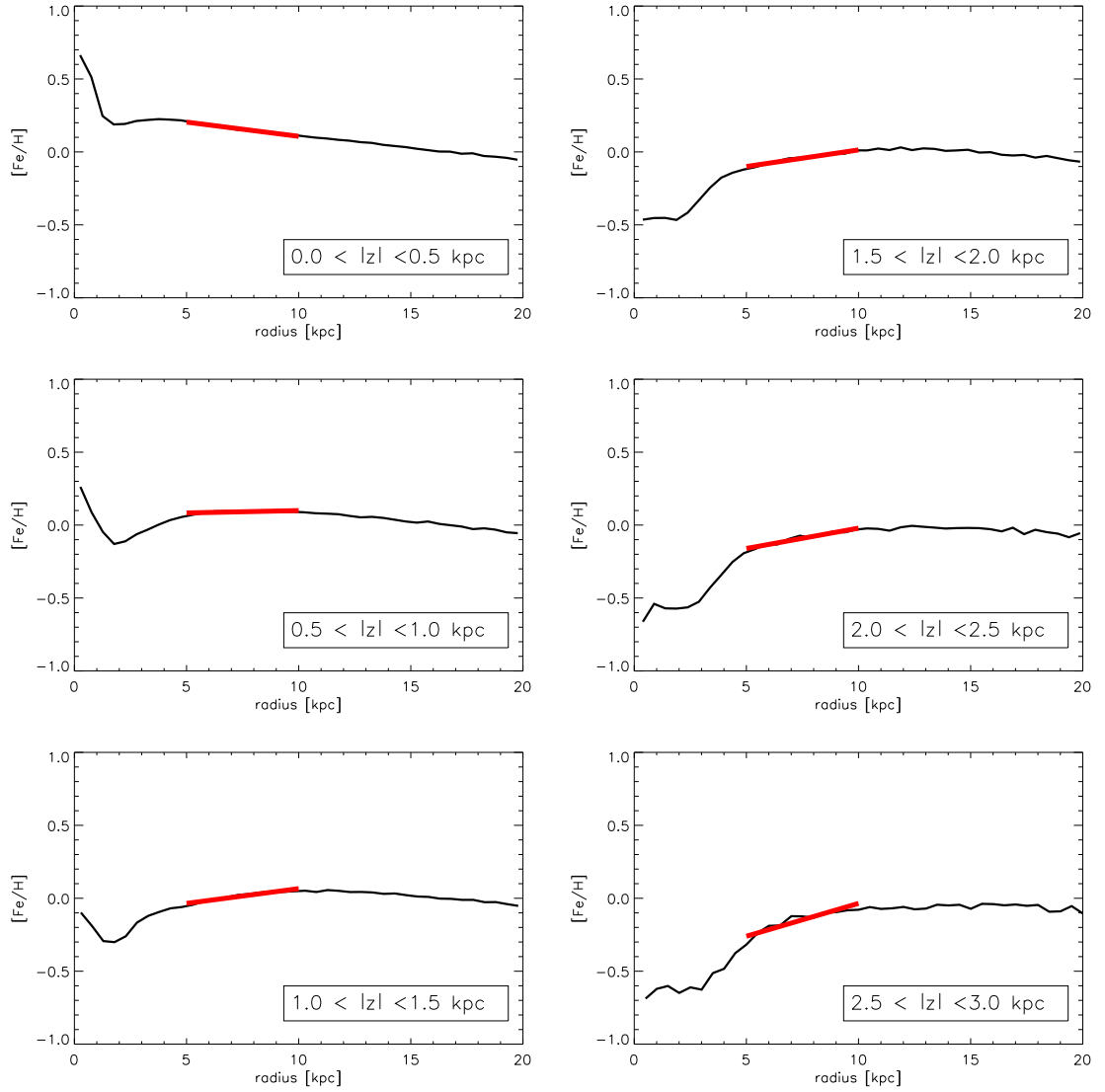
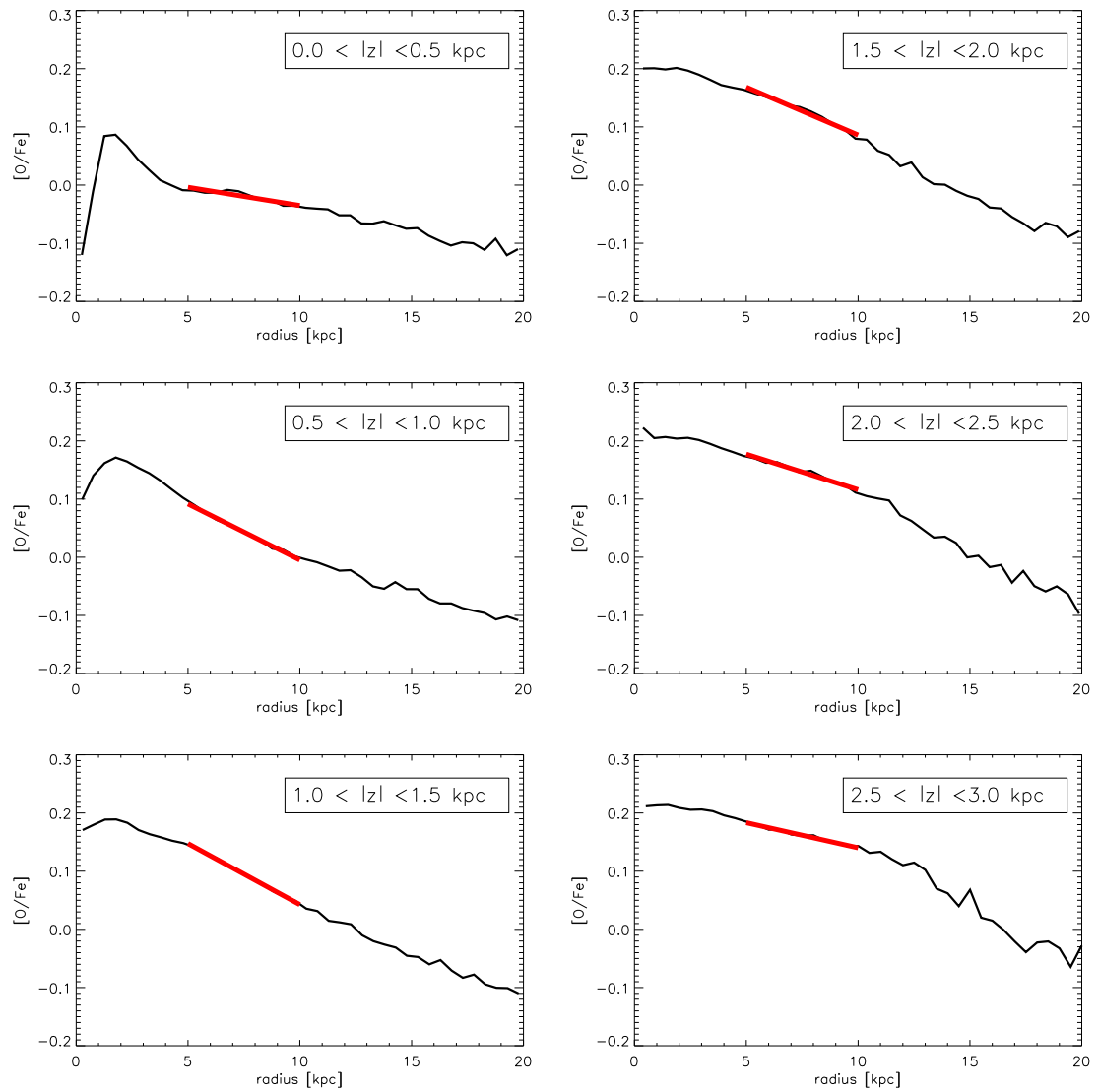


Figure A.1: Radial metallicity profile for all disc stars in the radial range $r < 20$ kpc, for galaxy MaGICC-g15784. Starting from the top-left panel, and moving down, and then right, we are shifting to higher heights from the mid-plane, as indicated in the inset of each panel.

Figure A.2: Same as Fig. A.1 but for $[O/Fe]$.

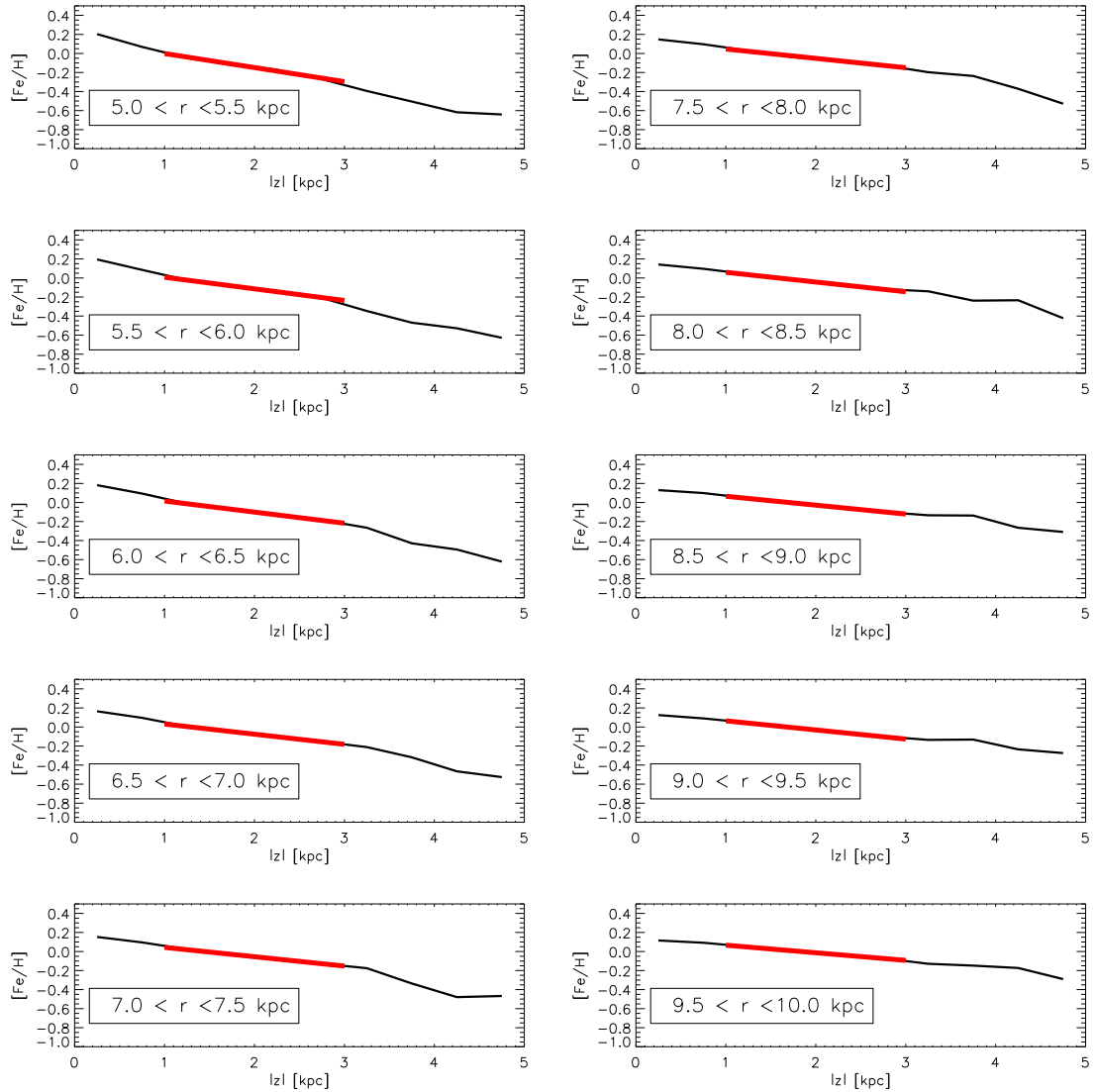


Figure A.3: Vertical metallicity with increasing radius for galaxy MaGICC-g15784. In each panel, the profile for all disc stars is shown in black, and the fit for the thick disc ($1 < |z| < 3$ kpc) in red.

d[Fe/H] / dr					
	MUGS-g1536	MUGS-g15784	MaGICC-g1536	MaGICC-g15784	109-CH
$ z < 0.5$ kpc	-0.042	-0.018	-0.019	-0.019	-0.012
$0.5 < z < 1.0$ kpc	-0.040	-0.007	-0.011	0.003	-0.002
$1.0 < z < 1.5$ kpc	-0.035	-0.005	-0.003	0.020	0.006
$1.5 < z < 2.0$ kpc	-0.026	-0.002	0.011	0.023	0.007
$2.0 < z < 2.5$ kpc	-0.025	-0.005	0.025	0.028	0.008
$2.5 < z < 3.0$ kpc	-0.011	-0.005	0.035	0.045	0.018

Table A.1: [Fe/H] radial gradients with increasing height for our five simulated Milky Way-like galaxies, measured in the radial range $5 < r < 10$ kpc. The values are in dex kpc⁻¹.

d[Fe/H] / dr for MaGICC–g15784				
[O/Fe]	> -0.05	> 0.05	> 0.15	< -0.05
$ z < 0.5$ kpc	-0.004	0.000	0.001	-0.034
$0.5 < z < 1.0$ kpc	0.004	0.006	0.004	-0.030
$1.0 < z < 1.5$ kpc	0.012	0.011	0.009	-0.028
$1.5 < z < 2.0$ kpc	0.015	0.013	0.011	-0.037
$2.0 < z < 2.5$ kpc	0.024	0.021	0.017	-0.051
$2.5 < z < 3.0$ kpc	0.035	0.035	0.029	-0.029

Table A.2: Same as Table A.1, but considering sub-populations selected by [O/Fe], for galaxy MaGICC–g15784. [O/Fe] is given in dex and the gradients in dex kpc⁻¹. The four chemical conditions studied are: [O/Fe] > -0.05 dex, [O/Fe] > 0.05 dex, [O/Fe] > 0.15 dex, and [O/Fe] < -0.05 dex.

d[O/Fe] / dr					
	MUGS-g1536	MUGS-g15784	MaGICC-g1536	MaGICC-g15784	109-CH
$ z < 0.5$ kpc	-0.003	-0.004	-0.000	-0.006	-0.001
$0.5 < z < 1.0$ kpc	-0.006	-0.009	-0.002	-0.019	-0.003
$1.0 < z < 1.5$ kpc	-0.013	-0.009	-0.003	-0.021	-0.005
$1.5 < z < 2.0$ kpc	-0.011	-0.009	-0.006	-0.016	-0.004
$2.0 < z < 2.5$ kpc	-0.010	-0.008	-0.006	-0.012	-0.004
$2.5 < z < 3.0$ kpc	-0.012	-0.008	-0.007	-0.009	-0.007

Table A.3: [O/Fe] radial gradients (in dex kpc⁻¹) with increasing height for our five simulated Milky Way-like galaxies. The radial range used is $5 < r < 10$ kpc.

	d[Fe/H] / d z				
	MUGS-g1536	MUGS-g15784	MaGICC-g1536	MaGICC-g15784	109-CH
5.0 < r < 5.5 kpc	-0.046	-0.040	-0.229	-0.148	-0.138
5.5 < r < 6.0 kpc	-0.038	-0.031	-0.203	-0.122	-0.180
6.0 < r < 6.5 kpc	-0.052	-0.016	-0.193	-0.117	-0.088
6.5 < r < 7.0 kpc	-0.049	-0.048	-0.173	-0.107	-0.085
7.0 < r < 7.5 kpc	-0.053	-0.023	-0.166	-0.098	-0.101
7.5 < r < 8.0 kpc	-0.022	-0.023	-0.130	-0.098	-0.097
8.0 < r < 8.5 kpc	-0.017	-0.030	-0.127	-0.102	-0.093
8.5 < r < 9.0 kpc	0.012	-0.025	-0.132	-0.093	-0.084
9.0 < r < 9.5 kpc	-0.002	-0.034	-0.105	-0.096	-0.113
9.5 < r < 10.0 kpc	-0.005	-0.025	-0.115	-0.080	-0.088

Table A.4: [Fe/H] vertical gradients with increasing radius for our five simulated Milky Way-like galaxies. We have selected the disc stars with height $1 < |z| < 3$ kpc. The unit used for the gradients is dex kpc⁻¹.

Appendix B

EXTRA MATERIAL

REGARDING CHAPTER 3

In this appendix we include all the extra material related to the six CALIFA galaxies analysed in this thesis, say: age against radius, radial age gradient with height, metallicity against radius, radial metallicity gradient with height, velocity curve and surface brightness profile. The age and metallicity profiles and radial gradients are included twice, first weighted by light and then by mass. The trends weighted by mass have not been used throughout the study due to their lower accurateness when comparing to the light weighted ones. In the age (or metallicity) vs. radius panels we only fit an exponential when there really exists a trend; in the cases where there are not enough points or the scatter is big we do not make any fitting.

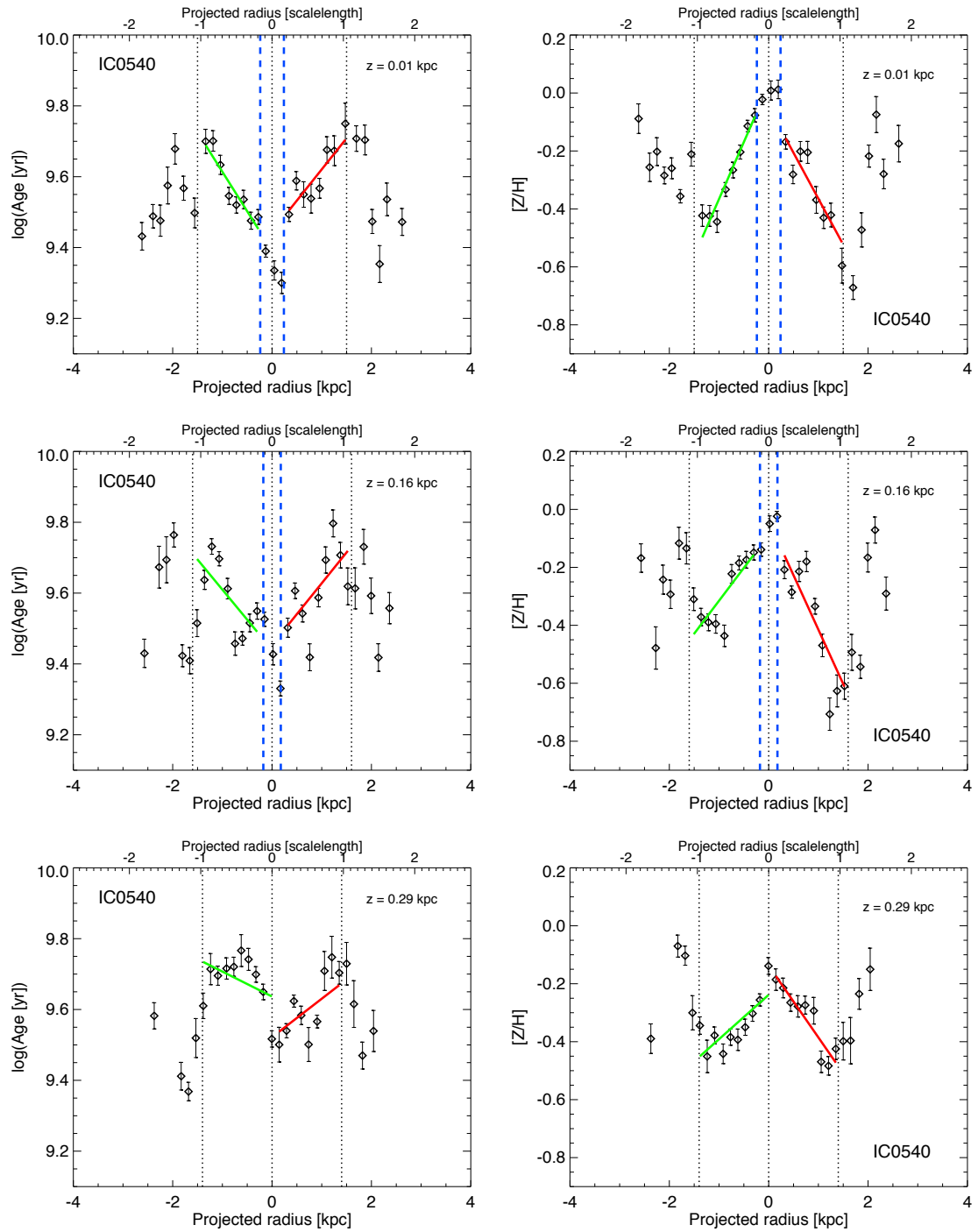


Figure B.1: Galaxy IC0540, age vs. radius on the left and metallicity vs. radius on the right – weighted by light

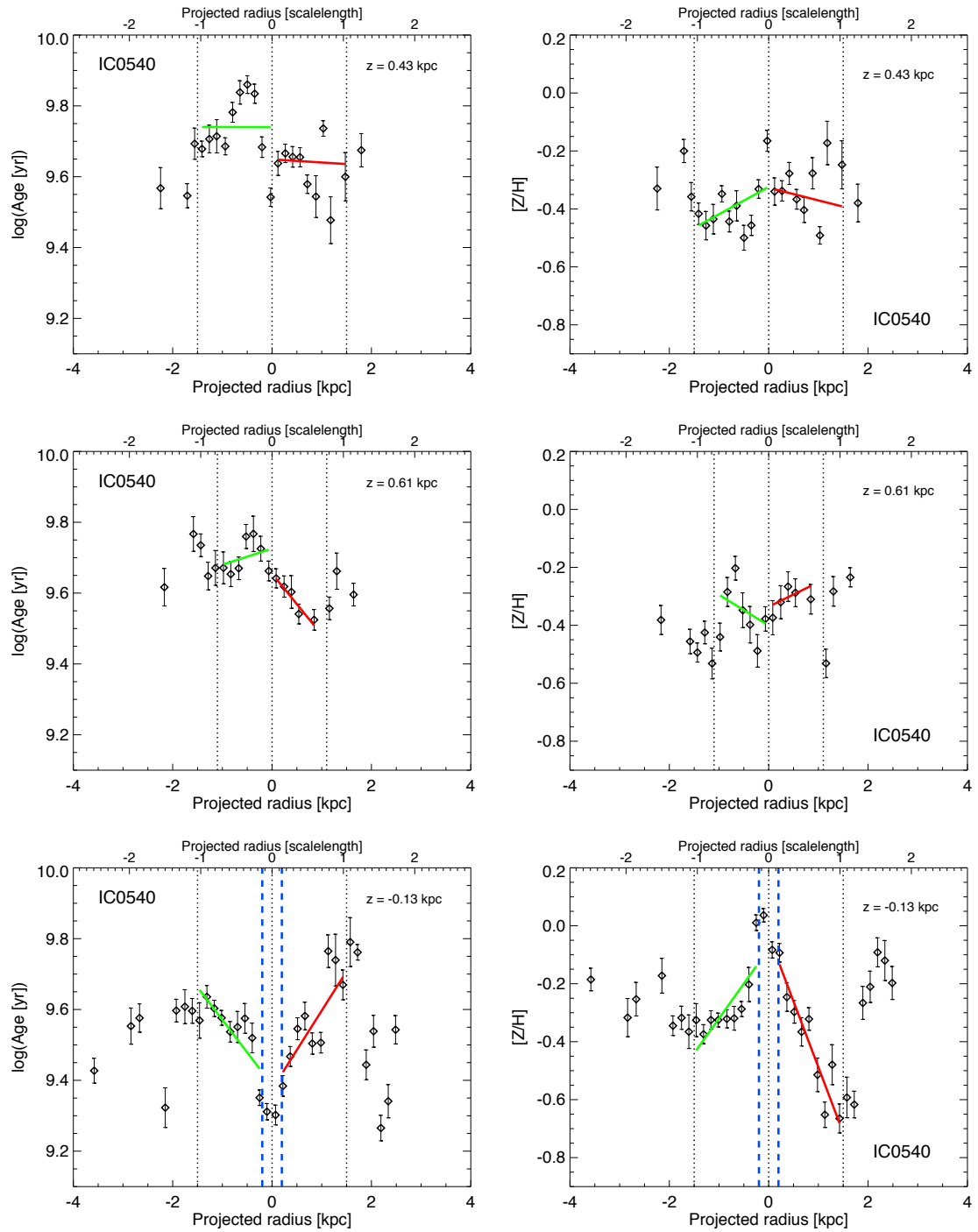


Figure B.2: Galaxy IC0540, age vs. radius on the left and metallicity vs. radius on the right – weighted by light

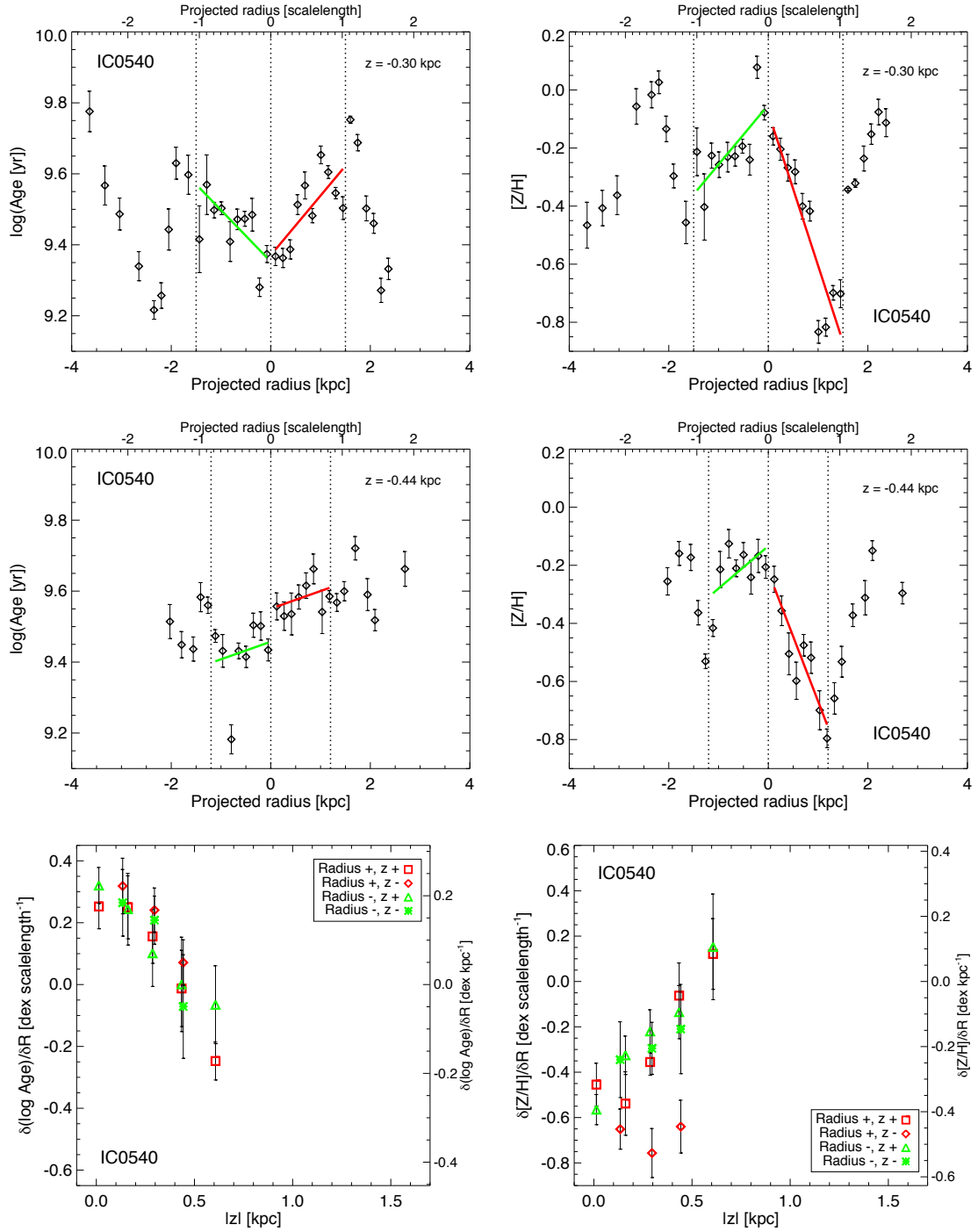


Figure B.3: Galaxy IC0540, age vs. radius on the left and metallicity vs. radius on the right. Bottom row: radial age gradient with height on the left and the same for metallicity on the right – weighted by light

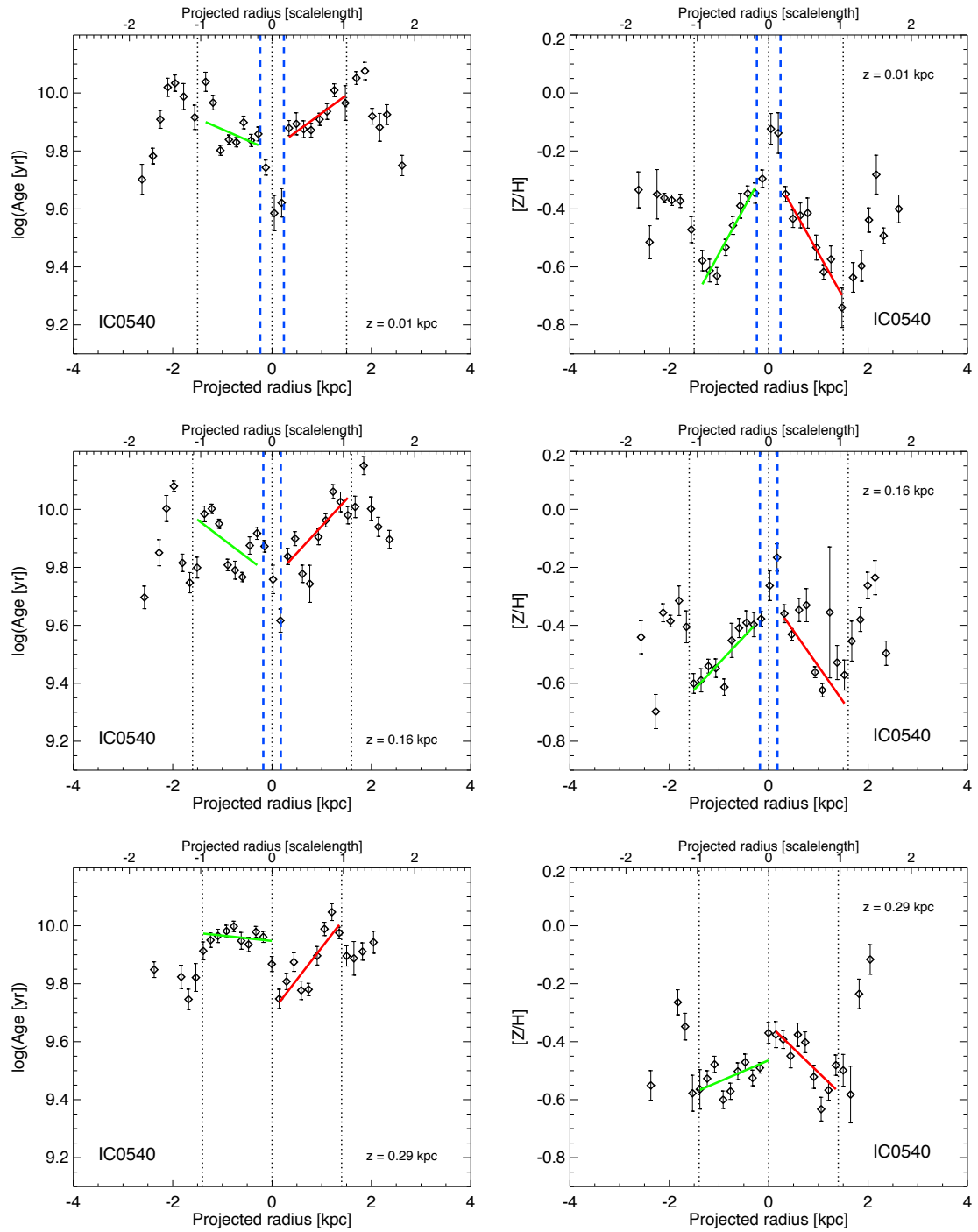


Figure B.4: Galaxy IC0540, age vs. radius on the left and metallicity vs. radius on the right – weighted by mass

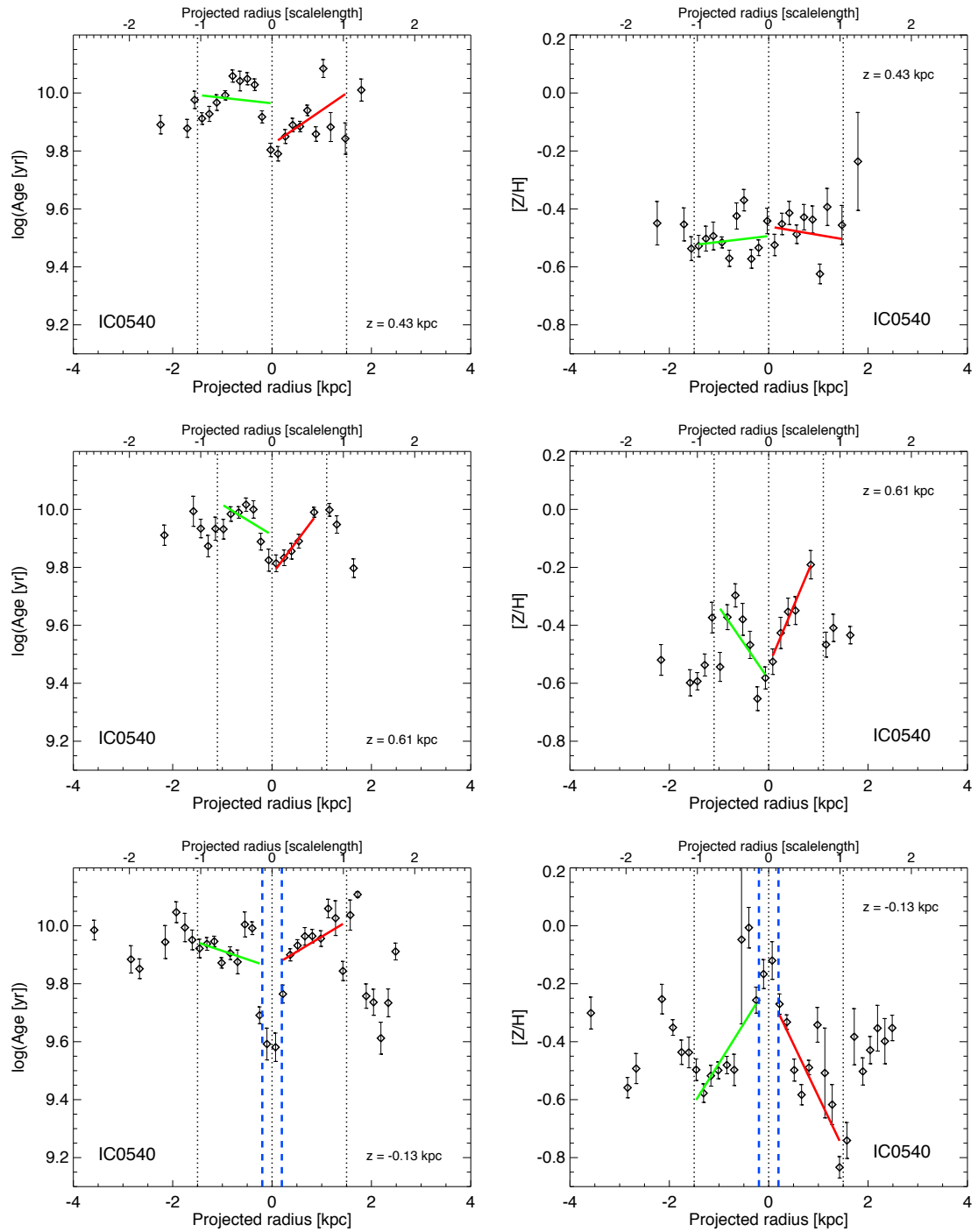


Figure B.5: Galaxy IC0540, age vs. radius on the left and metallicity vs. radius on the right – weighted by mass

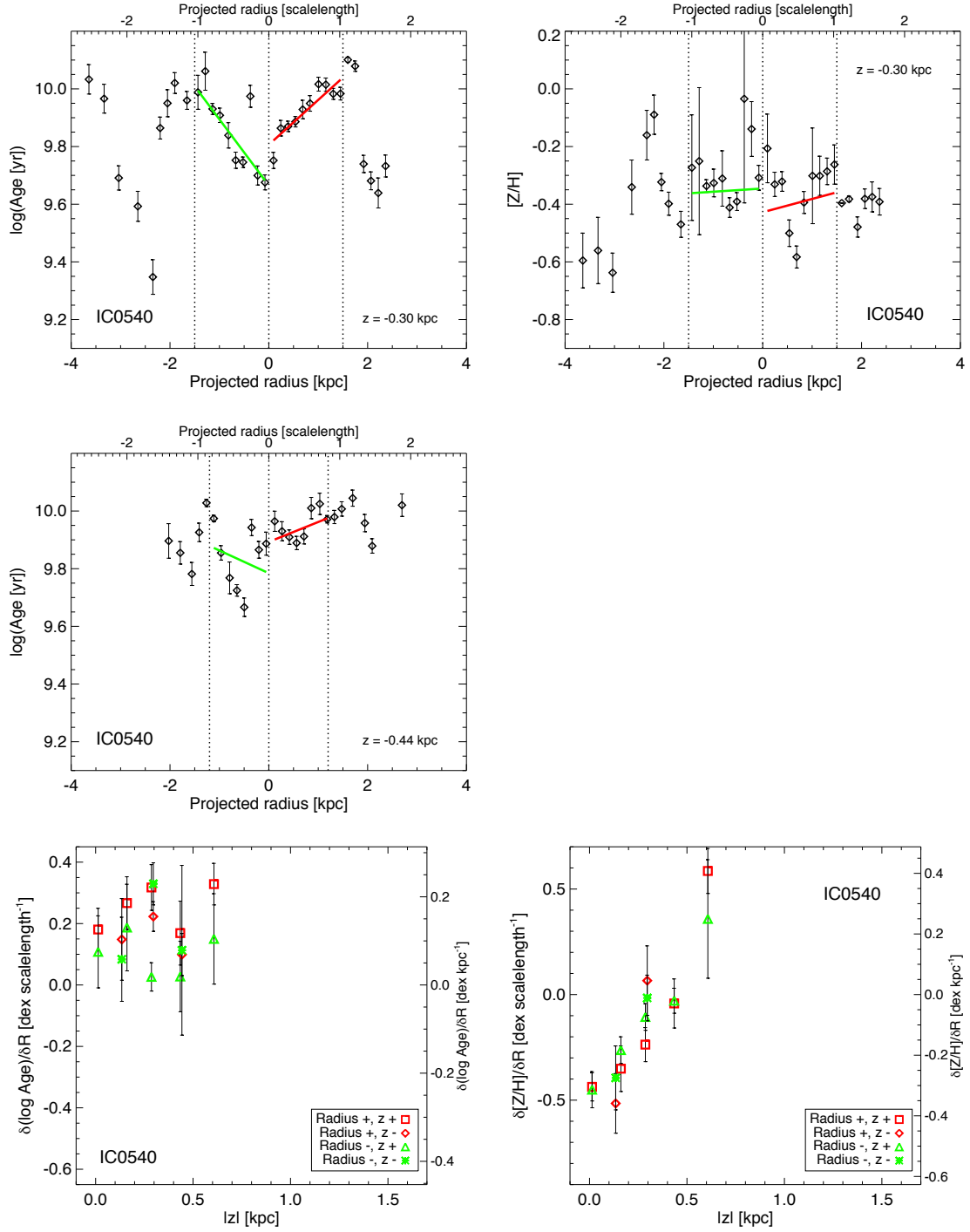


Figure B.6: Galaxy IC0540, age vs. radius on the left and metallicity vs. radius on the right. Bottom row: radial age gradient with height on the left and the same for metallicity on the right – weighted by mass

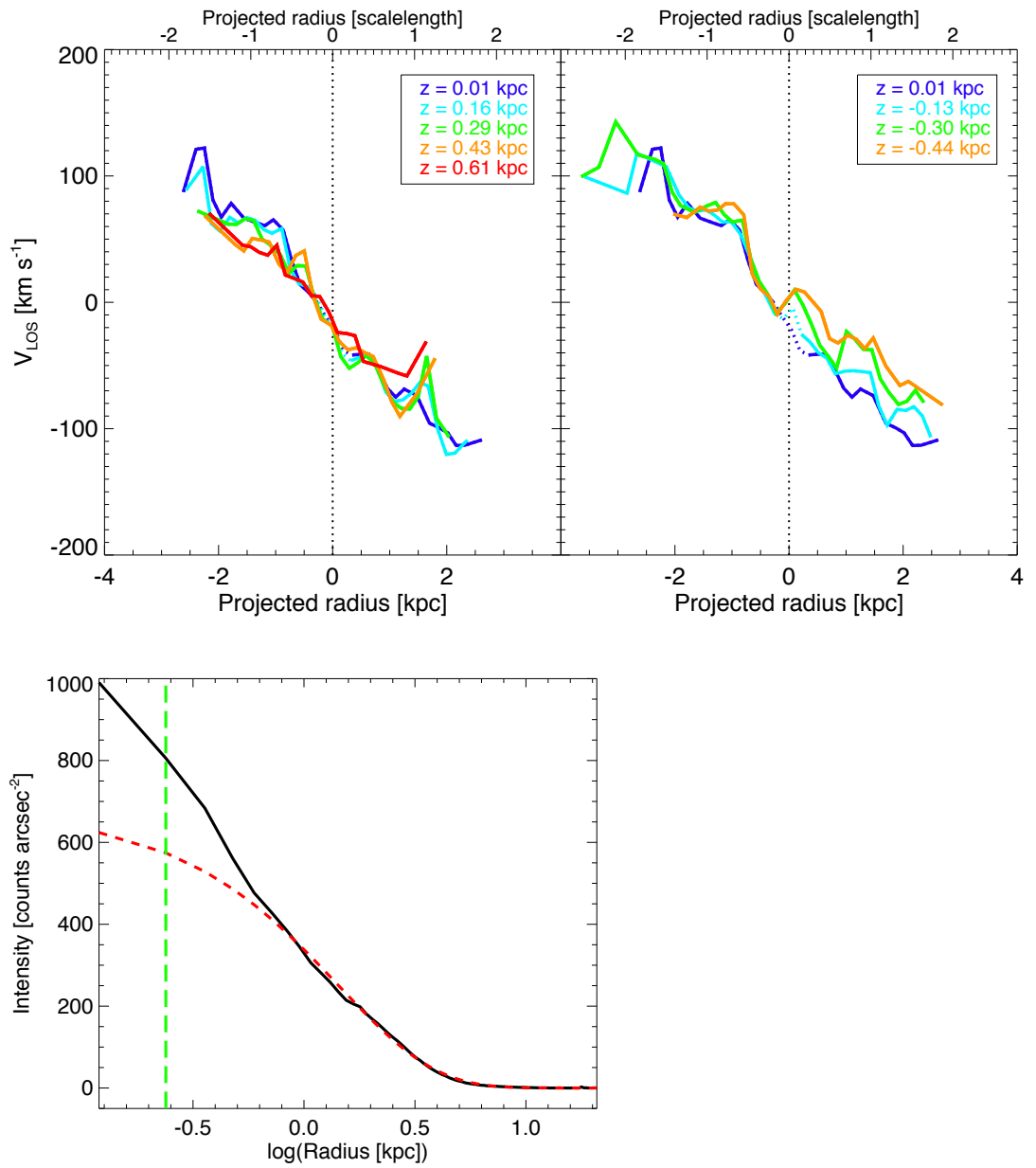


Figure B.7: Galaxy IC0540, rotation curve in the top and radial surface brightness profile in the bottom

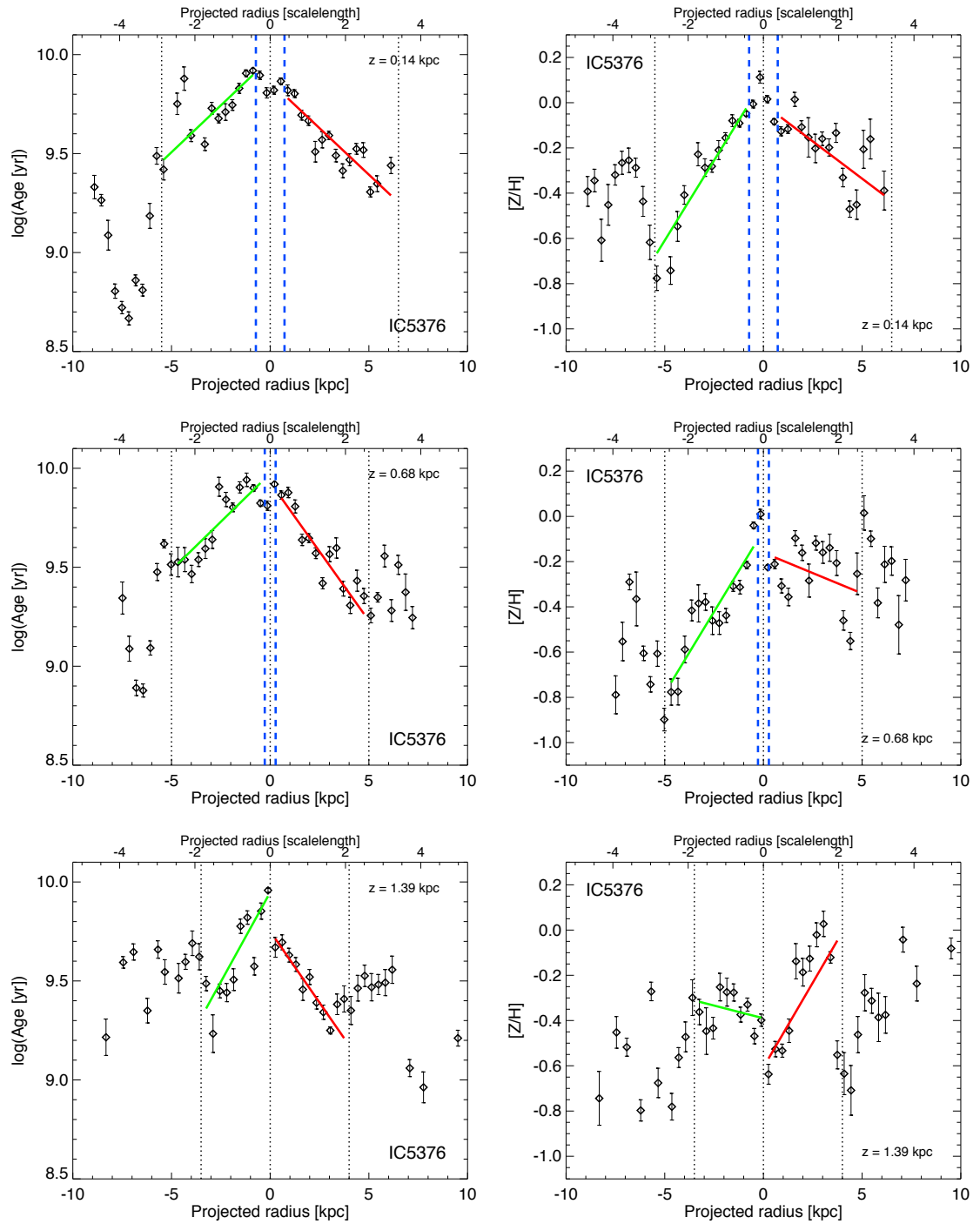


Figure B.8: Galaxy IC5376, age vs. radius on the left and metallicity vs. radius on the right – weighted by light

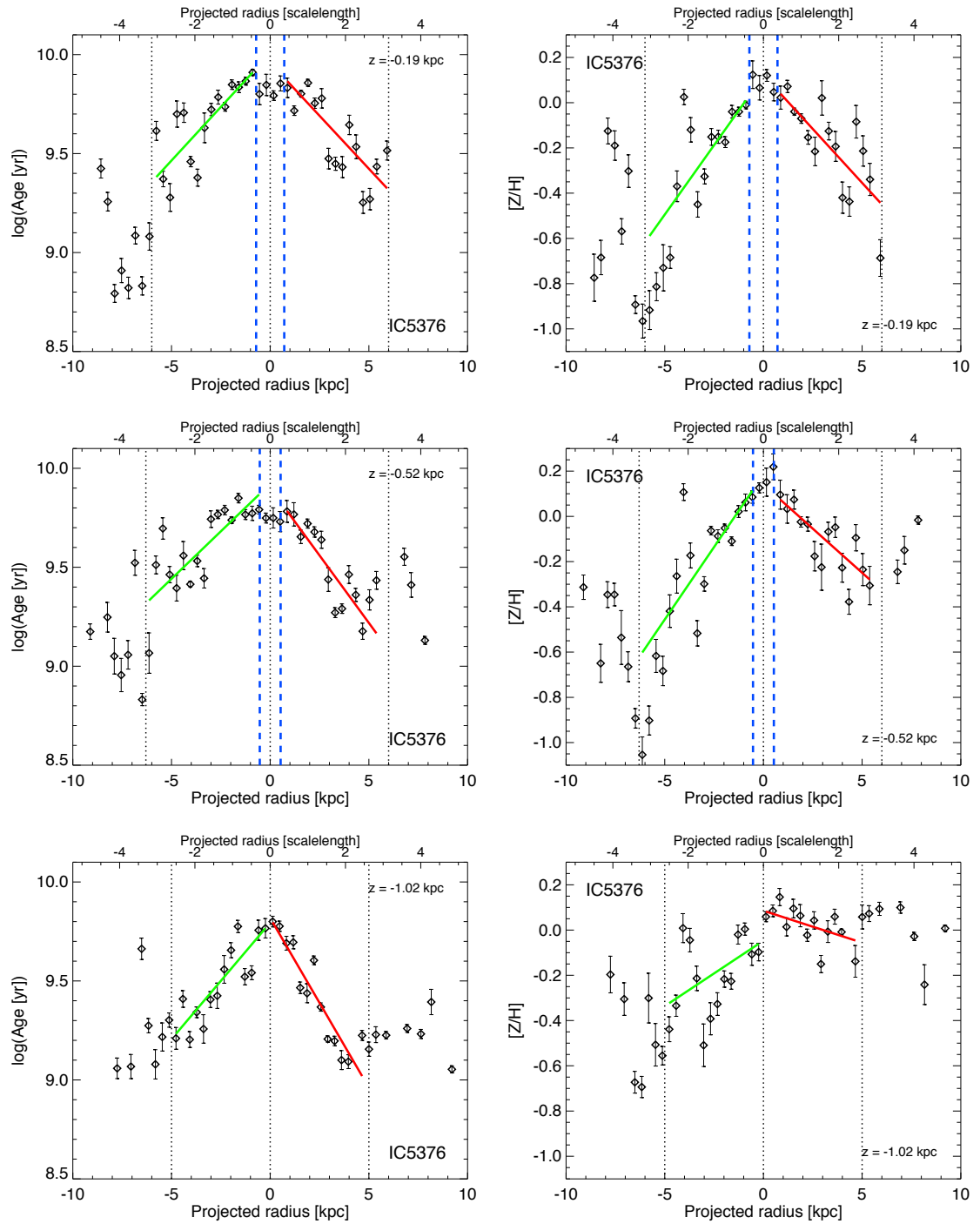


Figure B.9: Galaxy IC5376, age vs. radius on the left and metallicity vs. radius on the right – weighted by light

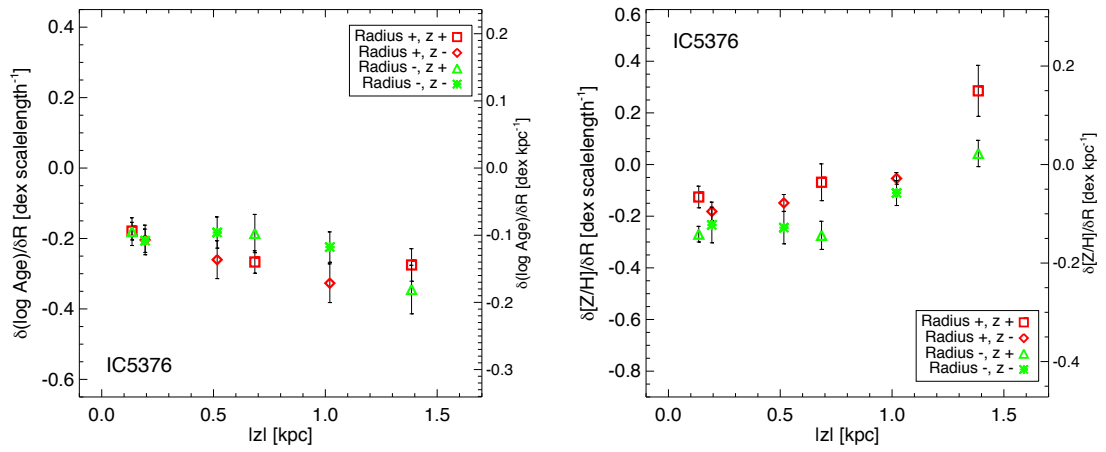


Figure B.10: Galaxy IC5376, radial age gradient with height on the left and the same for metallicity on the right – weighted by light

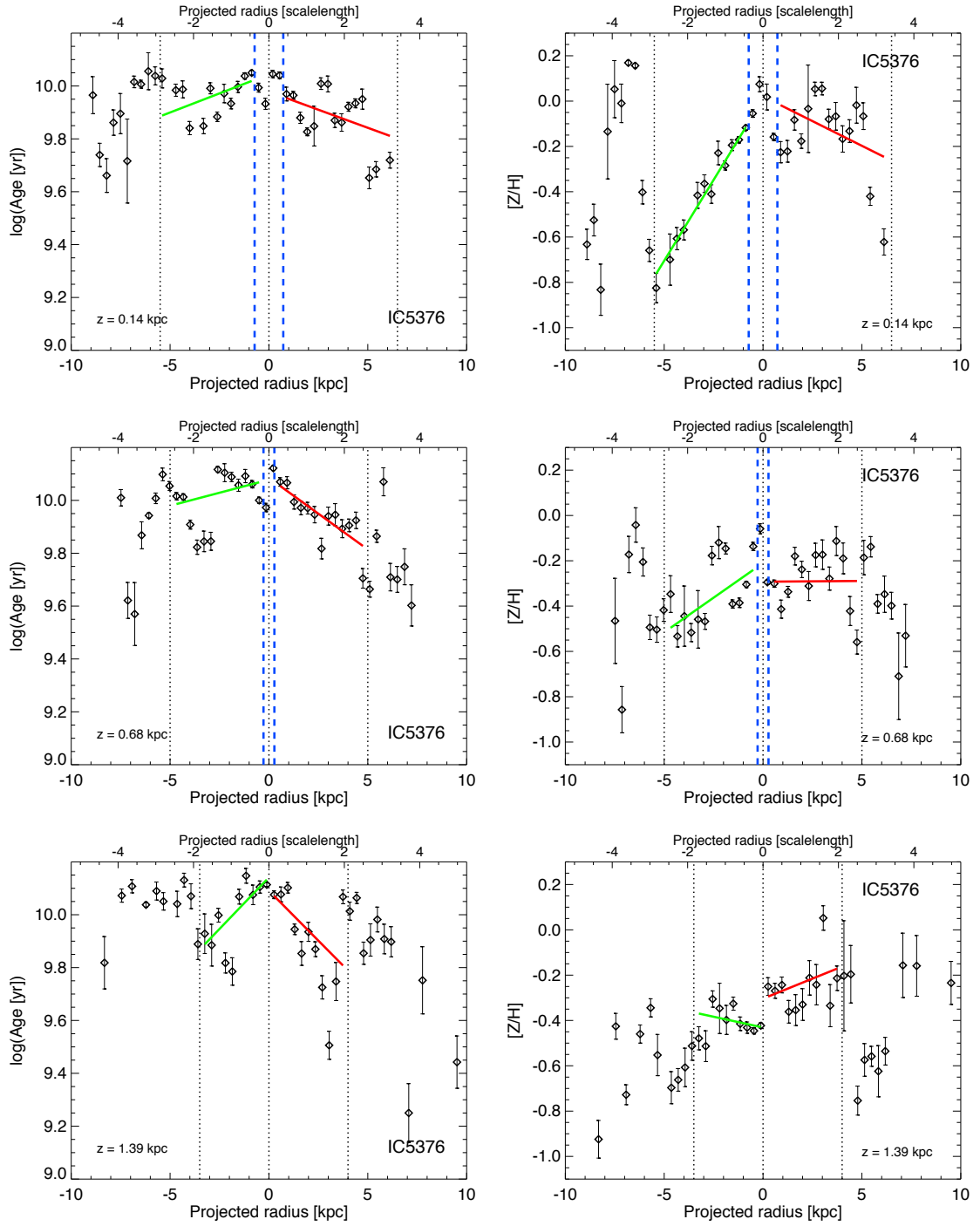


Figure B.11: Galaxy IC5376, age vs. radius on the left and metallicity vs. radius on the right – weighted by mass

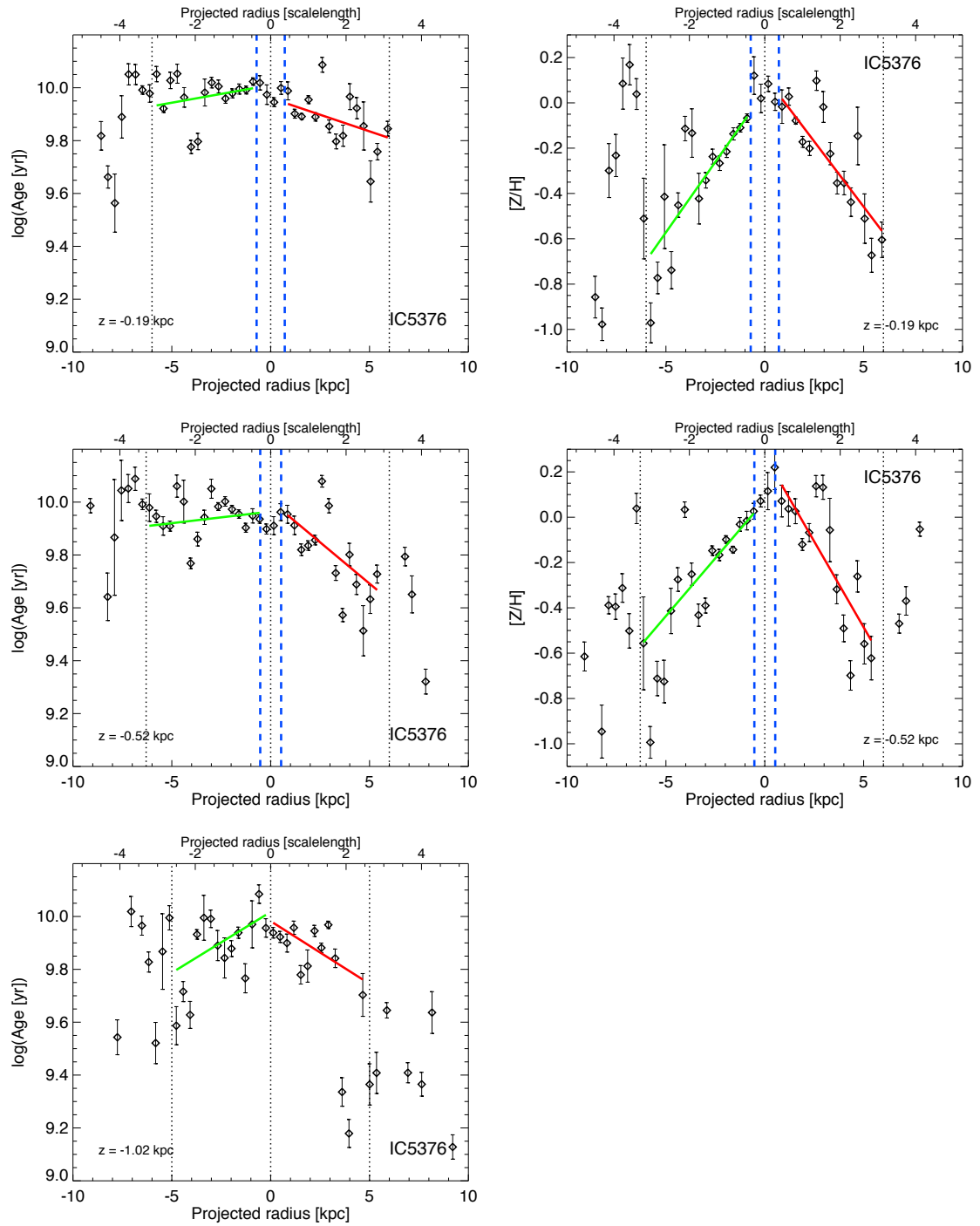


Figure B.12: Galaxy IC5376, age vs. radius on the left and metallicity vs. radius on the right – weighted by mass

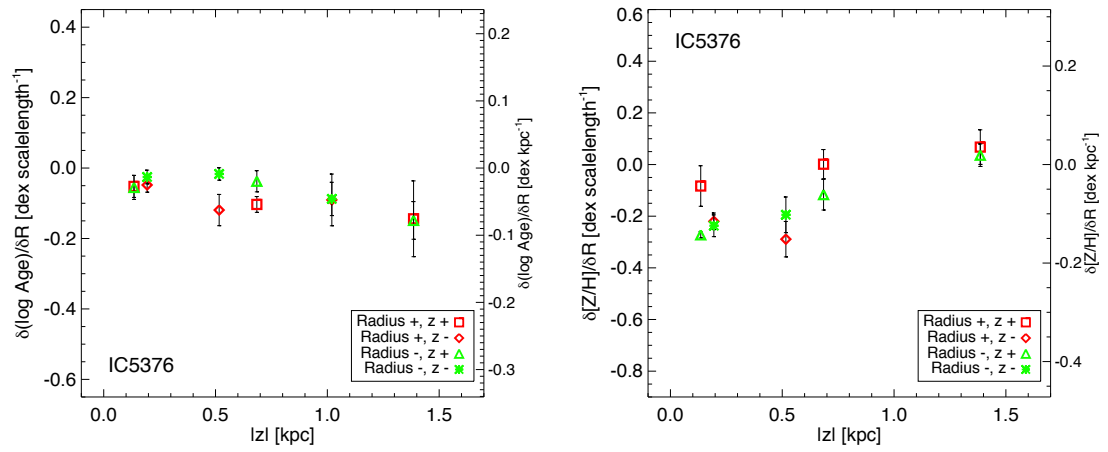


Figure B.13: Galaxy IC5376, radial age gradient with height on the left and the same for metallicity on the right – weighted by mass

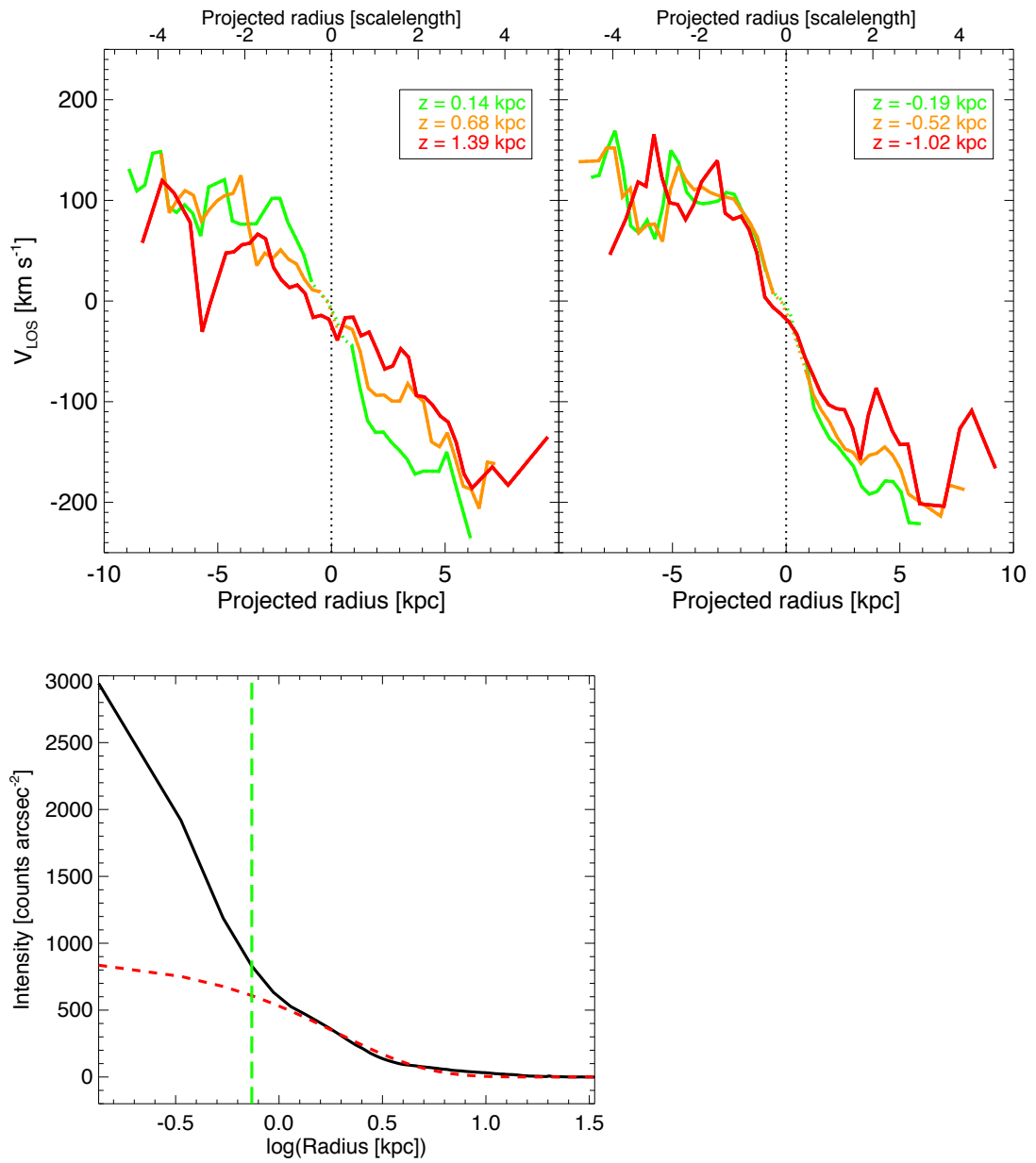


Figure B.14: Galaxy IC5376, rotation curve in the top and radial surface brightness profile in the bottom

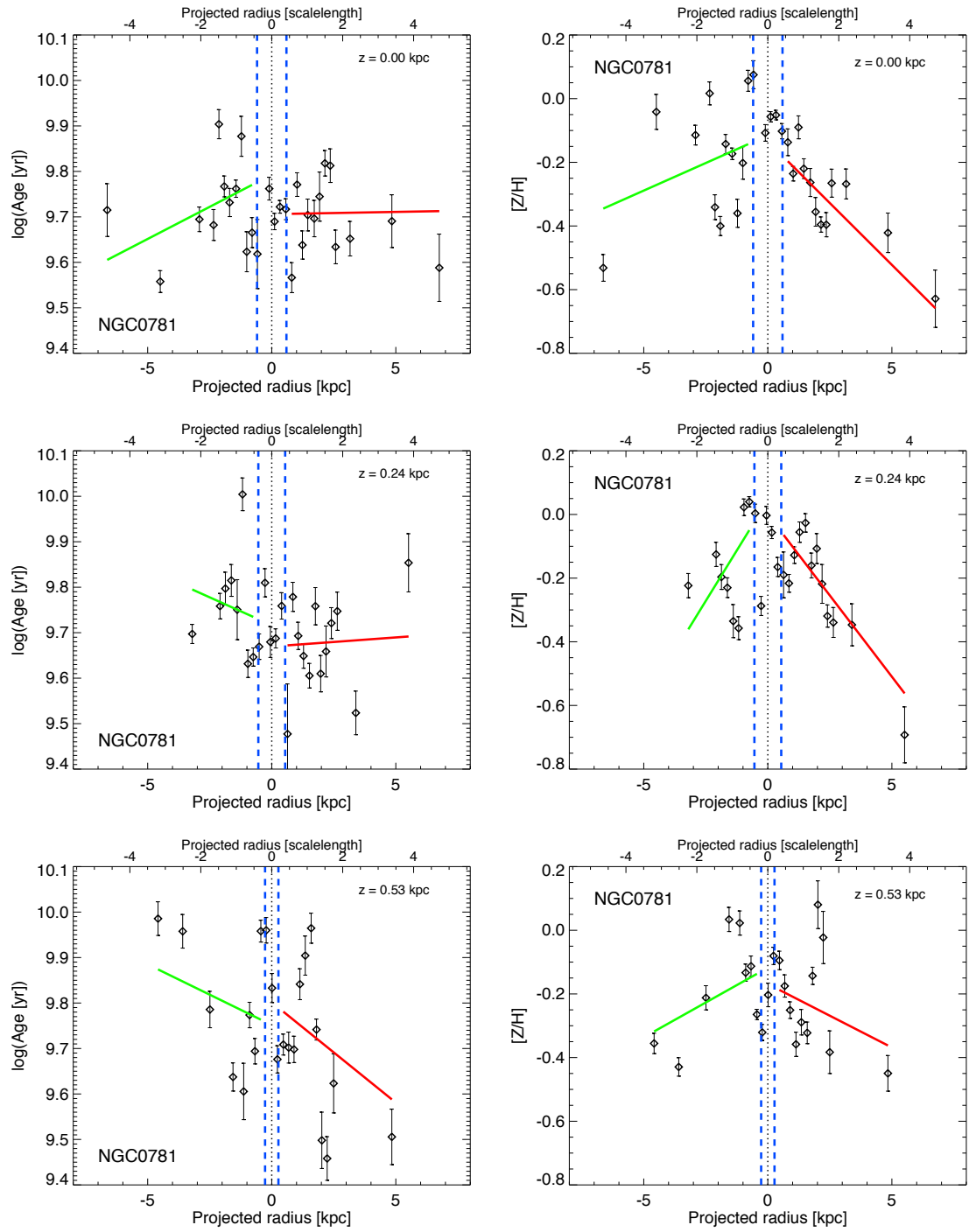


Figure B.15: Galaxy NGC0781, age vs. radius on the left and metallicity vs. radius on the right – weighted by light

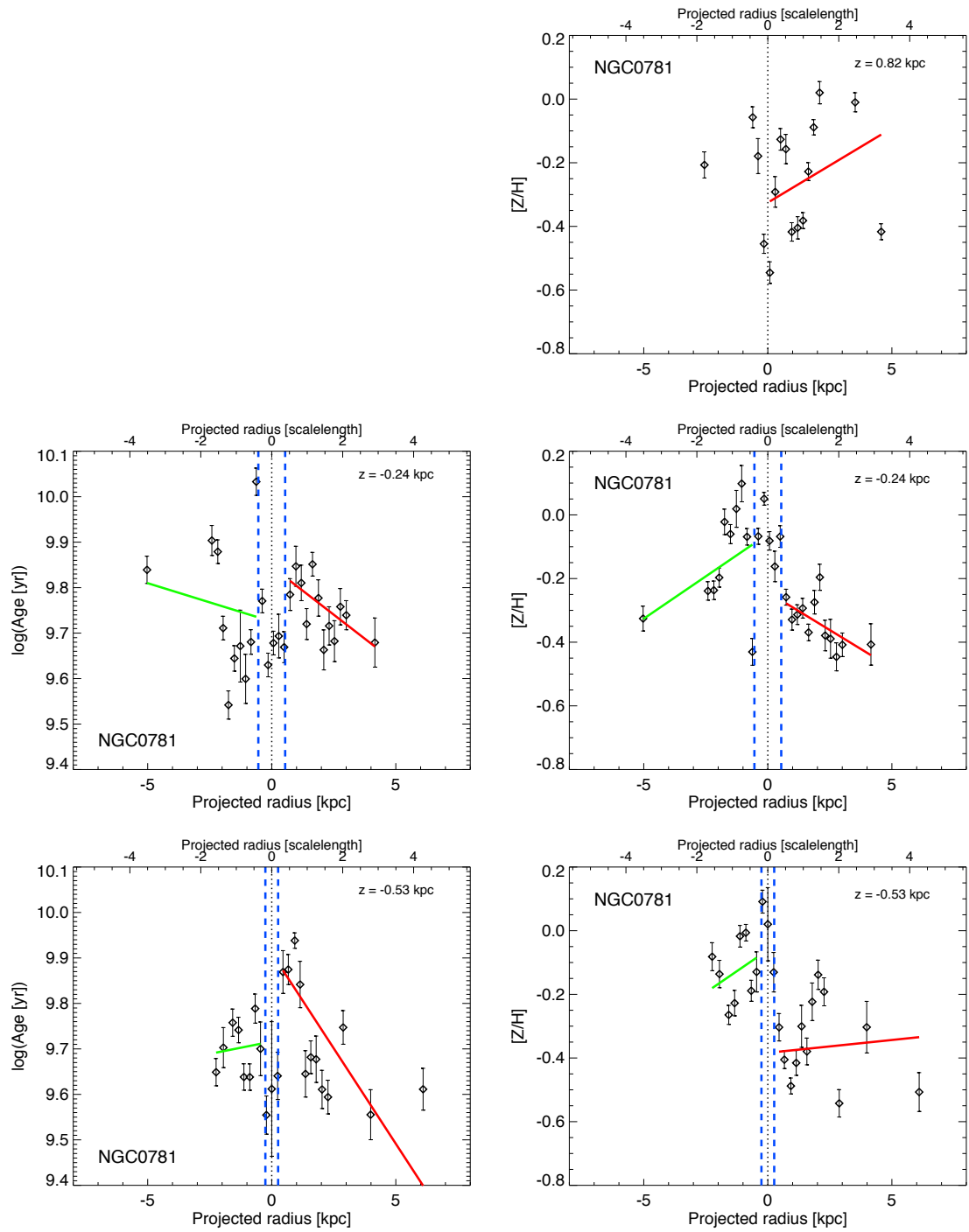


Figure B.16: Galaxy NGC0781, age vs. radius on the left and metallicity vs. radius on the right – weighted by light

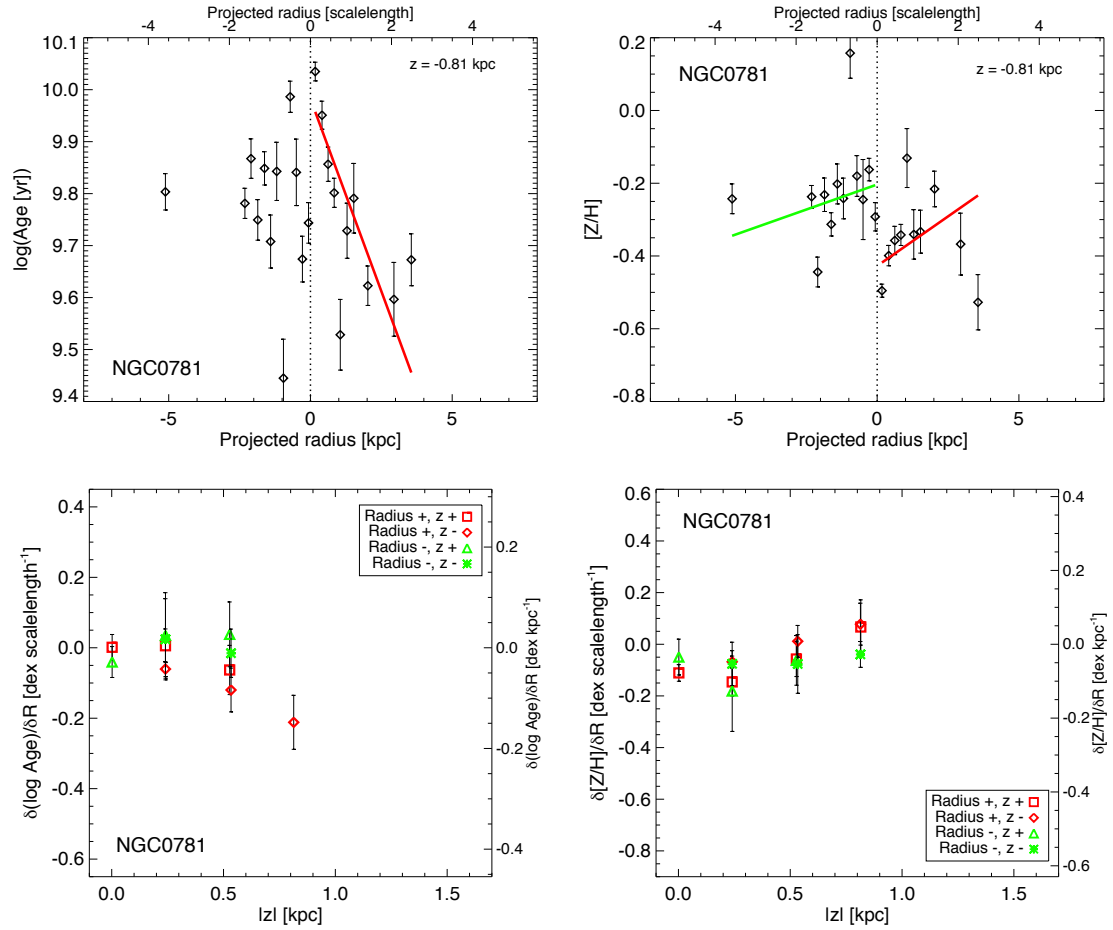


Figure B.17: Galaxy NGC0781, age vs. radius on the left and metallicity vs. radius on the right. Bottom row: radial age gradient with height on the left and the same for metallicity on the right – weighted by light

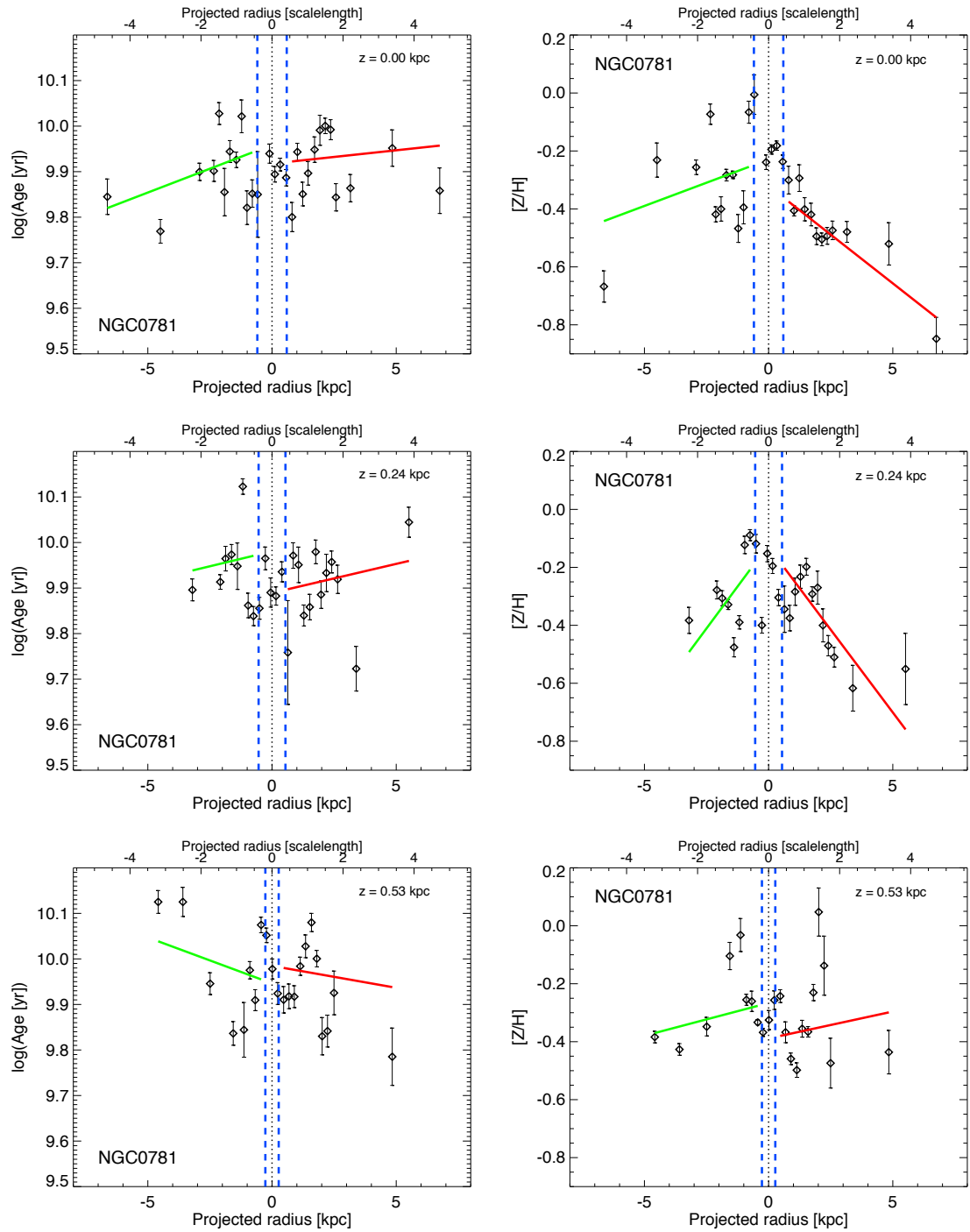


Figure B.18: Galaxy NGC0781, age vs. radius on the left and metallicity vs. radius on the right – weighted by mass

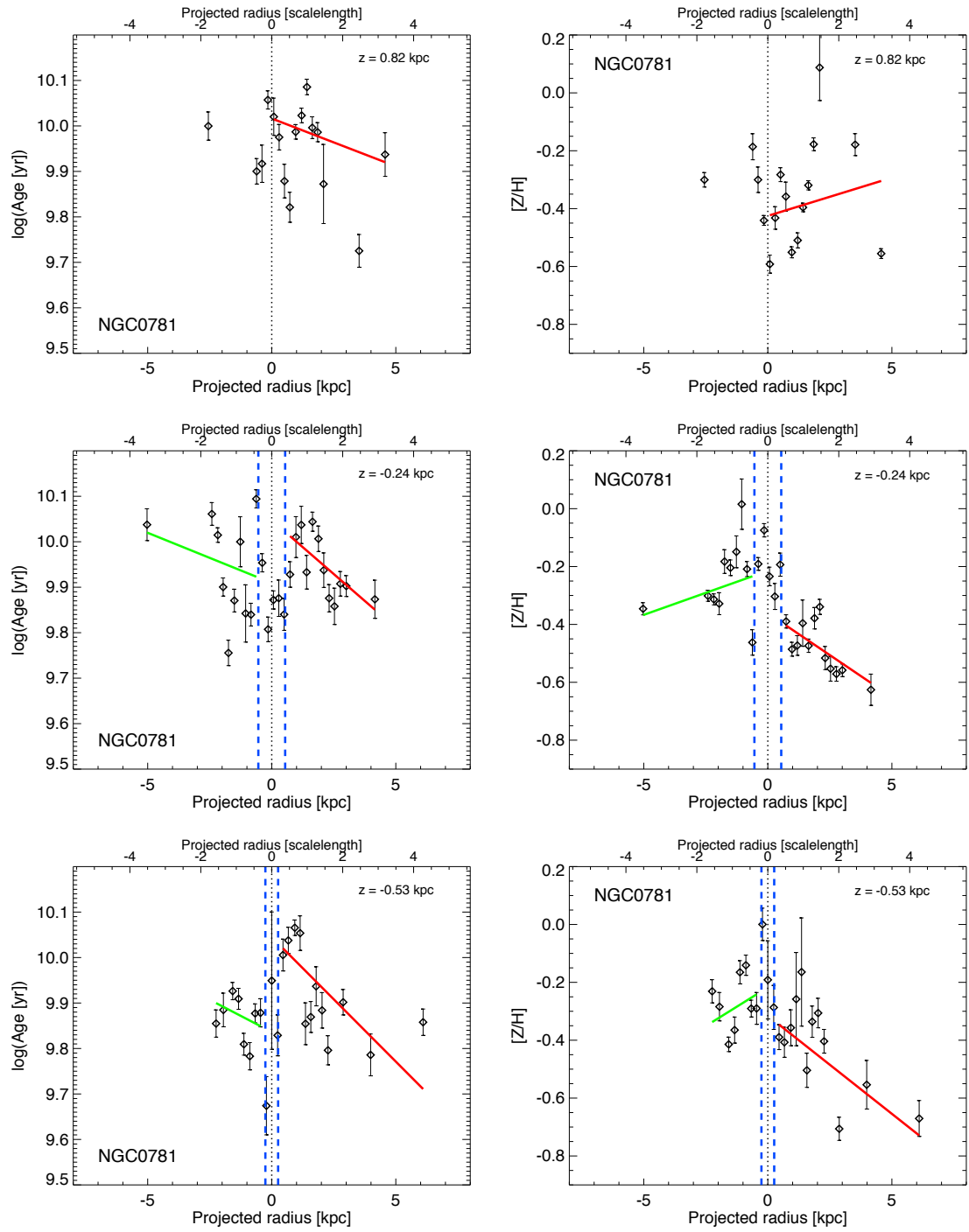


Figure B.19: Galaxy NGC0781, age vs. radius on the left and metallicity vs. radius on the right – weighted by mass

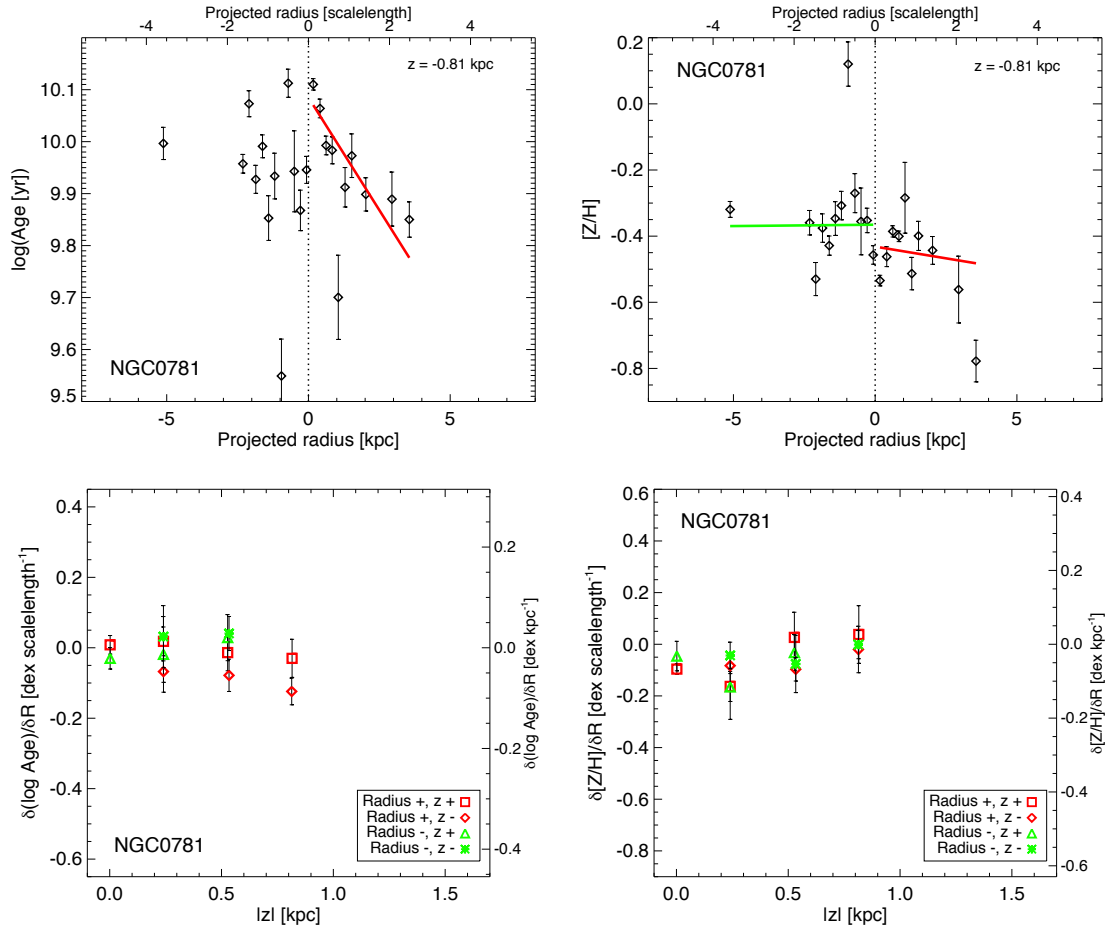


Figure B.20: Galaxy NGC0781, age vs. radius on the left and metallicity vs. radius on the right. Bottom row: radial age gradient with height on the left and the same for metallicity on the right – weighted by mass

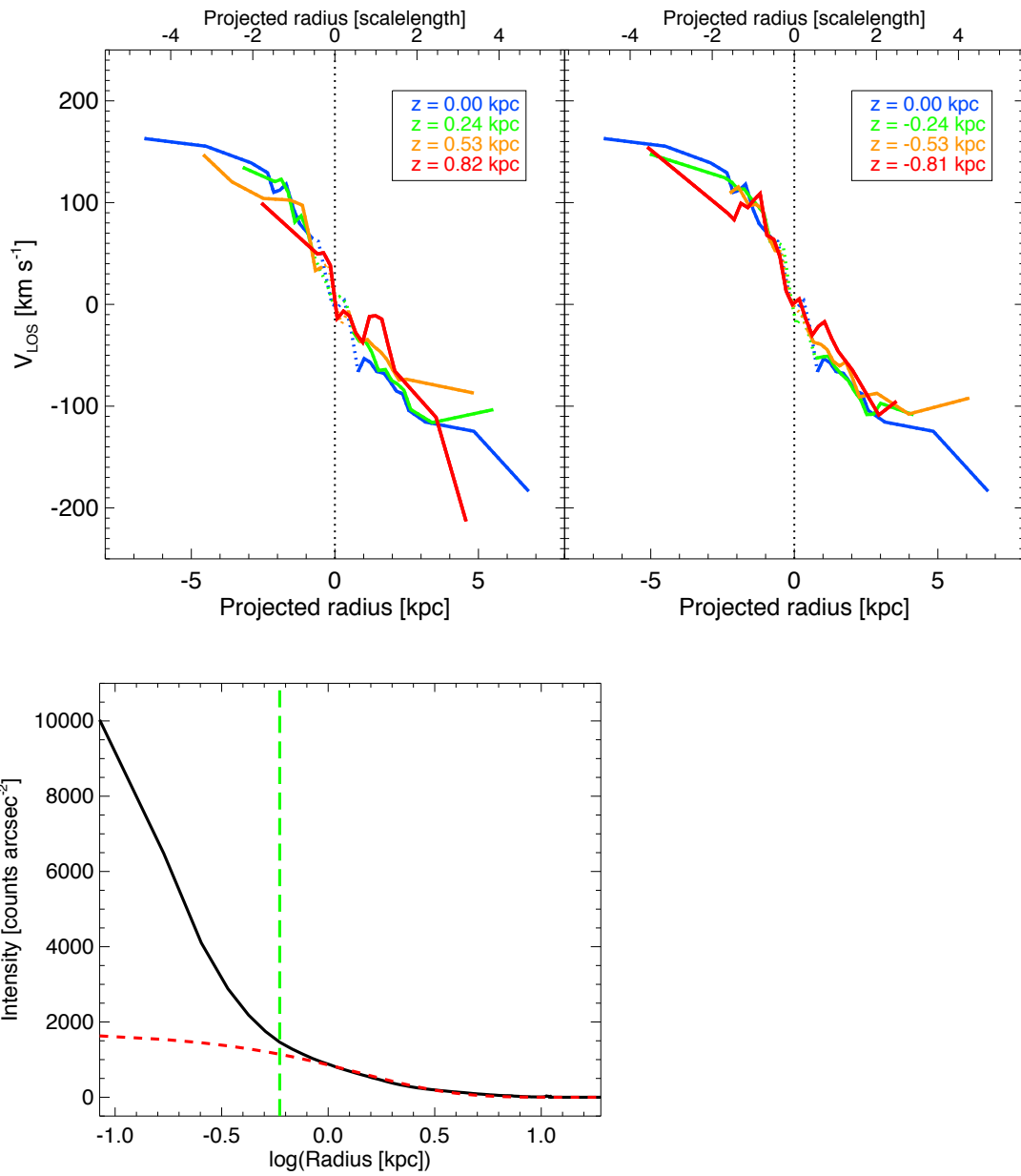


Figure B.21: Galaxy NGC0781, rotation curve in the top and radial surface brightness profile in the bottom

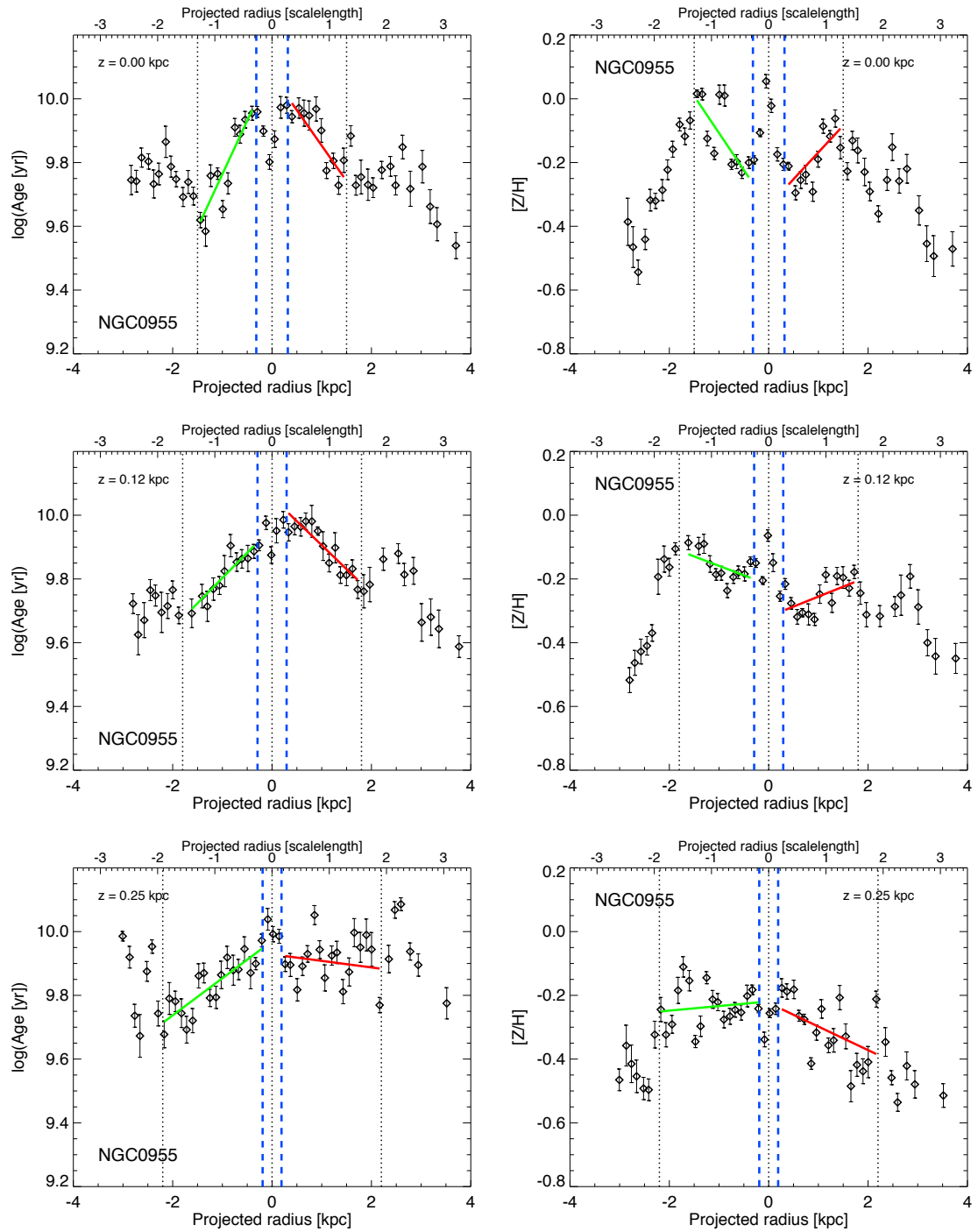


Figure B.22: Galaxy NGC0955, age vs. radius on the left and metallicity vs. radius on the right – weighted by light

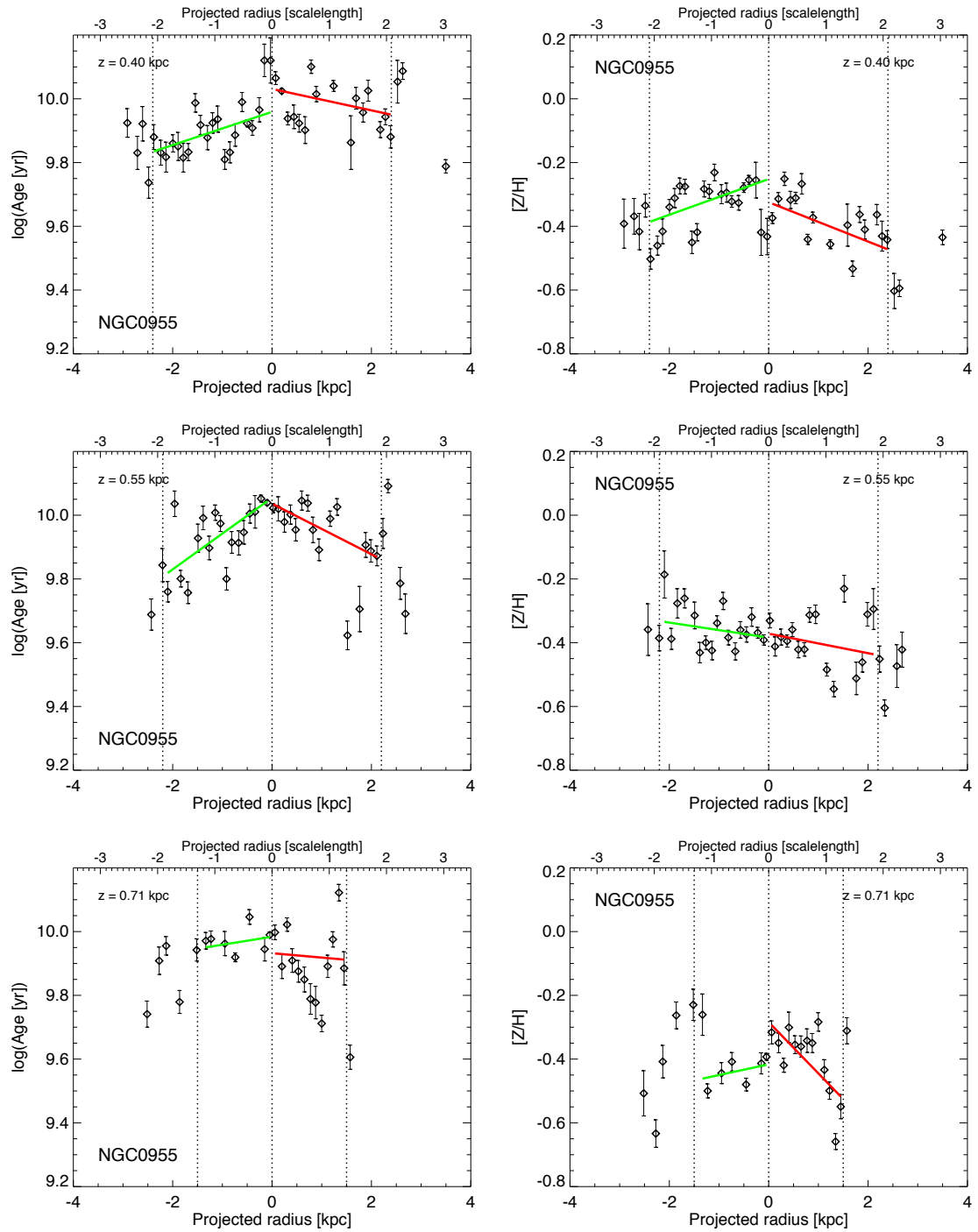


Figure B.23: Galaxy NGC0955, age vs. radius on the left and metallicity vs. radius on the right – weighted by light

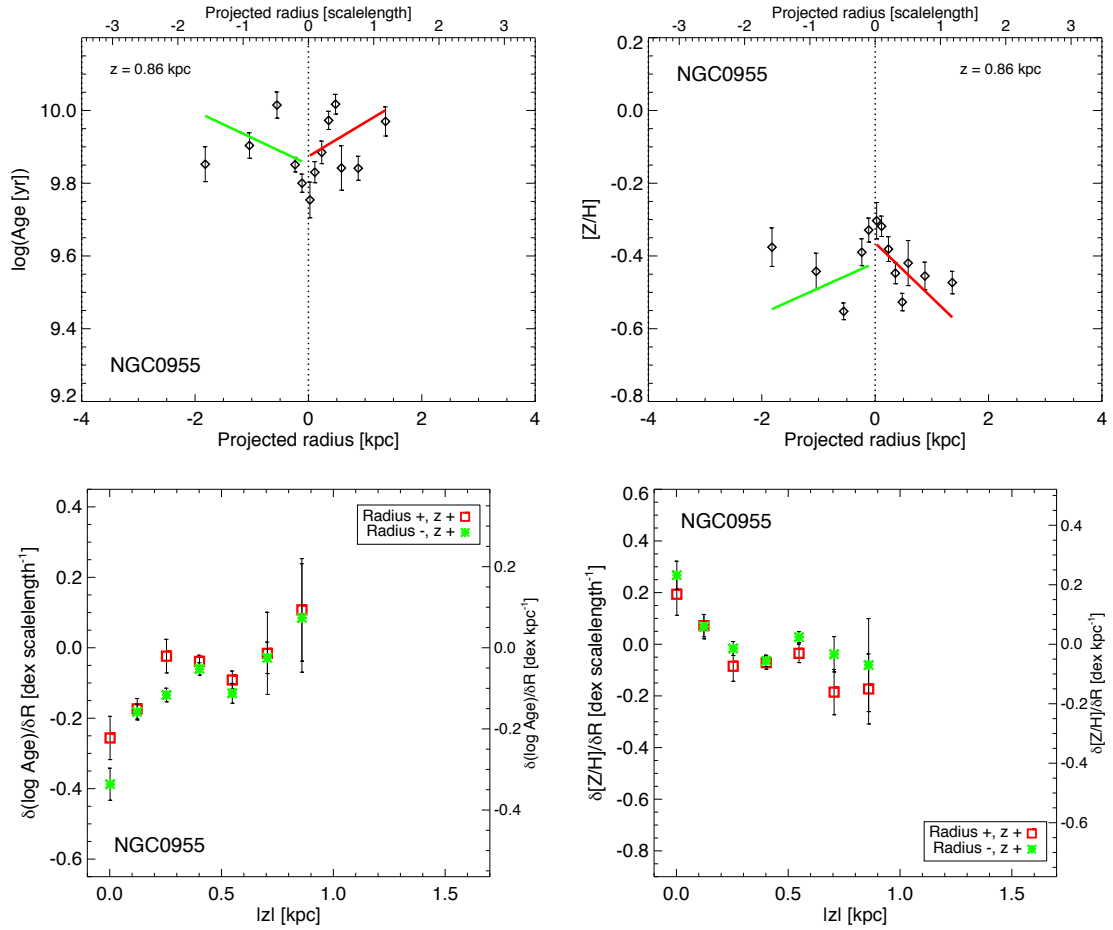


Figure B.24: Galaxy NGC0955, age vs. radius on the left and metallicity vs. radius on the right. Bottom row: radial age gradient with height on the left and the same for metallicity on the right – weighted by light

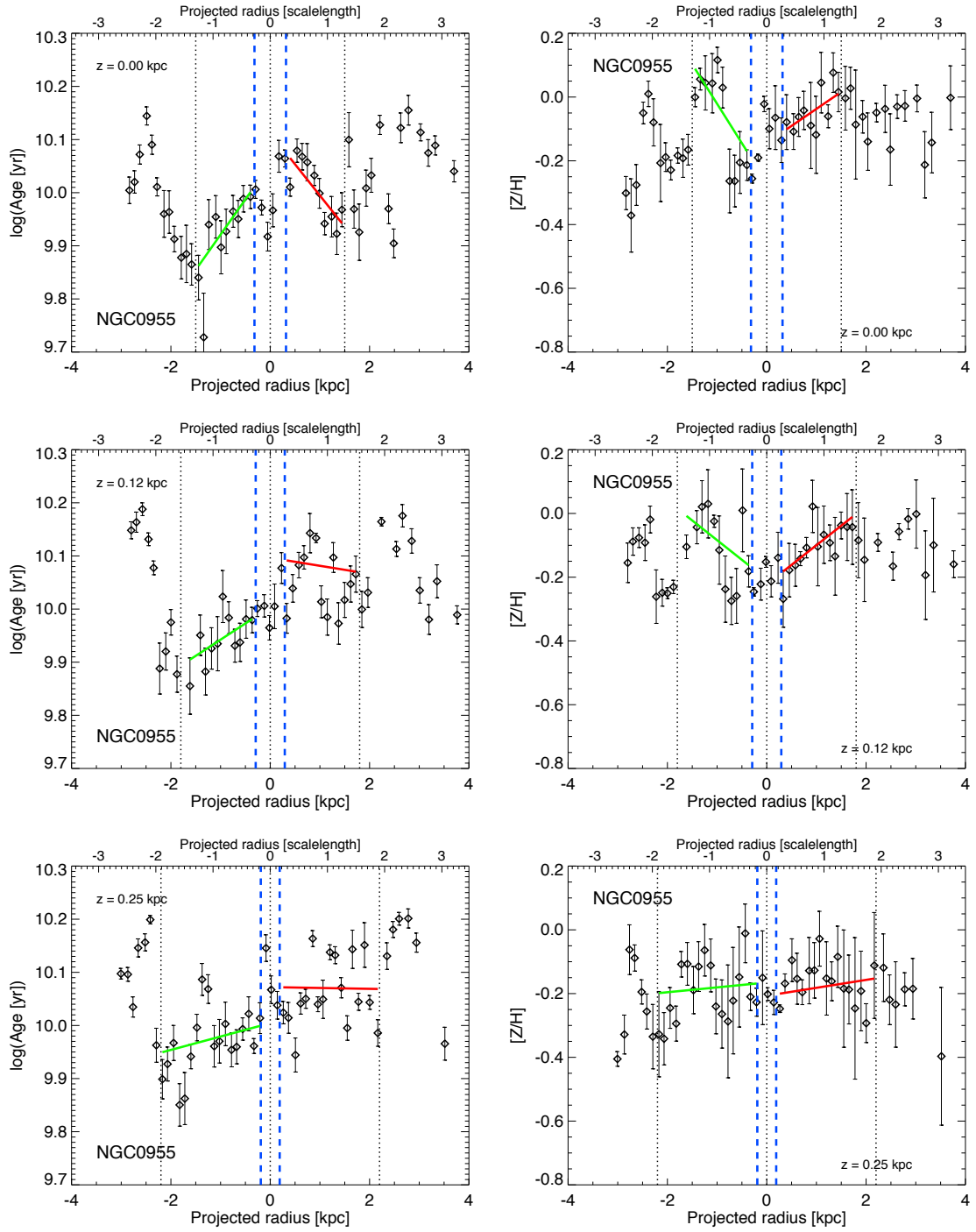


Figure B.25: Galaxy NGC0955, age vs. radius on the left and metallicity vs. radius on the right – weighted by mass

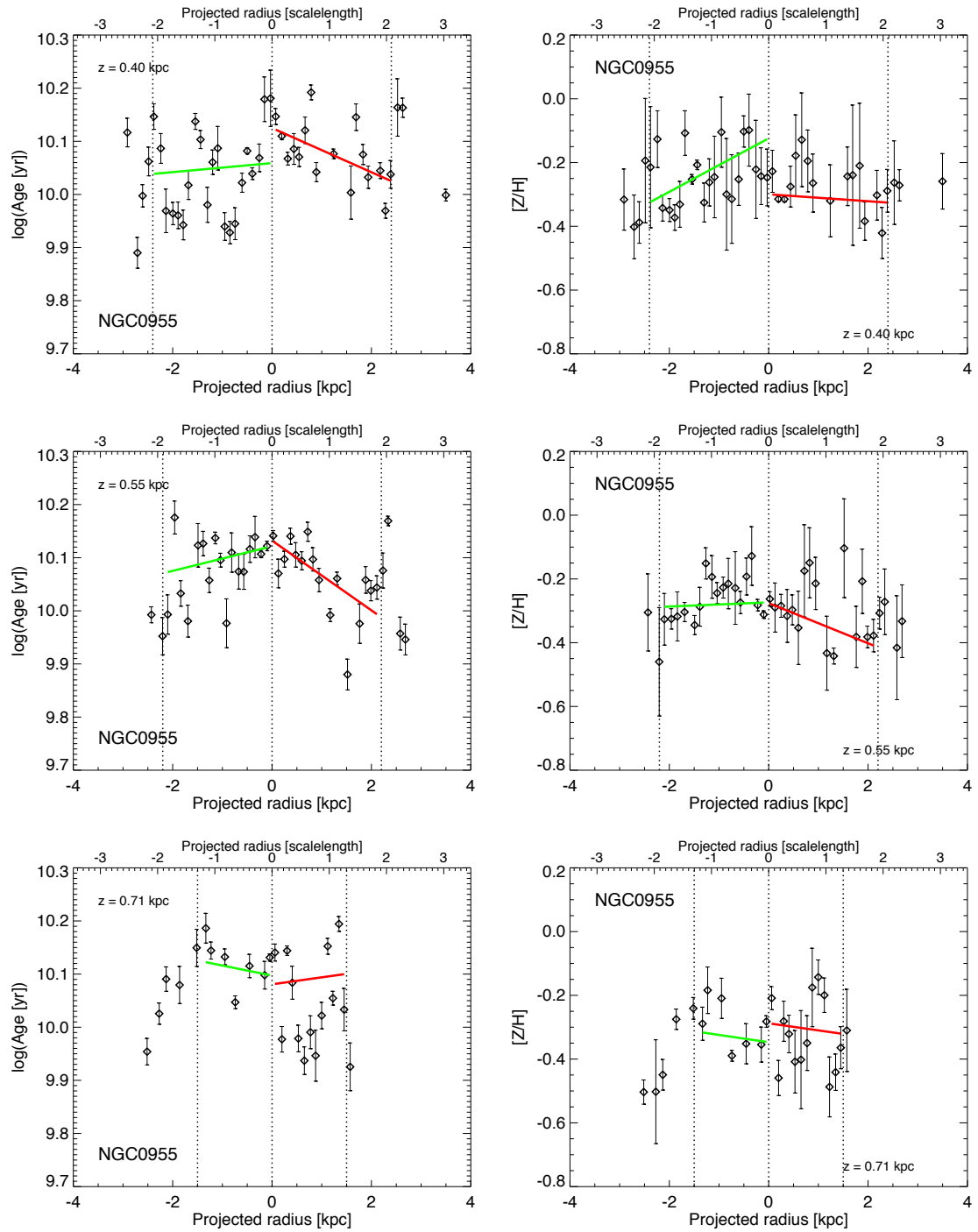


Figure B.26: Galaxy NGC0955, age vs. radius on the left and metallicity vs. radius on the right – weighted by mass

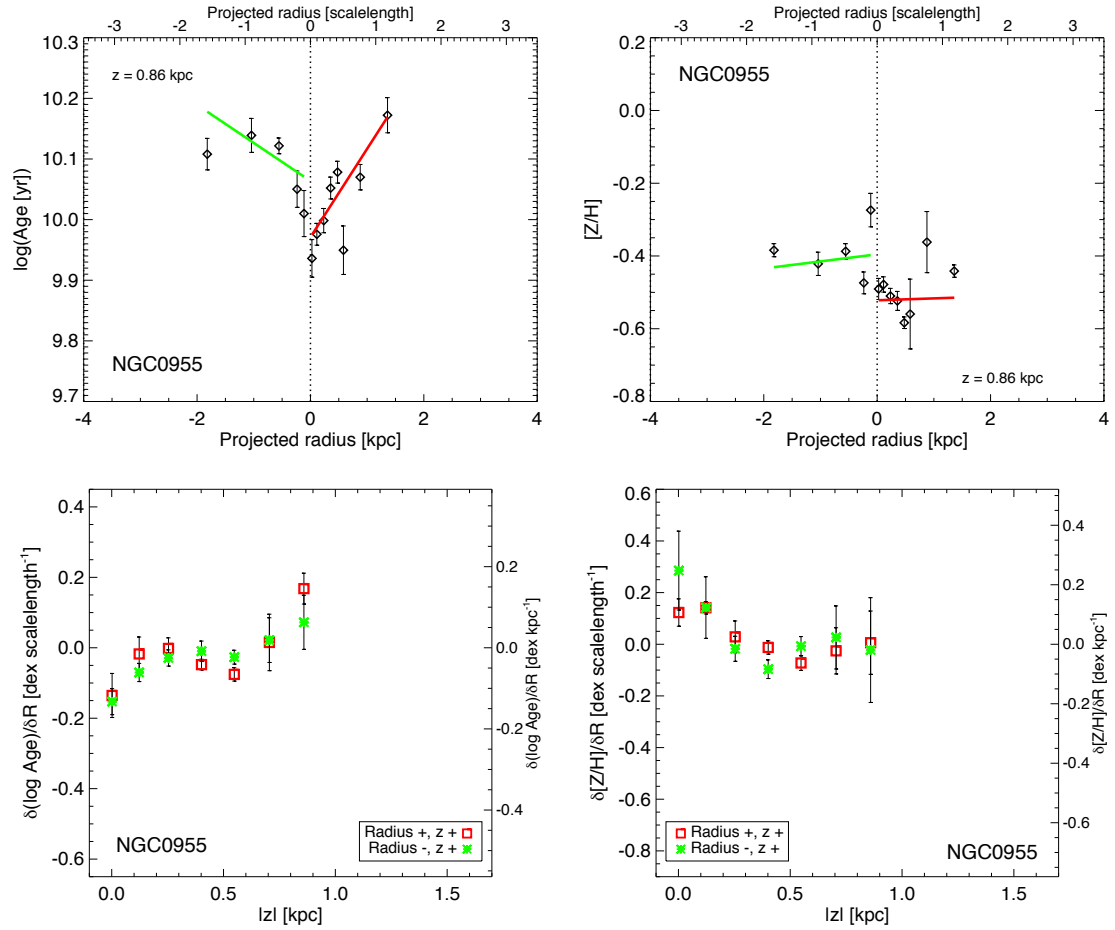


Figure B.27: Galaxy NGC0955, age vs. radius on the left and metallicity vs. radius on the right. Bottom row: radial age gradient with height on the left and the same for metallicity on the right – weighted by mass

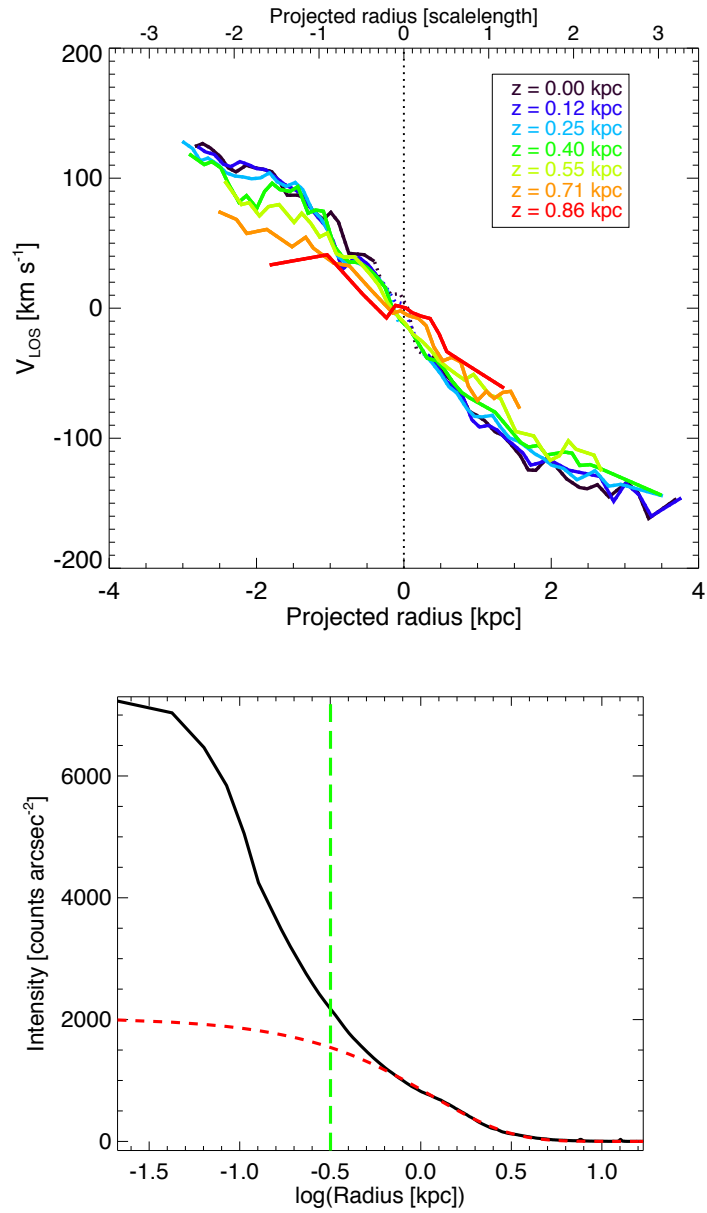


Figure B.28: Galaxy NGC0955, rotation curve in the top and radial surface brightness profile in the bottom

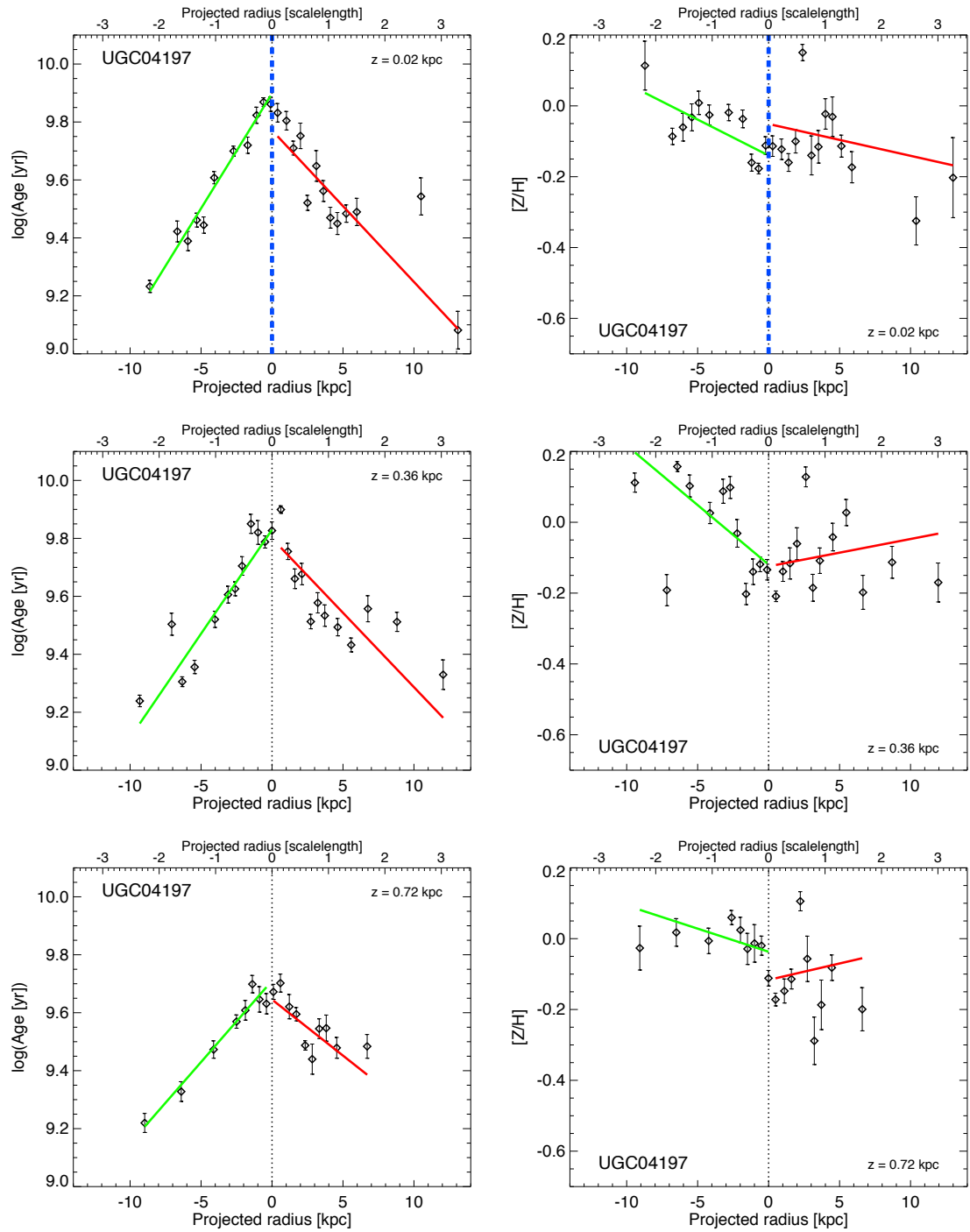


Figure B.29: Galaxy UGC04197, age vs. radius on the left and metallicity vs. radius on the right – weighted by light

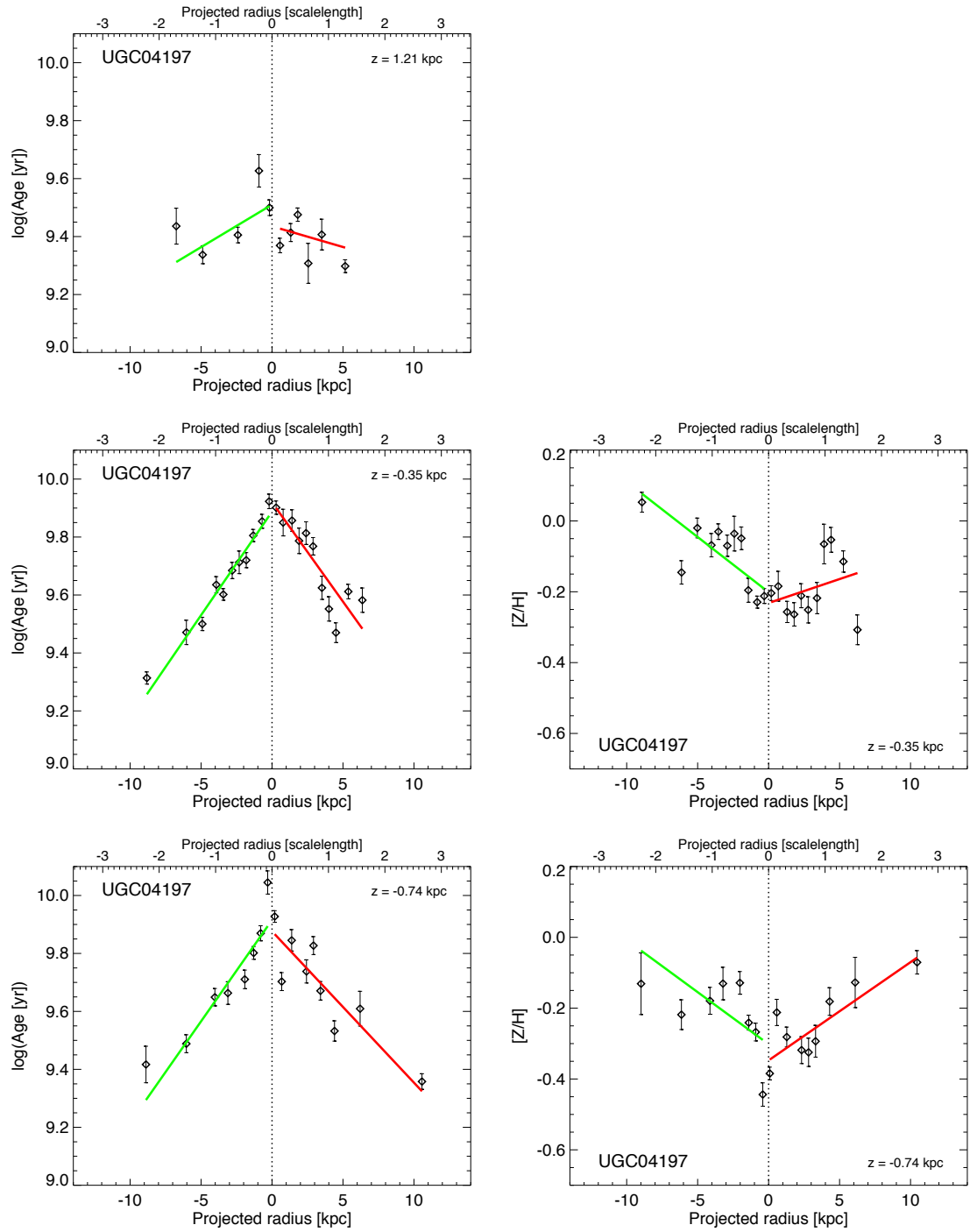


Figure B.30: Galaxy UGC04197, age vs. radius on the left and metallicity vs. radius on the right – weighted by light

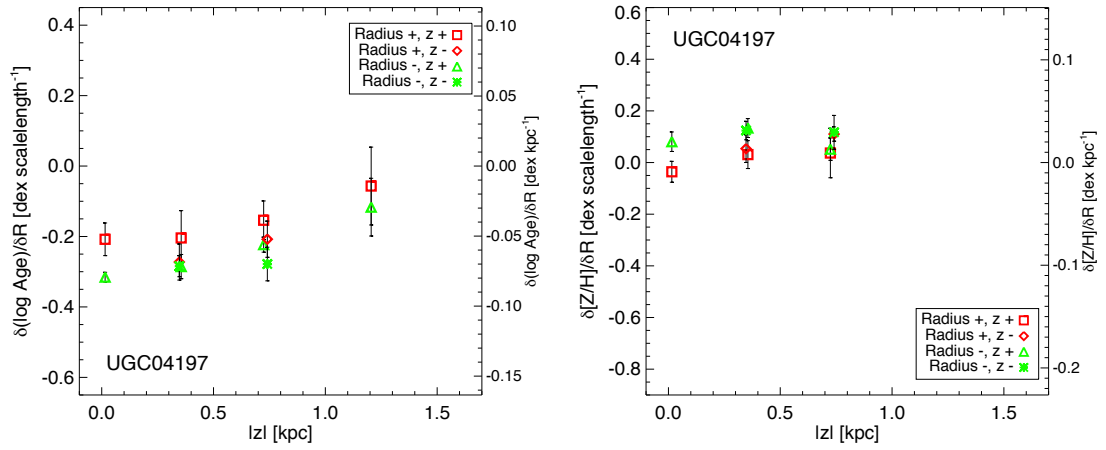


Figure B.31: Galaxy UGC04197, radial age gradient with height on the left and the same for metallicity on the right – weighted by light

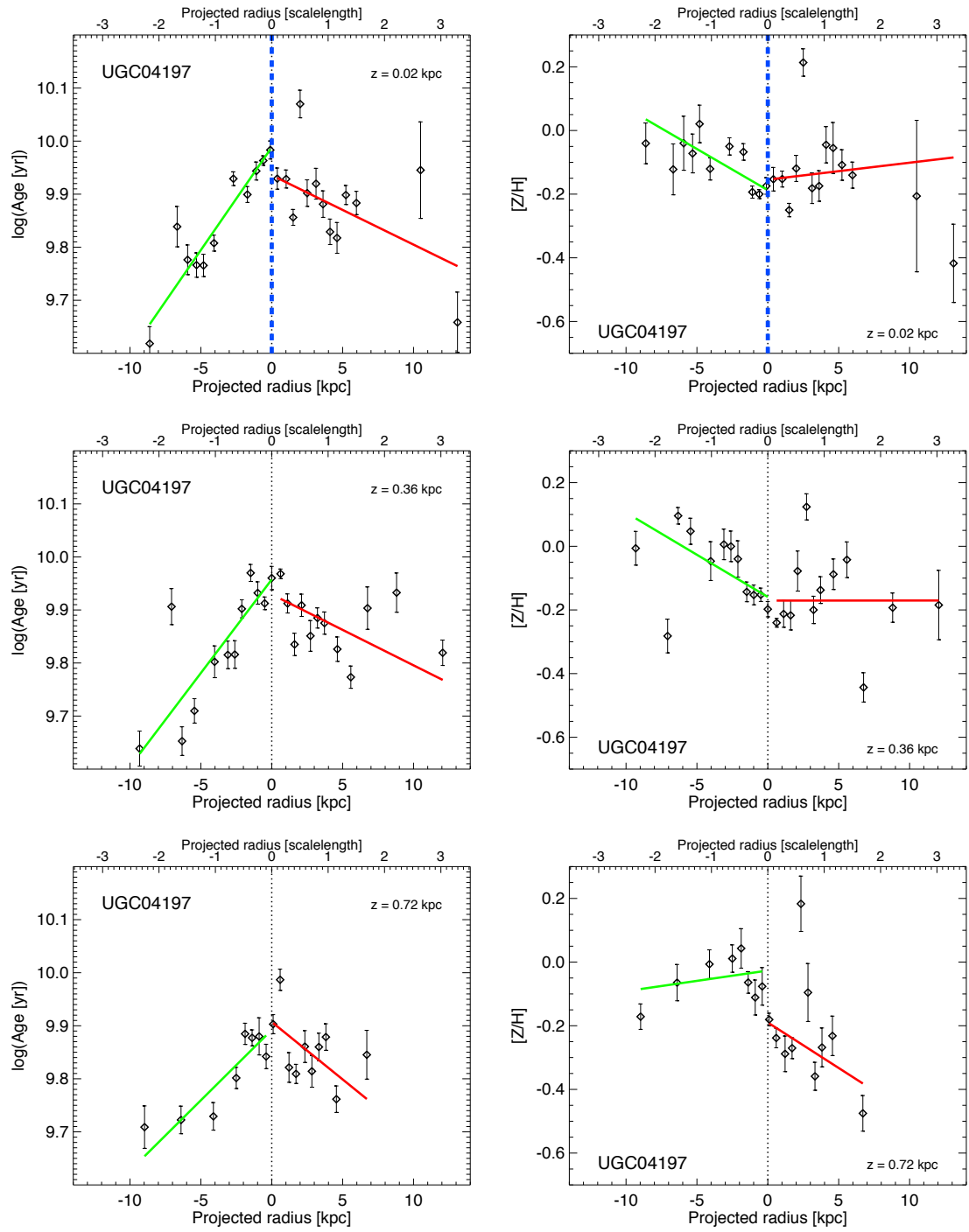


Figure B.32: Galaxy UGC04197, age vs. radius on the left and metallicity vs. radius on the right – weighted by mass

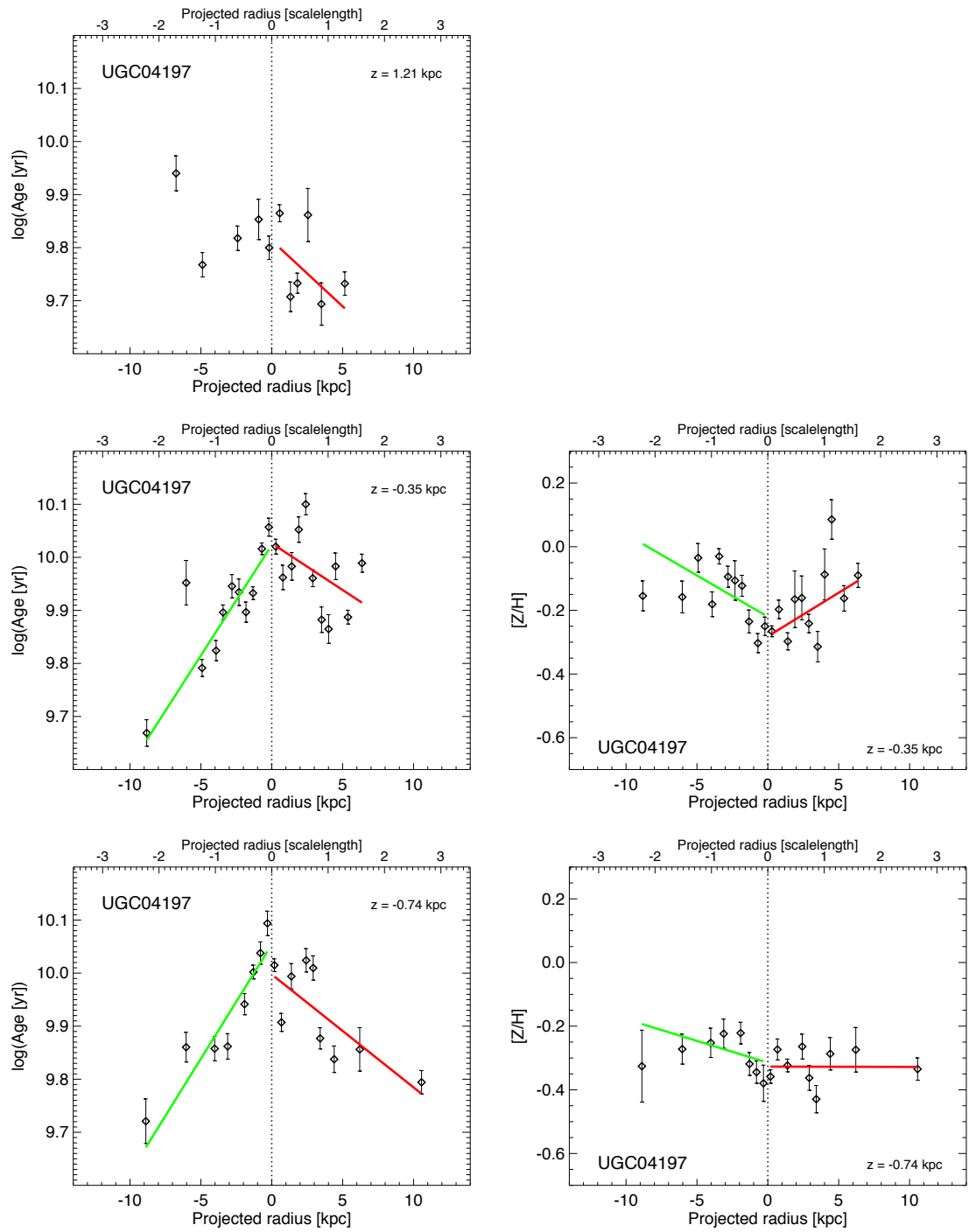


Figure B.33: Galaxy UGC04197, age vs. radius on the left and metallicity vs. radius on the right – weighted by mass

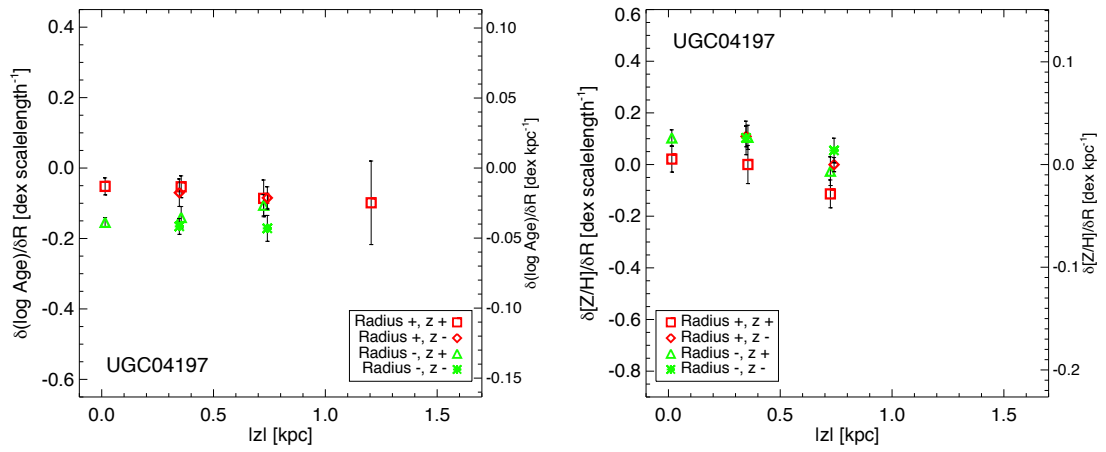


Figure B.34: Galaxy UGC04197, radial age gradient with height on the left and the same for metallicity on the right – weighted by mass

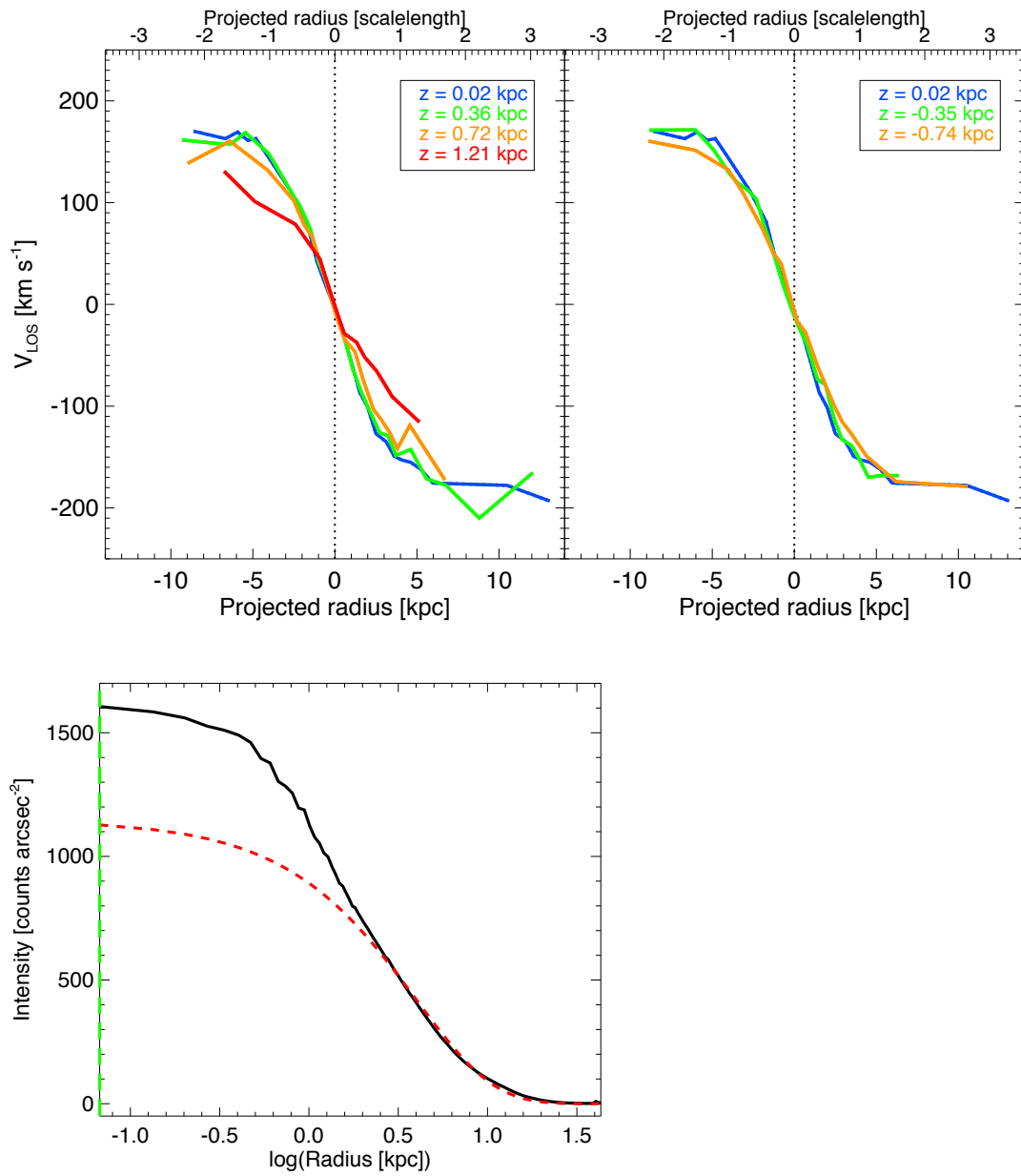


Figure B.35: Galaxy UGC04197, rotation curve in the top and radial surface brightness profile in the bottom

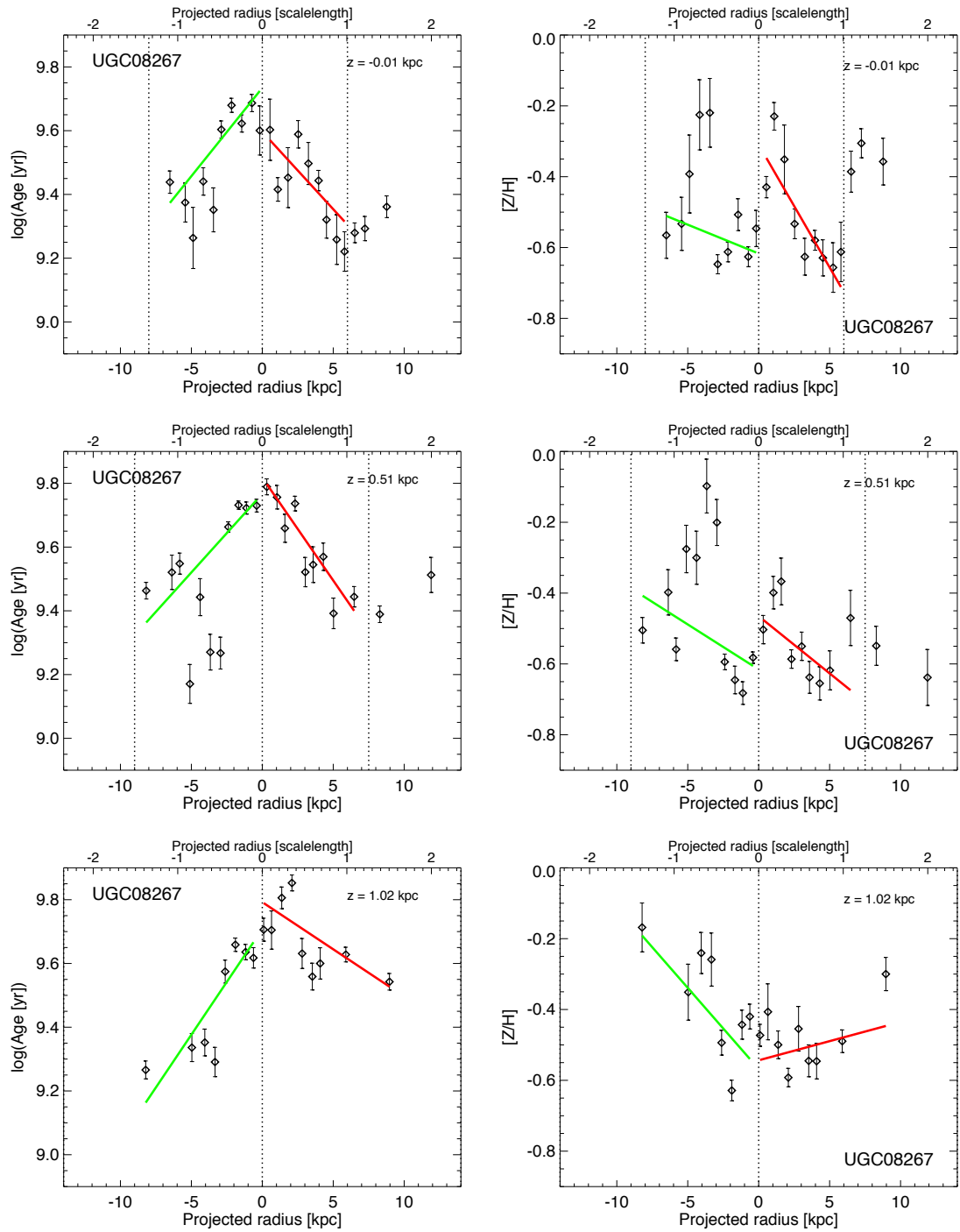


Figure B.36: Galaxy UGC08267, age vs. radius on the left and metallicity vs. radius on the right – weighted by light

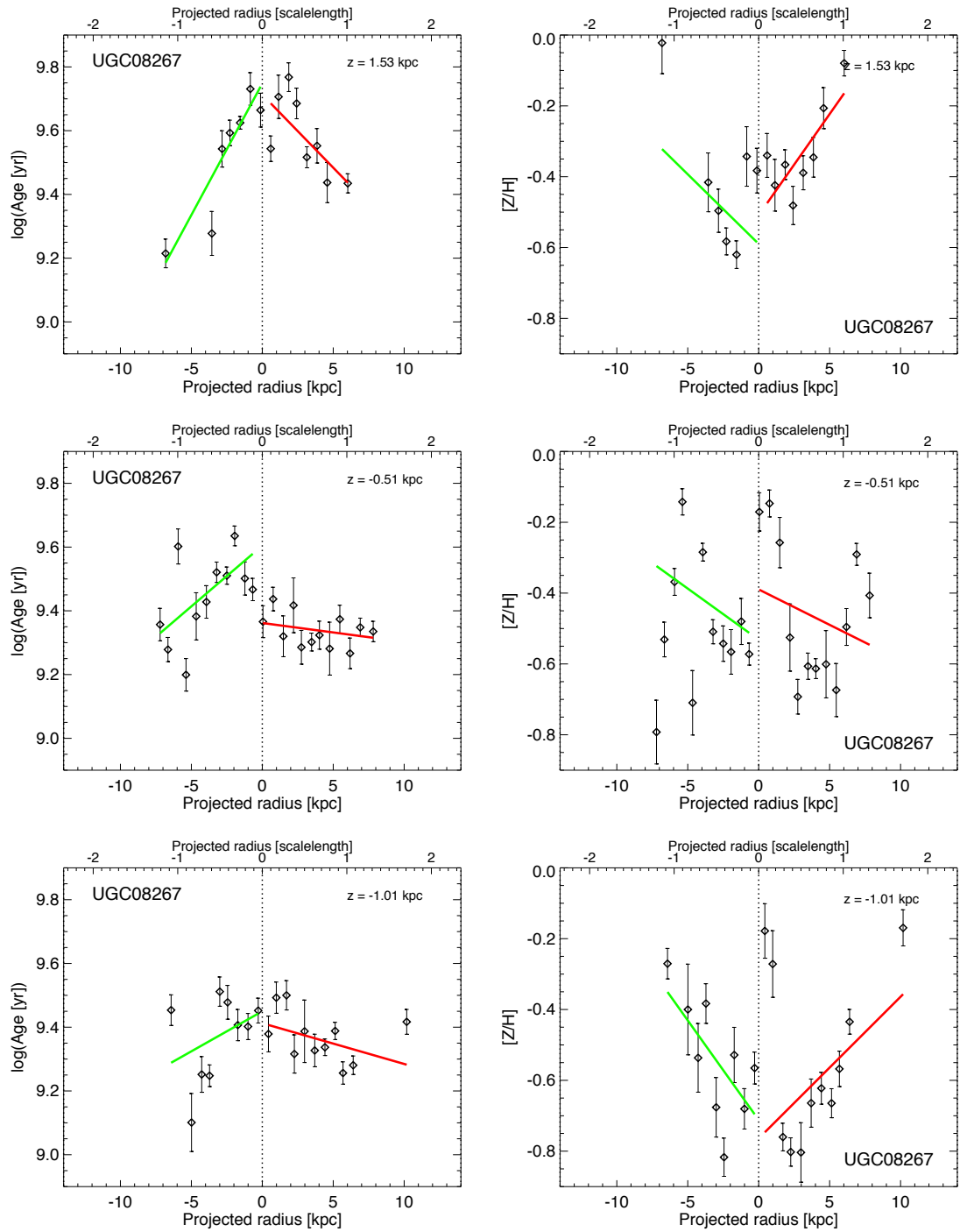


Figure B.37: Galaxy UGC08267, age vs. radius on the left and metallicity vs. radius on the right – weighted by light

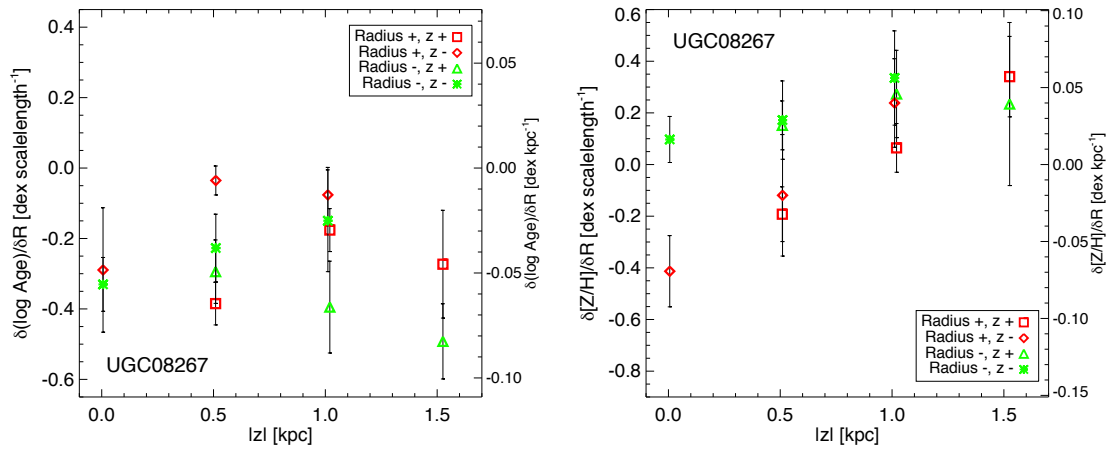


Figure B.38: Galaxy UGC08267, radial age gradient with height on the left and the same for metallicity on the right – weighted by light

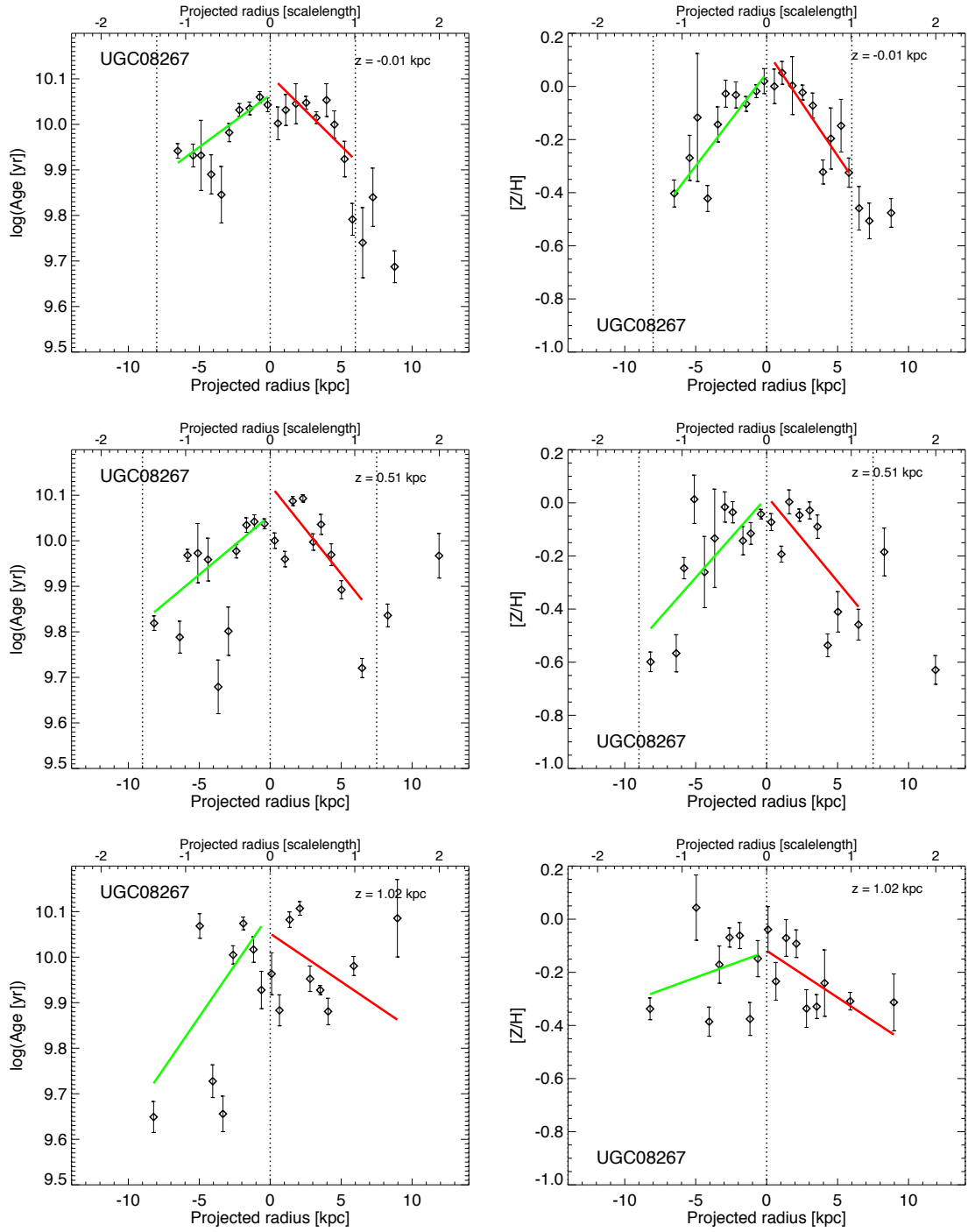


Figure B.39: Galaxy UGC08267, age vs. radius on the left and metallicity vs. radius on the right – weighted by mass

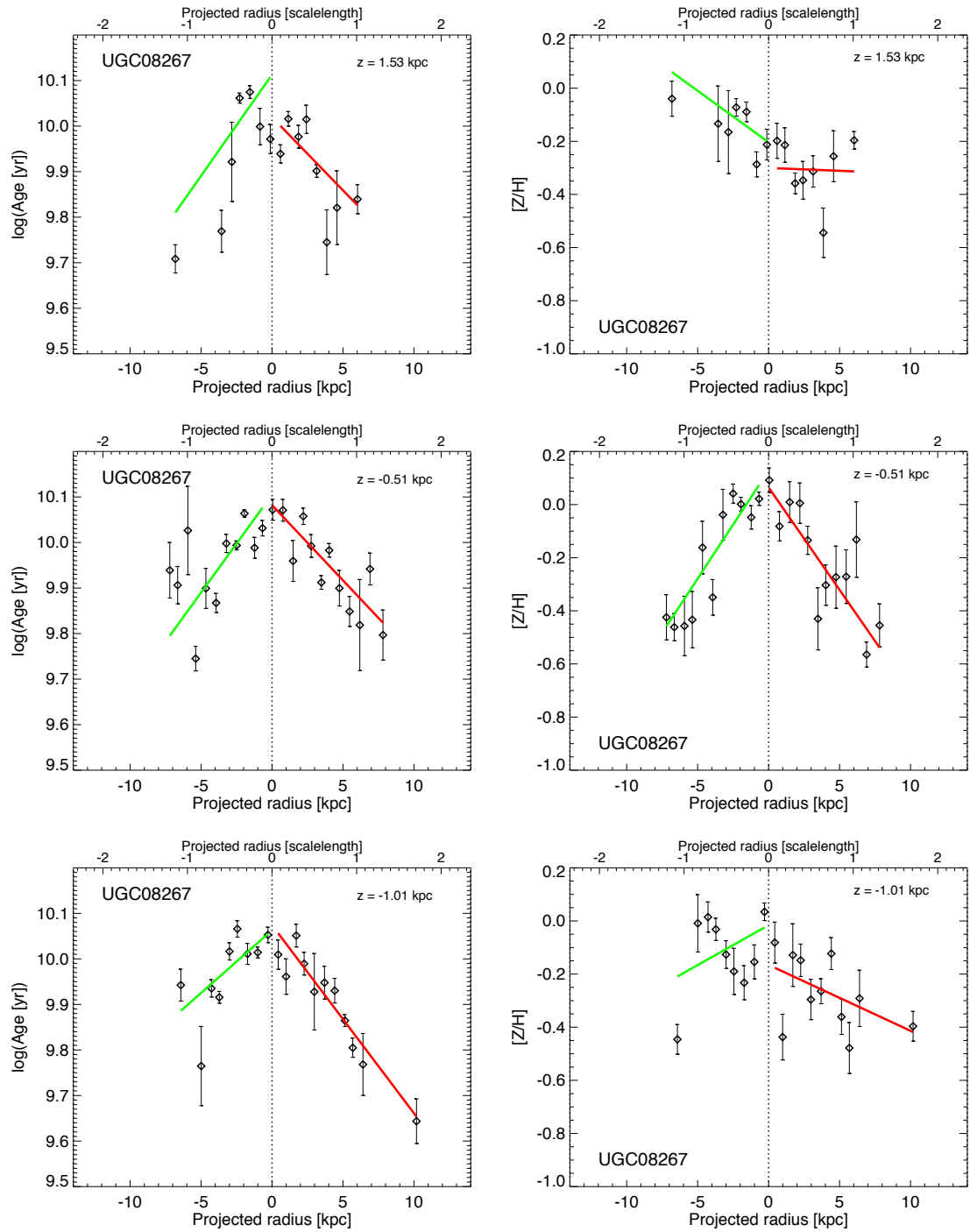


Figure B.40: Galaxy UGC08267, age vs. radius on the left and metallicity vs. radius on the right – weighted by mass

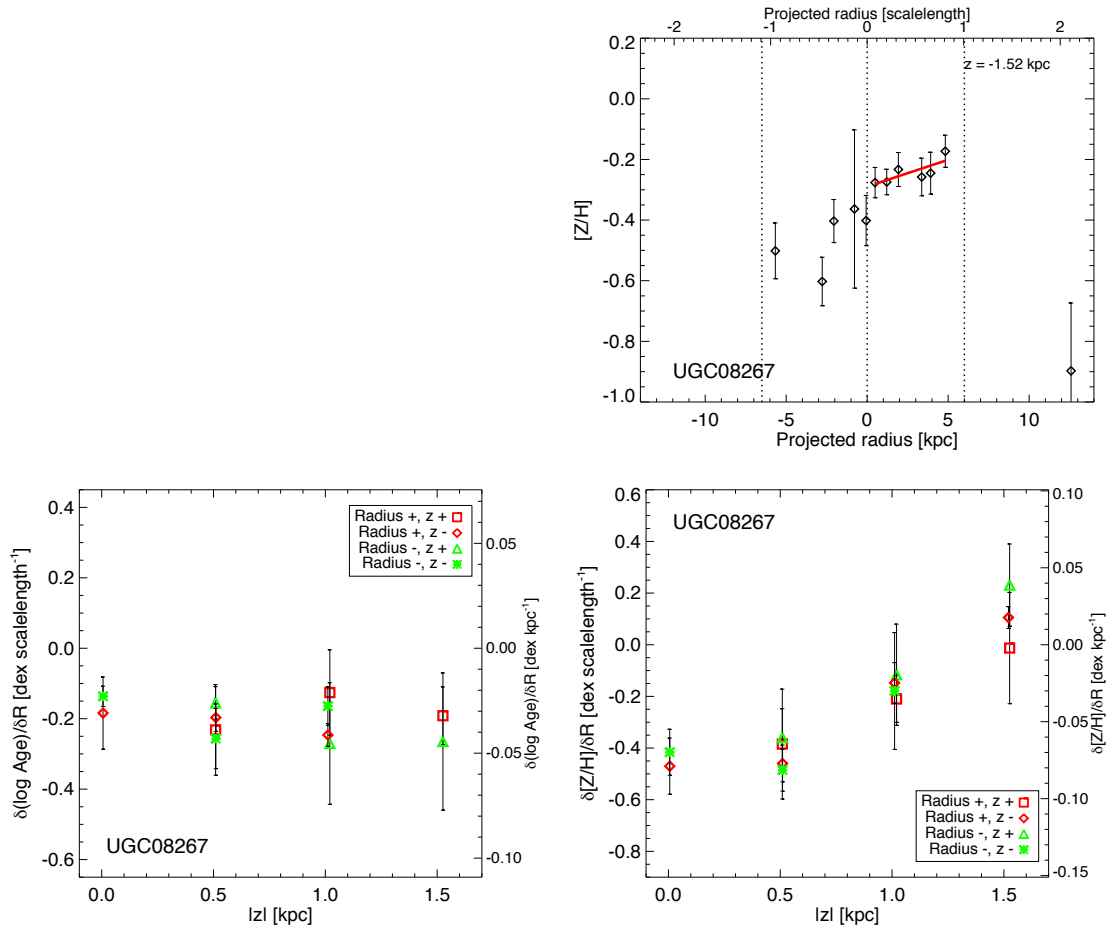


Figure B.41: Galaxy UGC08267. Top row: metallicity vs. radius. Bottom row: radial age gradient with height on the left and the same for metallicity on the right – weighted by mass

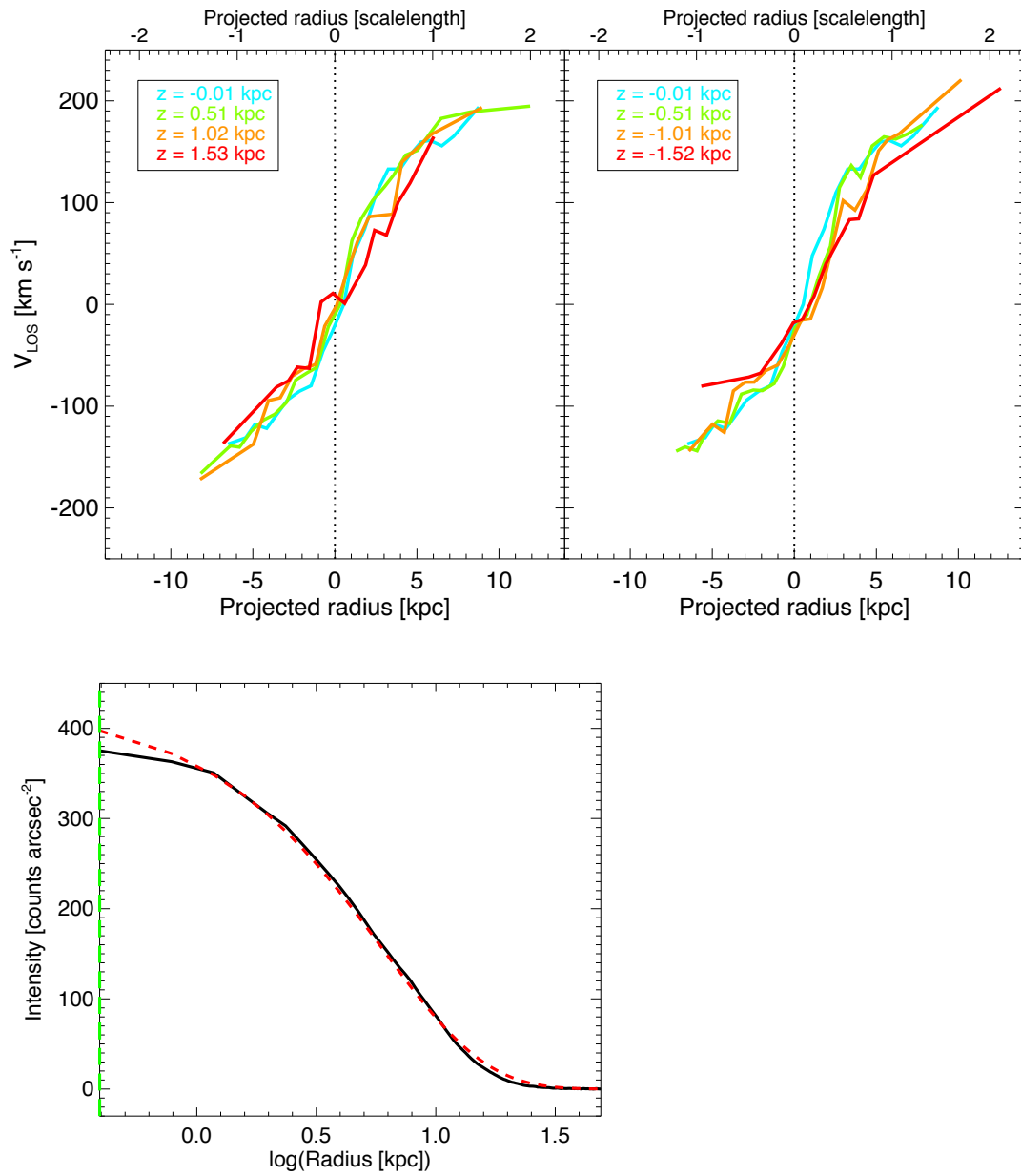


Figure B.42: Galaxy UGC08267, rotation curve in the top and radial surface brightness profile in the bottom

Appendix C

LIST OF PUBLISHED ARTICLES FROM THIS WORK

Articles published or submitted to journals during the course of this thesis:

- Chapter 2 of this thesis is related to ‘Origin of the Metallicity Distribution in the Thick Disc’ by M. S. Miranda, K. Pilkington, B. K. Gibson, C. B. Brook, P. Sanchez-Blazquez, I. Minchev, C. G. Few, R. Smith, R. Dominguez-Tenreiro, A. Obreja, J. Bailin and G. S. Stinson, published in *A&A* 587, A10, 2016
It is available at: <http://adsabs.harvard.edu/abs/2016A%26A...587A..10M>
- Chapter 3 of this thesis is related to ‘There is Not a Unique Thick Disc Formation Scenario’ by M. S. Miranda, P. Sanchez-Blazquez, C. B. Brook and B. K. Gibson, submitted to *MNRAS* in January 2017

Bibliography

- Abadi, M. G., Navarro, J. F., Steinmetz, M., & Eke, V. R. 2003a, *Astrophys. J.*, 591, 499
- Abadi, M. G., Navarro, J. F., Steinmetz, M., & Eke, V. R. 2003b, *Astrophys. J.*, 597, 21
- Abazajian, K. N., Adelman-McCarthy, J. K., Agüeros, M. A., et al. 2009, *Astrophys. J. Supple.*, 182, 543
- Adibekyan, V. Z., Sousa, S. G., Santos, N. C., et al. 2012, *Astron. Astrophys.*, 545, A32
- Afflerbach, A., Churchwell, E., & Werner, M. W. 1997, *Astrophys. J.*, 478, 190
- Anders, E. & Grevesse, N. 1989, *Geochimica et Cosmochimica Acta*, 53
- Anders, F., Chiappini, C., Santiago, B. X., et al. 2014, *Astron. Astrophys.*, 564, 115
- Assmann, P., Fellhauer, M., Kroupa, P., Bruens, R. C., & Smith, R. 2011, *Mon. Not. Roy. Astron. Soc.*, 415, 1280
- Bensby, T., Feltzing, S., & Lundström, I. 2003, *Astron. Astrophys.*, 410, 527
- Bensby, T., Feltzing, S., & Oey, M. S. 2014, *Astron. Astrophys.*, 562, A71
- Bland-Hawthorn, J. 2015, *Proceedings of the International Astronomical Union*, 309, 21

- Boeche, C., Siebert, A., Piffl, T., et al. 2014, *Astron. Astrophys.*, 568, A71
- Boeche, C., Siebert, A., Piffl, T., et al. 2013, *Astron. Astrophys.*, 559, A59
- Bond, N. A., Ivezić, Ž., Sesar, B., et al. 2010, *Astrophys. J.*, 716, 1
- Bournaud, F., Elmegreen, B. G., & Martig, M. 2009, *Astrophys. J.*, 707, 1
- Bouwens, R. J., Cayón, L., & Silk, J. 1997, *Astrophys. J.*, 489, L21
- Bovy, J. & Rix, H. W. 2013, *Astrophys. J.*, 779, 115
- Bovy, J., Rix, H.-W., & Hogg, D. W. 2012, *Astrophys. J.*, 751, 131
- Bovy, J. & Tremaine, S. 2012, *Astrophys. J.*, 756, 89
- Brook, C. B., Kawata, D., Gibson, B. K., & Freeman, K. C. 2004, *Astrophys. J.*, 612, 894
- Brook, C. B., Stinson, G., Gibson, B. K., Wadsley, J., & Quinn, T. 2012a, *Mon. Not. Roy. Astron. Soc.*, 424, 1275
- Brook, C. B., Stinson, G. S., Gibson, B. K., et al. 2012b, *Mon. Not. Roy. Astron. Soc.*, 426, 690
- Bundy, K., Bershady, M. A., Law, D. R., et al. 2015, *Astrophys. J.*, 798, 24
- Burstein, D. 1979, *ApJ*, 234, 829
- Calura, F., Pipino, A., Chiappini, C., Matteucci, F., & Maiolino, R. 2009, *Astron. Astrophys.*, 504, 373
- Camm, G. L. 1950, *Mon. Not. Roy. Astron. Soc.*, 110, 305
- Cappellari, M. & Emsellem, E. 2004, *Pub. Astron. Soc. Pac.*, 116, 138
- Carollo, D., Beers, T. C., Chiba, M., et al. 2010, *Astrophys. J.*, 712, 692

- Carrell, K., Chen, Y., & Zhao, G. 2012, *Astron. J.*, 144, 185
- Casetti-Dinescu, D. I., Girard, T. M., Korchagin, V. I., & van Altena, W. F. 2011, *Astrophys. J.*, 728, 7
- Cenarro, A. J., Peletier, R. F., Sánchez-Blázquez, P., et al. 2007, *Mon. Not. Roy. Astron. Soc.*, 374, 664
- Chabrier, G. 2003, *Pub. Astron. Soc. Pac.*, 115, 763
- Chen, Y. Q., Zhao, G., Carrell, K., & Zhao, J. K. 2011, *Astron. J.*, 142, 184
- Cheng, J. Y., Rockosi, C. M., Morrison, H. L., et al. 2012a, *Astrophys. J.*, 752, 51
- Cheng, J. Y., Rockosi, C. M., Morrison, H. L., et al. 2012b, *Astrophys. J.*, 746, 149
- Chiappini, C., Matteucci, F., & Gratton, R. 1997, *Astrophys. J.*, 477, 765
- Chiappini, C., Matteucci, F., & Romano, D. 2001, *Astrophys. J.*, 554, 1044
- Chiba, M. & Beers, T. C. 2000, *Astron. J.*, 119, 2843
- Cid Fernandes, R., Mateus, A., Sodré, L., Stasińska, G., & Gomes, J. M. 2005, *Mon. Not. Roy. Astron. Soc.*, 358, 363
- Comerón, S., Elmegreen, B. G., Knapen, J. H., et al. 2011a, *Astrophys. J.*, 741, 28
- Comerón, S., Knapen, J. H., Sheth, K., et al. 2011b, *Astrophys. J.*, 729, 18
- Comerón, S., Salo, H., Janz, J., Laurikainen, E., & Yoachim, P. 2015, *Astron. Astrophys.*, 584, A34
- Comerón, S., Salo, H., Peletier, R. F., & Mentz, J. 2016, *Astron. Astrophys.*, 593, L6
- Conselice, C. J., Wilkinson, A., Duncan, K., & Mortlock, A. 2016, *Astrophys. J.*, 830, 83

- Courteau, S., Dutton, A. A., van den Bosch, F. C., et al. 2007, *Astrophys. J.*, 671, 203
- Cresci, G., Mannucci, F., Maiolino, R., et al. 2010, *Nature*, 467, 811
- Croom, S. M., Lawrence, J. S., Bland-Hawthorn, J., et al. 2012, *Mon. Not. Roy. Astron. Soc.*, 421, 872
- Dalcanton, J. J., Yoachim, P., & Bernstein, R. A. 2004, *Astrophys. J.*, 608, 189
- Davé, R., Finlator, K., & Oppenheimer, B. D. 2011, *Mon. Not. Roy. Astron. Soc.*, 416, 1354
- de Vaucouleurs, G. 1948, *Ann. d'Astrophys.*, 11, 247
- de Vaucouleurs, G. 1958, *Astrophys. J.*, 128, 465
- de Vaucouleurs, G. 1959, *Handb. Phys.*, 53, 275
- Di Matteo, P., Haywood, M., Combes, F., Semelin, B., & Snaith, O. N. 2013, *Astron. Astrophys.*, 553, A102
- Domínguez-Tenreiro, R., Obreja, A., Brook, C. B., et al. 2015, *Astrophys. J. Letters*, 800, 30
- Domínguez-Tenreiro, R., Obreja, A., Granato, G. L., et al. 2014, *Mon. Not. Roy. Astron. Soc.*, 439, 3868
- El-Badry, K., Wetzel, A., Geha, M., et al. 2016, *Astrophys. J.*, 820, 17
- Erb, D. K., Shapley, A. E., Pettini, M., et al. 2006, *Astrophys. J.*, 644, 813
- Falcón-Barroso, J., Sánchez-Blázquez, P., Vazdekis, A., et al. 2011, *Astron. Astrophys.*, 532, A95
- Feltzing, S., Bensby, T., & Lundström, I. 2003, *Astron. Astrophys.*, 397, L1

- Ferland, G. J., Korista, K. T., Verner, D. A., et al. 1998, *Pub. Astron. Soc. Pac.*, 110, 761
- Few, C. G., Courty, S., Gibson, B. K., et al. 2012a, *Mon. Not. Roy. Astron. Soc.*, 424, 11
- Few, C. G., Courty, S., Gibson, B. K., Michel-Dansac, L., & Calura, F. 2014, *Mon. Not. Roy. Astron. Soc.*, 444, 3845
- Few, C. G., Gibson, B. K., Courty, S., et al. 2012b, *Astron. Astrophys.*, 547, 63
- Freeman, K. 2012, *Structure and Evolution of the Milky Way*, ed. A. Miglio, J. Montalbán, & A. Noels, 137
- Freeman, K. & Bland-Hawthorn, J. 2002, *Ann. Rev. Astron. Astrophys.*, 40, 487
- Fry, A. M., Morrison, H. L., Harding, P., & Boroson, T. A. 1999, *Astron. J.*, 118, 1209
- Fuhrmann, K. 2011, *Mon. Not. Roy. Astron. Soc.*, 414, 2893
- Gallazzi, A., Charlot, S., Brinchmann, J., & White, S. D. M. and Tremonti, C. A. 2005, *Mon. Not. Roy. Astron. Soc.*, 362, 41
- Gibson, B. K., Pilkington, K., Brook, C. B., Stinson, G. S., & Bailin, J. 2013, *Astron. Astrophys.*, 554, 47
- Gilmore, G. 2004, *Science*, 304, 1915
- Gilmore, G. & Reid, N. 1983, *Mon. Not. Roy. Astron. Soc.*, 202, 1025
- Gilmore, G. & Wyse, R. F. G. 1985, *Astron. J.*, 90, 2015
- Gilmore, G., Wyse, R. F. G., & Norris, J. E. 2002, *Astrophys. J. Letters*, 574, L39

- Girard, T. M., Korchagin, V. I., Casetti-Dinescu, D. I., et al. 2006, *Astron. J.*, 132, 1768
- González Delgado, R. M., García-Benito, R., Pérez, E., et al. 2015, *Astron. Astrophys.*, 581, A103
- Guérou, A., Emsellem, E., Krajnović, D., et al. 2016, *Astron. Astrophys.*, 591, A143
- Haardt, F. & Madau, P. 1996, *Astrophys. J.*, 461, 20
- Halle, A., Di Matteo, P., Haywood, M., & Combes, F. 2015, *Astron. Astrophys.*, 578, A58
- Hayden, M. R., Bovy, J., Holtzman, J. A., et al. 2015, *ApJ*, 808, 132
- Haywood, M., Di Matteo, P., Lehnert, M. D., Katz, D., & Gómez, A. 2013, *Astron. Astrophys.*, 560, 109
- Heavens, A., Panter, B., Jimenez, R., & Dunlop, J. 2004, *Nature*, 428, 625
- Heavens, A. F., Jimenez, R., & Lahav, O. 2000, *Mon. Not. Roy. Astron. Soc.*, 317, 965
- Ho, I. T., Kudritzki, R. P., Kewley, L. J., et al. 2015, *Mon. Not. Roy. Astron. Soc.*, 448, 2030
- Hopkins, P. F., Quataert, E., & Murray, N. 2011, *Mon. Not. Roy. Astron. Soc.*, 417, 950
- Hubble, E. & Rosseland, S. 1936, *The Realm of the Nebulae*, Vol. 84, 509
- Husemann, B., Jahnke, K., Sánchez, S. F., et al. 2013, *Astron. Astrophys.*, 549, A87
- Ivezić, Ž., Sesar, B., Jurić, M., et al. 2008, *Astrophys. J.*, 684, 287

- Jones, T., Ellis, R. S., Richard, J., & Jullo, E. 2013, *Astrophys. J.*, 765, 20
- Jurić, M., Ivezić, Ž., Brooks, A., et al. 2008, *ApJ*, 673, 864
- Kasparova, A. V., Katkov, I. Y., Chilingarian, I. V., et al. 2016, *Mon. Not. Roy. Astron. Soc.*, 460, L89
- Katz, N. 1992, *Astrophys. J.*, 391, 502
- Kauffmann, G., Heckman, T. M., White, S. D. M., et al. 2003, *Mon. Not. Roy. Astron. Soc.*, 341, 33
- Kay, S. T., Pearce, F. R., Frenk, C. S., & Jenkins, A. 2002, *Mon. Not. Roy. Astron. Soc.*, 330, 113
- Kazantzidis, S., Bullock, J. S., Zentner, A. R., Kravtsov, A. V., & Moustakas, L. A. 2008, *ApJ*, 688, 254
- Kepner, J. V. 1999, *Astrophys. J.*, 520, 59
- Kewley, L. J., Geller, M. J., & Barton, E. J. 2006, *Astron. J.*, 131, 2004
- Kobayashi, C., Umeda, H., Nomoto, K., Tominaga, N., & Ohkubo, T. 2006, *Astrophys. J.*, 653, 1145
- Koleva, M., Prugniel, P., Bouchard, A., & Wu, Y. 2009, *Astron. Astrophys.*, 501, 1269
- Koleva, M., Prugniel, P., Ocvirk, P., Le Borgne, D., & Soubiran, C. 2008, *Mon. Not. Roy. Astron. Soc.*, 385, 1998
- Kordopatis, G., Hill, V., Irwin, M., et al. 2013, *Astron. Astrophys.*, 555, 12
- Kroupa, P. 2001, *Mon. Not. Roy. Astron. Soc.*, 322, 231
- Kroupa, P. 2002, *Mon. Not. Roy. Astron. Soc.*, 330, 707

- Kroupa, P., Tout, C. A., & Gilmore, G. 1993, *Mon. Not. Roy. Astron. Soc.*, 262, 545
- Kubryk, M., Prantzos, N., & Athanassoula, E. 2013, *MNRAS*, 436, 1479
- Larson, R. B. 1974, *Mon. Not. Roy. Astron. Soc.*, 169, 229
- Lee, H., Skillman, E. D., Cannon, J. M., et al. 2006, *Astrophys. J.*, 647, 970
- Lee, Y. S., Beers, T. C., An, D., et al. 2011, *Astrophys. J.*, 738, 187
- Leethochawalit, N., Jones, T. A., Ellis, R. S., et al. 2016, *Astrophys. J.*, 820, 18
- Lequeux, J., Peimbert, M., Rayo, J. F., Serrano, A., & Torres-Peimbert, S. 1979, *Astron. Astrophys.*, 80, 155
- Loebman, S. R., Roskar, R., Debattista, V. P., et al. 2011, *Astrophys. J.*, 737, 8
- Luck, R. E., Andrievsky, S. M., Kovtyukh, V. V., Gieren, W., & Graczyk, D. 2011, *Astron. J.*, 142, 51
- Luck, R. E., Kovtyukh, V. V., & Andrievsky, S. M. 2006, *Astron. J.*, 132, 902
- Lynden-Bell, D. & Kalnajs, A. J. 1972, *Mon. Not. Roy. Astron. Soc.*, 157, 1
- Ma, X., Hopkins, P. F., Faucher-Giguère, C. A., et al. 2016a, *Mon. Not. Roy. Astron. Soc.*, 456, 2140
- Ma, X., Hopkins, P. F., Feldmann, R., et al. 2016b
- Magrini, L., Corbelli, E., & Galli, D. 2007, *Astron. Astrophys.*, 470, 843
- Makarov, D., Prugniel, P., Terekhova, N., Courtois, H., & Vauglin, I. 2014, *Astron. Astrophys.*, 570, A13
- Marsakov, V. A. & Borkova, T. V. 2005, *Astronomy Letters*, 31, 515

- Marsakov, V. A. & Borkova, T. V. 2006, *Astronomy Letters*, 32, 376
- Martig, M., Minchev, I., Ness, M., Fouesneau, M., & Rix, H.-W. 2016, ArXiv e-prints
- Martínez-Serrano, F. J., Serna, A., Doménech-Moral, M., & Domínguez-Tenreiro, R. 2009, *Astrophys. J.*, 705, 133
- Martínez-Serrano, F. J., Serna, A., Domínguez-Tenreiro, R., & Mollá, M. 2008, *Mon. Not. Roy. Astron. Soc.*, 388, 39
- Mast, D., Rosales-Ortega, F. F., Sánchez, S. F., et al. 2014, *Astron. Astrophys.*, 561, A129
- McWilliam, A. 1990, *Astrophys. J. Supple.*, 74, 1075
- Mikolaitis, Š., Hill, V., Recio-Blanco, A., et al. 2014, *Astron. Astrophys.*, 572, A33
- Minchev, I., Chiappini, C., & Martig, M. 2014, *Astron. Astrophys.*, 572, 92
- Minchev, I., Famaey, B., Quillen, A. C., et al. 2012, *Astron. Astrophys.*, 548, 127
- Minchev, I., Martig, M., Streich, D., et al. 2015, *Astrophys. J. Letters*, 804, 9
- Miranda, M. S., Pilkington, K., Gibson, B. K., et al. 2016, *Astron. Astrophys.*, 587, A10
- Moni Bidin, C., Carraro, G., & Méndez, R. A. 2012, *Astrophys. J.*, 747, 101
- Navarro, J. F., Abadi, M. G., Venn, K. A., Freeman, K. C., & Anguiano, B. 2011, *Mon. Not. Roy. Astron. Soc.*, 412, 1203
- Nemec, J. M. & Nemec, A. F. L. 1993, *Astron. J.*, 105, 1455
- Nomoto, K., Hashimoto, M., Tsujimoto, T., et al. 1997, *Nuclear Phys. A*, 616, 79

- Nordström, B., Mayor, M., Andersen, J., et al. 2004, *Astron. Astrophys.*, 418, 989
- Obreja, A., Domínguez-Tenreiro, R., Brook, C., et al. 2013, *Astrophys. J.*, 763, 26
- Ocvirk, P., Pichon, C., Lançon, A., & Thiébaud, E. 2006a, *Mon. Not. Roy. Astron. Soc.*, 365, 74
- Ocvirk, P., Pichon, C., Lançon, A., & Thiébaud, E. 2006b, *Mon. Not. Roy. Astron. Soc.*, 365, 46
- Ojha, D. K. 2001, *Mon. Not. Roy. Astron. Soc.*, 322, 426
- Ostriker, J. P. & Peebles, P. J. E. 1973, *Astrophys. J.*, 186, 467
- Pagel, B. E. J. 1997, *Nucleosynthesis and Chemical Evolution of Galaxies*, 392
- Pappalardo, C., Lançon, A., Vollmer, B., et al. 2010, *Astron. Astrophys.*, 514, A33
- Pasetto, S., Grebel, E. K., Zwitter, T., et al. 2012, *Astron. Astrophys.*, 547, A71
- Peng, X., Du, C., Wu, Z., Ma, J., & Zhou, X. 2013, *MNRAS*, 434, 3165
- Perez, J., Michel-Dansac, L., & Tissera, P. B. 2011, *Mon. Not. Roy. Astron. Soc.*, 417, 580
- Pilkington, K., Few, C. G., Gibson, B. K., et al. 2012a, *Astron. Astrophys.*, 540, 56
- Pilkington, K. & Gibson, B. K. 2012, in *Astronomical Society of the Pacific Conference Series*, Vol. 458, *Galactic Archaeology: Near-Field Cosmology and the Formation of the Milky Way*, ed. W. Aoki, M. Ishigaki, T. Suda, T. Tsujimoto, & N. Arimoto, 241
- Pilkington, K., Gibson, B. K., Brook, C. B., et al. 2012b, *Mon. Not. Roy. Astron. Soc.*, 425, 969

- Pilyugin, L. S., Grebel, E. K., & Zinchenko, I. A. 2015, *Mon. Not. Roy. Astron. Soc.*, 450, 3254
- Planck Collaboration, D. e. a. 2014, *Astron. Astrophys.*, 571, A16
- Prochaska, J. X., Naumov, S. O., Carney, B. W., McWilliam, A., & Wolfe, A. M. 2000, *Astron. J.*, 120, 2513
- Qu, Y., Di Matteo, P., Lehnert, M. D., & van Driel, W. 2011, *Astron. Astrophys.*, 530, 10
- Quinn, T. & Binney, J. 1992, *Mon. Not. Roy. Astron. Soc.*, 255, 729
- Rahimi, A., Carrell, K., & Kawata, D. 2013, *RAA*, 14, 1406
- Raiteri, C. M., Villata, M., & Navarro, J. F. 1996, *Memorie della Societ Astronomia Italiana*, 67, 817
- Reddy, B. E., Lambert, D. L., & Allende Prieto, C. 2006, *Mon. Not. Roy. Astron. Soc.*, 367, 1329
- Rix, H. W. & Bovy, J. 2013, *Astron. Astrophys. Rev.*, 21, 61
- Robin, A. C., Haywood, M., Creze, M., Ojha, D. K., & Bienayme, O. 1996, *Astron. Astrophys.*, 305, 125
- Rosales-Ortega, F. F. 2011, *New Astron.*, 16, 220
- Rosen, A. & Bregman, J. N. 1995, *Astrophys. J.*, 440, 634
- Roy, J.-R., Belley, J., Dutil, Y., & Martin, P. 1996, *Astrophys. J.*, 460, 284
- Rubin, V. C., Ford, W. K. J., & Thonnard, N. 1980, *Astrophys. J.*, 238, 471
- Ruchti, G. R., Fulbright, J. P., Wyse, R. F., et al. 2011, *Astrophys. J.*, 737, 9

- Ruiz-Lara, T., Few, C. G., Gibson, B. K., et al. 2016, *Astron. Astrophys.*, 586, A112
- Rupke, D. S. N., Kewley, L. J., & Barnes, J. E. 2010a, *Astrophys. J. Letters*, 710, L156
- Rupke, D. S. N., Kewley, L. J., & Chien, L. 2010b, *Astrophys. J.*, 723, 1255
- Rupke, D. S. N., Veilleux, S., & Baker, A. J. 2008, *Astrophys. J.*, 674, 172
- Sánchez, S. F., Kennicutt, R. C., Gil de Paz, A., et al. 2012a, *Astron. Astrophys.*, 538, A8
- Sánchez, S. F., Rosales-Ortega, F. F., Iglesias-Páramo, J., et al. 2014, *Astron. Astrophys.*, 563, A49
- Sánchez, S. F., Rosales-Ortega, F. F., Marino, R. A., et al. 2012b, *Astron. Astrophys.*, 546, A2
- Sánchez-Blázquez, P., Ocvirk, P., Gibson, B. K., Perez, I., & Peletier, R. F. 2011, *Mon. Not. Roy. Astron. Soc.*, 415, 709
- Sánchez-Blázquez, P., Peletier, R. F., Jiménez-Vicente, J., et al. 2006, *Mon. Not. Roy. Astron. Soc.*, 371, 703
- Sánchez-Blázquez, P., Rosales-Ortega, F. F., Méndez-Abreu, J., et al. 2014, *Astron. Astrophys.*, 570, A6
- Sandage, A., Freeman, K. C., & Stokes, N. R. 1970, *Astrophys. J.*, 160, 831
- Sanders, J. L. & Binney, J. 2015, *Mon. Not. Roy. Astron. Soc.*, 449, 3479
- Sarzi, M., Falcón-Barroso, J., Davies, R. L., et al. 2006, *Mon. Not. Roy. Astron. Soc.*, 366, 1151

- Schmidt, M. 1959, *Astrophys. J.*, 129, 243
- Schmidt, M. 1963, *Astrophys. J.*, 137, 758
- Schönrich, R. & Binney, J. 2009, *Mon. Not. Roy. Astron. Soc.*, 396, 203
- Searle, L. 1971, *Astrophys. J.*, 168, 327
- Sellwood, J. A. & Binney, J. J. 2002, *Mon. Not. Roy. Astron. Soc.*, 336, 785
- Sharina, M. & Davoust, E. 2009, *Astron. Astrophys.*, 497, 65
- Shaver, P. A., McGee, R. X., Newton, L. M., Danks, A. C., & Pottasch, S. R. 1983, *Mon. Not. Roy. Astron. Soc.*, 204, 53
- Shen, S., Wadsley, J., & Stinson, G. 2010, *Mon. Not. Roy. Astron. Soc.*, 407, 1581
- Simpson, J. P., Colgan, S. W. J., Rubin, R. H., Erickson, E. F., & Haas, M. R. 1995, *Astrophys. J.*, 444, 721
- Snaith, O. N., Bailin, J., Gibson, B. K., et al. 2015, *Mon. Not. Roy. Astron. Soc.*, accepted
- Soubiran, C., Bienaymé, O., Mishenina, T. V., & Kovtyukh, V. V. 2008, *Astron. Astrophys.*, 480, 91
- Soubiran, C., Bienaymé, O., & Siebert, A. 2003, *Astron. Astrophys.*, 398, 141
- Stanghellini, L. & Haywood, M. 2010, *Astrophys. J.*, 714, 1096
- Steinmetz, M., Zwitter, T., Siebert, A., et al. 2006, *Astron. J.*, 132, 1645
- Stinson, G., Seth, A., Katz, N., et al. 2006, *Mon. Not. Roy. Astron. Soc.*, 373, 1074
- Stinson, G. S., Bailin, J., Couchman, H., et al. 2010, *Mon. Not. Roy. Astron. Soc.*, 408, 812

- Stinson, G. S., Bovy, J., Rix, H.-W., et al. 2013a, *Mon. Not. Roy. Astron. Soc.*, 436, 625
- Stinson, G. S., Brook, C., Macciò, A. V., et al. 2013b, *Mon. Not. Roy. Astron. Soc.*, 428, 129
- Stinson, G. S., Brook, C., Prochaska, J. X., et al. 2012, *Mon. Not. Roy. Astron. Soc.*, 425, 1270
- Swinbank, A. M., Sobral, D., Smail, I., et al. 2012, *Mon. Not. Roy. Astron. Soc.*, 426, 935
- Tassis, K., Kravtsov, A. V., & Gnedin, N. Y. 2008, *Astrophys. J.*, 672, 888
- Teyssier, R. 2002, *Astron. Astrophys.*, 385, 337
- Tinsley, B. M. 1980, *Fundamentals of Cosmic Physic*, 5, 287
- Tissera, P. B., Pedrosa, S. E., Sillero, E., & Vilchez, J. M. 2016, *Mon. Not. Roy. Astron. Soc.*, 456, 2982
- Tojeiro, R., Heavens, A. F., Jimenez, R., & Panter, B. 2007, *Mon. Not. Roy. Astron. Soc.*, 381, 1252
- Tomkin, J., Lambert, D. L., & Balachandran, S. 1985, *Astrophys. J.*, 290, 289
- Torrey, P., Cox, T. J., Kewley, L., & Hernquist, L. 2012, *Astrophys. J.*, 746, 108
- Torrey, P., Vogelsberger, M., Genel, S., et al. 2014, *Mon. Not. Roy. Astron. Soc.*, 438, 1985
- Tremonti, C. A., Heckman, T. M., Kauffmann, G., et al. 2004, *Astrophys. J.*, 613, 898
- Tsikoudi, V. 1979, *ApJ*, 234, 842

- Tully, R. B. & Fisher, J. R. 1977, *Astron. Astrophys.*, 54, 661
- van der Kruit, P. C. & Freeman, K. C. 2011, *Ann. Rev. Astron. Astrophys.*, 49, 301
- van der Kruit, P. C. & Searle, L. 1981, *Astron. Astrophys.*, 95, 105
- van Zee, L., Salzer, J. J., Haynes, M. P., O'Donoghue, A. A., & Balonek, T. J. 1998, *Astron. J.*, 116, 2805
- Vazdekis, A., Sánchez-Blázquez, P., Falcón-Barroso, J., et al. 2010, *Mon. Not. Roy. Astron. Soc.*, 404, 1639
- Vera-Ciro, C., D'Onghia, E., Navarro, J., & Abadi, M. 2014, *Astrophys. J.*, 794, 173
- Vila-Costas, M. B. & Edmunds, M. G. 1992, *Mon. Not. Roy. Astron. Soc.*, 259, 121
- Villalobos, Á. & Helmi, A. 2008, *MNRAS*, 391, 1806
- Wadsley, J. W., Stadel, J., & Quinn, T. 2004, *New Astronomy*, 9, 137
- Werk, J. K., Putman, M. E., Meurer, G. R., & Santiago-Figueroa, N. 2011, *Astrophys. J.*, 735, 21
- White, S. D. M. & Rees, M. J. 1978, *Mon. Not. Roy. Astron. Soc.*, 183, 341
- Williams, M. J., Bureau, M., & Cappellari, M. 2009, *Mon. Not. Roy. Astron. Soc.*, 400, 1665
- Willman, B. & Strader, J. 2012, *Astron. J.*, 144, 76
- Woolley, S. E. & Weaver, T. A. 1995, *Astrophys. J. Supple.*, 101, 181
- Wuyts, E., Wisnioski, E., Fossati, M., et al. 2016, *Astrophys. J.*, 827, 18
- Wyse, R. F. G. & Gilmore, G. 1995, *Astron. J.*, 110, 2771

- Wyse, R. F. G., Gilmore, G., Norris, J. E., et al. 2006, *Astrophys. J. Letters*, 639, L13
- Xiang, M.-S., Liu, X.-W., Yuan, H.-B., et al. 2015, *RAA*, 15, 1209
- Yoachim, P. & Dalcanton, J. J. 2005, *Astrophys. J.*, 624, 701
- Yoachim, P. & Dalcanton, J. J. 2006, *Astron. J.*, 131, 226
- Yoachim, P. & Dalcanton, J. J. 2008, *Astrophys. J.*, 682, 1004
- Yuan, T.-T., Kewley, L. J., Swinbank, A. M., Richard, J., & Livermore, R. C. 2011, *Astrophys. J. Letters*, 732, L14
- Zahid, H. J., Geller, M. J., Kewley, L. J., et al. 2013, *Astrophys. J. Letters*, 771, 6
- Zaritsky, D., Kennicutt, Jr., R. C., & Huchra, J. P. 1994, *Astrophys. J.*, 420, 87